Engineering Surface for Next Generation Fluid Separation

A thesis submitted to the University of Manchester for the degree of Doctor of Philosophy (Materials) in the Faculty of Science and Engineering

2021

Usama Zulfiqar

Department of Materials

Table of Contents

Word count= 44464

List of figures

List of tables

List of abbreviations

SEM	Scanning electron microscope
EDS	Energy Dispersive X-ray Spectroscopy
TEM	Transmission Electron Microscopy
XRD	X-ray Diffraction
TGA	Thermogravimetric Analysis
WCA	Water contact angle
PDMS	Polydimethylsiloxane
AFM	Atomic force microscopy
TOC	Total organic carbon analysis
PU	Polyurethane
PVDF	Polyvinylidene fluoride
THF	Tetrahydrofuran
PTFE	Polytetrafluoroethylene
XPS	X-ray Photoelectron Spectroscopy
SDS	Sodium dodecylbenzene sulfonate
BET	Brunauer–Emmett–Teller
CNTs	Carbon nanotubes
APTES	3-aminopropyltriethoxysilane
QC	Quaternized chitosan
RMS	Root mean square

Abstract

Oil/water mixtures are produced in upstream and downstream operations during the extraction and refining of crude oil. Separating oily water is essential in industries for product specification and to avoid corrosion in pipelines. Besides, removing oily products from water is imperative before it can be discharged into the environment. Several techniques are in practice to deal with industrial oil/water mixtures, such as in situ burning, bioremediation, and solidifiers that change the physical shape of oil via chemical interaction. Physical separation of oil/water mixtures is in industrial practice; however, the existing technologies to do so often require either dissipation of large amounts of energy (such as in cyclones and hydrocyclones) or significant residence times or inventories of fluids (such as in decanters). Recently, materials with selective wettability have gained attention for application in the separation of oil/water mixtures, and surfactant stabilized emulsions. For example, a superhydrophobic material is selectively wettable towards oil whilst having a poor affinity for the aqueous phase. Therefore a superhydrophobic porous material can efficiently adsorb the oil while rejecting the water from an oil/water mixture, thus physically separating the two components. The ease of separation, low cost, and low energy requirements and potential for scale-up are some of the advantages of these materials over existing oil/water separation practices. This work studied the nanoscale engineering of various materials to separate biphasic mixtures and broader application in environmental remediation and energy. The first chapter of this thesis provides a background of the project and a state of the art literature review of various nanomaterials for oil/water separation. Research work on renewable nanocomposite adsorbent for emulsion separation has been presented in the second chapter. Nanocomposites were prepared by coating sawdust particles with a thin layer of alumina nanoparticles and a nanoscale

siloxane coating to make them superhydrophobic. The synthesis conditions were extensively studied, and nanocomposites were thoroughly characterized to establish a structure-property relationship. Optimised samples were used for the separation of surfactant stabilized oil/water emulsions.

Findings from the 2nd chapter inspired the research work on magnetic adsorbent for the separation of emulsions (3rd chapter). High surface area silica-based magnetic nanocomposites were synthesised for fast separation of stable emulsions. Both sawdust and magnetic nanocomposites were used for batch scale separation of emulsions. The findings from those works and guidance from industrial partners lead to macroscopic superhydrophobic materials for continuous separation. Chapter 4 presents a new spray based method for the fabrication of nanofibrous superhydrophobic membranes. Very small (13 nm) hydrophobic alumina nanoparticles were mixed with thermoplastic polyurethane and spray-coated on a water interface to acquire porous membranes. The membrane's pore size and surface properties were adjusted, and optimized samples were used to separate oil/water mixtures and emulsions.

Declaration

No portion of the work referred to in the thesis has been submitted in support of an application for another degree or qualification of this or any other university or other institute of learning.

Copyright statement

Acknowledgements

I would like to express my most profound appreciation to esteemed supervisor, Prof. Allan Matthews and co-supervisors Dr David J. Lewis and Dr Andrew Thomas, for their unwavering support, supervision and contributions throughout this research work. Their in-depth knowledge and wealth of experience working with industrial partners have been instrumental in completing this project.

I want to extend my sincere gratitude to Dr Leslie Bolton and Dr Kathryn Yearsley. Their vast industrial experience and insightful suggestions have been imperative in guiding the course of this research. I am deeply grateful to all of the bp-ICAM community to provide me with the opportunity and then supporting via resources to conduct this research. It has been a privilege to work with bp-ICAM as a PhD researcher. The learning and experiences gained through this platform will benefit me for the rest of my life. It is truly a unique program that instils various essential qualifications to the new generation of young researchers, and I feel honoured to be part of it.

I am deeply grateful to the University of Manchester staff, research officers and colleagues for training, help with characterisations, and for being an excellent company for the last few years.

Finally, I would like to thank my family for their support and for having faith in me despite challenging times.

Chapter 1: Introduction and literature review

Citation: U. Zulfiqar, A. G. Thomas, A. Matthews, and D. J. Lewis, "Surface Engineering of Ceramic Nanomaterials for Separation of Oil/Water Mixtures," Frontiers in Chemistry, vol. 8. Frontiers Media S.A., p. 578, Nov. 19, 2020, doi: 10.3389/fchem.2020.00578.

Author contributions:

All authors listed have made a substantial, direct and intellectual contribution to the work and approved it for publication. U. Zulfiqar collected and compiled the data and wrote the manuscript whilst A. G. Thomas, A. Matthews, and D. J. Lewis contributed to writing, editing, and revising the manuscript.

1.1 Introduction

There has been a growing interest in utilizing smart bioinspired materials with selective functional wettability to separate oil/water mixtures and emulsions. Surfaces can be engineered to have an affinity towards one class of fluid whilst being repellent to others. This implies that if an absorbent repels one phase, it can effectively collect the second phase from a biphasic mixture. The inspiration of using bioinspired materials for oil water separation is based on the so-called lotus leaf effect described by Barthlott and Neinhuis who observed that the self-cleaning property of the leaves of the lotus plant or water lilly (*Nelumbo nucifera*) is due to a rough surface with microscale villi and is also waxy and therefore hydrophobic(**Figure 1-*1***) [1]. This hierarchical structure imparts low surface energy to the leaf, making it extremely repellent to water and is said to be 'superhydrophobic' (water contact angle (WCA) > 150°). The evolutionary benefit to the plant is that it can efficiently reject water, so the leaves do not sink. As water droplets roll off the leaf, it is also passively self-cleaning, which allows efficient photosynthesis.

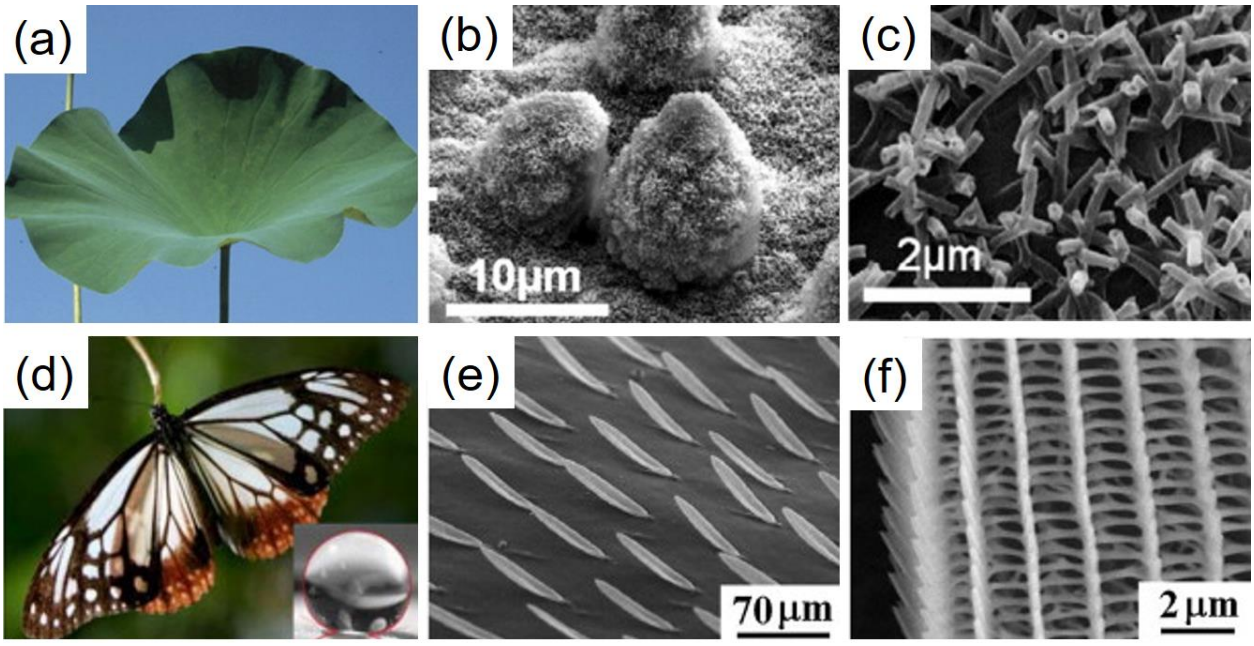

Figure 1-1: Figure showing the digital images and SEM images of different natural species which display hydrophobic properties (a- c) Nelumbo nucifera (Lotus) (d-f) butterfly wings. (a-c)Adapted from [2,3]. With permission from Elsevier and NPG, respectively.

This, of course, is not a feature exclusive to the lotus leaf; other insects and plants also have features that may display superhydrophobic properties with varying micro and nanoscale surface features. For example, Indian canna plants contain wax platelets that are randomly distributed on microscale rods (WCA~165°) whilst the Taro leaves comprise a surface containing nanoscale elliptic features that are uniformly distributed on micron-sized features (WCA~159°) [4]. Insects such as water striders (*Gerridae),* dragonflies (*Anisoptera),* cicadae *(Cicadoidea)* and butterflies (*Papilionoidea*) also possess anti-wetting and anti-fogging adaptations. The wings of the dragonfly *Hemianax papuensis* contains nanopillars which form a fractal structure resulting in an extremely water repellent surface (WCA~161°) [4,5]. Since the advent of electron microscopies, which allowed the discovery of the surface features that allow the superhydrophobic phenomenon in biological species, scientists have sought to engineer artificial superhydrophobic surfaces [6–8]. Mimicking of superhydrophobic surfaces has since been successfully achieved in labs worldwide, and this branch of *biomimicry* has found many applications in self-cleaning, protection of the building, corrosion resistance, anti-icing, drag reduction, biomedical and separation of oil/water mixtures and emulsions [9,10,19–21,11–18]. Although separation of oil/water mixtures had been demonstrated successfully using superhydrophobic surfaces, the separation of emulsions is not easy as the oil droplets are uniformly distributed and often stabilized within the water phase. Surfactant stabilised emulsions make a significant fraction of water contaminants and are created due to industrial operations or the extraction/refining of crude oil. A typical refining process for one ton of crude oil produces ca. 3.5–5 m^3 oil/water mixture. Worldwide production of produced water reached an

average of 210 million barrels in 1999 [22]. Unsolicited discharge of these mixtures and industrial effluents risks contaminating freshwater streams through adsorption in soil or direct mixing [23]. Finely distributed oil droplets in the water phase make an oil/water mixture more toxic and immune to conventional septation techniques. Typical oil/water separation methods lack efficiency in removing emulsion formed in the presence of natural additives and environmental stressors. Methods such as on spot burning and dispersants cause further pollution and are not sustainable for long term applications. An efficient and scalable separation method will have environmental remediation applications and enhance industrial processes economic value.

Superhydrophobic materials have the potential to separate oil/water mixtures due to their selective affinity towards oil [24–28]. Several types of superhydrophobic nanocomposites, including nanoparticle-grafted meshes, membranes, foams and textiles have been developed for this purpose [29–33]. For example, carbon-based nanofibers were grafted on a polydimethylsiloxane framework to enhance roughness, hydrophobicity, and capillaries to absorb oil/water mixtures [25]. Another work reported a nanofibrous electrospun polyimide membrane containing zeolitic imidazolate framework-8@thiolated graphene [34]. The hierarchical zeolitic imidazolate framework created a superhydrophobic/superoleophilic membrane that separated oil/water mixtures and emulsions with 99% efficiency. Industrial applications of current superhydrophobic formulations are impeded by low durability and further compounded by complicated manufacturing routes [35]. A range of methods involving superwettable materials have been explored to realize the separation of emulsions, and in some cases, surfactant stabilized emulsions [36–40]. This chapter covers a brief introduction of various types of oil/water mixtures and super wetting interfaces for the separation of such mixtures. Later, a state of the art literature review on surface engineering of nanomaterials for oil/water separation is presented.

1.2 Immiscible fluidic mixtures

1.2.1 Oil/water mixtures

Oil/water mixtures are produced in the petrochemical, leather, food, metallurgical and beverage industries on a regular basis. In the oil industry, the oil/water mixture volume is greatly increased by enhanced oil recovery techniques during the drilling from the reservoir. At the end of reservoir life, enhanced oil recovery techniques are employed to acquire 20- 40% more oil. Recovering the oil from oil/water mixture is of paramount interest to increase the economic value of operations in petrochemical industries [41]. These techniques are accompanied by many drawbacks including oil/water mixtures being produced in stable emulsions. Usually, oil/water mixtures don't exist as two separate phases. Instead, they are produced in the form of emulsions which are further modified with some natural surface active agents to stabilize the oil phase in water making the separation process extremely difficult.

Organic contaminants are produced in these processes, and if released into marine and river waters, they can affect biological organisms in many negative ways, as well as causing atmospheric pollution, destroying crops for consumption and causing a potential fire hazard [42,43].Oil/water mixtures are a potential problem due to the unprecedented harmful effects of hydrocarbons in water streams on the environment, on natural habitats and on human health [44454647].

Accidents during production or transportation of oil are another cause of oil/water mixtures discharged to the environment. Major accidents such as the Exxon Valdez spill (1987), the Deepwater Horizon fire and spill (2010) and the Chennai oil spill (2017) have all been deleterious to the marine environment [48,49]. As the oil comes to the surface of water due to its low density, it affects the animals which have to go through air/water interface to breathe. The rise and fall of tides enable contact between oil and natural species and affect them in several ways, including

digestion of oil, inhalation of vapors and DNA damage [5051]. Accidents that happen close to the shore are difficult to clean and have adverse effects on human health and economy.

1.2.2 Emulsions in the petrochemical industry

An emulsion is a metastable mixture of two immiscible fluids where droplets of one liquid are distributed in the another liquid phase [52]. These mixtures are mostly formed in the presence of an emulsifier which could be either a surfactant molecule or solid particles. Emulsions have been studied extensively in the past few decades, and several definitions and classification of these systems exist. For example, they have been defined as a mixture of two immiscible liquids with one phase uniformly distributed in the other with the help of an emulsifying agent [5354]. They are thermodynamically unstable mixtures that eventually separate from each other to reduce the interfacial area. There exists different classification of emulsions such as oil in water, water in oil and complex emulsions. Oil in water emulsions are formed when the oil droplets are dispersed in the water while water in oil emulsions are formed when water droplets are dispersed in oil. In complex emulsions, water is dispersed in oil which is also mixed in continuous water phase (water/oil/water emulsion). Emulsions are stabilized by the presence of emulsifying agent and the balance of lipophilic and hydrophilic properties of the agent is one of the important factors in dictating the emulsion type. The emulsifying agents are the surface active agents which makes the interfacial film leading to the reduction of interfacial tension and suspension of the droplets. Emulsions are also characterized as tight (small droplets) or loose (large droplets) based on the size of droplets dispersed in continuous phase. According to another work, an emulsion can be called a *macro emulsion* if the size of droplets is bigger than 0.1 µm and a *micro emulsion* when the size of dispersed droplets is less than 0.1 µm [55]

Emulsion generation is a severe problem in several industrial operations such as pharmaceuticals, cosmetics, food and especially in the petrochemical industry where emulsions are formed at the wellbore, during enhanced oil recovery operations and downstream processing [56,57]. These emulsions often contain salts which may cause corrosion in pipelines. The amount of water is increased in crude oil near the end of the life of a reservoir [58], and both immiscible liquids undergo intense pressure causing mixing and the generation of emulsions [59]. Emulsification like this makes cleanup difficult in the event of an oil spill as it alters the viscosity and density of oil. It can also enhance the volume of the mixture as observed in previous studies where an increase in volume of spilled material up to five times has been observed due to emulsification [606152]. Crude oil also contains several minerals and compounds such as asphaltene, organic acids, solid particles, organometallics, corrosion products and waxes and some of these compounds help to create stable emulsion with water. The solid particles of clays, silica and iron oxide are naturally hydrophilic but can become hydrophobic after prolonged contact with oil. This combined with asphaltenes and resins can help water droplets uniformly disperse in oil or vice versa, generating very stable emulsions.

1.3 Separation of oil/water mixtures

There are several approaches to separate oil/water mixtures in different situations. The US Environmental Protection Agency classifies the separation in three different categories in the event of an oil spill. These include mechanical recovery (booms, skimmers, sorbents), chemical and biological methods (gelling agents, dispersants, biological agents) and physical separation (pressure washing and sorbents) [62]. In situ burning of oil is sometimes used for the urgent treatment of oil spills but is limited by many factors [63]. For example, if the oil contains a significant amount of water, then ignition becomes very difficult; moreover, gases produced as a byproduct of combustion may cause secondary environmental pollution. There is a natural tendency in certain

organisms to consume hydrocarbons for the production of carbon and energy to create new microbial cells [64], which could be an ecologically viable and elegant way to remove oil from oil/water mixtures. However, these processes are slow and rely on conditions conducive to the microbes used.

Floatation and coagulation are some of the more widely used methods to treat emulsions. In floatation, air bubbles are introduced which become attached to the light fractions of the mixture (oil or particles) and transport them to the surface. Flotation is more beneficial than gravity separation in terms of efficiency for removing small particles [65]. Starting from the generation of air bubbles of a specific size which become attached the oil droplets, this is followed by aggregation of droplets which subsequently float to the top surface to form a layer which can be skimmed [66]. Coagulation is another method in which chemical agents are added to moderate the surface charge of oil droplets to help them aggregate and settle. The oil droplets are negatively charged due to adsorption of moieties which restrict their aggregation. Some chemical agents with opposite charges are introduced in the system which mitigates the charges on oil droplets and destabilises the colloids promoting their coalescence. For example, long-chain polymers have been introduced which act as a bridge to connect different colloidal particles to assist aggregation [43,67–69].

Other approaches towards separation are mechanical devices such as booms, skimmers or centrifugal devices such as hydro cyclones. Physical separation of the immiscible mixtures using absorbents is advantageous from many perspectives; however, traditional absorbents face limitations due to their affinity towards both oil and water. The absorbent may not be efficient in the separation of emulsion, especially those stabilized with surfactants. A method to improve absorbent efficiency is to engineer the surface properties to tune their wettability towards particular

liquid type. For example, if an absorbent is to be made oleophilic and hydrophobic, it will only absorb oil from an oil/water mixture leaving behind the clean water. Generally, the adsorption starts by the interaction of oil droplets with a sorbent surface followed by its entrapment in the porous framework of the sorbent. It is one of the easiest methods to separate the oil/water mixtures, however, the surface properties of adsorbents greatly influence their interaction with liquid.

Physical separation using membranes is a simple approach to physically separate the mixtures without using additional chemicals. The membrane acts as a porous layer and controls the transportation between oil and water [70]. The membranes can block the penetration of solids through their pores while letting the liquid pass through. Sorbents and membranes are useful materials for the remediation of oil/water mixtures and physical collection of oil. The surface engineering of these materials to tune their affinities towards oil or water is extremely important for efficient separation. The wetting properties of a surface such as high repellency towards water (superhydrophobic), affinity towards water (superhydrophilic), high repellency towards oil (superoleophobic), affinity towards oil (superoleophilic) mainly depend upon the chemical structure and geometry of the surface. Surface engineered absorbents and membranes can be an effective way to separate stable oil/water mixtures and emulsions.

1.4 Surface properties for physical separation

The surface of a material can be engineered to have a combination of wetting properties to be used for separation of oil/water mixtures. This combination could be superhydrophobic/ superoleophilic [71,72] or superoleophobic/superhydrophilic [73,74] depending upon the type of material and nature of application environment. Generally, surfaces with superhydrophobic properties are used to repel the water in a mixture and attract the oil. Hence, if an absorbent is to collect oil from an emulsion whilst repelling water, it will have a surface that is both superhydrophobic and

superoleophilic. For example, hierarchically structured MnO_2 particles have been used to separate oil from emulsions [75]. The particles were modified with stearic acid to render them superhydrophobic and superoleophilic.

1.4.1 Superhydrophobic/Superoleophilic Surfaces

Generally, the materials with these properties have been constructed by coating porous substrates with a superhydrophobic coating. A superhydrophobic coating can provide excellent resistance to water but allows the permeation of low surface tension liquids. When water is introduced to the surface of these materials, it forms a spherical droplet (CA > 150°) while an oil droplet completely spreads over it (CA < 10°). These surfaces are mostly inspired by nature as several natural species can repel water due to certain physicochemical features of their surface (e.g. lotus leaf, *vide supra*). Superhydrophobic surfaces can be created by combining nanoscale hierarchical roughness with low surface energy materials. For example, flourosilane modified silica nanoparticles have been used in combination with epoxy resin to create an artificial superhydrophobic surface. The nanoscale particles helped to achieve a hierarchical structure with low surface energy [76]. A dual scale modification was recently carried out on a melamine sponge to create a combination of superhydrophobic and superoleophilic properties [77]. The sponge was coated with graphene oxide followed by decoration with hydrophobic magnetite nanoparticles. After the modification, the sponge was able to collect oil while rejecting the water effectively There are other examples where this combination of properties has been used to engineer materials for oil/water separation [78–80]. A variety of nanomaterials have been used to create meshes [81–86], membranes [87–93], sponges [38], [42],[95,96] and fabrics [97–101] with superhydrophobic and superoleophilic properties for oil/water separation [30,31,102–105]. Most of these materials separate oil either by filtration, absorption or both. These materials have certain limitations in case as most of the separation is gravity driven in case of filtration which could be very slow or may not even work

in case of emulsions. Another problem is fouling of membranes or mesh pores by oil adsorption. The solid content in oil, especially in crude oil, can easily block the pores affecting the whole separation process. In the case of oil in water emulsions when stabilized by surfactant, the oil is uniformly distributed in the water phase and does not come in direct contact with separation materials thus making it ineffective for separation. However, there is recent trend in engineering micro scale absorbents with superhydrophobic and superoleophilic properties which can go into the emulsion under mechanical agitation and collect the dispersed oil phase from it [106–109]. This approach is reported to be effective for removing oil in several scenarios (present on the surface of water or uniformly distributed in water). Further details on surface engineering of different materials for this approach will be discussed in the next sections.

1.4.2 Superoleophobic/Superhydrophilic Surfaces

Rendering superoleophobic properties to a surface is not simple because there is a vast difference in surface tension between water and organic liquids. For example, water has surface tension of 72.8 mN m^{-1} whilst the surface tension of *n*-hexane is 18.4 mN m^{-1}. Recently some strategies such as modification of different nanomaterials with flourosilanes [110,111] engineering of re-entrant surface geometry for supeproleophobic properties [112] and underwater superoleophobicity have been studied in detail [113,114]. From an applications point of view, superoleophobic surfaces can be divided into several categories but this literature review is focused on surfaces which have both superoleophobic and superhydrophilic properties. This combination of properties can be used for oil/water separation via oil rejection whilst allowing water to pass through. In a typical example, a surface with a combination of superoleophobic and superhydrophilic properties was formed by using titania nanoparticles and fluorinated compounds containing hydrophilic units (Na^+) and its application in oil/water separation was demonstrated [73]. Titania nanoparticles and fluorinated compounds containing hydrophilic units (Na^+) were used to

construct these coatings on substrates such as steel mesh, sponge and cotton. The hydrophilic unit bestows hydrophilic properties while fluorine groups are responsible for the oleophobic character of the coating. The coatings were used to separate stabilized emulsion and mixtures of water and vegetable oil. Similarly, nanoparticles with thiol−acrylate components were used to create a coating with similar properties [115].

Introducing a liquid into nanostructured surfaces is a different approach to achieve a combination of superoleophobic and superhydrophilic properties. This method is inspired by fish scales which possess oil repellent properties in water enabling them to swim in oil contaminated water. The fish scales are made of protein and calcium phosphate which is a hydrophilic material. These scales have an affinity towards both water and oil in air; however, once water is penetrated in this structure, it becomes superoleophobic with an oil contact angle of 156 ° (1,2-dichloroethane). There are micropapillae with the rough structure distributed on the surface of fish skin which when soaked with water provides a superoleophobic platform. Several types of artificial materials especially membranes have been synthesized with underwater superoleophobic properties for oil/water separation [116–119120]. Recently, Ni $(OH)_2$ particles have been coated on a piece of fabric to create a hierarchical porous platform [121]. The composite fabric is superhydrophilic while demonstrating superoleophobic properties underwater. Moreover, the fabric can be made superhydrophobic after modification with stearic acid. The fabric separated oil/water mixtures with a separation efficiency more than 96% for both light and heavy oils. In another approach, $Cu(OH)_2$ was deposited on steel felts which had an underwater contact angle of 154 ° for n-octane. The material was able to separate the oil/water mixtures by allowing the water to permeate while retaining oil.

1.5 Theoretical background of superwetting interfaces for physical separation of immiscible fluids

1.5.1 Air/Water/Solid interface

Wetting of a surface is an important phenomenon which can affect many functional properties of a material. It is important to first highlight the concepts of surface energy and surface tension before discussing the wetting properties of a surface. Surface energy (solid surfaces) and surface tension (fluid surfaces) originates from unsymmetrical bonding of the atoms present at the surface of solid or liquid. It can be ascribed as the energy required to generate a liquid or solid surface in vacuum or gas. It is measured in mN/m. This is the energy related to bonding with other atoms. When a liquid comes in contact with a surface, there are several possibilities ranging from entirely spreading over the surface, to forming spherical droplets. The behavior of a liquid on a surface depends upon the physicochemical properties of surface and is reflected by the angle formed by liquid droplet. For example, water will completely wet a surface of high surface energy e.g. glass [122]. On the other hand, water droplets tend to form a spherical shape on a low surface energy surfaces such as polytetrafluoroethylene (PTFE). Schematic (**Figure 1-*2***) shows the possible states of water droplet on a surface.

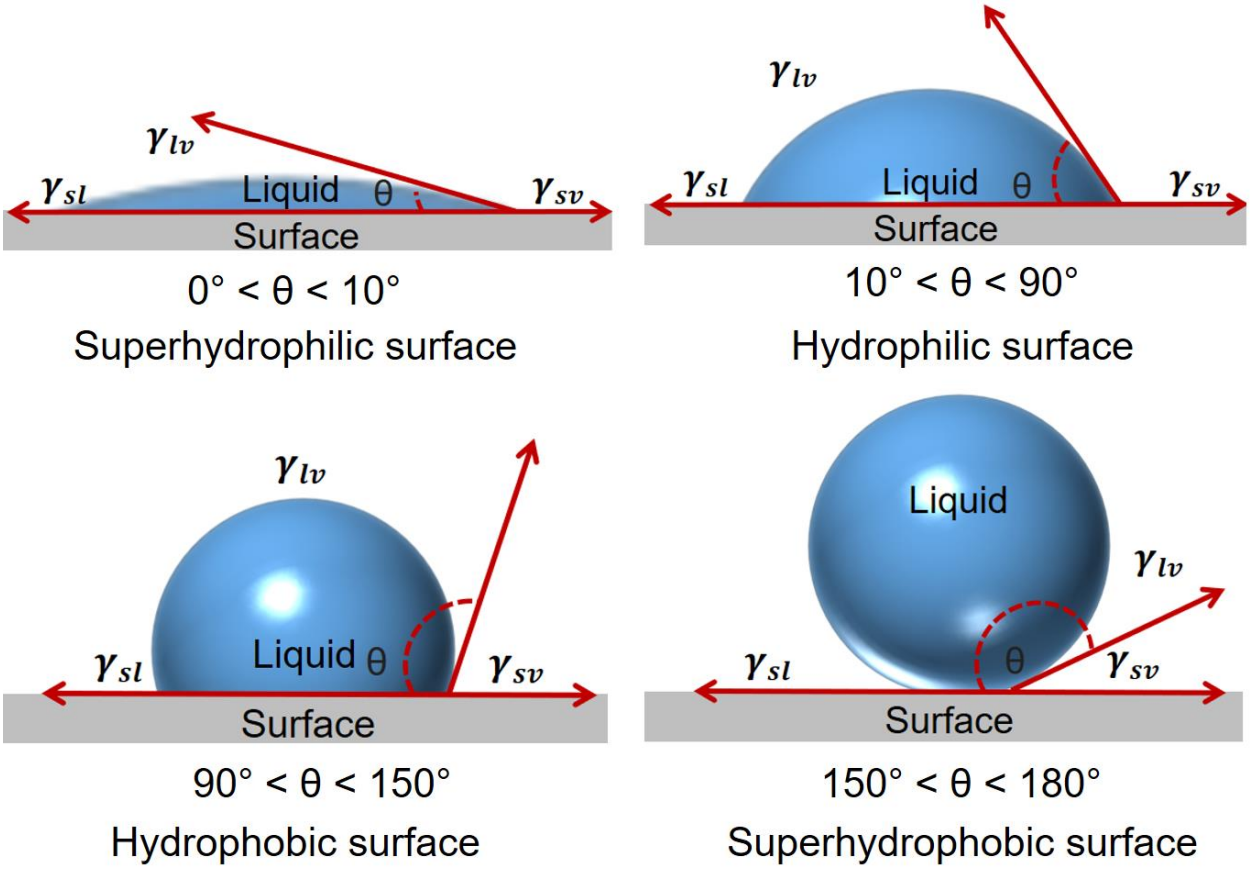

Figure 1-2: Schematic showing the four possible states of water droplet on a surface.

Surface properties have been defined by the nature of their interaction with water. If a liquid droplet is suspended in air, its shape is determined by gravity and the surface tension on the liquid/vapor interface [123]. The liquid molecules at the interface are drawn inwards to maintain the minimum surface area. The smallest surface area can be achieved by forming a sphere; however, gravitational pull acts to flatten the droplet. The effect of gravitational force can be ignored if the size of drop is less than the capillary length of water (2.7 mm). In this case, the shape of water drop will be determined solely by the surface tension of water [124]. Hence, if a small droplet (d < 2.7 mm) is placed on a flat surface there exists three different interfaces and the corresponding surface tensions. Young's equation [120,125]defines wettability under these conditions:

$$\cos\theta = \frac{\gamma_{sv}-\gamma_{sl}}{\gamma_{lv}} \quad (1)$$

Where:

θ^o = Contact angle of a water droplet on a flat surface;

γ_{sv}= Interfacial tension of solid vapor phase;

γ_{sl}= Interfacial tension of solid liquid phase;

γ_{lv}= Interfacial tension of liquid vapor phase.

Young's equation is derived by considering an ideally smooth surface; however, almost every surface has some inhomogeneity in practical cases imperfections or defects contribute to the surface roughness and can greatly influence its wetting properties. Therefore, Wenzel proposed a modification to account for surface roughness in relation to contact angle:

$$cos\theta_w = r\left(\frac{\gamma_{sv}-\gamma_{sl}}{\gamma_{lv}}\right) \quad (2)$$

Which by substitution into equation (1) becomes:

$$cos\theta_w = rcos\theta \quad (3)$$

And where:

θ_w= Contact angle of the rough surface (Wenzel contact angle);

θ= Contact angle on a perfectly flat surface (Young's contact angle).

r = Surface roughness

The Wenzel equation [122] explains the role of surface roughness in controlling the wettability of a surface. For a hydrophilic material, the roughness will increase the wettability of a surface. Similarly, the roughness will further decrease the wettability of a hydrophobic surface. This equation not only includes rough surface but also explains the wettability of smooth surfaces. For example, if the roughness value (ratio actual surface versus projected surface r < 1 for a rough surface) is 1 (for a perfectly planar surface), the contact angle from Young's equation is obtained.

The Cassie- Baxter model [122,126] proposes a heterogeneous structure for superhydrophobic surfaces. The water droplet rests on the asperities of a rough surface rather than entirely penetrating the features, thus making a solid-liquid-air interface, and the following relationship applies:

$$\boldsymbol{cos\theta = f_1 cos\theta_1 + f_2 cos\theta_2} \quad (4)$$

Where:

θ = Contact angle of a water droplet (Cassie-Baxter)

f_1 = Fraction of material 1 in contact with surface

θ_1 = Contact angle of a water droplet with surface

f_2 = Fraction of material 2 in contact with air

θ_2 = Contact angle of a water droplet with air

If the surface features have been made by one solid, then f1 represents the solid fraction that interacts with water and $f_2(1\text{-}f_1)$ is the area fraction of air pockets in contact with the water droplet. Water contact angle with air is 180°; therefore the equation can be simplified to the following form:

$$\boldsymbol{cos\theta = f_s(1 + cos\theta_s) - 1} \quad (5)$$

Where f_s denotes the fractional area of solid with contact angle θ_s in contact with water droplet.

Therefore, increasing the roughness on a surface will increase its hydrophilic or hydrophobic properties depending upon the surface's chemical composition. If a hydrophobic material is considered, the contact angle or water repellent properties of a surface will substantially increase if the surface features are capable of hosting air pockets in them. Thus, a hierarchically structured surface will give rise to a superhydrophobic surface due to surface roughness, air pockets and low surface energy chemistry. The schematic explains a water droplet's behaviour on a surface by all three models (**Figure 1-*3***).

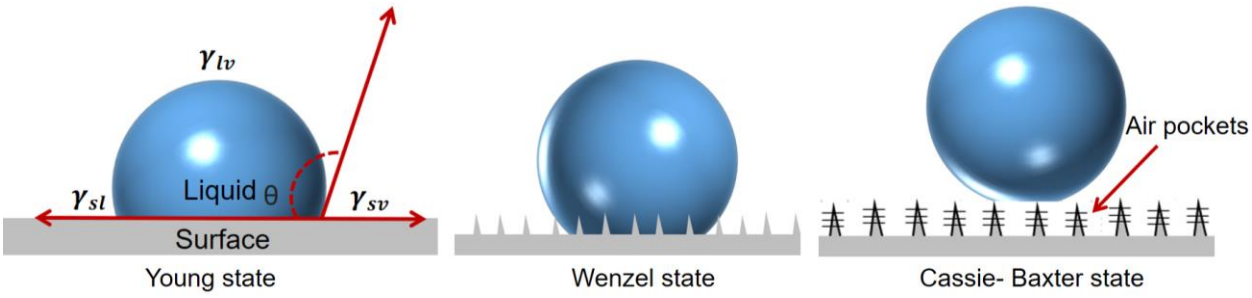

Figure 1-3: Schematic showing the behavior of water droplet in three different modals

1.5.2 Oil/Water/Solid interface

To apply superoleophobic surfaces in oil/water separation, it is important for them to possess an affinity towards water. There has been recent trend in the fabrication of underwater superoleophobic surface with superhydrophilic properties. These types of surfaces are generally engineered by infusing water into the nanostructured surface. The water together with the rough texture blocks ingress of oil whilst letting water pass through. The Young's equation can present the corresponding oil contact angle formed in Oil/Water/Solid interface.

$$\boldsymbol{cos}\theta_{ow} = \frac{\boldsymbol{\gamma_{sw}-\gamma_{so}}}{\boldsymbol{\gamma_{ow}}} \quad \textbf{(6)}$$

θow= Contact angle of an oil droplet on a smooth surface in water

γ_{sw}= Interfacial tension of solid water phase

γ_{so}= Interfacial tension of solid oil phase

γ_{ow}= Interfacial tension of oil water phase

Young's equation (1) is valid for both oil and water droplets and can be written by replacing the values of γ_{sw} and γ_{so}. By replacing these values, we get the following equation:

$$\boldsymbol{cos}\theta_{ow} = \frac{\boldsymbol{\gamma_{ov}\ \cos\theta_o-\gamma_{wv}\ \cos\theta_w}}{\boldsymbol{\gamma_{ow}}} \quad (7)$$

Hence a hydrophilic surface can become oleophobic in underwater conditions. In the previous section, it was discussed in details that a heterogeneous interface (solid/air) is required to create the superhydrophobic phenomenon. Similarly, the Wenzel and Cassie Baxter modals can be generalized for the solid water interface, which means an underwater rough surface with solid/water interface will exhibit superoleophobic properties [125]. The Wenzel model for underwater surfaces can be given as follows:

$$\boldsymbol{cos\theta_w = r cos\theta_{ow}} \quad (8)$$

And Cassie Baxter modal

$$\boldsymbol{cos\theta_{CB} = f_{so}\cos\theta_{ow} + f_{so} - 1} \quad (9)$$

Like the superhydrophobic surface where air /solid interface helps increase the water contact angle, underwater superoleophobic surfaces exploit water/solid interface. The water layer sticks to the very rough solid structure and provides superoleophobic character due to its oil-repellent nature.

1.6 Literature review- surface engineering of ceramic nanomaterials

1.6.1 Silica-based materials

In silica (SiO_2), the silicon atom is surrounded by four oxygen atoms to form a tetrahedral vertex which is further bridged with others by a shared oxygen atom to form a three-dimensional network. Silica possesses a unique combination of properties which make it a material of choice for several applications. For example, it has thermal stability up to 1500 °C along with good mechanical strength. Moreover, the silanol groups (Si−OH) present on the surface of silica makes it a suitable support for the grafting of several moieties. The synthesis of silica nanoparticles is generally carried out by sol-gel processing using silicates or alkoxides [127,128]. The steps in the synthesis of nanoparticles include hydrolysis of precursors followed by condensation. A typical sol-gel process is sometimes combined with other modifications to produce silica nanomaterials of desirable features. For example, the templates such as polystyrene and chitosan have been utilized to synthesise silica by a sol-gel process to create desired shapes in final particles [129,130]. Hydrolysis greatly depends upon several factors, including precursor, pH, temperature and additives. The ease of shape control by using different templates and reaction parameters makes silica material of choice for several applications including drug delivery, water purification, bioimaging and selectively wettable surfaces for oil/water separation. Regarding the oil water separation, silica has been used in various forms such as nanoparticles, nanostructured micro particles and nanostructure scaffolds [131–133].

Silane modification is therefore performed to alter the hydrophobic character of silica by replacing hydroxyl bonds with the silane functional group. In a typical modification process, OH groups present on the surface of silica would react with the chlorine of dichlorosilane leading to the replacement of surface functional groups [134]. The hydrophobic character combined with the nanoscale features creates a hierarchical structure suitable to impart superhydrophobic properties.

1.6.1.1 Nanoparticles

Silica nanoparticles have been used to develop materials for the separation of oil/water mixtures [13,135–140]. For example, silica nanoparticles in the size range of 40-60 nm and the silane coupling agent hexadecyltrimethoxysilane were coated on a filter paper via a dip coating method to prepare a hydrophobic separation medium for oil/water mixtures [141]. Similarly, spherical silica nanoparticles with diameter 20 nm were modified with octadecyltrichlorosilane followed by deposition on the surface with the aid of polyfluorowax to make a superhydrophobic textile which effectively separated a mixture of hexadecane and water [142]. In another study, silica nanoparticles of diameter 12 nm were modified with octylsilane and were decorated on a polyurethane sponge to construct a superhydrophobic platform for adsorption of oil from oil/water mixtures [143]. Recently, silica nanoparticles were used in combination with epoxy resin to form superhydrophobic coatings by spray deposition. Nanoparticle surfaces were modified by reaction with hexamethyldisilazane (HMDS) during synthesis [144]. It was suggested that HMDS produces trimethylsilyl and ammonia which further reacts with hydroxyl groups of silica nanoparticles to form a layer on its surface. The introduction of the trimethylsilyl group introduces steric hindrance which prevents the agglomeration and growth of silica nanoparticles. The hydrophobic nature of particles enabled them to be dispersed in an organic solvent, as shown in **Figure 1-*4***a. Transmission electron microscopy (TEM) and powder X-ray diffraction (PXRD) suggested that the silica clusters (**Figure 1-*4***b) were amorphous (**Figure 1-*4***e). Thermogravimetric analysis (TGA) profiles show a significant weight loss (7.8 wt.%) in the temperature range 200°C - 725°C (**Figure 1-*4***f), which the authors ascribe to the loss of functionalities from the surface of silica. Superhydrophobic materials were formed by depositing the silica nanoparticles combined with an adhesive (polyurethane (PU)) onto a glass surface. (**Figure 1-*4***c). **Figure 1-*4***g shows the coating

formed by silica nanoparticles and epoxy. The difference in transmittance of these coatings is shown in **Figure 1-*4***(d and h), the coating formed by PU and silica showed better transmittance.

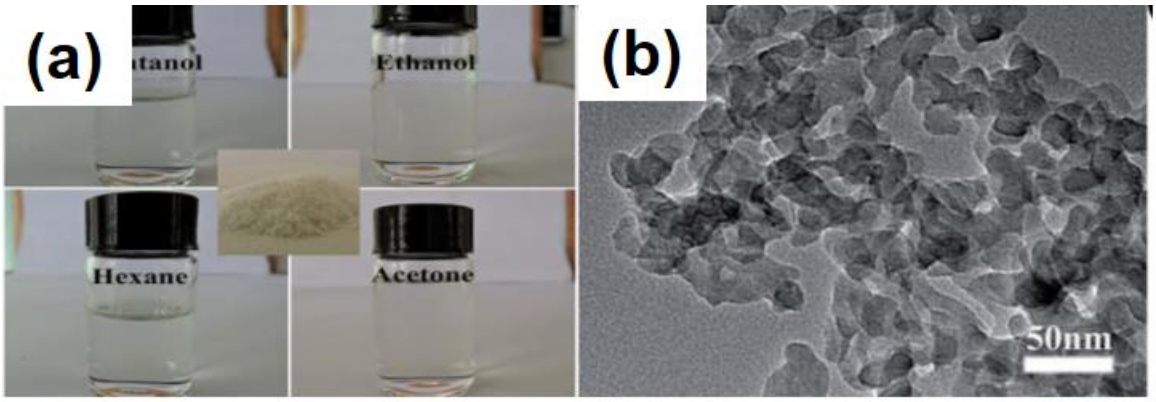
(a)
Ethanol
Hexane
Acetone
(b)
50nm

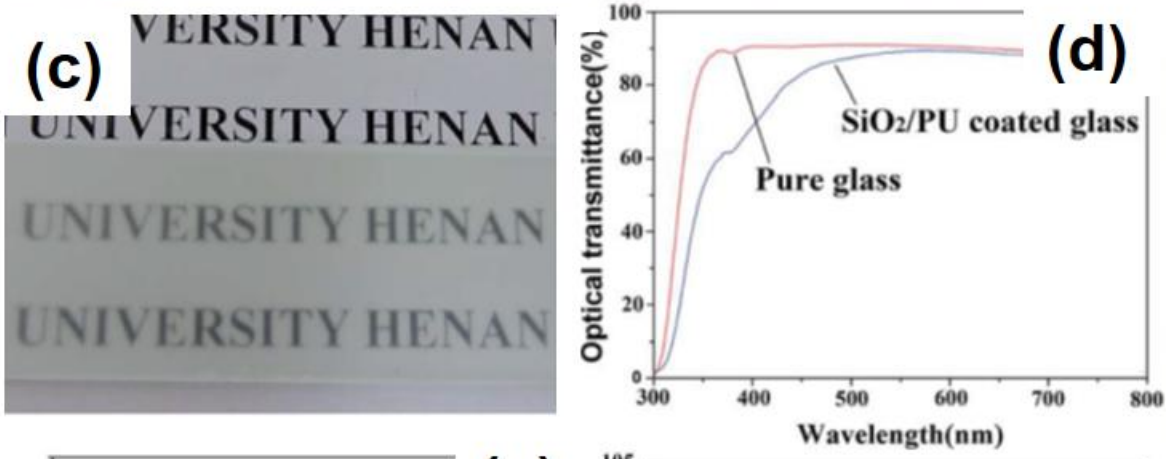
(c)
VERSITY HENAN
UNIVERSITY HENAN
UNIVERSITY HENAN
UNIVERSITY HENAN
(d)
Optical transmittance(%)
SiO2/PU coated glass
Pure glass
Wavelength(nm)

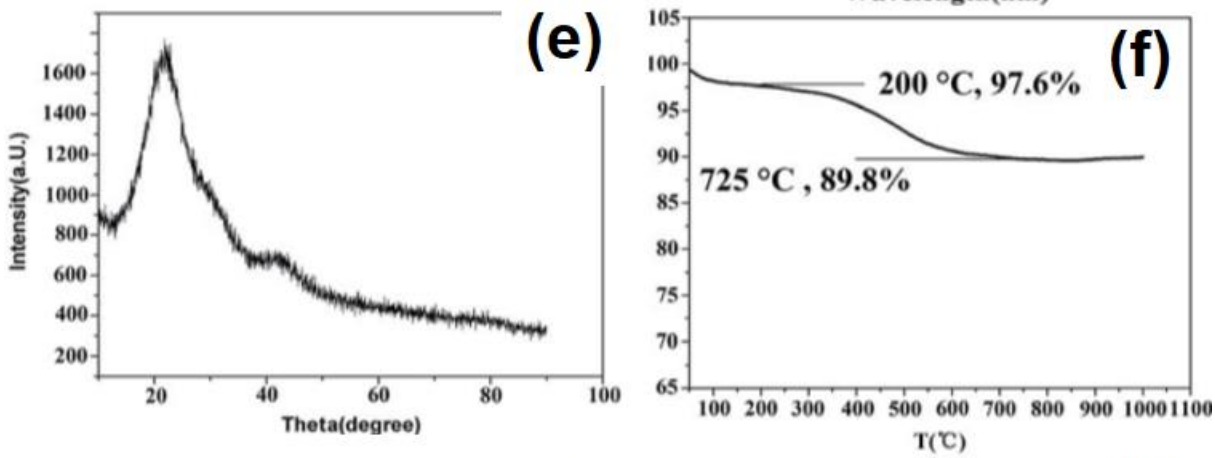
(e)
Intensity(a.u.)
Theta(degree)
(f)
200 °C, 97.6%
725 °C , 89.8%
T(℃)

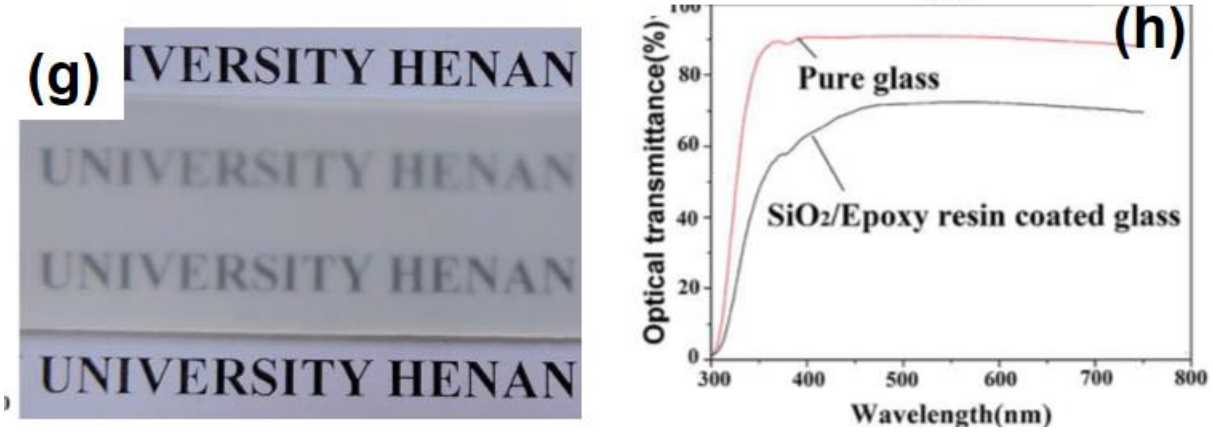
(g)
IVERSITY HENAN
UNIVERSITY HENAN
UNIVERSITY HENAN
UNIVERSITY HENAN
(h)
Optical transmittance(%)
Pure glass
SiO2/Epoxy resin coated glass
Wavelength(nm)

Figure 1-4: (a) Digital images showing the silica nanoparticles dispersion in different solvents while inset is showing the silica powder. (b) TEM of silica nanoparticles, (c) X-ray diffraction spectrum of silica nanoparticles (d) Thermal analysis of the silica nanoparticles. (e) Digital image showing the coating of silica/polyurethane on glass, (f) Difference in transmittance of glass slide before and after coating silica/polyurethane (g) Digital images showing the coating of silica/epoxy resin on glass. (h) Difference in transmittance of glass slide before and after coating silica/epoxy). Adapted from[144]. With permission from The Royal Society of Chemistry, 2017.

The coatings were applied to several substrates including glass, fabric and paper and sponge. The WCA in all cases was more than 150°. A superhydrophobic sponge was prepared, which was used for the separation of oil/water mixtures by mounting in a vacuum system (**Figure 1-5**a and b). The separation efficiency was observed to be more than 95 % in most cases as shown in **Figure 1-5**c and d. The separation efficiency was measured by calculating the difference in the volume of liquids before and after separation.

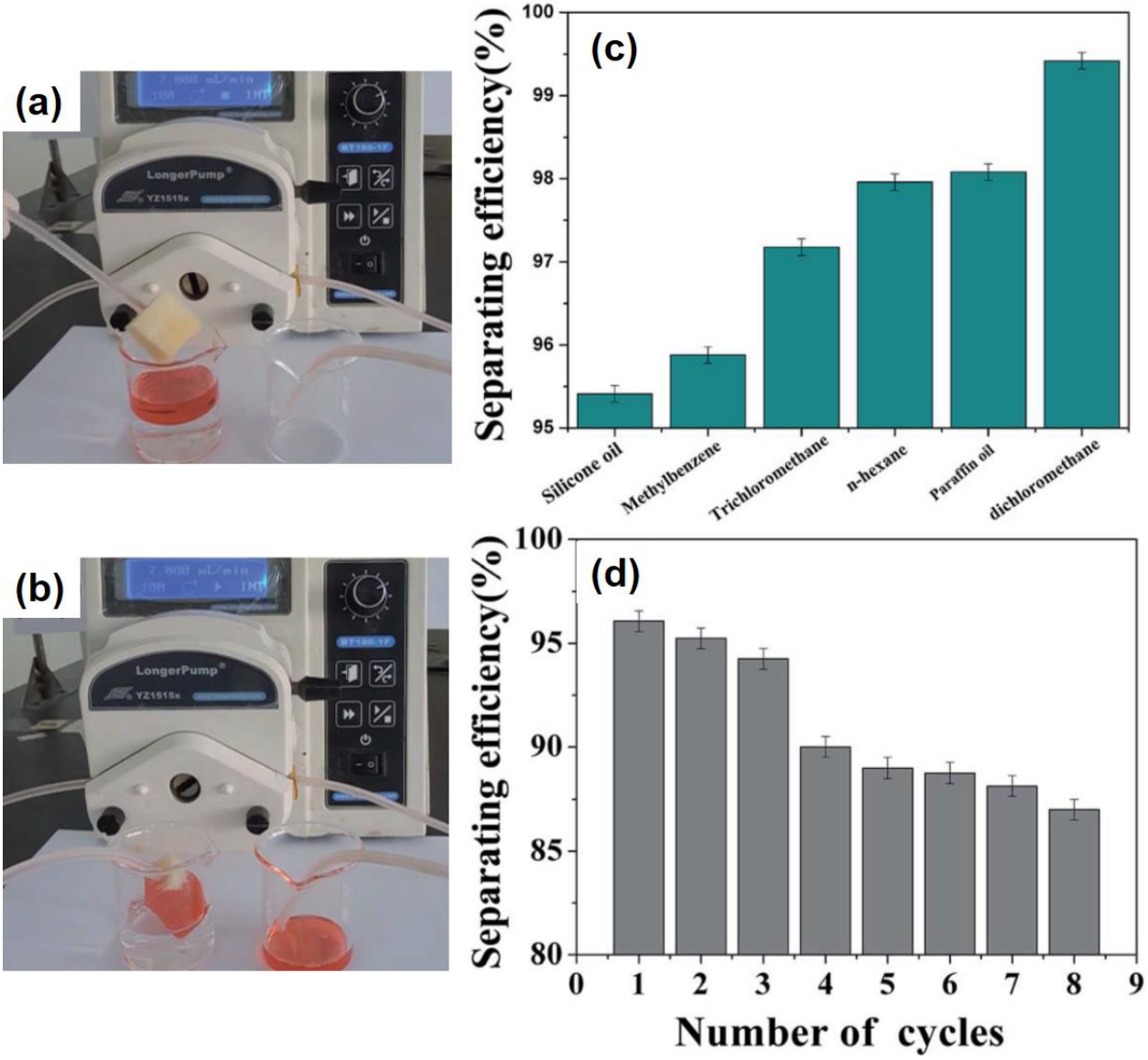

Figure 1-5: Digital images showing (a and b) the absorption of red dyed silicone oil (c) Separating efficiency and (d) recyclability of the sponge. Adapted from[144]. With permission from The Royal Society of Chemistry, 2017.

In addition to the superhydrophobic materials, silica nanoparticles have also been used to engineer underwater oleophobic separation media for oil/water separations. For example, a superhydrophilic and underwater superoleophobic fabric was prepared by employing a vapour-liquid interfacial reaction to decorate thiol-ene/silica hybrids on fabrics [138]

1.6.1.2 Nanostructured Microparticles

Nanostructured microparticles in different shapes (hollow, hierarchical) have been synthesized using sol-gel chemistry and used to separate oil water mixtures and emulsions. For example, silica particles were prepared by using polystyrene (PS) microspheres as a template [145]. Briefly, the surface of PS was made positively charged by hexadecyltrimethylammonium bromide (CTAB) so as to coat silica on it by hydrolysis of TEOS in an alkaline environment. Silica particles on micro PS particles created a hierarchical structure which was retained even after removal of PS particles via calcination as shown in **Figure 1-*6***. Hollow microspheres of silica were formed which were further modified with 1H,1H,2H,2H-perfluorodeyltriethoxysilane (PDES) to make them superhydrophobic. The PDES assembles on the surface and lowers the surface free energy thus changing the wettability of particles.

The modification of a silica surface by self-assembly of the low energy material was confirmed by XPS and FTIR spectroscopy (**Figure 1-*6***). The XPS survey spectrum indicated the presence of fluorine which suggested the modification of pristine silica by PDES. Moreover, the intensity of hydroxyl groups in FTIR was observed to decrease after modification which is another evidence of functionalization of silica as pristine silica demonstrates a very strong band in this range due to presence of hydroxyl groups on its surface.

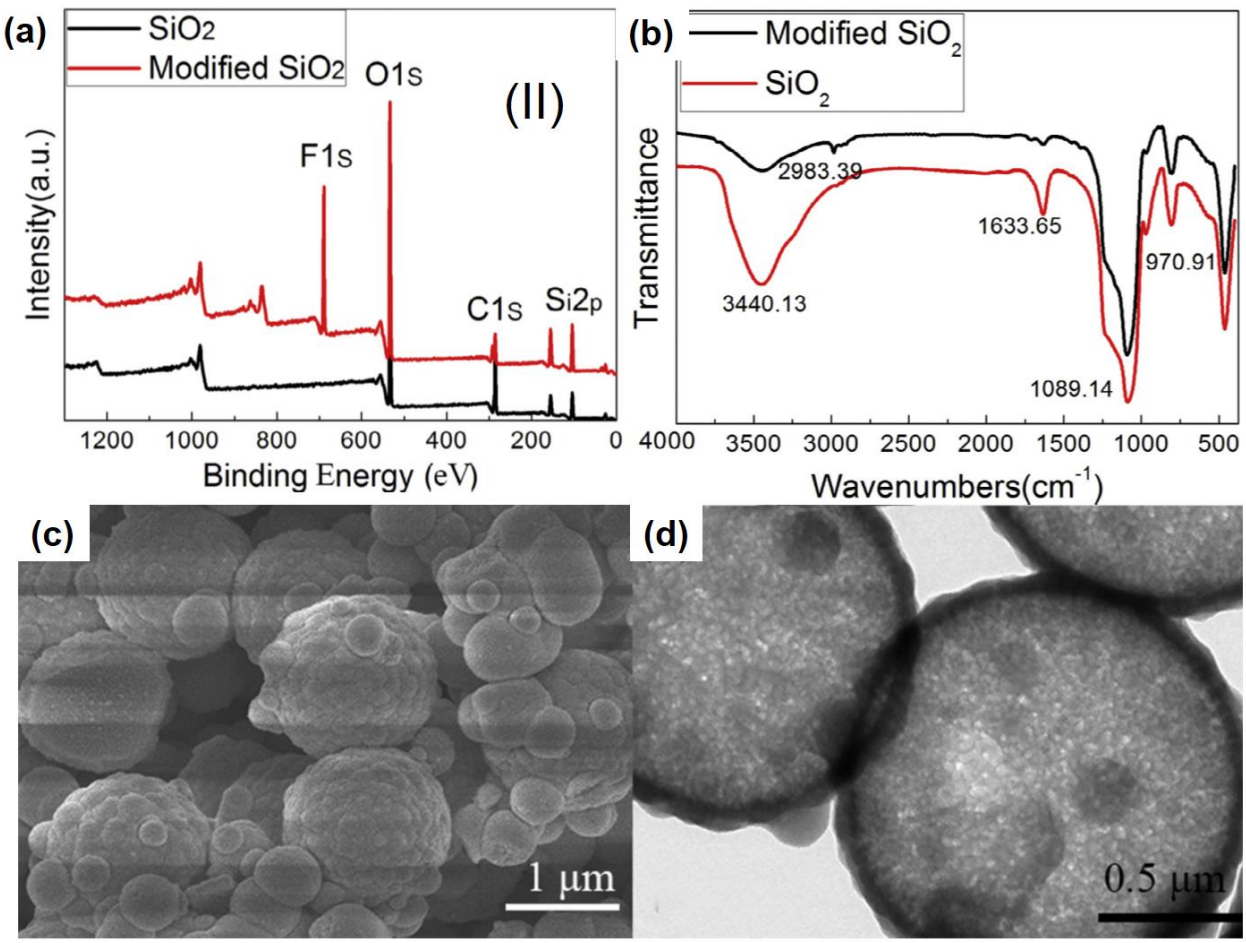

Figure 1-6: (a) XPS spectra and (b) FTIR spectra of silica before and after modification and (c) SEM and (d) TEM images of superhydrophobic Silica microspheres. Adapted from [145]. With permission from Elsevier, copyright 2017.

The superhydrophobic powder was produced to fabricate superhydrophobic surfaces on different substrates. A sponge coated with the superhydrophobic powder was used to demonstrate the separation of oil/water mixtures while the modified powder was used to separate oil/water emulsions.

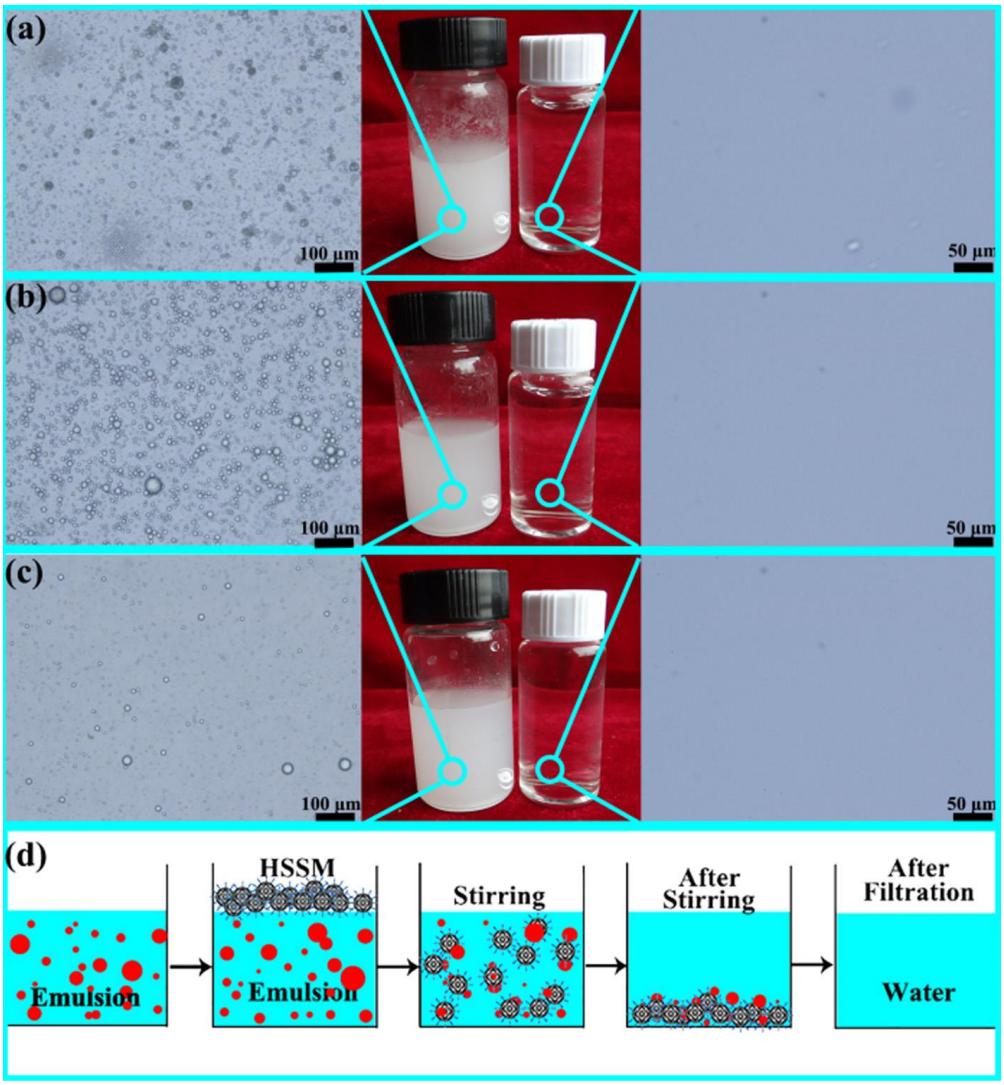

Figure 1-7: (a) Optical microscopy of lubricating oil in water emulsions stabilized by sodium dodecylbenzene sulfonate (SDS) before (left) and after separation (right) digital images of emulsion and separation product (middle) (b), Optical microscopy of diesel oil in water emulsions stabilized by SDS before (left) and after separation (right) digital images of emulsion and separation product (middle) (c), Optical microscopy of n-hexadecane in water emulsions stabilized by SDS before (left) and after separation (right) Digital images of emulsion and separation product (middle) (d), Schematic showing the separation process of oil/water emulsions (d). Adapted from [145]. With permission from Elsevier, copyright 2017.

Three different types of oil in water emulsion were prepared by using diesel oil (**Figure 1-*7***), lubricating oil (**Figure 1-*7***), and hexadecane (**Figure 1-*7***). The oils were mixed with water in volume ratio of 1:100 followed by addition of 0.1 g/L sodium dodecylbenzene sulfonate. The

stable emulsions were obtained by vigorously stirring the mixture. For the separation of emulsion, the superhydrophobic powder was introduced under vigorous stirring. The microspheres captured the oil phase from the surfactant stabilized emulsion due to the combination of superoleophilic and superhydrophobic properties. The opaque emulsion was turned transparent which indicates that the microspheres removed the oil, leaving the water behind. Optical microscopy of the emulsified solution before and after separation demonstrated that most of the oil phase was removed by the superhydrophobic microspheres.

Similarly, polystyrene (PS) was used in another study as a template to fabricate raspberry-like silica microspheres [146]. Similar to the previous study TEOS was used as a precursor of silica and the surface roughness was controlled by tuning the concentration of ammonia, water and molecular weight of polyvinylpyrrolidone. However, the PS beads were not removed and used for dual scale roughness on the surface. The surface of silica microspheres was rendered hydrophobic by modification with hexadecyltrimethoxysilane. The modified particles were used to generate superhydrophobic surfaces on various substrates including steel mesh, paper, cotton and sponge. The particles were anchored on a steel mesh to devise a platform for separation of oil/water mixtures. The superhydrophobic mesh separated mixtures of water and chloroform with a separation efficiency of more than 95% was achieved up to 5 cycles of separation.

In another study, core-shell particles were produced by deposition of silica on the surface of polyvinylidene fluoride (PVDF) microspheres with hierarchical micro and nanoscale roughness (**Figure 1-*8***) [147]. Silane modified silica nanoparticles and PVDF were mixed in an organic solvent followed by electrospraying which resulted in precipitation of PVDF and evaporation of the solvent. At an appropriate concentration of silica, i.e. 8%, a core-shell structure was synthesized

where PVDF particles acted as an organic core while silica nanoparticles formed a continuous inorganic shell (**Figure 1-*8***c-d).

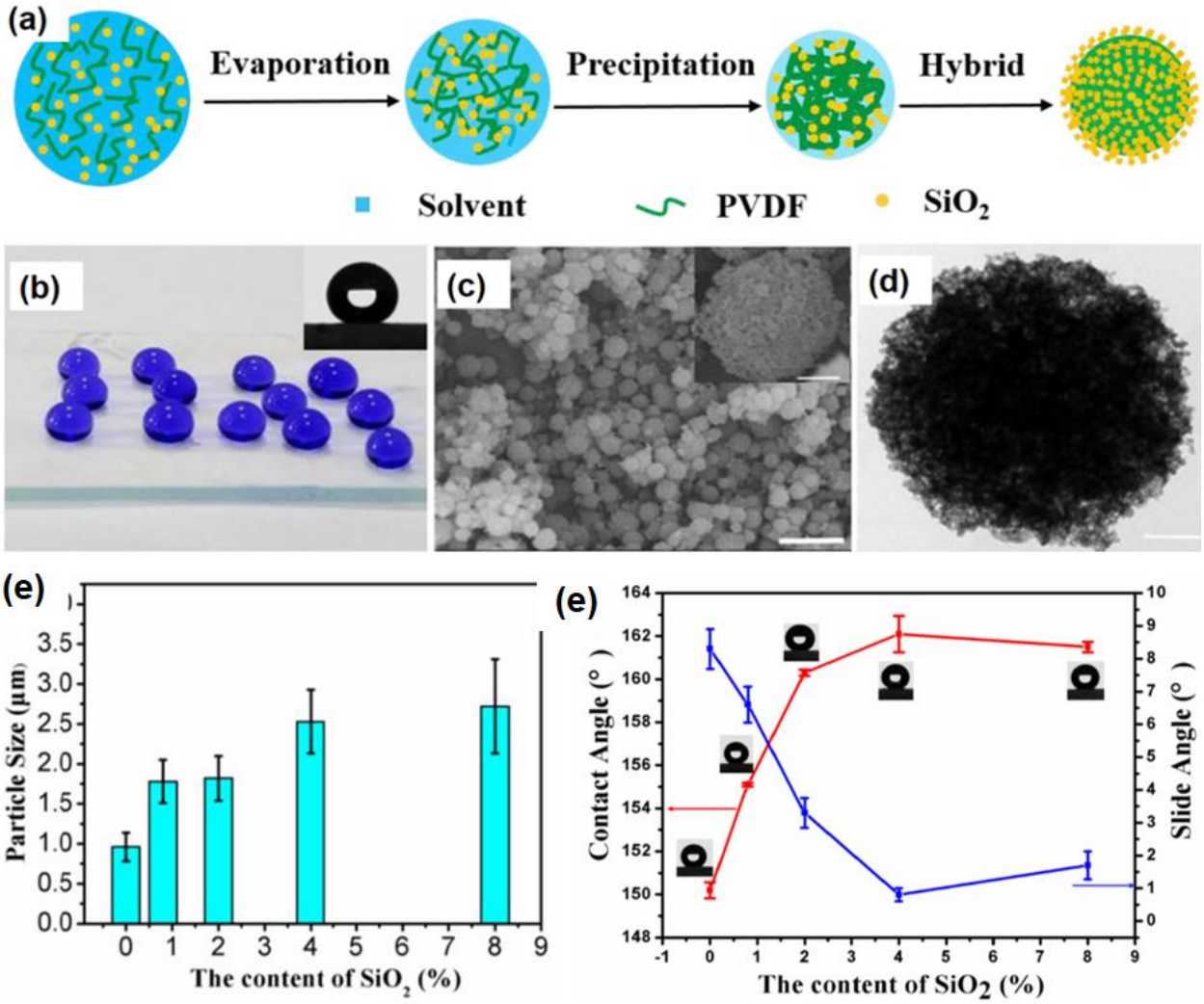

Figure 1-8: (a) Schematic showing the procedure for synthesis of hierarchical hybrid microspheres (b) Digital images showing the water droplets on the superhydrphobic surface while optical photograph in inset is representing contact angle measurement (c) SEM (c, scale bar = 10 μm and 1 μm for inset) and (d) TEM images showing the morphology of electro sprayed hybrid microspheres. (e) Plot showing the change in diameter of hybrid particles as a function of silica concentration (f) the graph showing the effect of silica content on contact angles and sliding angles of water drops Adapted from 144. With permission from Elsevier, copyright 2017.

The size of PVDF particles increased gradually with increasing amount of silica (**Figure 1-*8***) which is probably due to an increase in the thickness of shell. Surface coated silica plays an essential role in dictating the superhydrophobic properties as evidenced by the increasing contact angle with increasing amount of silica (**Figure 1-*8***). This behaviour was attributed to the increased roughness with increasing content of silica. In addition to the superhydrophobic coating by electrospraying, (**Figure 1-*8***) a free-standing membrane was formed by using the same materials; however, the membrane demonstrated low water contact angle as compared with the superhydrophobic coating.

The superhydrophobic coating was applied on filter paper to demonstrate its application in oil/water separations. The coated filter paper proved to be effective in separation of oil/water mixtures and resisted corrosive liquids (**Figure 1-*8***). However, the filter paper took 3 min to separate 100 ml of the mixture. On the other hand, a membrane formed by electrospraying PVDF and silica took only 30s to separate the same volume. It was suggested that the superior properties of the membrane were due to superoleophilic properties and the capillary tubes formed by voids between the microspheres and threads resulting in quick and continuous transportation of oil across the membrane during the separation process. The increased separation time in the case of modified filter paper was attributed to the poor transportation of oil through filter paper structure. The membrane separated an oil/water mixture with flux 2050 L m^{-2} h^{-1} and separation efficiency of 97.5% up to 20 cycles (**Figure 1-*8***).

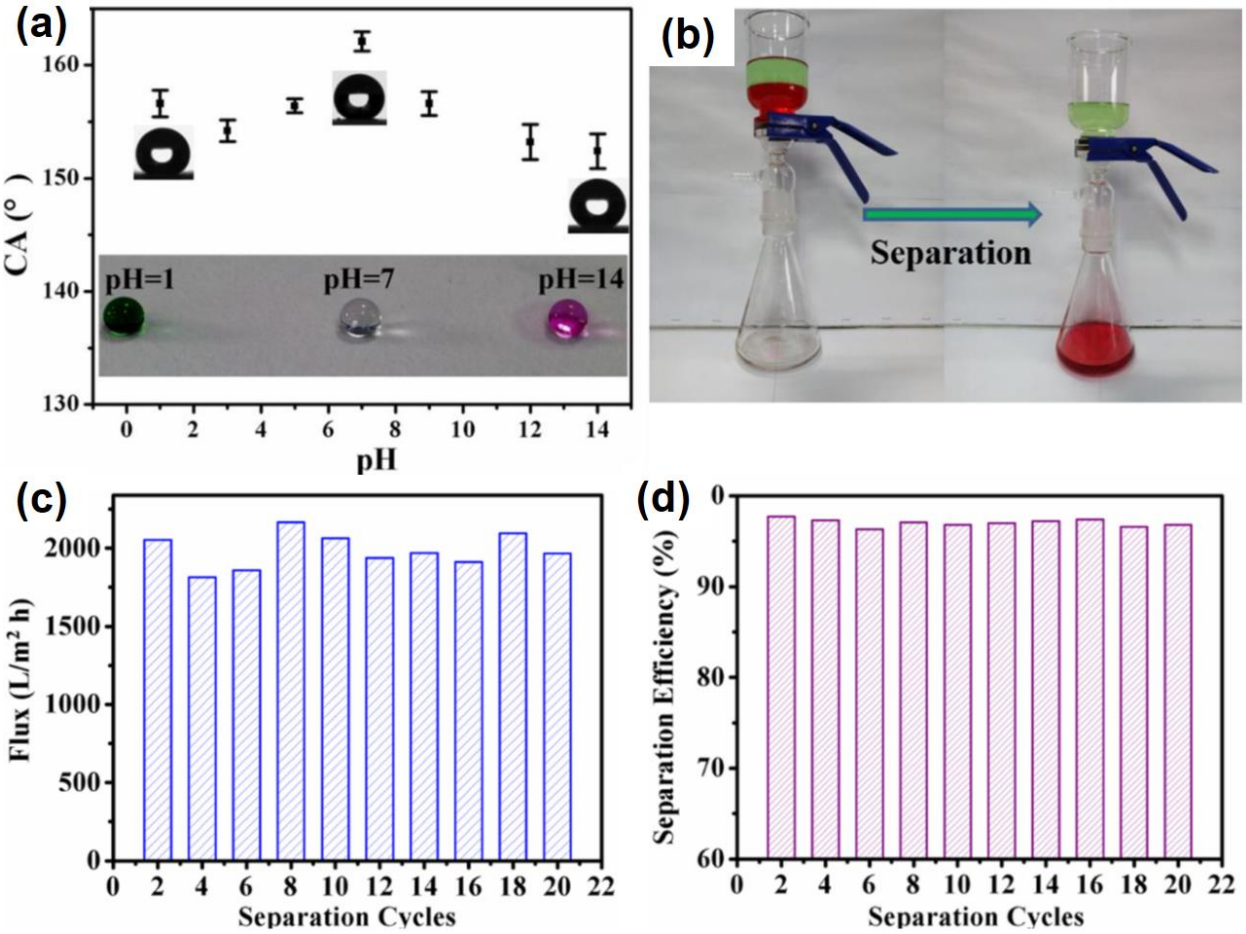

Figure 1-9: Graph showing the variation of water contact angles at different pH while the shape of water droplets can be observed in the inset (a) Separation of dichloromethane and water under harsh conditions (b) the flux (c) and efficiency (d) for the oil-water separation with different cycles by using the PVDF/Silica membrane. Adapted from [147]. With permission from Elsevier, copyright 2017.

1.6.1.3 Nanostructured Scaffolds

Nanostrucutred scaffolds of silica have been fabricated and used to adsorb and remove oil from oil/water mixtures. In comparison to particles, they are interconnected networks and offer multiple advantages such as recyclability, easy handling and good absorption.

A solvothermal process has been used for fabrication of nanoporous hybrid materials from divinylbenzene and silica for the separation of different types of emulsions [148]. The fabrication procedure involves the reaction of fumed silica (0.2–0.3 μm) with DVB monomer in the presence

of a radical initiator (AIBN) (Fig. 1-8a). The interconnected porous material that results from this reaction was isolated by evaporating the ethyl acetate.

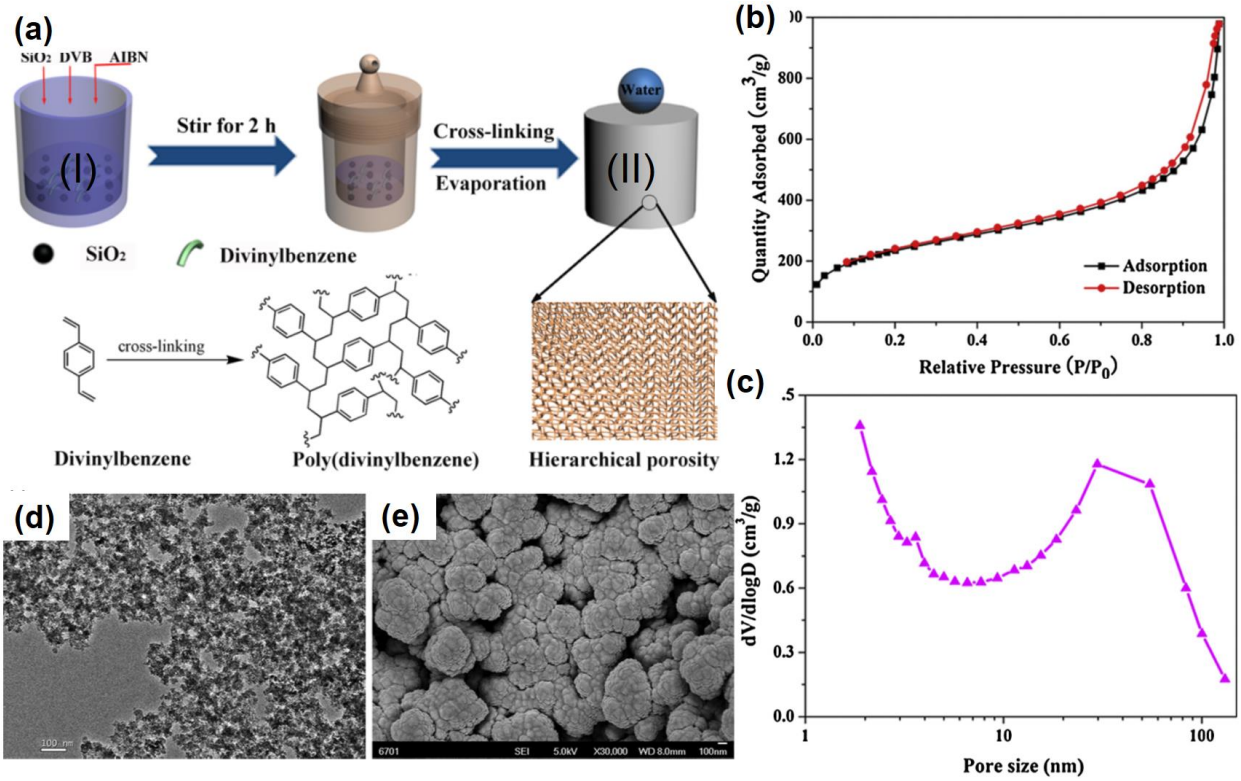

Figure 1-10: (a) Schematic showing the fabrication process of hybrid material (b) Gas adsorption isotherms and (c) pore size distribution confirm the nanoporous structure of hybrid material, (d) TEM images (e) and SEM images of hybrid material. Adapted from [148]. With permission from Elsevier, copyright 2017.

Characterisation of the surface by BET adsorption isotherms and SEM revealed mesopores with diameters from 10 nm to 100 nm (**Figure 1-*9***). SEM and TEM revealed an overall hierarchical structure constituted by different types of nanoparticles (**Figure 1-*9***). This unique hierarchical structure provides air pockets during interaction with liquid droplets and renders the material superhydrophobic.

Indeed, the prepared material demonstrated a water contact angle of 160° and complete repellence of water. Due to excellent superhydrophobic properties and selective wetting towards oil, the

material immediately adsorbed the hexadecane from water/hexadecane mixture. Different types of common organic pollutants were separated, and the respective absorbance capacity was reported. It was found that the absorbance of the material is as high as 21.9 g/g.

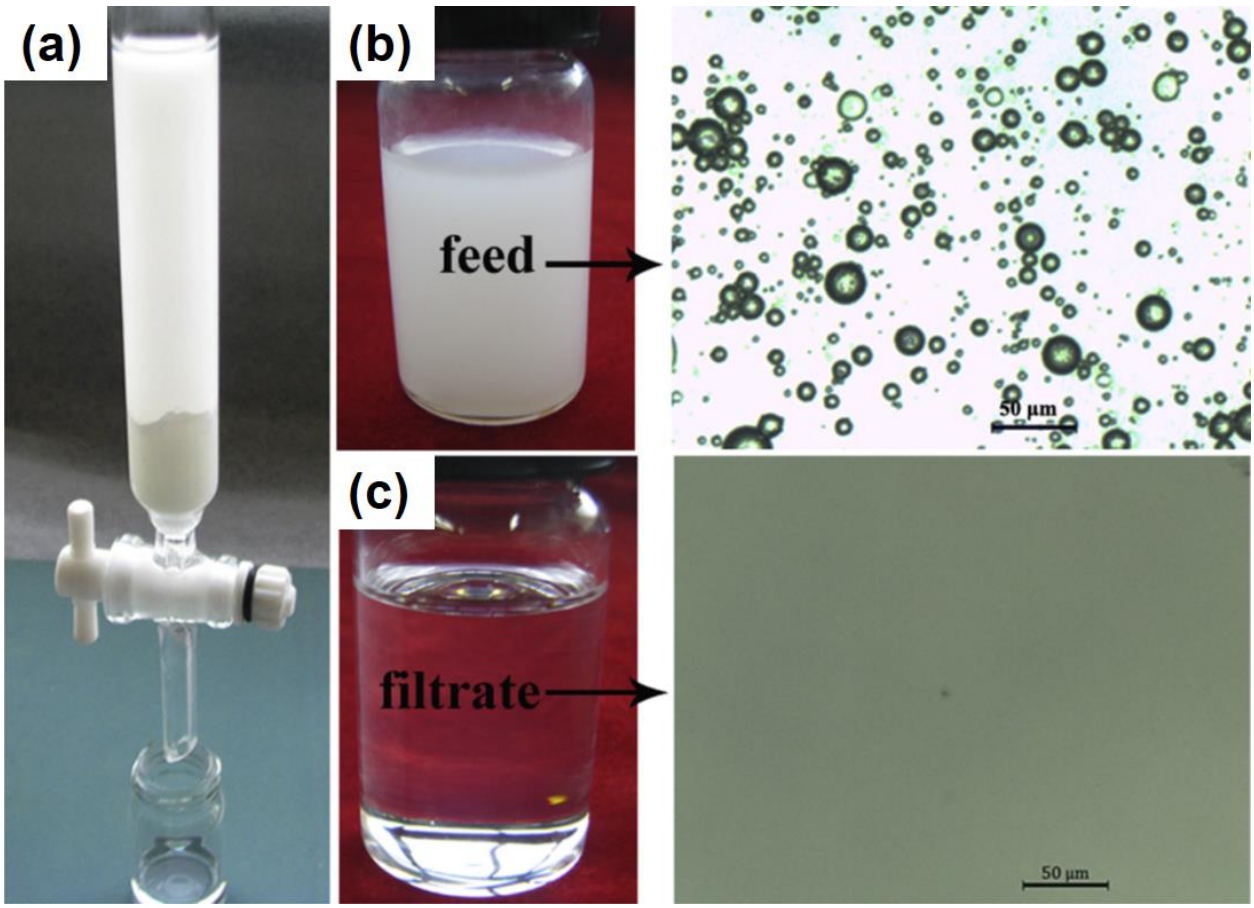

Figure 1-11: (a) Digital images showing the setup for separation of water in oil emulsion (b), optical microscope DLS results of water in toluene emulsion before (c) after (c) and separation. Adapted from [148]. With permission from Elsevier, copyright 2017.

The material was also tested to separate surfactant stabilized oil in water or water in oil emulsions (**Figure 1-*9***). These emulsions were prepared by mixing the fluids in 1:100 ratios, stabilizing them with the commercially available nonionic surfactants Tween 80 or Span 80 with stirring for 15 h. In case of a water in toluene emulsion, the toluene easily passed through the porous channels while

water was completely rejected due to the superhydrophobic properties of the membrane. It was further confirmed from optical microscopy that de-emulsification took place, as effectively indicated by the significant difference in the phase-contrast observed before and after separation (**Figure 1-*11***). Moreover, DLS measurements also verified the substantial change in droplet sizes before and after separation of emulsion. Gas chromatography confirmed that the separated toluene was 99.73% pure which proved the high separation efficiency of the process.

1.6.2 Carbon

Elemental carbon is an important element which exists in both crystalline (diamond and graphite) and non-crystalline bulk allotropes (coal, charcoal and carbon black). It contains six electrons with four in its valence electrons with three different hybridizations sp^3, sp^2, and sp^1. The $1s^2$, $2s^2$, $2p^2$ electronic configuration of carbon allows it to have several types of structures with unique properties. For example, diamond is the hardest material as every carbon atom is covalently bonded to four other carbon atoms in tetrahedral fashion. At the same time, graphite is a soft material as it consists of 2D sheets of carbon atoms joined by Van der Waals forces. The weak bonding (ca. 2kJ mol^{-1}) between the sheets allows sliding, which makes graphite a soft material. The carbon atoms in graphene sheets are bonded via covalent bonds. The nanoscale allotropes of carbon including graphene, carbon nanotubes, fullerenes and nanodiamonds offer a wide range of properties such as high thermal and electrical conductivity, corrosion resistance, optical, mechanical and electrochemical properties [149]. The use of carbon-based nanomaterials has been extended to structural materials, electronic, sensing, biomedical, energy storage, catalysis, cardiac scaffolds, desalination and water purification [149–152]. Different forms of carbon have been explored to prepare materials for separation of oil/water mixtures and emulsions. Carbon foam fabricated by using polyurethane foam as a template and lignin phenol formaldehyde as a carbon source is

just one example of carbon-based materials for oil/water separation [153]. Several other forms of carbon have also been used for this purpose and are discussed in detail in the following sections.

1.6.2.1 Graphene

Graphene is a single layer formed by hexagonally arranged sp^2 hybridized carbon atoms. Graphene exhibits interesting properties such as very high electron mobility (250,000 cm^2/Vs at room temperature), high Young's modulus (1 TPa) and thermal conductivity of 5000 $W\ m^{-1}\ K^{-1}$. [154,155]. Graphene has been utilized to produce materials for oil/water separation [156–158]. It has strong tendency towards absorption of oils, and this property was employed to create a superhydrophobic foam by dip coating a polyurethane sponge in suspensions of graphene and cellulose nanowhiskers. The superhydrophobic foam displayed effective separation of several organic solvents and maintained its superhydrophobicity after 50 cycles of separations [159]. In another example, graphene was introduced in the framework of polyurethane sponge by in situ polymerization in the presence of *N*-methyl pyrrolidone [160]. The resulting sponge showed a water contact angle of 151.8° ± 0.5° and an oil contact angle of 0.5° and was subsequently used for the separation of various types of oil/water mixtures and emulsions.

Magnetic graphene oxide sheets were synthesized for the separation of oil/water emulsion emulsions [161]. Magnetic ferrite particles were prepared from iron carbonyls by oxidation/decomposition method followed by a thin coating of silica to enhance the chemical stability and to provide a medium for functionalization with silane coupling agent (3-APTES). The amine groups on the surface were then utilized for the reaction with graphene oxide (GO) sheets prepared by Hummer's method. Separation experiments were performed using a crude oil in water emulsion which was stable up to 12 h. A small quantity of M-GO was introduced in the mixture which immediately changed its color, indicating the emulsion breaking.

Recently, reduced graphene oxide-based composites with hierarchical structure have been fabricated by embedding metal-organic framework nanoparticles in rGO sheets [162]. The material possesses a combination of superhydrophobic and superoleophilic properties allowing it to capture oil from an oil/water mixture selectively. The composite was fabricated by immobilizing zeolitic imidazolate frameworks (ZIF-8) on rGO sheets at room temperature. The microdroplets of suspension of the composite were produced by an ultrasonic spray nozzle. The droplets were mixed with silicon oil (continuous stirring at 165ºC) to allow the wrinkling and self-assembly of composite microspheres. **Figure 1-*12*** shows the schematic of the synthesis process.

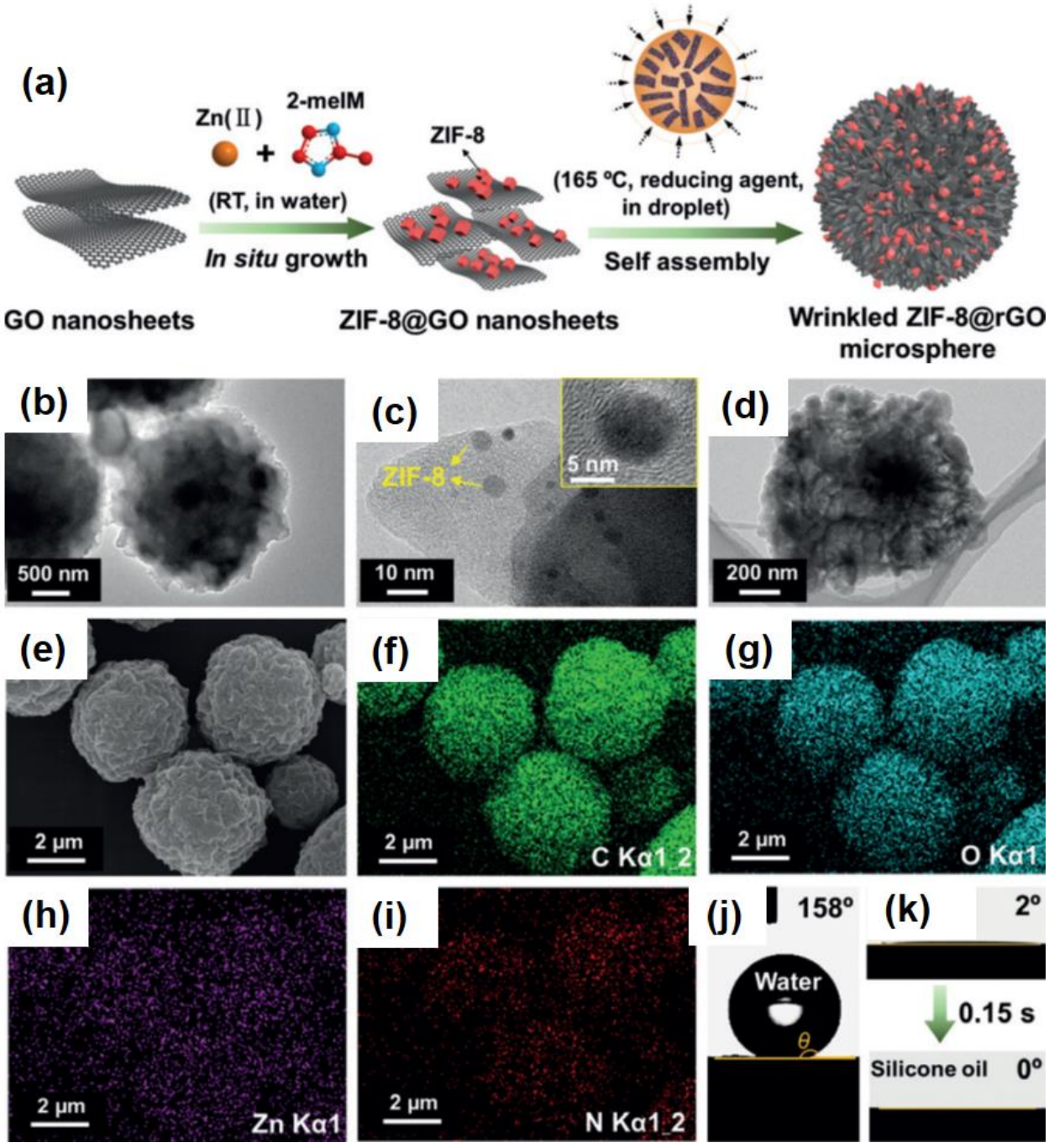

Figure 1-12: (a) Schematic showing the formation process of ZIF-8@rGO spheres, (b-d) TEM images showing the structure of the wrinkled ZIF-8@rGO (e) SEM and (f-i) EDS of ZIF-8@rGO (j) contact angle of water (k) and silicone oil on ZIF-8@rGO. [162]

Figure 1-*12* (b-d) shows the TEM images of ZIF-8@rGO microparticles. These are composed of ZIF-8 nanoparticles uniformly distributed on wrinkled rGO sheets. The spatial uniformity and dispersion of ZIF-8 can be observed from the EDX **Figure 1-*12***(e-i). The combination of nanoparticles and sheet structure creates mesoscale roughness, which helps achieve a very high contact angle of 158º along with oleophilic properties **Figure 1-*12***(j-k). The produced particles were coated on a PU foam by dip coating, and the resulting composite superhydrophobic foam was used for the separation of organic solvents from water

1.6.2.2 Carbon nanotubes/fibers

Carbon nanotubes (CNTs) can be imagined as a cylinder in which individual carbon atoms are sp^2 bonded to each other. There are different types of CNTs, including the single wall, double wall or multiwall depending upon the number of rolled graphene sheets. They have very high surface area and can be easily functionalized both covalently and non-covalently to host new properties for specific applications. CNTs can be chemically modified by carboxylation, amidation, acrylation and PEGylation and esterification. Another interesting advantage of CNT is their dual-scale roughness due to the cylindrical structures. This feature is significant in the fabrication of superhydrophobic materials [163,164]. A composite membrane for the separation of oil/water emulsion was fabricated using CNTs and polysulfone as support. A thin layer of Pebax was coated, and different concentrations of functionalized CNTs (FCNTs) were used to study the effect on morphology and separation characteristic of the membrane [165]. It was observed that increasing the concentration of FCNTs improved the mechanical and thermal properties and increased the hydrophilicity of the membrane. Silanized CNTs have been used to fabricate ethyl cellulose-based composite sponges. The sponges were coated by nanoparticles of SiO_2 which were further modified with hexadecyltrimethoxysilane to obtain a superhydrophobic and

superoleophilic sponge. The resulting sponge was then used to separate oil/water mixtures and emulsions [166]. In another study, a superhydrophobic and superoleophilic membrane was prepared by assembling carbon nanofibers and single-walled carbon nanotubes on an etched stainless steel mesh. The composite membrane was then modified with polydimethylsiloxane and used to separate water from an emulsion [167].

Superhydrophobic surfaces have been fabricated via two-step fabrication of carbon nanofibers by plasma sputtering followed by CVD at 300 °C to achieve superhydrophobic properties[14]. This represents a route which does not involve complicated processing and avoids toxic chemicals. Initially, the copper was deposited on different substrates as a catalyst by plasma sputtering. Later, the samples were placed in a CVD chamber for carbon deposition. The flow of hydrogen was maintained until the temperature reached 300 °C and then acetylene was introduced for 30 min. Finally, the chamber was cooled to room temperature under nitrogen.

Digital images show the wetting behaviour of glass and fabric before and after deposition of CNF (**Figure 1-*13***). It can be observed that the water drop has formed a bead shape on superhdyrophobic materials compared to complete absorption or very low contact angle in case of pristine materials.

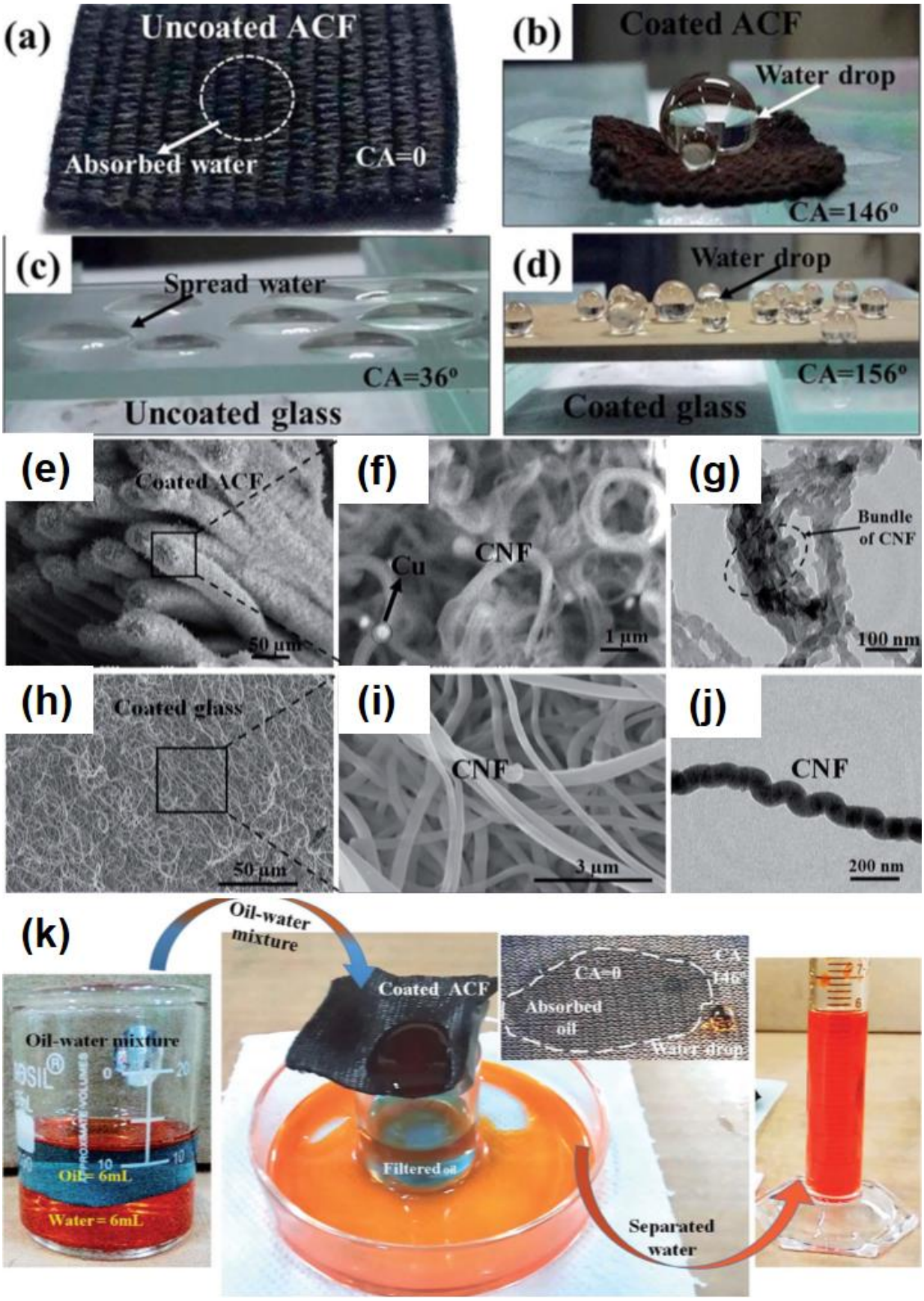
(a)
Uncoated ACF
Absorbed water
CA=0
(b)
Coated ACF
Water drop
CA=146°
(c)
Spread water
CA=36°
Uncoated glass
(d)
Water drop
CA=156°
Coated glass
(e)
Coated ACF
50 μm
(f)
Cu
CNF
1 μm
(g)
Bundle of CNF
100 nm
(h)
Coated glass
50 μm
(i)
CNF
3 μm
(j)
CNF
200 nm
(k)
Oil-water mixture
Oil= 6mL
Water = 6mL
Oil-water mixture
Coated ACF
CA=0
CA 146°
Absorbed oil
Water drop
Filtered oil
Separated water

Figure 1-13: (a) Digital images showing pristine ACF (b) and modified ACF (c) pristine glass (d) and modified glass (e-j) SEM and TEM images of images of modified ACF and glass. (k) Separation of kerosene and water mixture by using modified ACF. With permission from The Royal Society of Chemistry, copyright 2017[14]

SEM and TEM results reveal the presence of entangled CNF structure with individual fiber with a diameter of 30 nm, whereas the Cu particles have been observed as bright spots (**Figure 1-*13***). Similarly, CNF structure on glass can also be seen with an individual fiber of diameter of <100 nm (**Figure 1-*13***). The porous structure formed by CNF is supposed to entrap more air, thus increasing surface superhydrophobicity [14].

The pristine fabric shows the water contact angle of 0°; however, the deposition of CNF increased the water contact angle to 146°. Similarly, CNF-coated the glass also demonstrated an increase in water contact angle from 36° to 156°. Surface energy measurements showed that the coated glass slide and fabric (46.56 mJm^{-2} and 55.91 mJm^{-2}, respectively) hold low surface energy as compared to the uncoated glass and fabric. XPS showed that the coated glass slide and fabric contained fewer carbonyl groups than the uncoated samples. The coated ACF has a combination of superhydrophobic and superoleophilic behaviour which means that oil can easily pass through it while water would be rejected entirely (**Figure 1-*13*** k). The property was used to separate different types of oil/water mixtures with a separation efficiency of 99% up to 50 cycles [14].

1.6.2.3 Carbon soot

Carbon nanoparticles (soot) are produced from incomplete combustion of organic molecules. A straightforward source of carbon nanoparticles is candles which are primarily made of paraffin wax. Incomplete combustion of candle wax results in the production of hydrophobic carbon nanoparticles. Despite some limitations in terms of stability and mechanical properties, it is an inexpensive and simple process to fabricate superhydrophobic materials. Candle soot has been used to produce a superhydrophobic and superamphiphobic surfaces whilst using

polydimethylsiloxane (PDMS) and hexane as base [168]. Carbon nanoparticles (CNPs) were embedded in PDMS, which was cured by the heat of the flame. This resulted in chemically and mechanically stable superhydrophobic surface.

Similarly, a robust superhydrophobic coating was produced by depositing a composite coating of camphor soot and PDMS [169]. In another study, CNPs dispersed in acetone were prepared by using a candle [170]. The dispersion was then used to prepare superhydrophobic coatings by the spray process. The coatings produced by this method were stable up to 400°C and demonstrated better water jet and drop impact resistance than the coatings prepared by direct deposition of soot from candle flame.

A one-step method was proposed to fabricate superhydrophobic and superoelophilic materials [171]. The proposed fabrication method does not require any chemicals, and short smoking for 5 min was enough to render the materials superhydrophobic. A folded copper foam was exposed to candle flame under suitable conditions to collect the carbon soot. The deposition of carbon soot created hierarchical structures with micro/nanoscale features absent in the bare copper foam, as shown in the SEM images (**Figure 1-*14*** a-d).

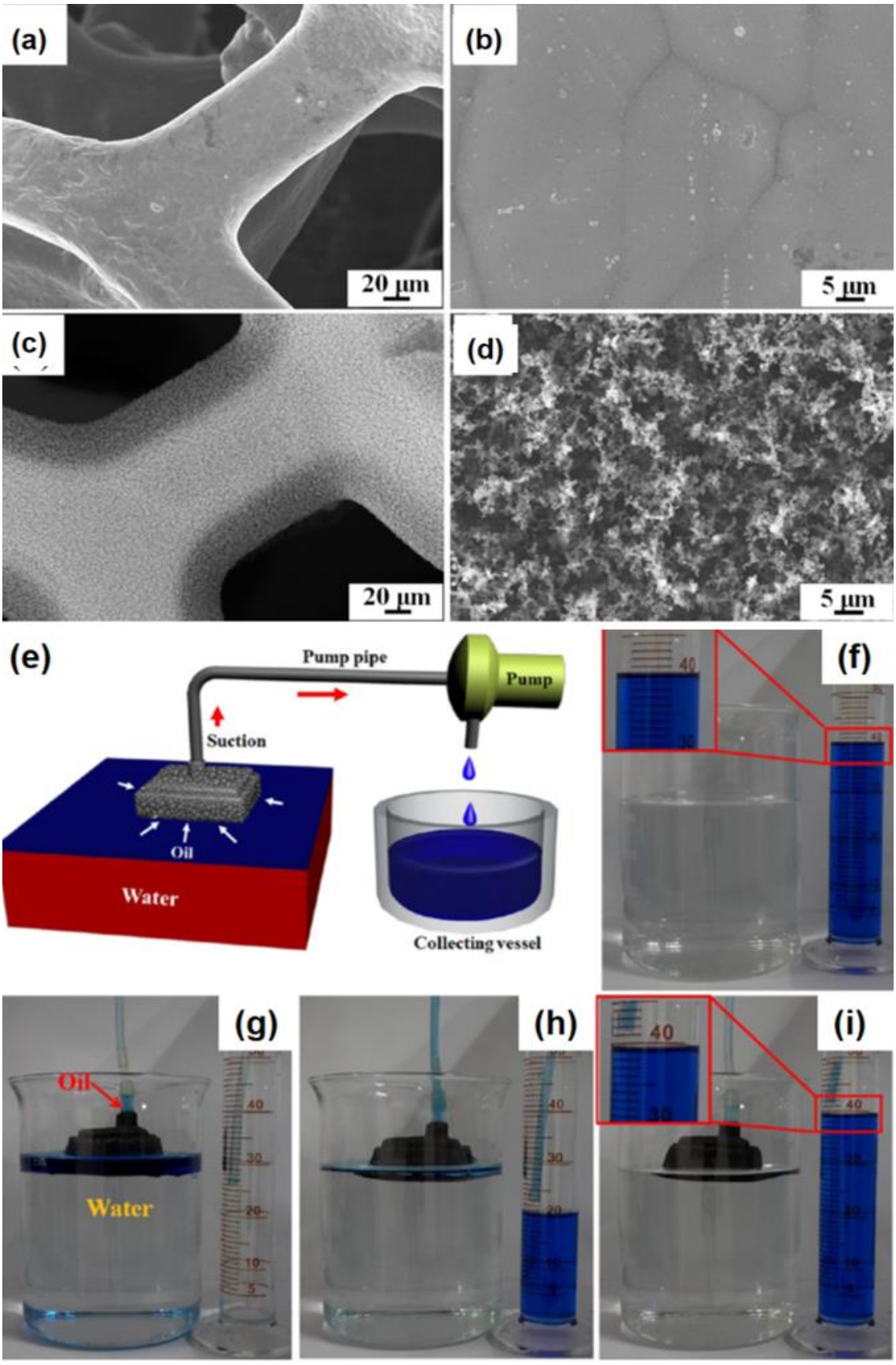
(a)
20 μm
(b)
5 μm
(c)
20 μm
(d)
5 μm
(e)
Pump pipe
Pump
Suction
Oil
Water
Collecting vessel
(f)
(g)
Oil
Water
(h)
(i)

Figure 1-14: (a-b) SEM images of copper foam before and (c-d) after coating with candle soot, (e) Schematic showing the separation apparatus (f-i) Digital images showing the separation of oil/water mixtures by using superhydrophobic copper foam. Adapted from [171]. With permission from American Chemical Society, copyright 2017.

SEM, XPS and EDS results confirmed the presence of 20 µm thick layer of carbon soot which wrapped the porous structure of the copper foam. The hierarchical structure and low surface energy of carbon soot realized the superhydrophobic coating without any chemical modification. Contrary to the superhydrophilic behaviour of pristine copper foam, it demonstrated a water contact angle of 155° after coating with carbon soot. Moreover, the superhydrophobic copper foam demonstrated superoleophilic behaviour as the oil droplet completely spread over it. The copper foam was used for the gravity-driven separation of oil/water mixture containing 15 ml red-dyed water and 30 ml blue-dyed toluene. The oil could easily pass through the foam while water was retained in the foam resulting in the complete separation of oil/water mixture [170].

In addition to the gravity separation, the continuous separation was performed from a device containing a peristaltic pump, as shown in **Figure 1-*14***e. The device efficiently separated the oil from an oil/water mixture containing 450 ml of water and 40 ml of toluene dyed with methylene blue **Figure 1-*14*** f-i. The device separated the mixture with a recovery rate of 98.8%, which was based on the comparison of gathered oil and the original amount in the mixture [170].

Following this approach, five different oil/water mixture of toluene, n-hexane, silicone oil, isobutanol, and dichloromethane were separated and their recycled rates (volume ratio of the collected oil and original amount of oil in mixture) were calculated. Moreover, the device demonstrated a recovery rate of more than 95% up to six cycles ensuring the reproducibility and durability.

1.6.2.4 Carbon gels

Aerogels are known for their porous structure and very low density. A typical synthesis approach for aerogels is to prepare wet gel by a sol-gel process followed by replacing the liquid phase with gas. The aerogels have high porosity which gives them distinct properties, including high surface area and very low thermal conductivity. As the porous structure of carbon aerogels are assembled from sp^2 carbon nanoparticles, they possess unique properties such as high thermal, mechanical and chemical stability, electrical conductivity, large surface area and very low density. These fascinating characteristics persuaded the researchers to find the application of carbon aerogels in many fields such as sensor, sorbents, energy, filtration and sensors [172]. Carbon-based aerogels can be divided into five different types based upon the allotrope of carbon used in the production of aerogel [172]. For example, graphene oxide has been used to prepare graphene-based aerogels [173]. Graphene oxide can be suspended in water and contains oxygen functionalities at basal planes and edges, which helps in covalent reaction with different compounds. This ability allows the preparations of new materials with tunable properties for specific applications. Similarly, CNTs have been used to prepare robust and conductive aerogels for a range of energy and environment applications[174]. Other examples of carbon aerogels are amorphous carbon, graphite and diamond aerogels [172,175,176].

Different types of carbon-based aerogels and their composites have been conceived for oil/water separation. For example, a PU foam reinforced porous graphene aerogel was fabricated by freeze casting to collect oil from an oil/water mixture [177]. The produced aerogel demonstrated superior mechanical and superhydrophobic properties making it applicable for the separation of oil/water mixtures for several cycles. In another study, light weight and electrically conductive carbon aerogels were fabricated from the oxidation-oven drying-carbonization method using waste paper as a source material [178]. The aerogel produced by this method is suitable for separation of oil/water

mixtures due to the combination of superhydrophobic/ superoleophilic properties, high absorption (33–70 g g^{-1}) and high compressibility. In a different study, popcorn was used as a carbon precursor to prepare superhydrophobic and magnetic carbon aerogel [179]. The popcorn was treated with the iron nitrate before carbonization to yield magnetic popcorn carbon which was further modified with octyltrichlorosilane to produce "superhydrophobic aerogels". The aerogel exhibits selective absorption towards oils and can be used to separate many types of oil/water mixtures up to several cycles. Similarly, pressure-sensitive carbon aerogels were fabricated from pyrolysis of cellulose aerogels which were composed of microfibers of poplar catkin (PC) [180]. For this, the PC fibers were activated by sodium chlorite followed by carbonization at 1000 °C under nitrogen atmosphere.

The PSC aerogels have a water contact angle of 150.3°, making them suitable candidates for absorbing the oil from oil/water mixtures (**Figure 1-*15***a). The PSC aerogel can separate oil/water mixtures under gravity, as shown in **Figure 1-*15***b. The oil was passed through the aerogel while water was retained on the surface. The aerogel displayed an absorbency of 81 to 161 g g^{-1} for a range of oils and organic solvents, as shown in **Figure 1-*15***c. Moreover, the aerogel can be re-used after drying in an oven and displayed absorbance 80 g g^{-1} when used for ten cycles. It was demonstrated that the oil absorbed aerogel could also be treated via combustion. The aerogel maintained its skeleton after complete combustion of oil in 45 s.

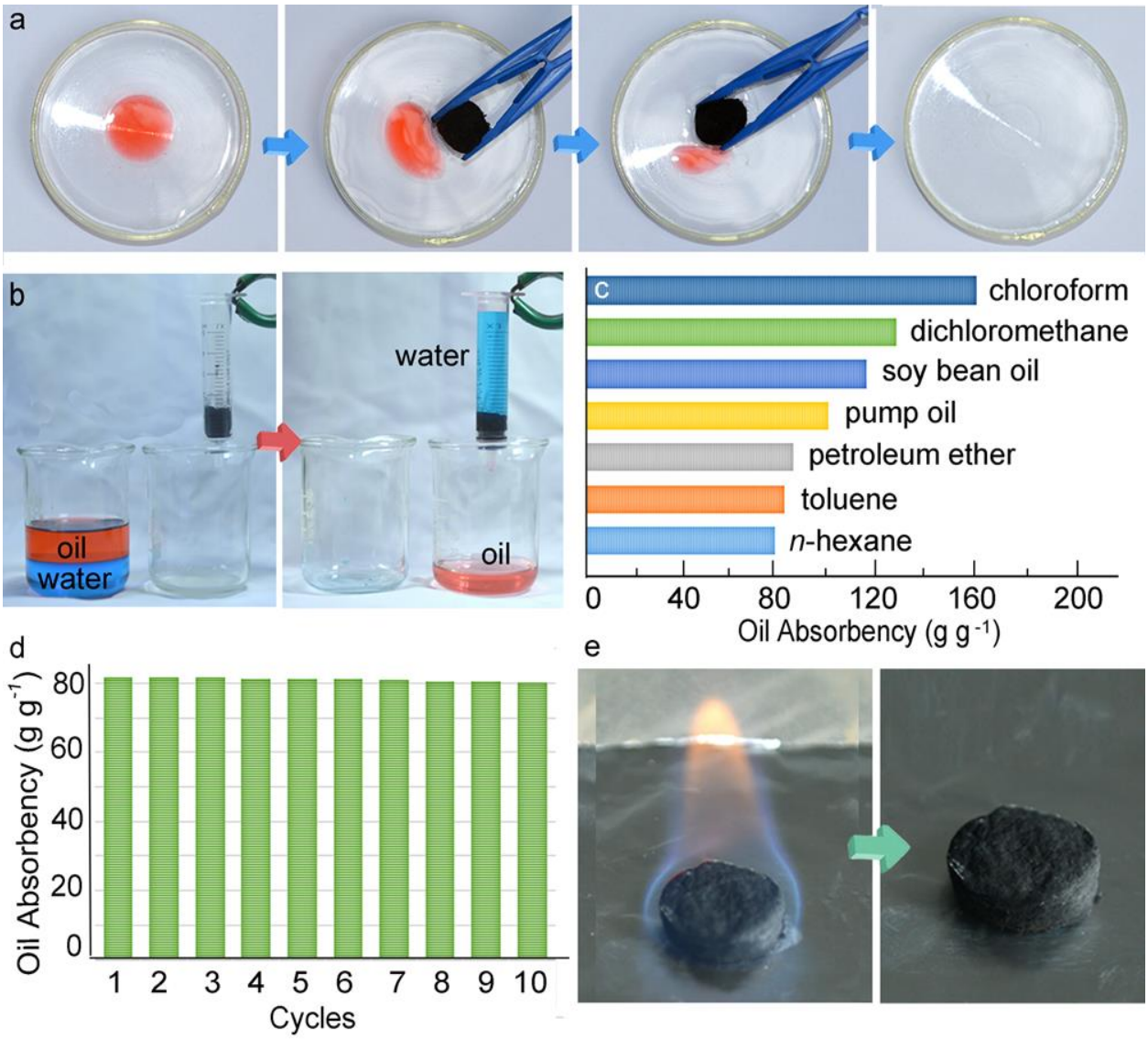

Figure 1-15: Images showing the absorption of oil (a) separation process (b) absorption capacity (c) cycles (d) and combustion of oil in PSC gel. Adapted from [180]. With permission from American Chemical Society, copyright 2017.

1.6.3 Iron Oxide

Iron oxides naturally exist in many forms; however, magnetite, (Fe_3O_4), maghemite (γ-Fe_2O_3) and hematite (α-Fe_2O_3) are technologically the most important types. These oxides have found applications in many fields due to their magnetic properties and biocompatibility. Magnetite (Fe_3O_4) and maghemite (γ- Fe_2O_3) have been explored extensively for biomedical applications including drug delivery, thermal therapy, magnetic hyperthermia and magnetic resonance imaging

[181–184] while hematite (α- Fe_2O_3) has been used in gas sensors, pigments and catalysts as it is an n-type semiconductor, have low cost and shows resistance against corrosion [185].

Inspired by its magnetic properties, Fe_3O_4 has been used in various studies alone or with other materials for separation of oil/water mixtures and emulsions [186–189]. For example, Fe_3O_4 were deposited on coco peat powder with the aid of polydopamine followed by modification with octadecylamine. The resulting product was magnetic and highly hydrophobic 135º ± 3º. These properties make it suitable for sorption of oil from an oil/water mixture [190]. Similarly, Fe_3O_4 was used to prepare magnetic and superhydrophobic polyurethane sponge [191]. The sponge was coated with straw soot and Fe_3O_4 nanoparticles via an immersion method. The sponge was later modified with PDMS to improve the water-repellant character of the sponge. The sponge exhibited water contact angle 154° and oil absorption 30 times its weight. Moreover, the sponge is recyclable up to 30 times and suitable for magnetic separation. In some other studies, Fe_3O_4 nanoparticles have been used in combination with other materials such as zinc oxide, stearic acid [192], silane [193,194], silica and fluoropolymer [195] to modify polyurethane sponge for oil/water separation.

Recently, Fe_2O_3 nanoparticles prepared by a co-precipitation method were coated with silica and 3-aminopropyltriethoxysilane (APTES) followed by grafting with quaternized chitosan (QC) [196]. The prepared material was then characterized for oil/water separation with respect to pH, reusability and as a function of dosage.

To study the oil/water separation ability of prepared materials, a 0.2 wt.% emulsion of diesel in water was made via sonication for 5 min. A known amount of nanoparticles was added, followed by manual shaking and separation of nanoparticles by applying a magnetic field. The nanoparticles were then washed with ethanol three times to remove the oil and reused for the separation experiments. The separation experiments were performed under different pH values and it was

found that QC coated nanoparticles show exceptional performance. The transmittance of water increased with increasing dosage of QC coated nanoparticles. The equilibrium value of 98% was achieved when the dosage was increased to 34 mh/L under both acidic and neutral condition. However, the separation efficiency was decreased under alkaline conditions, and 98% transmittance was achieved. It was discussed that negatively charged oil droplets were attracted towards positively charged QC coated nanoparticles via electrostatic attraction.

1.6.4 Titanium Oxide

Titania naturally exists as anatase, rutile and brookite. It is a n-type semiconductor (3.02 eV) and has very high refractive index 2.609 (rutile). When exposed to UV light, it generates an electron-hole pair which can be used for the production of electricity or photo catalysis [197]. Titania has been explored for many applications including degradation of organic pollutants, photovoltaics, air purification, self-cleaning surfaces, hydrogen evolution, sterilization, food additive, biomedical, degradation of pesticides, supercapacitors and lithium batteries [198–200]. An interesting feature of titania is its superhydrophilic property under UV exposure [201]. Inspired by the properties of titania, an underwater superoleophobic membrane was fabricated by spray depositing titania nanofibers and used for the separation oil/water mixture and photocatalytic degradation of organic molecules under UV [202]. In another study, magnetic titania nanotubes were prepared as a superhydrophobic sorbent for oil. Titania nanotubes were synthesized by a hydrothermal method in the presence of magnetic nanoparticles and modified with octadecylamine [203]. The prepared material was able to absorb oil more than 1.5 times its own weight and recyclable more than 5 times.

Similarly, a TiO_2 based superhydrophobic coating was constructed on cotton fabric via a hot pressing technique. The coating had a water contact angle of more than 150° and showed resistance to abrasion and machine washing [204]. The coating offered self-cleaning, antifouling, UV

protection properties. Coating with superhydrophobic characteristic was created by dip coating the fabric in a mixture of n-octyltriethoxysilane and Tetrabutyl titanate. The treatment caused the embedding of randomly dispersed TiO_2 on the surface of the cotton fibers. The surface roughness was further evaluated by atomic force microscopy. It was found that pristine fabric contained a relatively smooth structure with a root mean square value of 14.6 nm compared to the coated fabric which exhibited an increase value of RMS i.e. 48.2 nm. This highlighted the increased roughness of fabrics after deposition of TiO_2. The inherent structure of fabric combined with TiO_2 generated a hierarchical structure with micro and nanoscale features which are required for the Cassie-Baxter wetting state. A contact angle greater than 150° was observed. The XPS survey of the fabrics confirmed the deposition of TiO_2 and octyltriethoxysilane as the strong peaks of Ti 2p, Si 2p peak and Si 2 s were present in the coated fabrics as compared to pristine fabric. The fabric demonstrates outstanding UV resistance and mechanical properties as it can endure several abrasion and laundering cycles. The fabric was demonstrated to separate a mixture of dichloromethane and water with separation efficiency close to 100%. It can be seen that the water which was dyed as blue could not penetrate through the fabric due to superhdyrophobic property while oil easily permeated through the fabric. The fabric maintained this property even after five cycles of separation.

In another study, TiO_2 was deposited via spin coating on hierarchical polylactide (PLA) membrane to make it superhdyrophilic [205]. The PLA membrane was synthesized by a non-solvent induced phase separation (NIPS) method by using a non-woven fabric as a support. The PLA solution was cast on the fabric followed by immersing in water. The membrane was dried in air and peeled off from the fabric. A paint-like suspension of TiO_2 and as synthesized hydrophilic copolymer P(VP-VTES) was deposited PLA membrane via spin coating to fabricate superhydrophilic surface.

SEM images reveal the morphology of the PLA membrane and it can be observed that micro-scale groves, microspores and stretched nanofibrils have created a hierarchical microstructure. A robust coating of TiO2@P(VP-VTES) was formed on the PLA membrane via spin coating. The stretched nanofibrils seized the TiO2 nanoparticles to form a coral tentacle -like structure (**Figure 1-*16*** a-h). The high magnification images show that the TiO_2 nanoparticles have entirely covered the surface **Figure 1-*16*** g. Membrane maintained high flux, high separation efficiency and high rejection after ten separation cycles of oil/water mixtures.

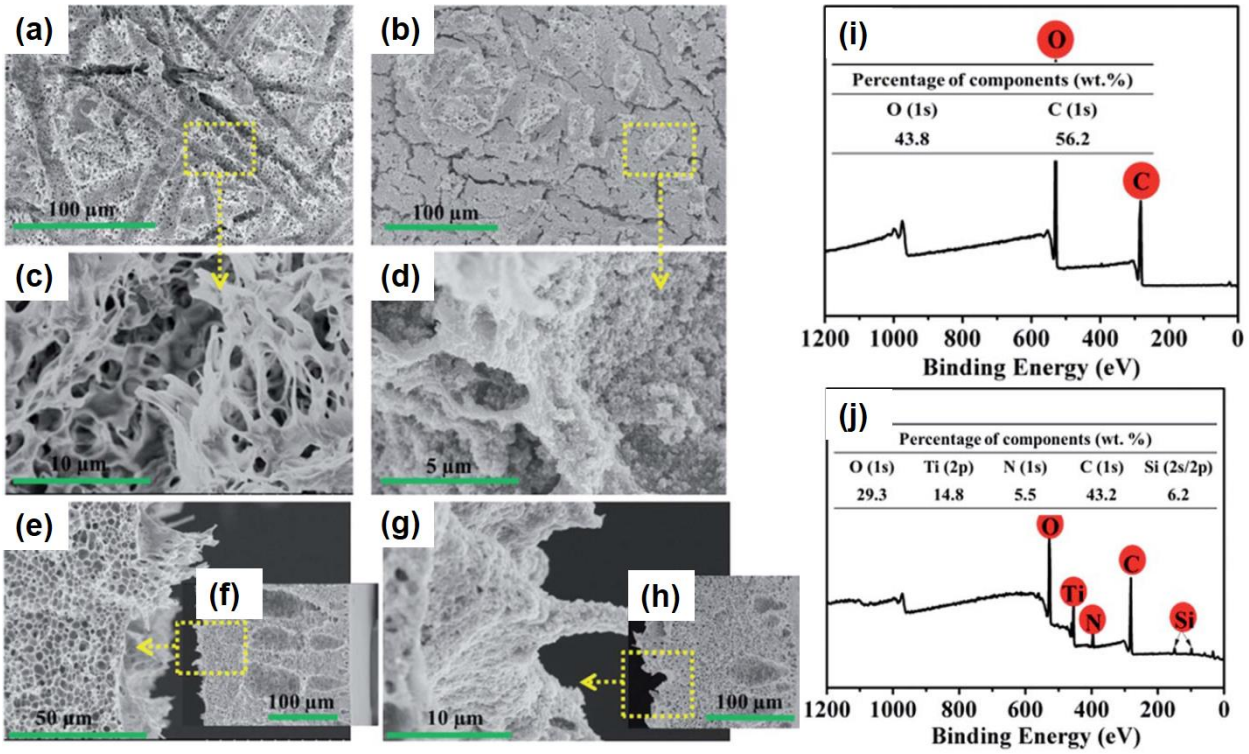

Figure 1-16: Front and cross sectional SEM images of (a, c, e, and f) pristine and (b, d, g, and h)TiO_2 modified membrane (i) XPS of pristine(j) and with TiO_2 membrane. With permission from The Royal Society of Chemistry, copyright 2017[205]

1.6.5 Zinc Oxide

ZnO is a semiconductor which has attracted attention due to its unique physical and chemical properties. ZnO has a large bandgap of 3.37 eV, large excitation binding energy of 60

meV, high photostability and radiation absorption over a broad range [206,207]. Moreover, ZnO is biocompatible, biodegradable and demonstrates antibacterial properties in nano sizes due to high surface reactivity [208]. The properties of ZnO has been studied for a wide range of applications including photo catalysis, antibacterial, energy, sensors and optoelectronics. A variety of ZnO based nanostructures has been explored, classified as 1D, 2D and 3D structures. Some examples include, nanorods, tubes, needles, belts, rings, sheets, flowers and snowflakes. Due to a wide range of nanostructures, ZnO has been used extensively to fabricate superhydrophobic surfaces [209–211]. For example, a superhydrophobic coating was fabricated by using ZnO nanoparticles of size 24 nm and wurtzite structure. The nanoparticles were prepared by a hydrothermal method and modified with palmitic acid. The coating demonstrated a water contact angle >160°; however, it became hydrophilic after heating at 230°. This behaviour was associated with the thermal degradation of palmitic acid [212]. Similarly, porous ZnO nanoparticles prepared by a combustion method were used with copper stearate to prepare a superhydrophobic coating with water contact angle 161°. In addition to the nanoparticles, flower-like structures of ZnO have also been explored [213,214] such as a flower-like ZnO hierarchical structure was used in combination with epoxy for the durable superhydrophobic surface. The coating demonstrated water contact angle more than 150° and sustained several abrasion cycles demonstrating its high durability. Inspired by the progress in ZnO based nanomaterials, a unique approach was adopted to develop a mesh for the separation of oil/water mixtures. A mesh was developed by growing ZnO nanowires stainless steel mesh by chemical vapour deposition, which demonstrated reversible wettability [215]. The mesh demonstrated superhydrophilic and underwater superoleophobic behaviour allowing it to let the water penetrate through its pores while blocking the oil. The mesh is able to become superhydrophilic or superhydrophobic depending upon thermal treatment under under hydrogen

or oxygen environments. The fabrication route of mesh involved the synthesis of ZnO nanowires produced by thermal chemical vapor deposition which were then suspended in ethanol and coated on steel mesh by drop casting. SEM images indicate the pore size of mesh (50 μm) and ZnO wires of diameter 100 nm and length 4.6 μm randomly distributed on the surface (**Figure 1-*17*a**). The XRD analysis of ZnO nanowires indicates the wurtzite phase of ZnO (**Figure 1-*17*b**). As prepared mesh demonstrates both superhydrophilic and superoleophilic properties with a water contact angle of 0°.

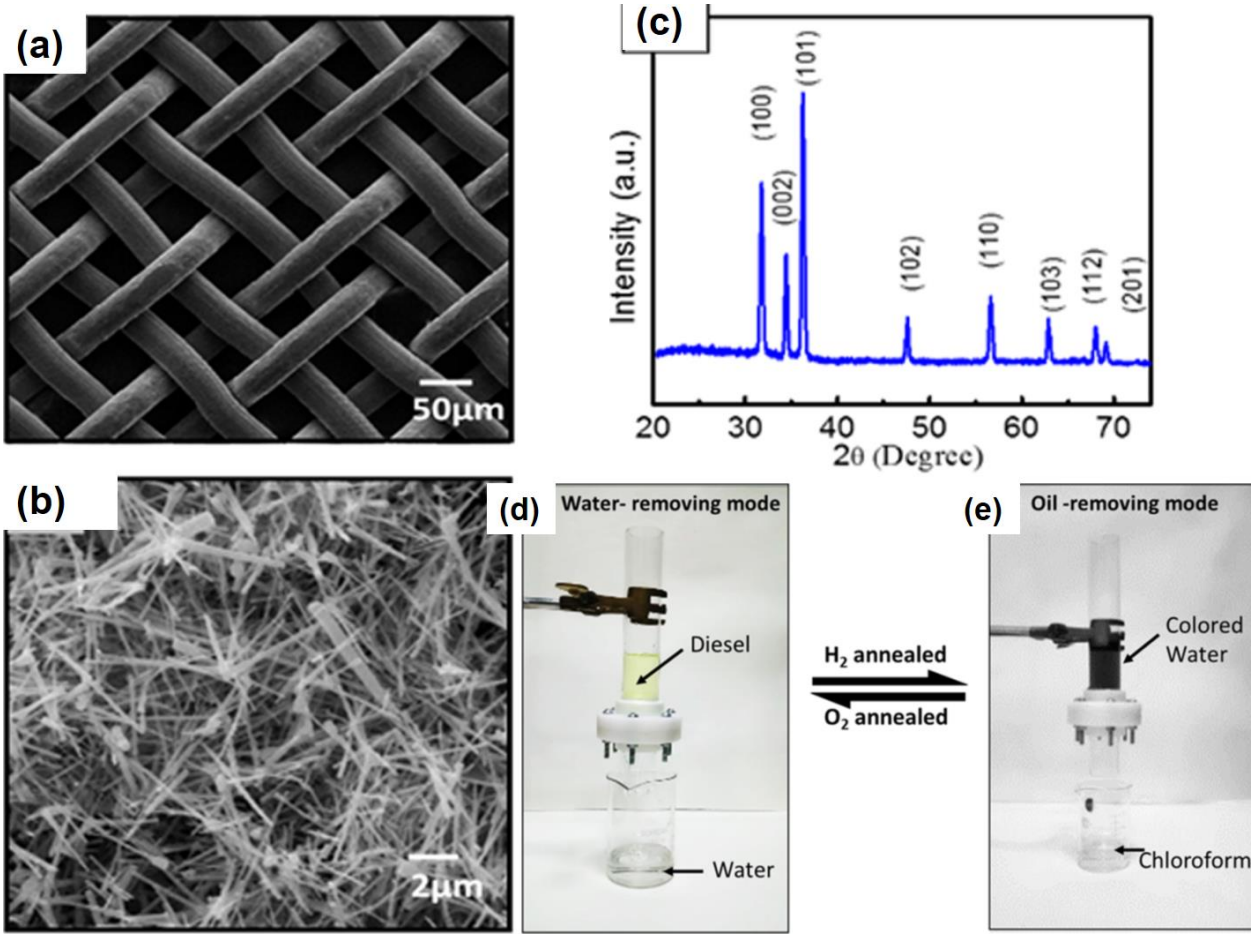

Figure 1-17: (a and b) SEM images showing the structure of pristine and ZnO coated mesh, (c) XRD pattern of ZnO coated mesh (d) The separation device used for the separation of oil/water mixtures by using ZnO coated mesh. Adapted from [215]. With permission from American Chemical Society, copyright 2017.

The mesh displayed underwater superoleophobic behaviour. The underwater contact angle is more than 150° for various types of oils indicating the high resistance of mesh towards oil penetration in the presence of water. Moreover, the oil rolls off at an angle of 5°, indicating the low adhesion due to the repulsion of polar water towards nonpolar oils. The trapped water decreases the effective contact area between oil and solid surface, resulting in triple-phase discontinuous line. This together with surface roughness result in underwater superoleophobic behaviour. The mesh was switched to superhydrophobic and superoleophilic by hydrogen annealing treatment. The annealing was performed under hydrogen at 300 °C, which resulted in the water contact angle of 154° without affecting the superoleophilic properties of the mesh. The reversible switching of mesh was demonstrated by annealing at 300 °C for 1 h under oxygen. The process is reversible and annealing treatments with hydrogen and oxygen control the wetting behavior.

A model device was fabricated using ZnO nanowire mesh (Fig. 1-15d). In the water removing mode, superhydrophilic and underwater superoleophobic was used, and a mixture of diesel and water in 1:2 ratios were poured through the device. The water easily penetrated through the mesh while diesel was blocked. Similarly, several other oils were also tested including gasoline, hexane, olive oil, mustard oil, and turpentine oil

For the oil removing mode, the mesh after hydrogen treatment was used. It has superhydrophobic/superoleophilic properties making it possible to remove mixtures of chloroform and 1,2-dichloroethane with water. The oil quickly passed through the mesh while blocking the water. The contact angle measurements demonstrated the recoverability of mesh for more than ten cycles. Moreover, mesh efficiency was more than 99.9% for mustard oil, diesel, gasoline, olive oil, and turpentine oil.

1.7 Summary and conclusions of the literature review

Whilst an understanding has been developed that superhydrophobic surfaces can be artificially created by combining a nanoscale structure with hydrophobic functionality, most of these surfaces are susceptible to damage upon application of mechanical force. Therefore, efforts are still ongoing to make robust superhydrophobic surfaces. In most cases, durability loss is associated with the damage to nanoscale topography and chemical functionality under mechanical forces or harsh service conditions. Most of the durable superhydrophobic surfaces have been made by combining hydrophobic nanoparticles with adhesive; however, the resistance of such surfaces to organic solvents is still questionable. The response of a robust superhydrophobic surface in a harsh environment such as pressure, wear and shear has been discussed in a study, and it was argued that surface roughness plays a vital role in the stability of Cassie Baxter wetting state [216]. A brief examination of the literature uncovers a deep concern regarding the stability of superhydrophobic surfaces used for engineering applications and the methods to characterise them [217]. With increasing interest in applying superhydrophobic surfaces for engineering materials, it has become essential to devise standard methods to characterise the durability of the superhydrophobic surface against different parameters such as mechanical or chemical environments. These characteristics will play a vital role in engineering superhydrophobic materials for emulsion and oil/water mixtures.

In addition to the durability, special design considerations are required for the application of superhydrophobic materials for oil/water separation. For example, most superhydrophobic materials have been used to separate oil/water mixtures where oil exists as a separate phase and can be separated by a simple filtration step. However, the separation becomes extremely difficult

if the oil phase is uniformly distributed in the aqueous phase and stabilised by surfactants. In this case, the design of superhydrophobic materials becomes vital because typical absorbents are either inefficient or do not separate very stable emulsions. For example, pore size and structure will play a key role in separating emulsions. Despite some work present in the literature, this is still a developing field with many unexplored facets, especially designing materials with switchable wettability to separate both oil/water and water/oil emulsions. In addition, there is a lack of characterisation of emulsion separation by superhydrophobic materials. Most presented in the literature have used different recipes for emulsions, and in some cases, emulsions were not stable even up to 48 hrs. In addition, durable superhydrophobic materials should be designed considering the surfactant stabilised emulsions and the recyclability of the adsorbent.

Various types of nanoparticles have been deposited on different substrates to engineer superhydrophobic materials for oil/water separation. The choice of materials comes down to the substrate and scenarios of application. For example, silica can be synthesised in different shapes (from nanometer pore to micrometre scaffold) and bind to various substrates due to surface silanol groups. The mesoporous structure of silica can offer sites for the adsorption of organic moieties. However, the surface of silica nanoparticles would need to be modified with low surface energy groups to impart hydrophobic properties and require further processing steps. The same is the case with most ceramic nanoparticles. They offer relatively high thermal stability and robust coatings in some cases; however, additional processing steps are required to tune surface chemistry and adherence to the substrate. Another criterion for choosing a nanomaterial for oil/water separation could be the inherent hydrophobic/hydrophilic structure. For example, carbon particles produced from candle soot or related methods offer hydrophobic behaviour.

Similarly, graphene-based materials have hydrophobic properties depending upon the nature of surface functional groups. These nanomaterials can avoid a step of surface modification needed for silica or most inorganic nanoparticles but require a suitable adhesive to bind them to the substrate. As explained in the previous sections, the key criterion for selecting a nanomaterial would be the surface chemistry, the magnitude of roughness, synthesis route, ease of functionalisation and adhesion behaviour with the substrate. Some materials such as rods, sheets or tubes, including CNT's and graphene composites, offer dual-scale roughness due to their unique geometrical features. A structure formed by these materials will provide a more rough structure, thus more air cushion and water repellent properties. Another exciting feature could be the magnetic properties as they could benefit reusable or fast separation systems for surfactant stabilising emulsions. In this regard, Iron-based oxides and their composites can provide a unique combination of high surface and area magnetic properties for fast separation of emulsions.

In addition to choosing the nanomaterial or modifying agent, the separation medium or substrate structure also plays an important role. Aerogels and foams produced from natural resources offer an environmentally friendly and economical solution. The 3D porous network offers very adsorption capacity most foams reported in the literature are reusable due to their elastic nature. Some examples include polymer-based foams such as polyurethane, melamine or carbon-based foams derived from natural resources or nickel, copper foams. The surface of these structures was modified to render them superhydrophobic. Some other structures, such as meshes and fabrics, have been explored. The suitability of these materials for emulsion separation is uncertain due to large pores. As mentioned in previous sections, the emulsion could contain tiny oil droplets uniformly distributed in the water phase or vice versa. An adsorbent or filtration medium with large pores would not sieve small droplets.

Typical oil/water separation materials lack efficiency in removing emulsions formed in the presence of natural additives and environmental stressors. Methods such as on spot burning and dispersants cause further pollution and are not sustainable for long term applications. An efficient and scalable separation method will have environmental remediation applications and enhance the economic value of industrial processes. Most studies used nanoparticle-based coatings that can fracture during infield application, thus changing the adsorbent properties. Adsorbents for oil/water separation must resist environmental stressors, and their manufacturing route should be scalable for commercial applications. In addition, the environmental impact of nanomaterials should also be considered before engineering superhydrophobic materials for oil/water separation. For this, fluorine-containing compounds must be avoided for surface modification and appropriate adhesive bind nanomaterials to the substrate. This research will focus on creating nanocomposites for emulsion separation whilst considering the recyclability, durability and potential impact on the environment. The nanoparticles coated filtration mediums risk causing secondary pollution by exposing toxic nanomaterials to the environment. Therefore, stable nanocomposites will be fabricated for batch scale separation of emulsion, whilst macroscopic superhydrophobic structure for potentially continuous separation will be studied in the second phase. The nanocomposite will be either prepared with a binder or magnetic properties for batch scale separation to retrieve the material quickly after separation.

Furthermore, the choice of formulations that are fluorine-free and relatively environment friendly will be considered. For example, the 2nd chapter of this thesis utilises alumina nanoparticles with a nanoscale polysiloxane layer deposited on sawdust particles. These materials are readily available and environment friendly as compared to fluorine-based compounds. In addition, the nanocomposite is compacted by a polydimethylsiloxane layer, which is a biocompatible polymer.

Similar considerations will be made for the materials used in the 3rd and 4th chapters. For example, the membranes reported in the 4th chapter contain nanoparticles embedded in the polyurethane network, thus reducing the risk of leakage during application.

1.8 Aims of research

This project aimed to establish surface engineering protocols using various nanomaterials and their composites to separate oil/water mixtures and emulsions. The project was started with an aim to first study particulate adsorbents for batch scale separation of surfactant stabilized emulsion. A sawdust based renewable and high surface area silica-based nanocomposite adsorbents were synthesised in the first phase. A clear understanding was established on the role of using particulate adsorbent superhydrophobic adsorbents in the removal of tiny oil droplets from emulsions. Later, the research was progressed towards the synthesis of macroscopic superhydrophobic materials after extensive consultation with industrial collaborators. Superhydrophobic platforms such as nanofibrous membranes and 3D porous frameworks were thought to be more practicable for large-scale industrial applications in treating emulsions. Therefore, a new spray based method was developed for the synthesis of membranes and durable superhydrophobic coatings.

Chapter 2: Renewable adsorbent for the separation of surfactant-stabilized oil in water emulsions based on nanostructured sawdust

Citation: U. Zulfiqar, A. G. Thomas, K. Yearsley, L. W. Bolton, A. Matthews, and D. J. Lewis, "Renewable Adsorbent for the Separation of Surfactant-Stabilized Oil in Water Emulsions Based on Nanostructured Sawdust," ACS Sustain. Chem. Eng., p. acssuschemeng.9b04294, Nov. 2019, doi: 10.1021/acssuschemeng.9b04294.

Author contributions:

All authors listed have made a substantial, direct and intellectual contribution to the work and approved it for publication. U. Zulfiqar carried out the experimental work and wrote the manuscript whilst A. Matthews, D. J. Lewis and A. G. Thomas were involved in supervision, critical analysis of results, editing and revision of the manuscript. A. G. Thomas helped with the XPS analysis of samples. K. Yearsley, L. W. Bolton provided supervision as industrial mentors and helped in editing the manuscript.

2.1 Abstract

This work reports the surface modification of sawdust particles with silane-modified alumina nanoparticles and polydimethylsiloxane to create smart micron sized absorbents for separation of surfactant stabilized emulsions. A very fine polysiloxane network (< 12 nm) was created on the surface of alumina nanoparticles which were then uniformly coated on the surface of sawdust particles to create a hierarchical film with a thickness < 500 nm. The composite particles were then coated with polydimethylsiloxane to create a stable superhydrophobic absorbent with contact angle > 150° and thermal stability up to 200 °C. The absorbent is preferentially wetted by oil and can be used to separate surfactant stabilized emulsion under mechanical agitation. The absorbent was able to remove most of the oil content from the emulsions; the optical transmittance of emulations increased from 0 to ca. 90% after separation and optical microscopy images showed very low trace of oil in the filtrate.

2.2 Introduction

Oil/water mixtures are generated through various processes and their volume is continually increasing with expanding industrial operations. Industries such as metal processing, pharmaceuticals, and oil generate large volumes of oily water as a consequence of their daily operations [218]. In the oil industry, oil/water mixtures are produced during extraction and refining of crude oil. It is important to remove water from oily products (i) to meet product specification, and (ii) to avoid corrosion in pipelines, but it is also important to remove oily products from water to allow water to be discharged into the environment. A separate problem is the need to clean up oil from accidental spillages, both of crude oil and of oil-based fuels, to the environment. Such spillages can have a devastating impact on natural habitats and ocean life [64] particularly due to the tendency of oil to concentrate at the water's surface. Typical methods to separate oil/water

mixtures include mechanical separation via bommers, skimmers, centrifugation and chemical or biological methods [43,65]. Mechanical methods have limited effectiveness while the chemical and biological methods either disperse the oil or convert it to other chemical species.

Recently, materials with selective affinity towards oil and repellent towards water have been used for the separation of these biphasic mixtures [219–221]. Inspired by natural superhydrophobic surfaces such as the lotus leaf, these materials are promising candidates for the physical separation of oil/water mixtures. Superhydrophobic surfaces repel water due to their distinctive rough surface features and low surface energy in range of 20–30 mN m^{-1}. Despite the strongly water repellent properties of a superhydrophobic surface, organic liquids with low surface energy are still attracted. This combination of oleophilicity and hydrophobicity can be used to selectively collect the oil from an oil/water mixture without affecting its chemical nature.

In the past few decades, efforts have been made to understand the phenomenon of superhydrophobicity and to artificially create superhydrophobic surfaces [219]. It has been found in many cases that surfaces with a combination of hierarchical roughness and non-polar surface chemistry can give rise to superhydrophobic properties, mainly by maintaining a large fraction of air within the surface texture. Following this approach, several types of superhydrophobic materials have been synthesized and their applications have been explored in different fields such as corrosion resistance, protective coatings for building materials, anti-fogging and anti-icing coatings and also for oil/water separation [10,76,228,220–227]. For oil/ water separation, a variety of porous substrates such as foams, meshes, filter papers, fabrics, gels, monoliths and fibers have been made superhydrophobic and oleophilic to collect oil from oil/water mixture [75,88,232–235,100,141,167,225,226,229–231]. However, the separation of oil from an emulsion where oil droplets are uniformly distributed in the water phase is not straightforward. In the oil industry, oil/water

mixtures have oil droplets as small as 100 nm which separate only slowly under the influence of gravity. The separation process becomes even more difficult if the oil droplets are stabilized by surfactants such as alkylbenzene sulfonates, fatty acids, as well as naturally-occurring solid particles [53]. Crude oil also contains solid matter such as clays, particles of silica and iron oxide which are naturally hydrophilic, but become hydrophobic following prolonged exposure to hydrocarbons. This, combined with the presence of asphaltenes and resins, can help water droplets to disperse uniformly in oil or vice versa generating very stable emulsions. Mixtures with small oil droplets stabilised by amphiphiles cannot readily be separated by conventional superhydrophobic materials because little of the oil phase comes into contact with the separation medium. One approach is to use micron sized superhydrophobic absorbents to collect the dispersed oil phase from the emulsion [75,107,109]. An example of this approach is the use of superhydrophobic hollow silica micro particles [109] which have been used for the separation of three different types of oil in water emulsions.

Sawdust (SD) provides a widely available and inexpensive micron size structure which can be decorated with nanoscale features to produce superhydrophic / oleophilic materials. The usefulness of SD as a micro-scale template has been demonstrated previously in production of activated carbon [236,237], and removal of cadmium [238], arsenic and sulfamethoxazole [239] from water. Sawdust has also been used as a reinforcement in polyethylene composites [240]. Sawdust was chemically modified with cetyltrimethylammonium bromide to alter its hydrophilic nature. The chemical functionalization was believed to improve the adhesion between sawdust and polymer matrix by reducing the polarity gap. Similarly, sawdust was chemically modified by decorating its surface with nanoparticles of zirconium or lanthanum oxide to prepare cost efficient absorbent for the removal of arsenic form water [241].

In this paper we report micron sized composite functional absorbents for the separation of oil water mixtures. SD particles were used as a micro-scale structural support, with size ranging up to several microns, on which a nanostructured absorbent was constructed based on Al_2O_3 nanoparticles (NPs) functionalized with hydrophobic silane groups. The composite particles are stabilized with polydimethylsiloxane (PDMS) to avoid the release of nanoparticles to the environment during application. The assembly of these so-called PDMS@Al_2O_3@SD nanocomposites is shown in Scheme 1. We then show how these nanostructured composites can be used for efficient demulsification of a surfactant-stabilized emulsion of toluene in water, with excellent recyclability.

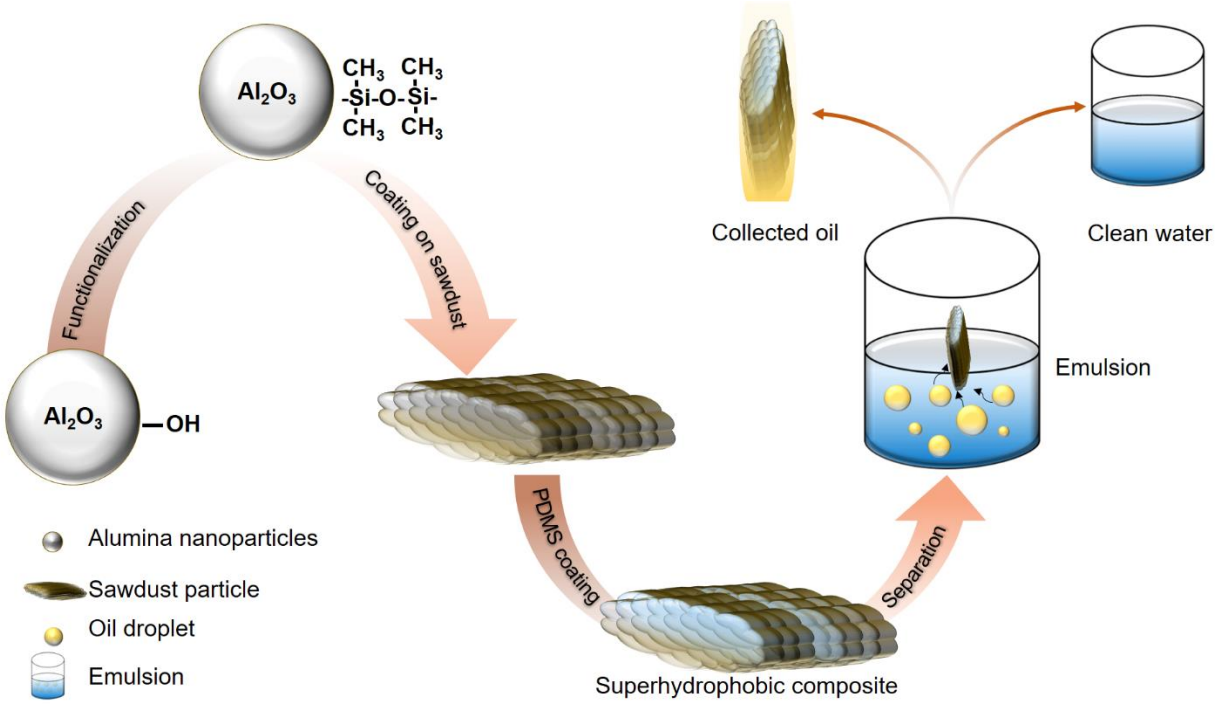

Scheme 1: Fabrication process of superhydrophobic composite particles and their application in separation of emulsions

2.3 Materials and Methods

2.3.1 Materials

Aluminium oxide (Al_2O_3- CAS Number 1344-28-1) nanopowder with diameter < 50 nm and surface area >40 m^2/g and dichlorodimethylsilane (CH_3SiHCl_2- CAS Number 75-78-5) (≥ 98.5% (GC) were purchased from Sigma Aldrich. Sawdust (SD) was washed with methanol several times and dried overnight in an oven at 90 °C followed by sieving to collect < 150 µm particles. The washed SD particles (<150 µm) were used without any other processing. SYLGARD® 184 silicone elastomer was used as a source of polydimethylsiloxane (PDMS) and was activated in a 10:1 ratio with curing agent. Span 80 ($C_{24}H_{44}O_6$-CAS Number 1338-43-8) with viscosity 1000-2000 mPa.s at 20 °C was procured from Sigma Aldrich and used as a surfactant to make stable oil in water emulsions.

2.3.2 Methods

1 g alumina nanoparticles (Al_2O_3 NPs) was added to 200 ml hexane under continuous stirring. 20 ml dichlorodimethylsilane (DCDMS) was introduced in the mixture and the temperature was raised to 200 °C until the solvent evaporated. The resulting powder was dried for 2 h. at 200 °C and washed with acetone four times. For preparation of superhydrophobic surfaces, functionalized Al_2O_3 NPs were suspended in acetone (4 wt.%) and ultrasonicated for 4 h. and then spray deposited on a variety of substrates using a Clarke DIY Air Brush Kit. The spray distance was maintained at 10 cm for all samples. After spray deposition, the substrates were dried at 90 °C for 1 h.

The Al_2O_3@SD particles were prepared by mixing 1 g SD particles in 10 ml suspensions containing different concentrations of nanoparticles (Table 1). The suspensions were made by ultrasonication of Al_2O_3 NPs in acetone for 4 h. After mixing SD particles, the mixture was

sonicated for 30 min and then left to dry overnight. For the deposition of PDMS layer, 3 wt.% PDMS and curing agent were mixed in two different beakers, each containing 50 ml hexane, and magnetically stirred for 1 h. Later, the two mixtures were mixed together and then stirred for 30 min. The prepared PDMS solution was mixed in different quantities (Table 2) with Al_2O_3@SD and dried for 2 h. The final product was washed with acetone twice and dried. After characterization, the optimized PDMS@Al_2O_3@SD particles were used for the separation experiments.

Table 1-1: Sample names for Al_2O_3 NP-coated SD particles

Specification	**Sample Name**
1 wt.% Alumina Nanoparticles	1-Al_2O_3@SD
3 wt.% Alumina Nanoparticles	2-Al_2O_3@SD
5 wt.% Alumina Nanoparticles	3-Al_2O_3@SD
7 wt.% Alumina Nanoparticles	4-Al_2O_3@SD
9 wt.% Alumina Nanoparticles	5-Al_2O_3@SD

Table 1-2: Sample names for Al_2O_3 NP-coated SD particles further coated with PDMS

Specification	**Sample Name**
Al_2O_3@SD coated with 10 ml PDMS solution	1-PDMS@Al_2O_3@SD
Al_2O_3@SD coated with 20 ml PDMS solution	2-PDMS@Al_2O_3@SD
Al_2O_3@SD coated with 30 ml PDMS solution	3-PDMS@Al_2O_3@SD

2.3.3 Characterization

The morphology of the nanoparticles, surfaces and absorbents was examined by using a field emission scanning electron microscope (SEM). The samples were coated with a layer of platinum before analysis to make them conductive. The cross section of sawdust particles was created by using a Focused Ion Beam (FIB) FEI Quanta 3D FIB + XUM. The thermal analysis was performed by thermal gravimetric analysis (TGA- Mettler Toledo TGA/DSC1) in air with a heating rate of 10 °C/min while the chemical structure and composition were analyzed by Fourier-transform infrared spectroscopy (FTIR- NICOLET 5700 spectrometer) and X-ray photoelectron spectroscopy (XPS). XPS was performed by using Kratos Axis Ultra with monochromatic Al k alpha X-ray source. The data analysis was done using CASA XPS software; spectra were corrected on the binding energy scale with respect to adventitious carbon (C 1s at 284.8 eV.). The Shirley background and Gaussian Lorentzian peak shape were used for the peak fitting. Contact angles were measured by using a Kruss drop shape analyser. Transmittance spectra were recorded using a UV/Vis spectrophotometer (Shimazu UV-1800) in the visible range. For separation experiments, test emulsions were produced by mixing toluene and water at 1000 rpm using a magnetic stirrer for 20 min with a surfactant to stabilize the emulsion (1g/l Span 80). The emulsions were characterized by optical microscopy (Olympus BH2 upright optical microscope, Zeiss camera) and UV/Vis absorption spectroscopy before and after separation.

2.4 Results and Discussion

SEM was used to assess the morphologies of the nanoparticles. **Figure 2-*1***a and b shows the SEM images of Al_2O_3 NPs before and after functionalization. The nanoparticles are randomly shaped and are in the size range < 50 nm according to their commercial specification. There is no obvious effect on physical structure of nanoparticles after functionalization.

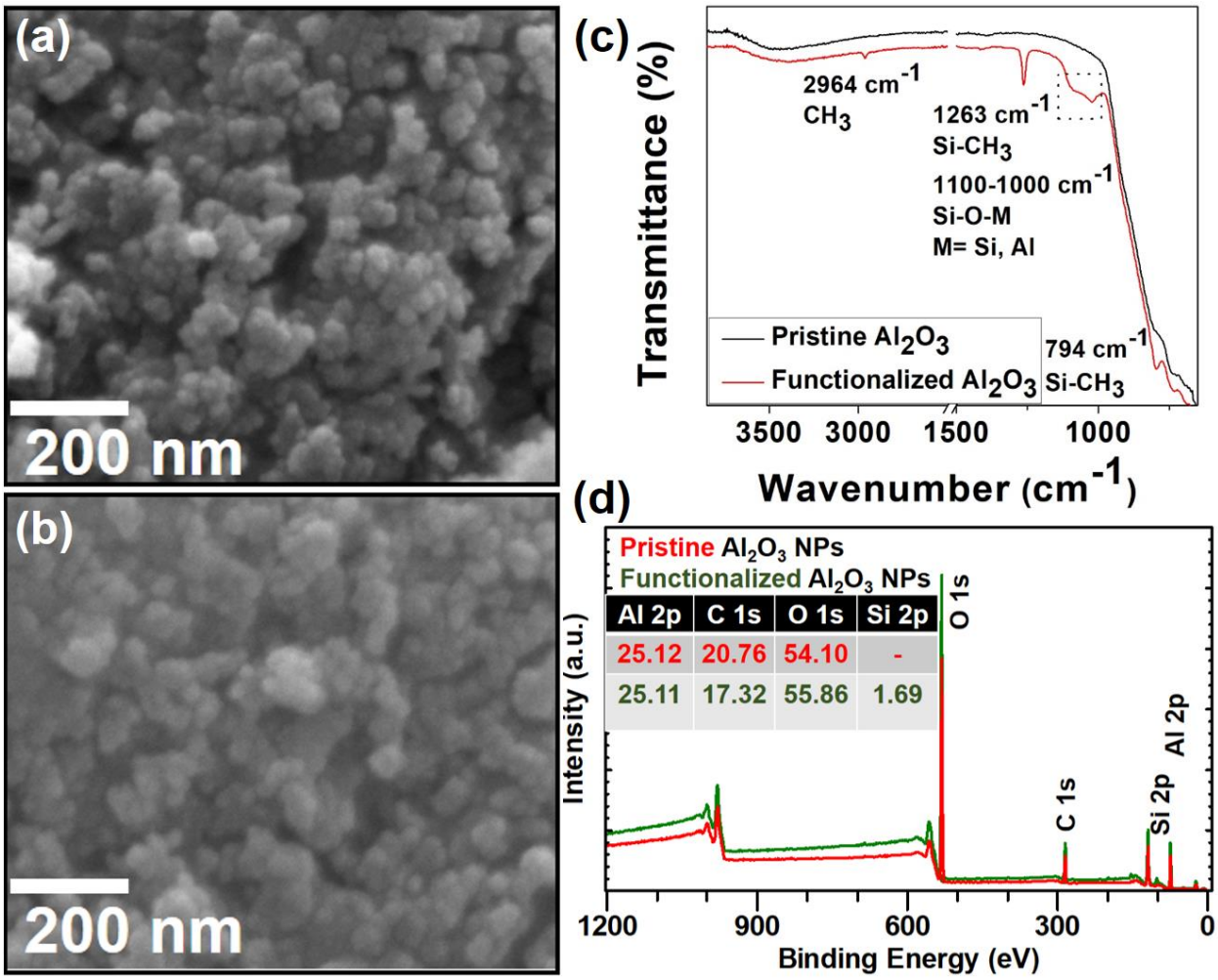

Figure 2-1: SEM images showing the morphology of the Al_2O_3 nanoparticles (a) before and (b) after functionalization (c) FTIR spectra of Al_2O_3 nanoparticles before and after functionalization; (d) XPS spectra of alumina nanoparticles before and after functionalization

The functionalized Al_2O_3 NPs were further characterized by FTIR and XPS to study the change in surface chemistry after functionalization. New peaks emerge post-functionalization which are absent in the spectra of pristine nanoparticles. The peaks at ~2964 cm^{-1} and ~1263 cm^{-1} indicate the presence of CH_3, while the peak at ~ 794 cm^{-1} indicates the presence of the siloxane Si-O bond (**Figure 2-*1***c). There is a broad band at 1000-1120 cm^{-1} which has been attributed previously to Si-O-Si and Al-O-Si bonds [242]. In other studies this has been attributed to vibrations from Si–O–

C, Si-O-Si and Si-O-Al bonds, [37 – 41] with no consensus arising as to a single identity for this broad peak. It is likely that the resonance contains vibrational elements of all three bonding types and hence spans a large manifold of energies.

Figure 2-*1*d shows the XPS analysis of Al_2O_3 NPs before and after functionalization. The quantification from high resolution spectra of Al_2O_3 NPs indicates the presence of 25.12at% aluminium, 20.76 at% carbon and 54.10 at% oxygen. The peak position of Al 2p (74.58 eV) indicates the presence of Al_2O_3. After functionalization of the alumina surface with silane groups, a Si 2p peak appears in the XPS spectrum at 101.97 eV which we attribute to introduction of the (-Si$(CH_3)_2$O-) groups at the surface. The quantification of high resolution spectra by peak fitting shows 25.11 at% aluminum, 17.32 at% carbon, 55.86 at% oxygen and 1.69 at% silicon. Keeping in view the results from FTIR and XPS, we conclude that reaction resulted in the formation of a very fine polysiloxane network on the surface of alumina. This modification is important in creating a low surface energy network to replace the hydroxyl groups present on the surface of Al_2O_3 NPs, probably due to reaction between hydroxyl and chlorine groups resulting in the formation of HCl as a byproduct and anchoring of dimethylsilyl group on the surface of nanoparticles. The presence of the siloxane bond, which is clear from the peak at ~795 cm^{-1} and 1000-1120 cm^{-1}, is possible if silane groups are forming a chain. There is a possibility that HCl, formed during the functionalization reaction, could react with the Al_2O_3 NPs to form aluminium chloride. To ensure that any aluminium chloride was removed, the NPs were dried at 200 °C and washed with acetone. The combination of these steps would be expected to remove all the byproducts since aluminium chloride has a boiling point of 180 °C and good solubility in acetone.

Figure 2-*2*a shows the TGA analysis of alumina nanoparticles before and after functionalization. The weight loss in nanoparticles before functionalization can be ascribed to the removal of

moisture and water produced due to polycondensation of hydroxyl groups from alumina nanoparticles. It has been previously noted that pure alumina nanoparticles lose mass due to dehydroxylation up to 800°C [243]. Silica nanoparticles are also known to exhibit weight loss in this temperature due to polycondensation of hydroxyl groups [244]. The TGA analysis of alumina nanoparticles after functionalization shows the two stages of weight loss. It starts with the removal of water molecules up to 180 °C with a weight loss of 1.48 wt.%, followed by a second stage starting at 180 °C with a major weight loss up to 530 °C but continuing more gradually to ~810 °C. The sample lost 5.17 % weight in this region which indicates the degradation of silyl methyl functional groups.

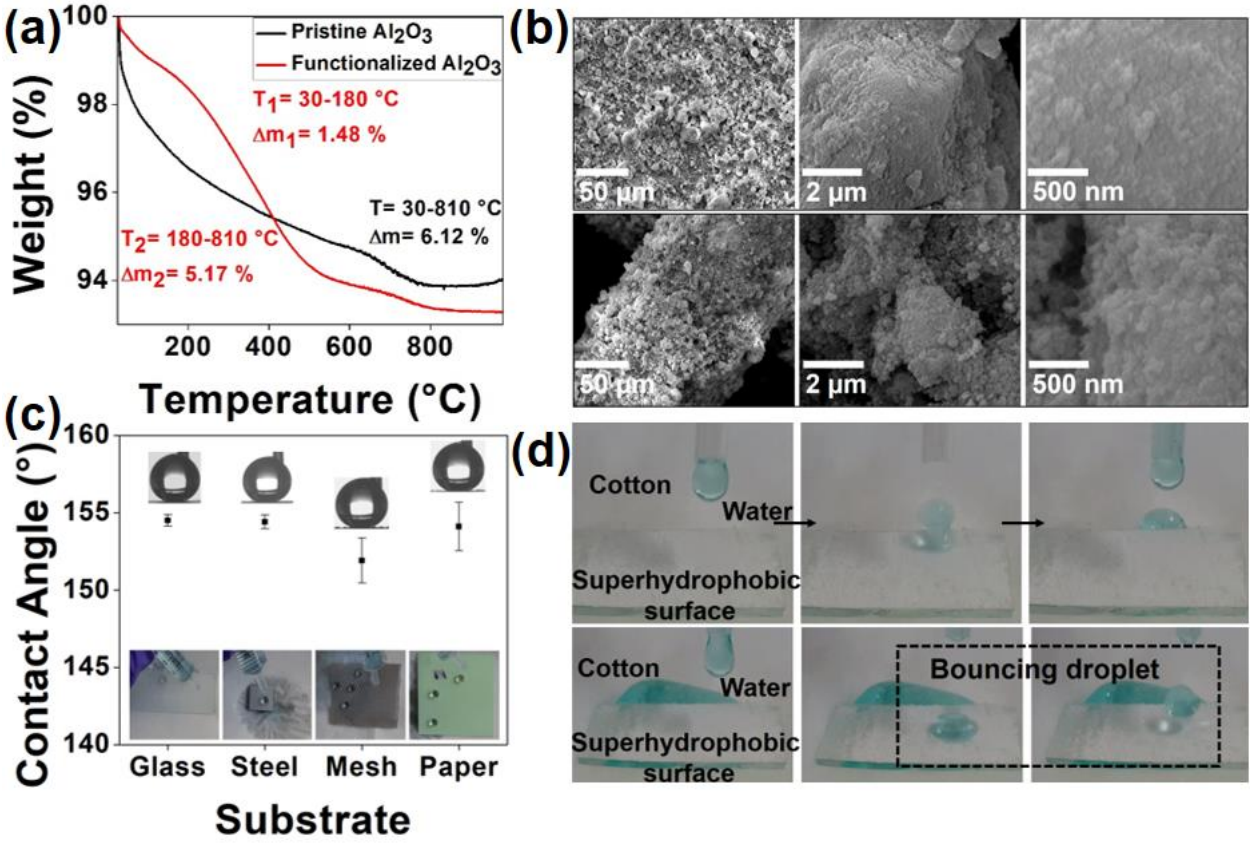

Figure 2-2: (a) Thermogravimetric analysis of the functionalized Al_2O_3 nanoparticles; (b) SEM images showing the morphology of the spray coated glass and mesh; (c) Water contact angle of different substrates sprayed with functionalized Al_2O_3 nanoparticles; (d) Digital images showing

the roll off and bouncing droplet on a superhydrophobic surface fabricated from functionalized Al_2O_3 nanoparticles

To demonstrate the application of functionalized Al_2O_3 NPs, they were used to make a 4 wt.% suspension in acetone which was deposited on various substrates by spraying. **Figure 2-2**b shows the morphology of the resulting coatings. The nanoparticles form a hierarchical structure which is uniformly distributed across the substrates. This process can be used to coat variety of substrates: paper, fabric, steel, mesh and glass were coated and the resulting contact angles were measured as shown in **Figure 2-2**c. All of these contact angles exceed 150° so these are regarded as superhydrophobic surfaces. The functionalized Al_2O_3 NPs were also deposited on a glass slide with the help of silicone adhesive to create a superhydrophobic surface. **Figure 2-2**d shows the behaviour of a water droplet on this superhydrophobic surface. The water droplet is rejected from the surface upon contact, indicating the extremely high repellence towards water. In another image, an occurrence of droplet bouncing on a surface can also be observed.

To prepare functional absorbents for the separation of surfactant-stabilized emulsions, the nanoparticles were coated on SD particles (< 150 μm). To determine the optimal loading of NPs on the SD substrate, different loadings of functionalized Al_2O_3 NPs were coated on the surface of SD to make composite particles Al_2O_3 @SD. The functionalized Al_2O_3 NPs coating significantly changed the surface wettability of SD particles. It can be seen in

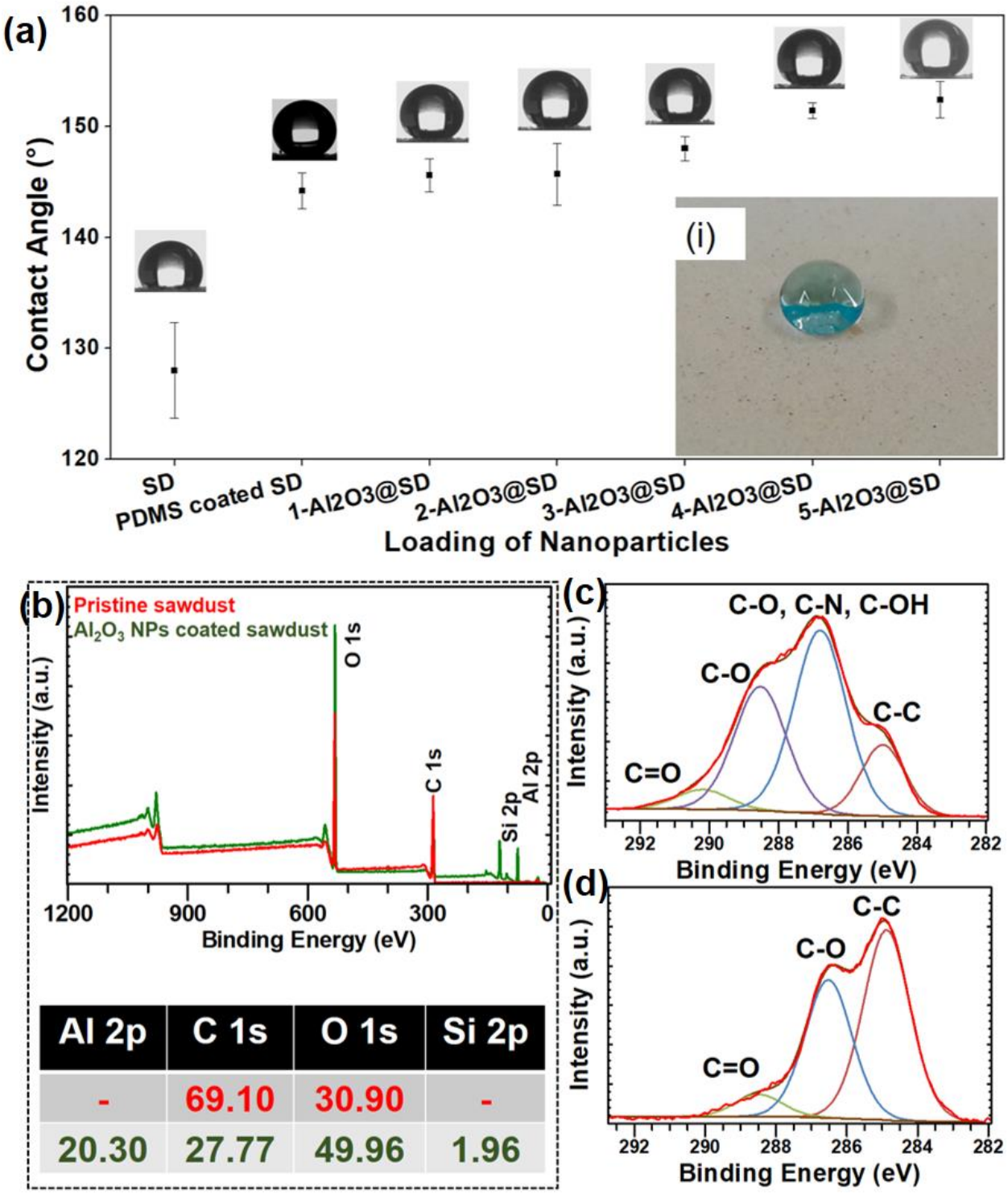

Al 2p	C 1s	O 1s	Si 2p
-	69.10	30.90	-
20.30	27.77	49.96	1.96

Figure 2-3a that the water contact angle of coated SD started to increase with increased loading of Al_2O_3 NPs until it reached about 150°, with the largest contact angle being achieved with the maximum loading, 5-Al_2O_3 @SD (152.4° ± 1.62) The inset shows the superhydrophobic surface

created from 5-Al_2O_3 @SD and its visual appearance after immersion in water coloured with methylene blue.

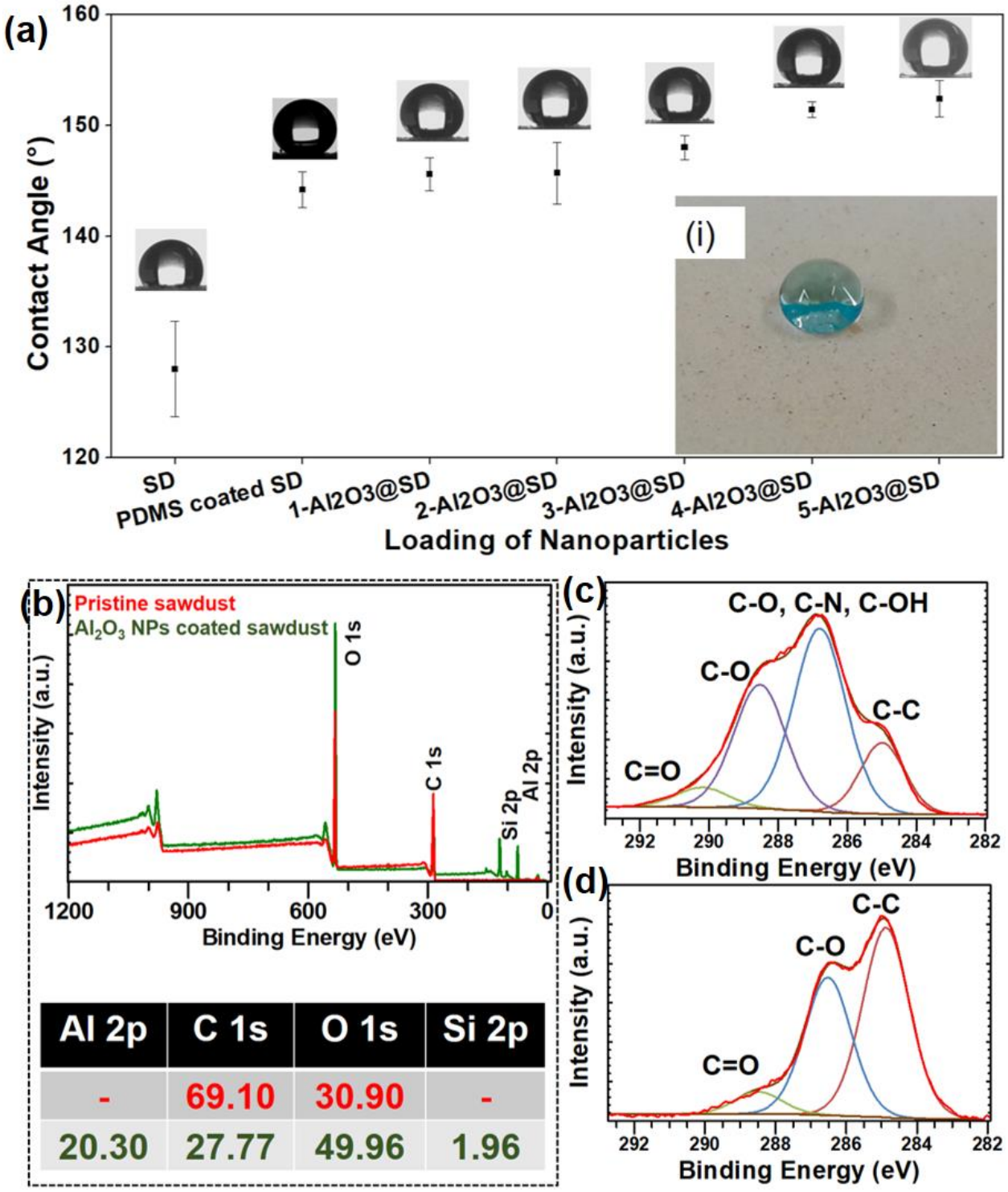

Al 2p	C 1s	O 1s	Si 2p
-	69.10	30.90	-
20.30	27.77	49.96	1.96

Figure 2-3: Graph showing the change in water contact angle with increasing loading of Al_2O_3 nanoparticles in sawdust, (i) inset showing the water droplet on 5-Al_2O_3@SD bonded to glass with silicone adhesive (b) XPS spectra of sawdust before and after coating with alumina nanoparticles; high resolution C1s (c) before and (d) after coating (5-Al_2O_3 @SD)

The changes in the surface chemistry of SD were observed by XPS and FTIR. The XPS spectrum

(

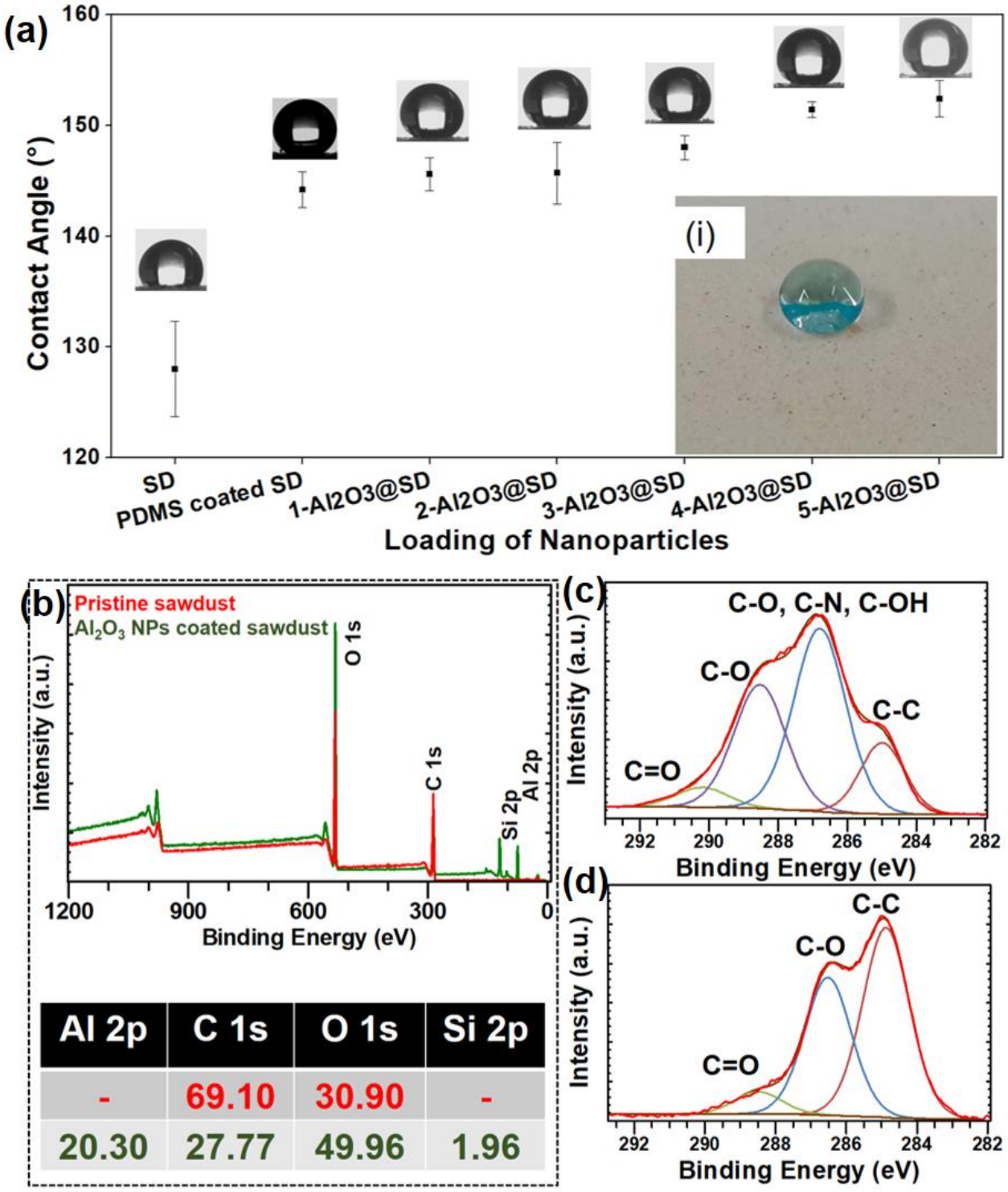

Al 2p	C 1s	O 1s	Si 2p
-	69.10	30.90	-
20.30	27.77	49.96	1.96

Figure 2-3b) of pristine SD shows carbon and oxygen peaks which are the main contents of

organic matter in SD. The deconvolution of C1s peak from sawdust indicated four chemical states

(

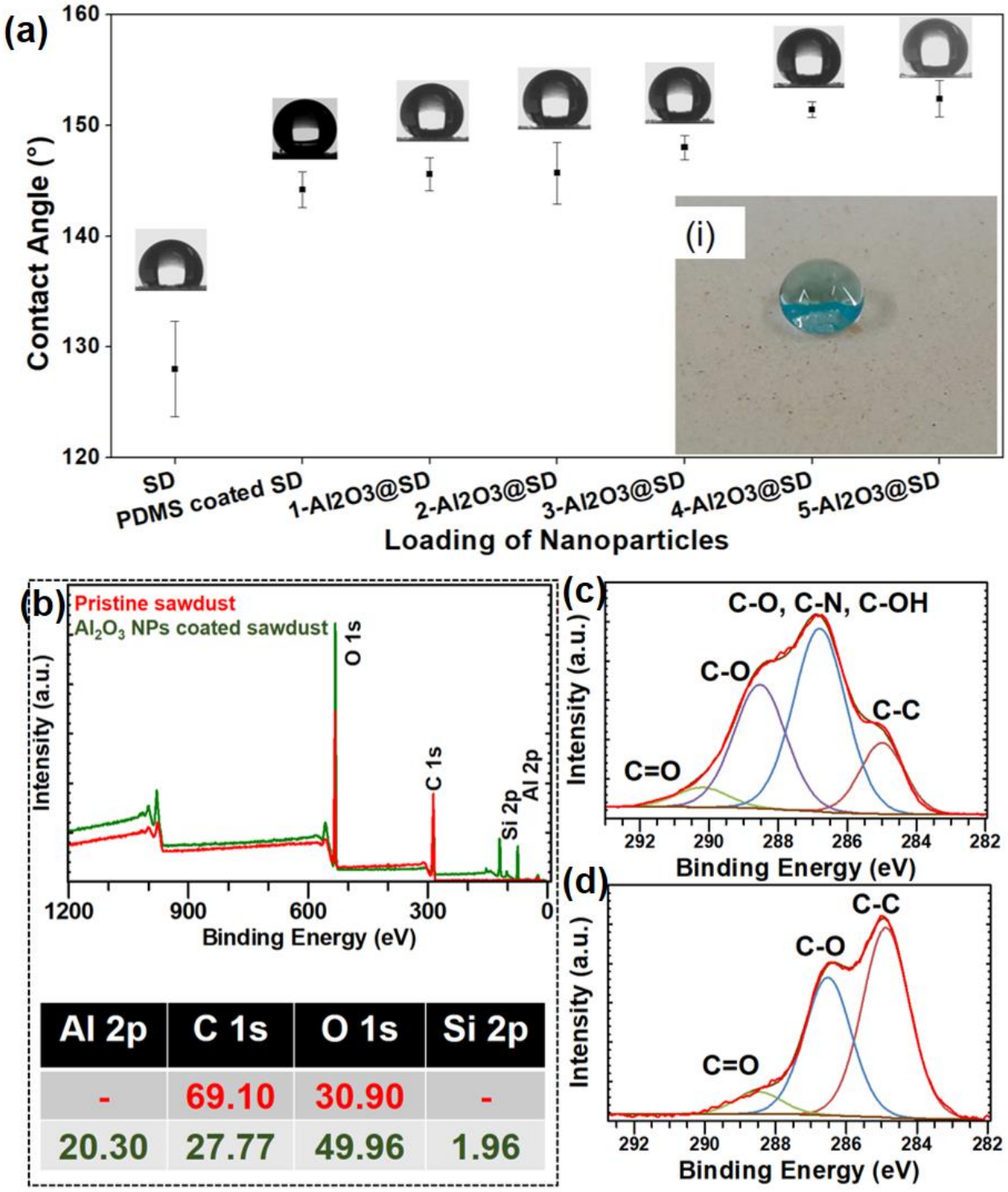

Al 2p	C 1s	O 1s	Si 2p
-	69.10	30.90	-
20.30	27.77	49.96	1.96

Figure 2-3c). SD is mainly composed of cellulose and lignin which are mainly C-O, C-OH C-OC, explaining why the peak at about 286.5 eV is the largest.

After coating with functionalized Al_2O_3 NPs (5-Al_2O_3@SD), new peaks for aluminium and silicon appear. These peaks indicate that the surface of sawdust has been covered with functionalized Al_2O_3 NPs. The quantification of high resolution spectra by peak fitting shows the presence of 20.30 at% aluminium, 27.77 at% carbon, 49.96 at% oxygen and 1.96 at% silicon. The deconvolution of C1s peak from functionalized sawdust also shows carbon bonds, suggesting that the nanoparticle coating is porous and carbon is showing through. Figure S6 shows the FTIR spectra of pristine SD and those coated with functionalized Al_2O_3 NPs. In pristine SD, peaks characteristic to lignin and cellulose (the main constituents of wood) can be seen. A broad band around 3330 cm^{-1} can be observed indicating the OH groups, while a peak at 2890 cm^{-1} indicates stretching vibrations from C-H bonds. The peak at 1732 cm^{-1} can be assigned to the carbonyl groups. Other peaks include 1260 cm^{-1}, 1154 cm^{-1} and 1036 cm^{-1} which can be ascribed to the vibrations from aromatic rings, and C-O bonds in different components of wood (cellulose and lignin). All of these values are in close agreement with literature [245,246]. The intensity of the characteristic peaks found in wood decrease with increased loading of Al_2O_3 NPs. The peaks at 1260 cm^{-1} and 796 cm^{-1} emerge due to increased loading of Al_2O_3 NPs and represent the vibrations from Si-CH_3 and Si-O bonds. These bonds are only present in the Al_2O_3 NPs due to functional groups.

The coating of Al_2O_3 NPs was further confirmed by secondary electron SEM imaging. The surface of SD particles is smooth before deposition of Al_2O_3 NPs (**Figure 2-4**a). A rough surface is observed in samples coated with Al_2O_3 NPs. A uniform film of Al_2O_3 NPs is formed with increasing loading of NPs in coating solution (Fig. S1 and 2). The best distribution is achieved in

the samples with the highest loading of NPs (4-Al_2O_3 @SD and 5-Al_2O_3 @SD) (**Figure 2-4**b). These are the same samples with highest contact angles which can be related to the distribution of Al_2O_3 NPs.

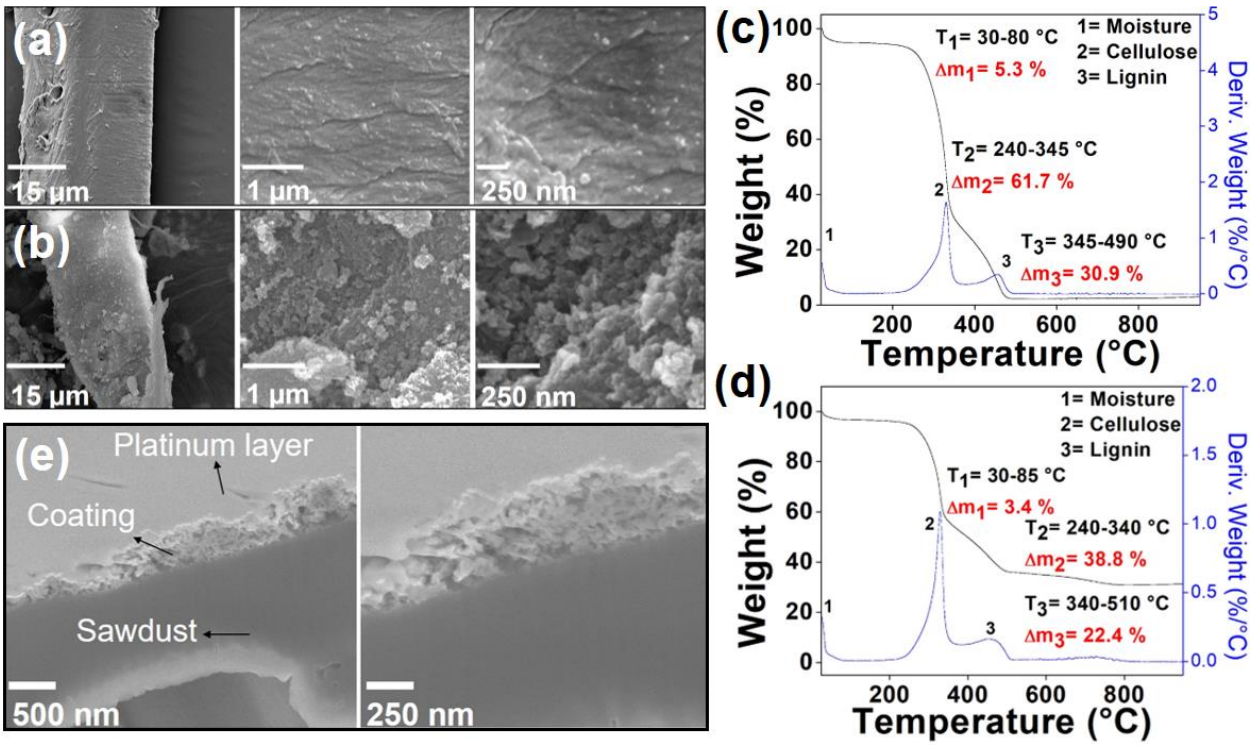

Figure 2-4: SEM images showing the morphology of (a)pristine sawdust and (b) 5- Al_2O_3 @SD. Samples of pristine SD and 5-Al_2O_3 @SD were subjected to thermal analysis in air and the results are shown in **Figure 2-*4*** c and d. There are three stages of weight loss from the pristine SD which we believe derive from the following steps: (i) removal of moisture from 30 to 80°C; (ii) loss of cellulose (61.7%) from 240 to 345°C; and (iii) loss of lignin (31%) from 345 to 490°C. After three stages of weight loss, the residue of SD was almost zero indicating that the SD was completely burned. There is some residue left in the TGA analysis of results of 5-Al_2O_3 @SD which is presumably from the coated Al_2O_3 NPs (**Figure 2-*4***d). Also, a small trend of weight loss above 500 °C can be observed which is identical to the TGA of Al_2O_3 NPs. We potentially ascribe this

to weight loss from the degradation of functional groups. The residue which is 30.9 % is from the Al_2O_3 NPs which were coated on the surface of sawdust. This value can be used to estimate the loading of NPs. However, due to the extremely irregular and rough morphology of SD it is likely that these data are prone to significant uncertainty.

Although the Al_2O_3 NPs coated SD has a superhydrophobic structure, there is a risk that the NPs may be detached from the SD surface if used in a practical process, particularly one using mechanical agitation, and hence a risk that this could lead to release of nanoparticles into the environment. Therefore, Al_2O_3 NPs were fixed on the surface of SD by using PDMS as binder. To deposit PDMS, a 3 wt.% solution of it was prepared in hexane and 5-Al_2O_3 @SD particles were soaked in three different volumes of this solution and then dried at 90 °C for 2 h. The stability of nanoparticles was checked by mixing the samples with methanol and the filtrate was collected for the measurement of transmittance. The samples were also characterized with by SEM and TGA to observe the morphology and estimate the quantity of PDMS which is binding nanoparticles to the SD particle surface. Further details can be found in the supporting information, Figures S3-S8 and accompanying text.. The best optical transmittance, and thus the most effective adherence of the nanoparticles to the sawdust, was achieved with the maximum amount of PDMS, i.e. 3-PDMS@ Al_2O_3 @SD.

Figure 2-*4*e shows SEM images of a cross section of the particle surface generated by focused ion beam (FIB) milling. The coating consisting of functionalized Al_2O_3 which can be observed between the sawdust and the platinum layer. Fig. S9 shows the EDX mapping of cross section showing that majority of carbon and oxygen is present in the sawdust while aluminium can be observed in the areas where alumina nanoparticles are present. There is a slight deviation between

the EDX map and the SEM image due to minor spatial drift during the EDX mapping because the sample is slightly insulating.

The deposition of PDMS was further confirmed by FTIR and **Figure 2-*5***a shows the spectra obtained. It can be observed that the intensity of characteristic peaks of PDMS increases with increasing loading. The 3-PDMS@ Al_2O_3 @SD powder sample was also analysed with XPS and the quantification from high resolution spectra shows the presence of 12.09 at% aluminium, 40.63 at% carbon, 39.03 at% oxygen and 8.23 at% silicon. The amount of silicon is significantly increased after PDMS coating which clearly indicates its blending within the Al_2O_3 NPs and sawdust structure. The Al 2p peak representing the alumina nanoparticles is also still present after PDMS coating. The deconvolution of C1s peak is shown in the inset of **Figure 2-*5***b: it shows three chemical states with a major peak appearing at 284.9 eV indicating C-C bonds, though it should be noted that the Si-C peak appears at same energy level so this might be a combination of two peaks. It can be concluded that the PDMS is finely distributed and alters neither the morphology nor the chemical structure significantly. A typical PDMS coating would normally be expected to form a layer hiding the structure of nanoparticles, but that appears not to be the case in the results presented here. The Si 2p appears at 102.38 which corresponds to a polysiloxane structure. Hence the PDMS is stabilizing the nanoparticles on sawdust surface thus generating a stable superhydrophobic surface on sawdust particles.

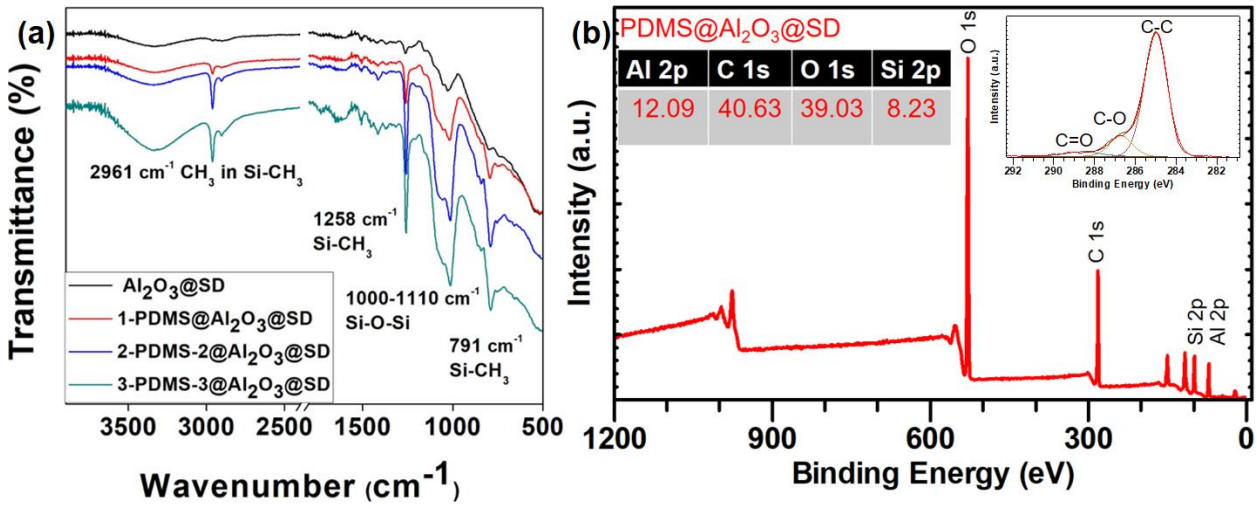

Figure 2-5: (a) FTIR and (b) XPS spectra of 3-PDMS@ Al_2O_3 @SD samples

After optimizing the deposition of PDMS, the 3-PDMS@ Al_2O_3 @SD was used for separation of surfactant stabilized emulsions. The nanocomposite particles can also be used for the collection of oil from the surface of water as shown in the **Figure 2-*6***a. The particle readily absorbs toluene (red, dyed with Sudan III) while repelling water due to their excellent superhydrophobic properties. **Figure 2-*6***b and c show the separation process in which 1g 3-PDMS@ Al_2O_3 @SD was added in 10 ml emulsion and manually shaken for 5 min and then filtered.

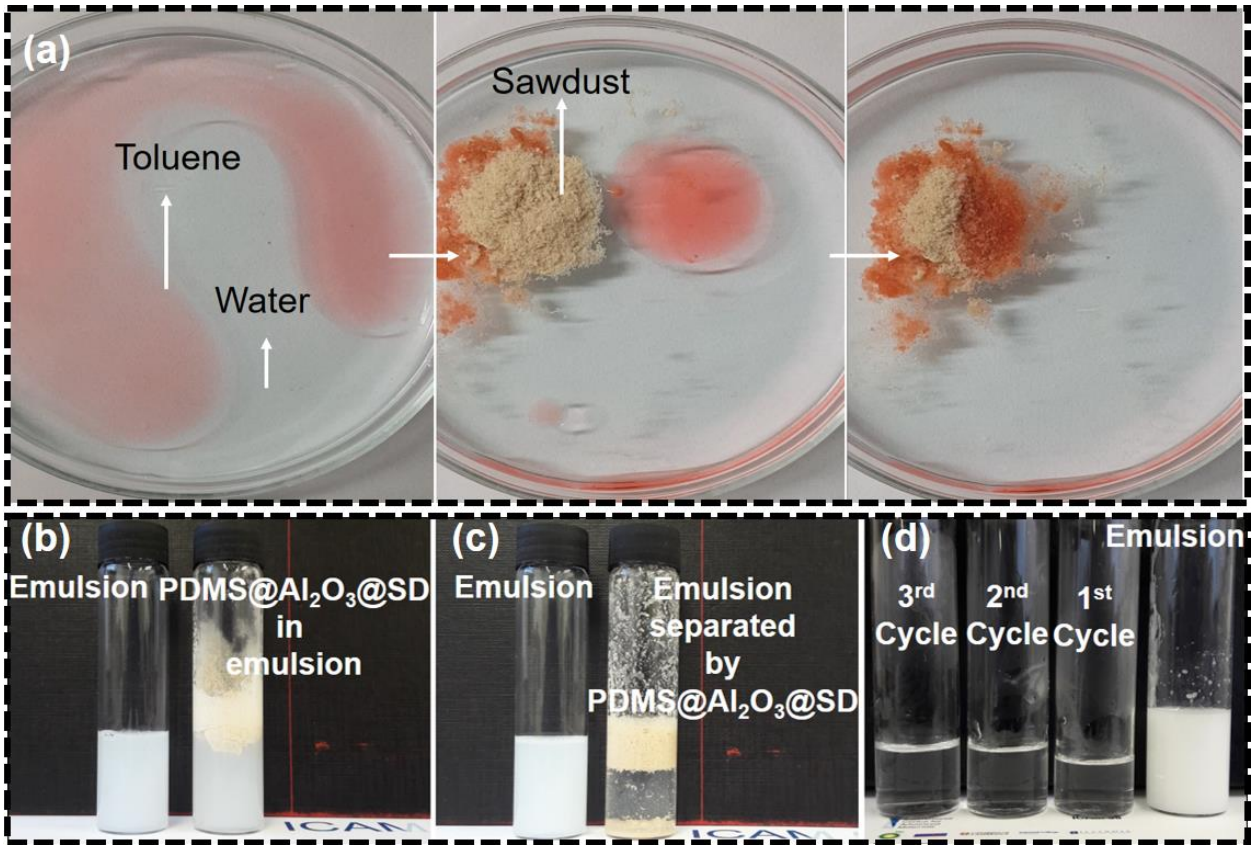

Figure 2-6: (a) Digital images showing the collection of toluene (red) from the surface of water (blue) by 3-PDMS@Al_2O_3@SD; (b, c) Digital images showing the separation of emulsion by 3-PDMS@Al_2O_3@SD; and (d), emulsion before and after separation for 3 cycles.

Four different loadings of toluene (5 ml= T_1, 10 ml= T_2, 15 ml= T_3, 20 ml= T_4 in 100 ml water) were studied and separation was performed for three cycles for each loading. The emulsions were characterized with optical microscopy to observe oil droplets in emulsion before and after separation. **Figure 2-7**a shows the transmittance of emulsion T_1 before and after separation. The transmittance results show that the emulsion has virtually zero transmittance while the transmittance becomes more than 80 % after treatment with 3-PDMS@ Al_2O_3 @SD. The recyclability was observed by using the same adsorbent again and introducing new emulsion. The absorbent was washed with acetone and dried in an oven before each cycle of separation. The

absorbent showed good recyclability as the transmittance of emulsion improved for all three cycles of separation.

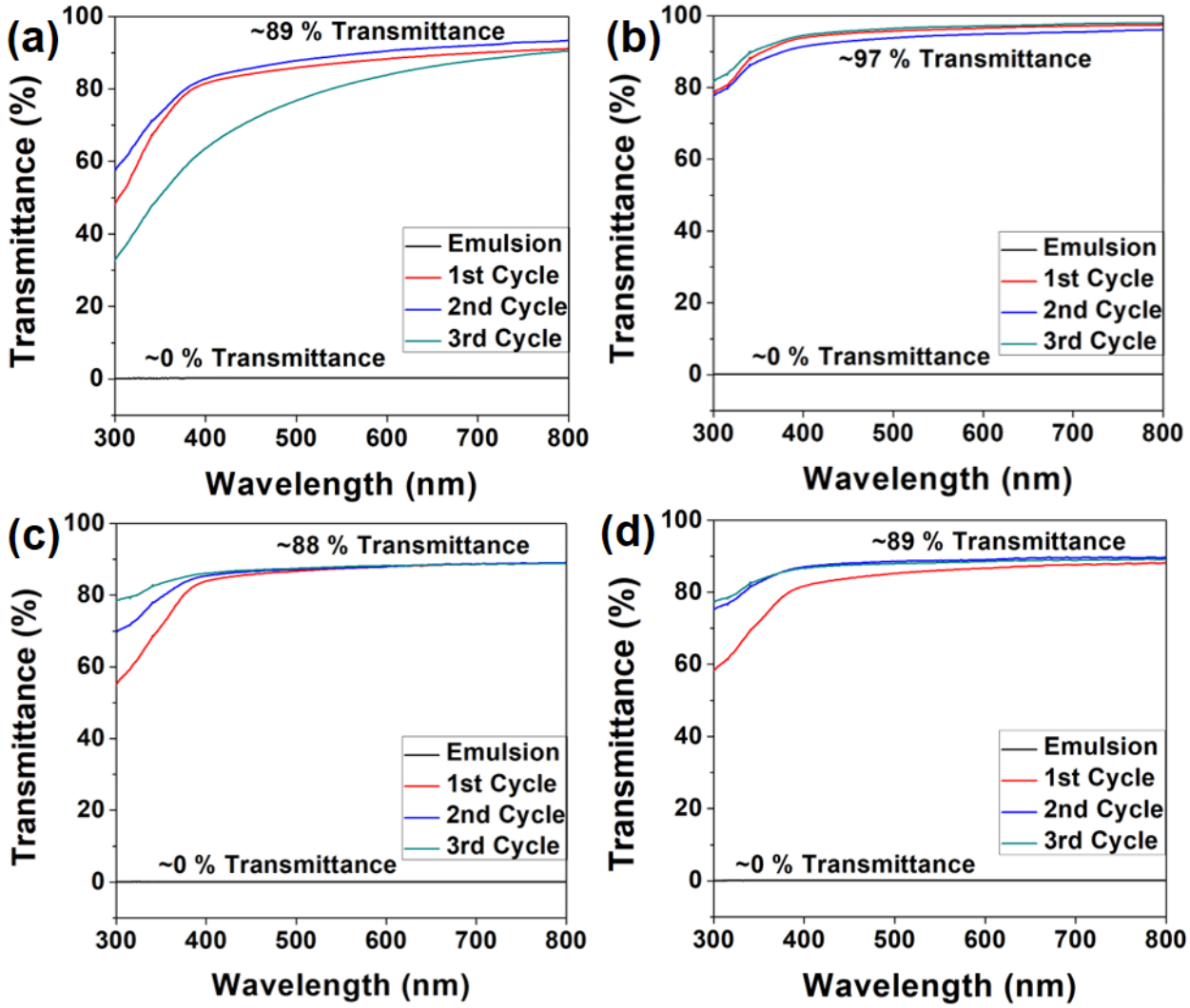

Figure 2-7: Transmittance of emulsion before and after separation (a) T_1, (b) T_2, (c) T_3, and (d) T_4.

Figure 2-*7*b shows the results for emulsion T_2, showing that 3-PDMS@ Al_2O_3 @SD effectively removes oil droplets from this emulsion as the transmittance is about 90 % in all cycles. The same is the case with T_3 and T_4 as evidenced in **Figure 2-*7***c and d. Optical microscopy images of emulsions before and after separation are shown in **Figure 2-*8***. The emulsions contain numerous droplets of toluene well dispersed in water and the quantity of droplets is increased with higher volume of toluene. After treatment with 3-PDMS@ Al_2O_3 @SD particles, most of the toluene is removed and optical microscopy images indicate very little oil for three cycles of separation. The particles are also fairly effective in separating other types of oils such as the complex mixtures of triglycerides in olive oil (Supporting Information).

Superhydrophobic absorbents follow a simple approach of physical separation via selective absorption of oil from an emulsion. The superhydrophobic nature of the absorbent prevents its interaction with water. The powder can easily go into the emulsions through mechanical agitation due to its small size and capture the uniformly distributed oil droplets in the water phase. Later, the absorbent can be separated from emulsion and can be washed for next cycle of separation. As this process follows simple selective absorption of oil from emulsion without using complex apparatus or processes, it is believed that this could be a simple and cost effective solution for the separation of oil/water mixtures and emulsions [107,108,247].

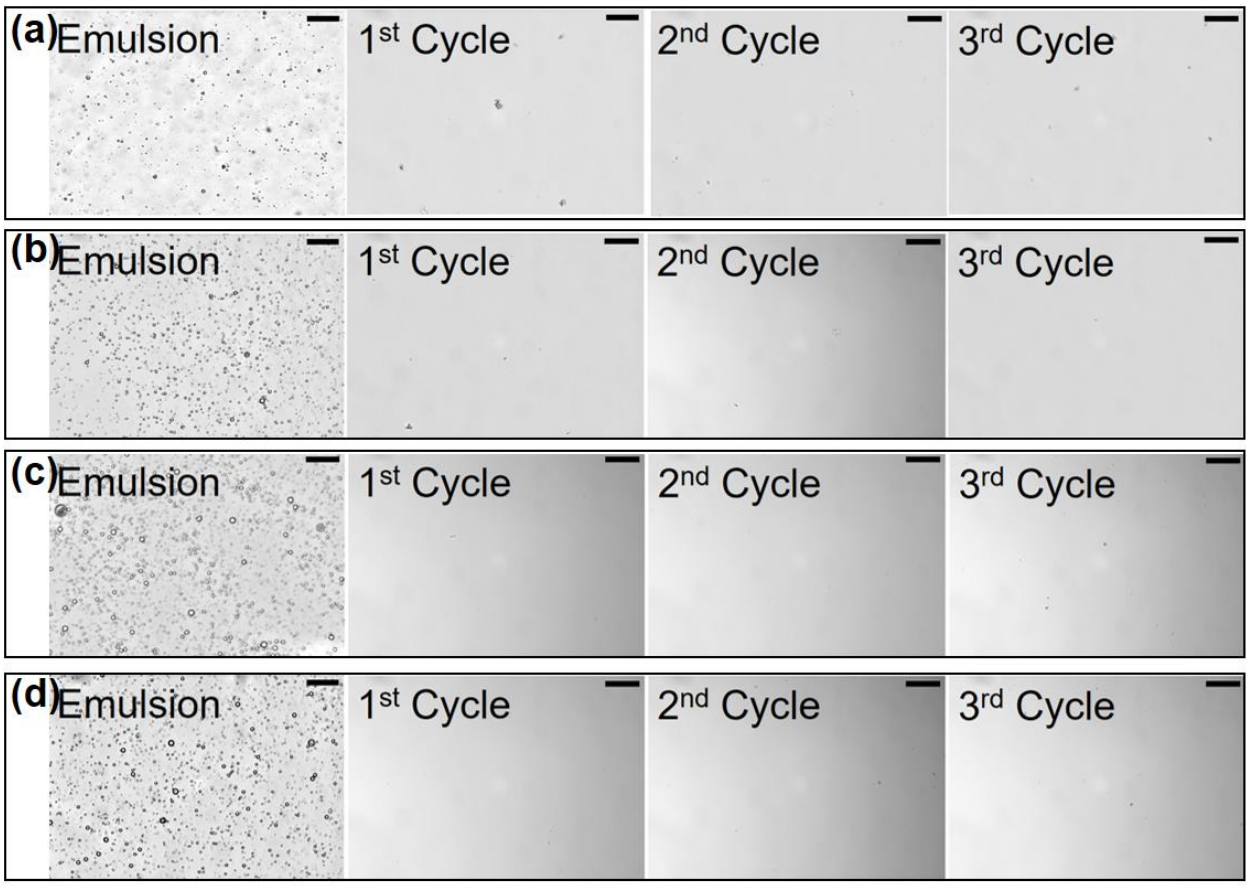

Figure 2-8: Optical microscope images before and after separation (a)T_1 (b), T_2 (c), T_3 and (d)T_4 Scale bar on all images is 50 µm.

2.5 Conclusion

Superhydrophobic composite particles were prepared by coating the surface of micron-sized sawdust particles with functionalized alumina nanoparticles followed by deposition of polydimethylsiloxane (PDMS). The uniform coating of alumina nanoparticles on sawdust particles imparts a superhydrophobic character while PDMS strengthens the nanoparticle network thus generating a stable superhydrophobic absorbent. The material was further characterized with XPS and FIB to investigate the role of alumina nanoparticles and PDMS in separation and recyclability. The composite particles effectively separate surfactant stabilized oil in water emulsions. It is found from the recyclability experiments that these composite particles can be used for multiple

separation cycles. If used industrially it could be envisaged that the particles will be mixed with the emulsion and then separated via pressure or in-line filtration once they have completely absorbed the oil and broken the emulsion.

2.6 Supplementary information

Results and Discussion

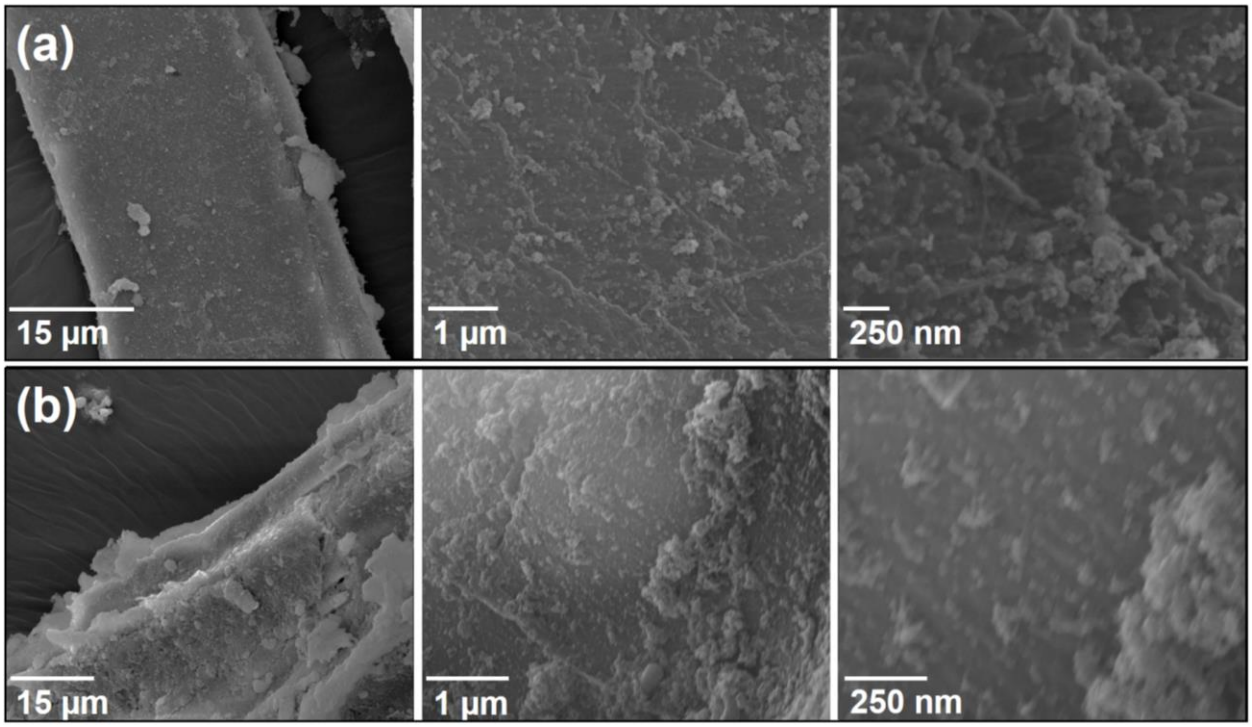

Figure S1: SEM images showing the morphology of the 1- Al_2O_3 @SD (a) and 2- Al_2O_3 @SD (b). Some nanoparticles are seen on the surface of sawdust under these conditions, however, they are not uniformly distributed and does not cover the entire surface

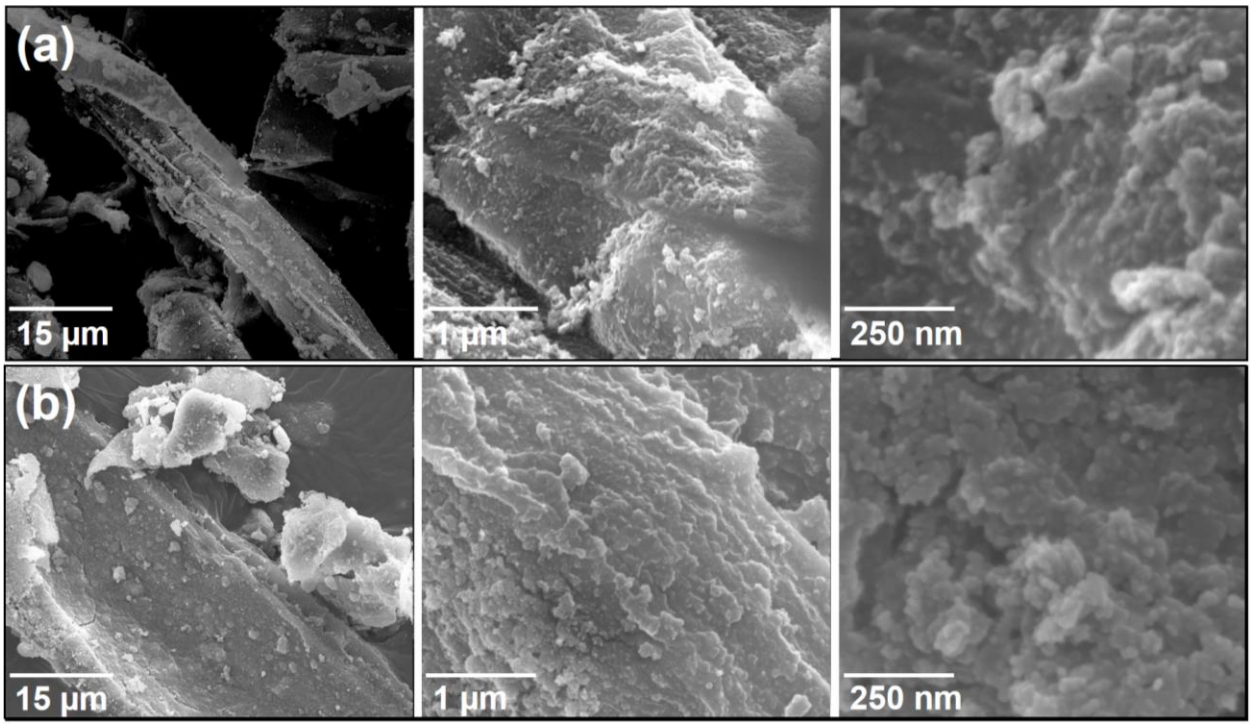

Figure S2: SEM images showing the morphology of the 3- Al_2O_3 @SD (a) and 4- Al_2O_3 @SD (b). The coating of nanoparticles becomes gradually uniform by increasing the laoding of nanoparticle in the suspension. The surface of sawdust is effectively covered in case of 4- Al_2O_3 @SD. The uniformity of this coating is directly linked with the contact angle as discussed in the main text.

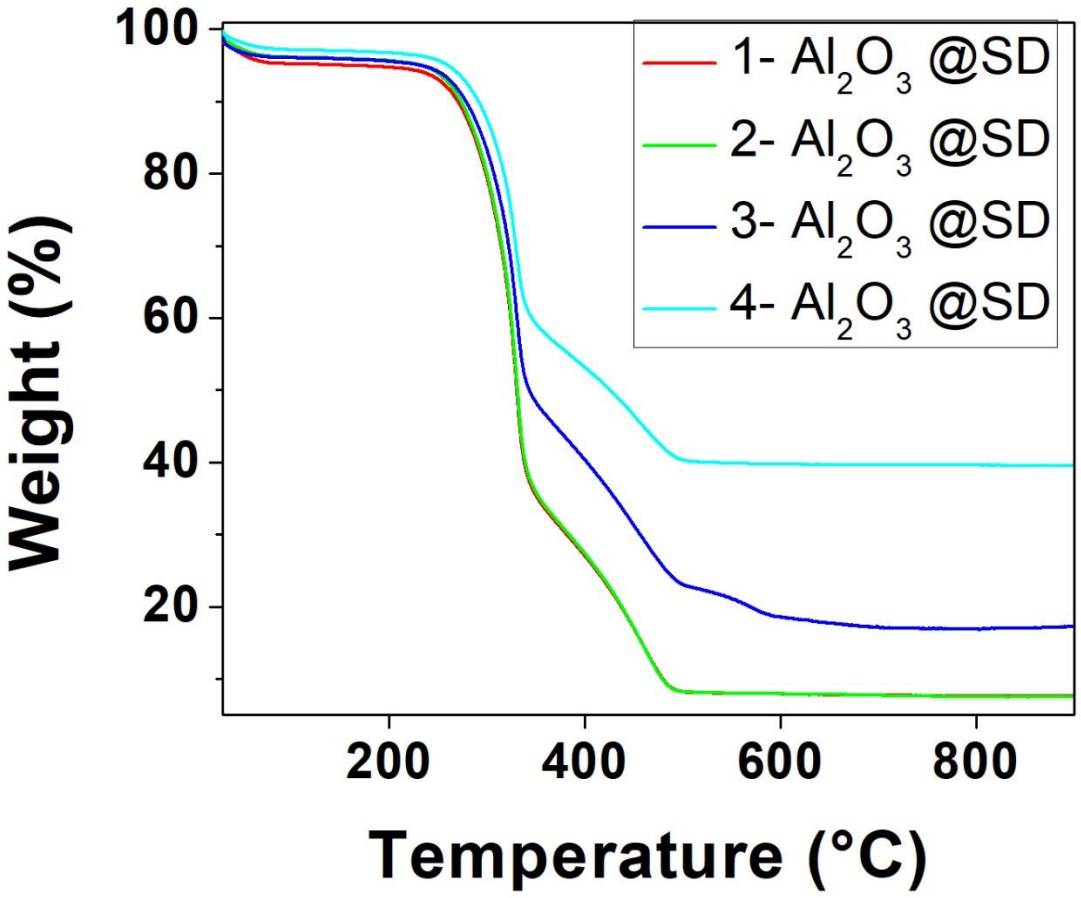

Figure S3: Thermogravimetric analysis of 1- Al_2O_3@SD, 2- Al_2O_3@SD, 3- Al_2O_3@SD and 4- Al_2O_3@SD.

Figure S3 shows the TGA analysis of samples 1- Al_2O_3@SD, 2- Al_2O_3@SD, 3- Al_2O_3@SD and 4- Al_2O_3@SD. The residue left after degradation of wood is increased with higher loading of nanoparticles. TGA provides weight loss and the residue left at the end gives an approximation of loading of nanoparticles. As the geometry of sawdust is very irregular and weight of residue (nanoparticles) would be different in every cycle that is why a direct relation cannot be established. However, an approximate loading can be inferred after which material achieve superhydrophobic properties. In this case, the sawdust becomes superhydrophobic for samples 4-Al_2O_3@SD and 5-Al_2O_3@SD. The loading of nanoparticles in these cases is more than 35%. Other samples show

low loadings (3-Al_2O_3@SD= ~22.5 %, 2-Al_2O_3@SD= 8.3%, 1-Al_2O_3@SD= 8.2%) and correspondingly low contact angles.

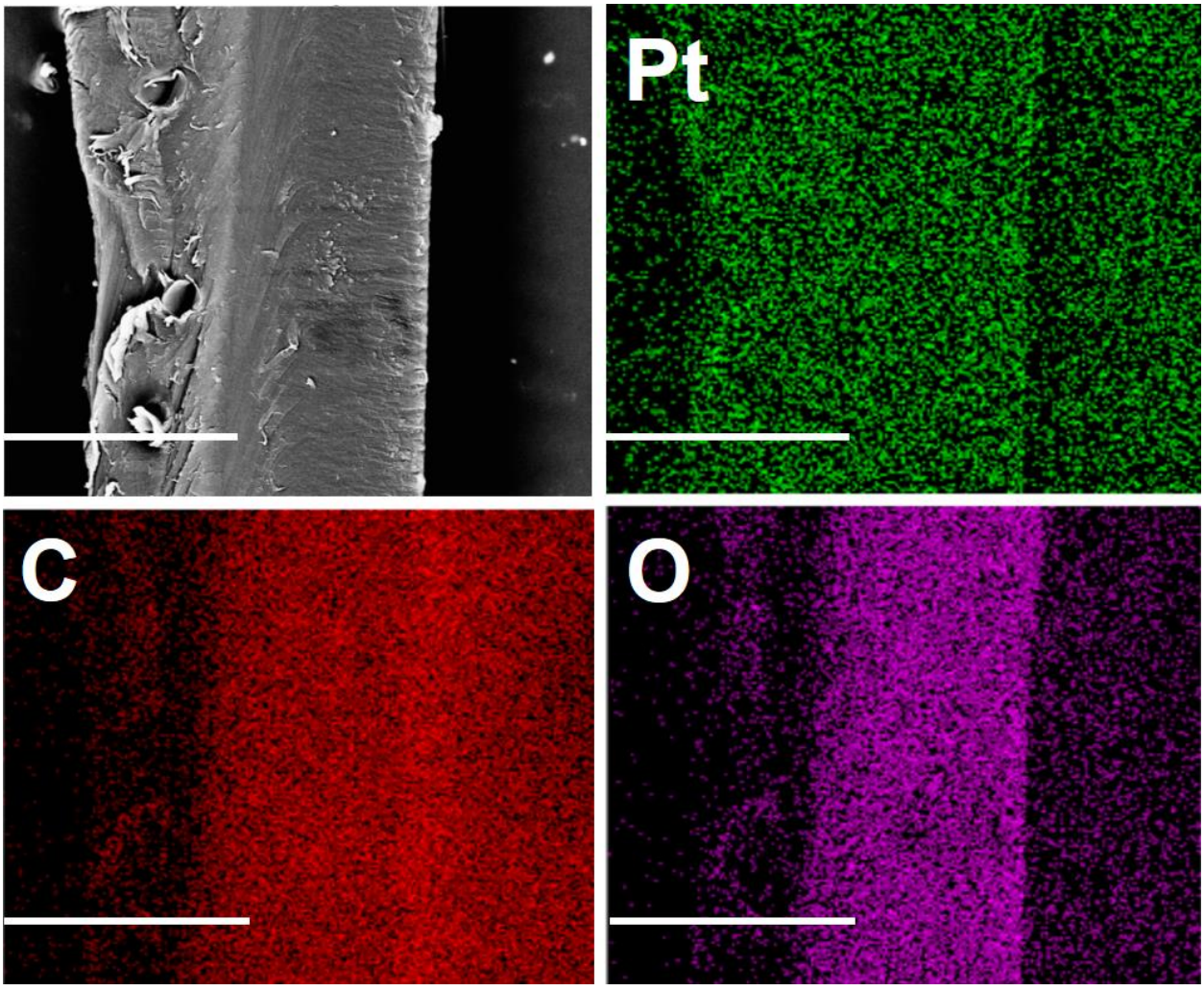

Figure S4: EDS analysis of pristine sawdust

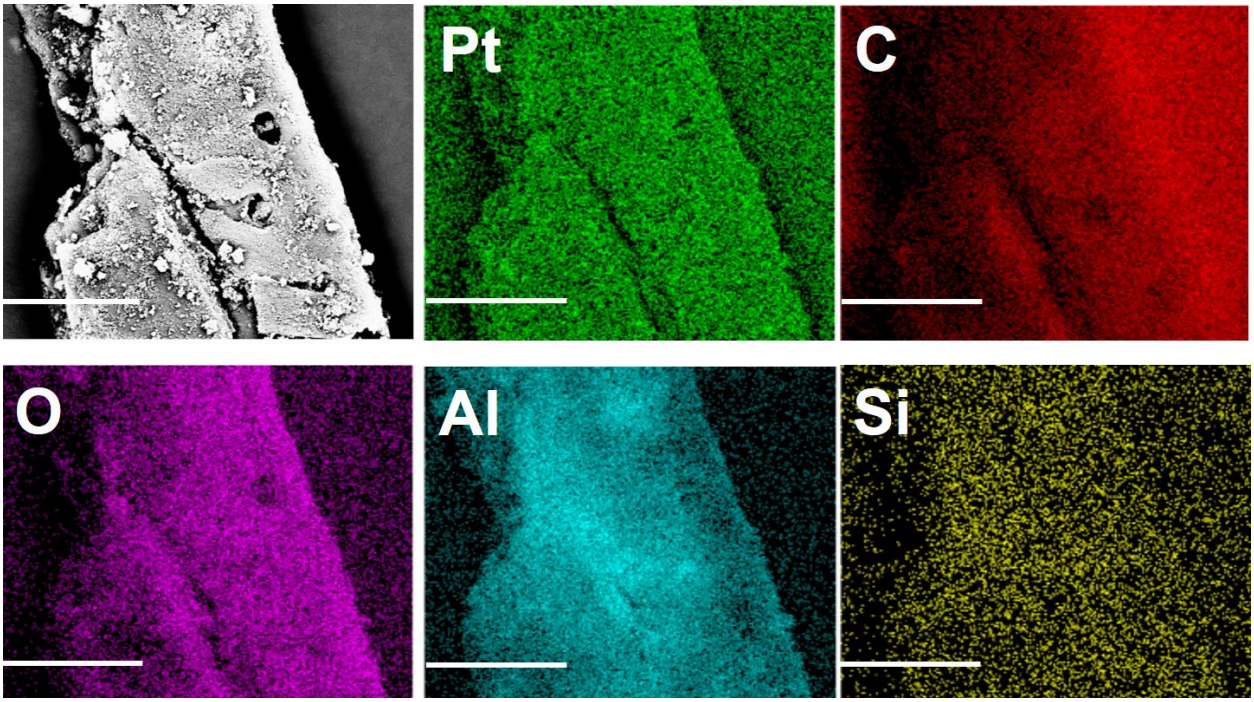

Figure S5: EDS analysis of coated sawdust (5-Al_2O_3 @SD)

Figure S4 and S5 shows the EDS mapping of sawdust before and after coating with Al_2O_3 nanoparticles. The pristine sawdust shows three different elements; platinum from the conductive coating on sample while carbon and oxygen are the main constituents of sawdust. When sawdust is coated with Al_2O_3 nanoparticles, two new elements appear; aluminium and silicon which are from functionalized nanoparticles. The signals for silicon are weak as compared to other elements as it is only present as functional groups. The EDS mapping confirms the uniform coating of Al_2O_3 nanoparticles on the surface of sawdust.

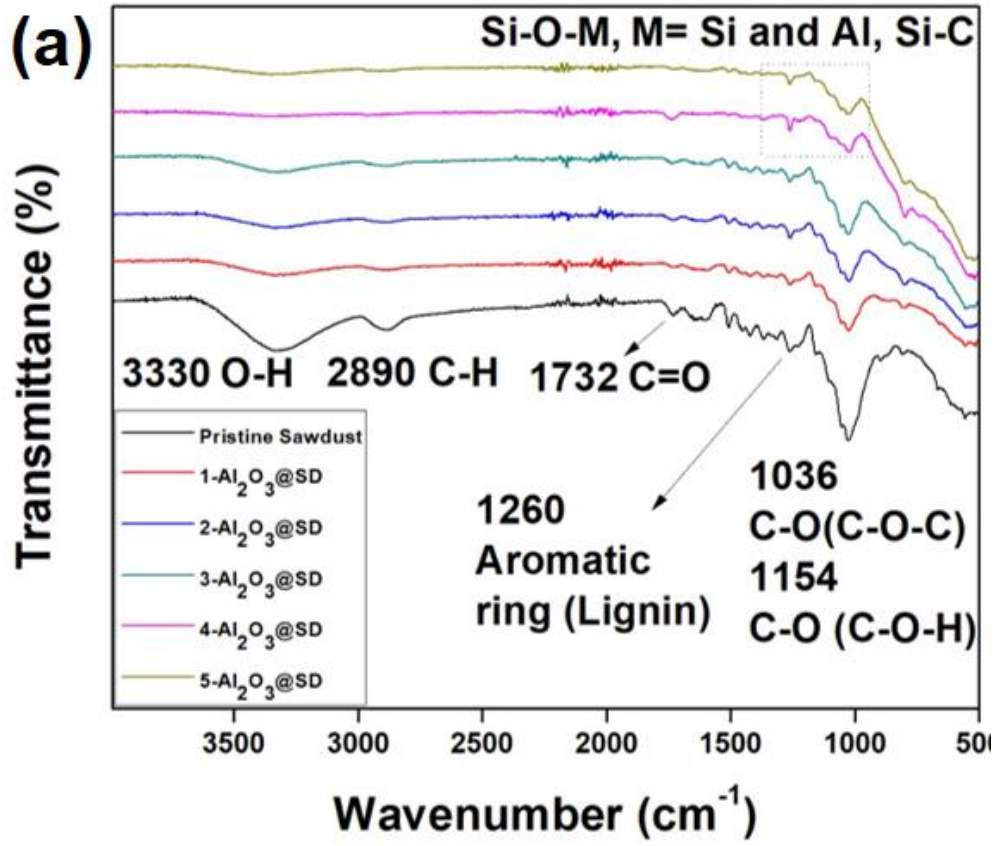
(a)
Si-O-M, M= Si and Al, Si-C
Transmittance (%)
3330 O-H
2890 C-H
1732 C=O
1260
Aromatic
ring (Lignin)
1036
C-O(C-O-C)
1154
C-O (C-O-H)
Pristine Sawdust
1-Al2O3@SD
2-Al2O3@SD
3-Al2O3@SD
4-Al2O3@SD
5-Al2O3@SD
3500
3000
2500
2000
1500
1000
Wavenumber (cm-1)

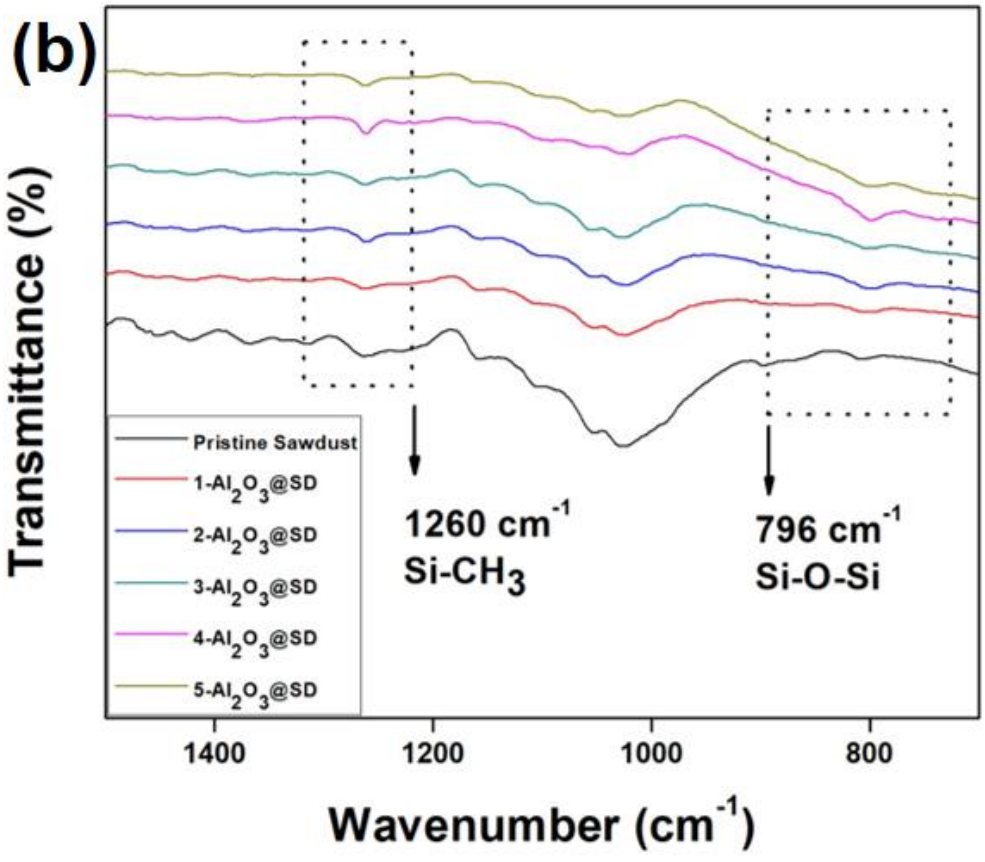
(b)
Transmittance (%)
1260 cm-1
Si-CH3
796 cm-1
Si-O-Si
Pristine Sawdust
1-Al2O3@SD
2-Al2O3@SD
3-Al2O3@SD
4-Al2O3@SD
5-Al2O3@SD
1400
1200
1000
800
Wavenumber (cm-1)

Figure S6: FTIR spectra of (a) sawdust coated with Al_2O_3 nanoparticles (magnified spectra)

To deposit PDMS, a 3 wt.% solution of it was prepared in hexane and 5-Al_2O_3 @SD particles were soaked in three different volumes of this solution and then dried at 90 °C for 2 h. This produces two different types of particles as shown in Fig.S7c: there is an agglomerated layer like structure on the surface, and a powder is present under that layer. To check the stability, 0.2 g 5- Al_2O_3 @SD particles before and after coating with different amount of PDMS were stirred (400 rpm for 2 min) in methanol and the filtrate was collected for analysis, as shown in Fig. S7a. Fig. S7b shows the optical transmittance of 5- Al_2O_3 @SD particles before and after deposition of PDMS. It is clear from the colour of filtrate that some of the Al_2O_3 NPs left the surface to make a suspension with methanol before PDMS coating and remained in it even after filtration. However, the filtrate became clear with increasing loading of PDMS as shown in the transmittance curve in visible range. The best optical transmittance was achieved in case of 3-PDMS@ Al_2O_3 @SD .

The Fig. S8 shows the SEM images of 1-PDM@ Al_2O_3 @SD and 2-PDM@ Al_2O_3 @SD while Fig. S9 shows the morphology of 3-PDM@ Al_2O_3 @SD. A change in surface morphology can be observed as PDMS tends to form a smooth surface; we conclude that while it is important to use sufficient PDMS to adhere the Al_2O_3 NPs effectively to the surface, too much will replace the rough structure created by Al_2O_3 NPs with a smooth structure, thereby reducing the superhydrophobic character of the surface. Fig. S9 shows the SEM images of two different particles of 3-PDM@ Al_2O_3 @SD. Rough surface morphologies caused by Al_2O_3 NPs can be observed in both images. Moreover, the water contact angle of the surface made by 3-PDMS@ Al_2O_3 @SD is 152.0° ± 1.7

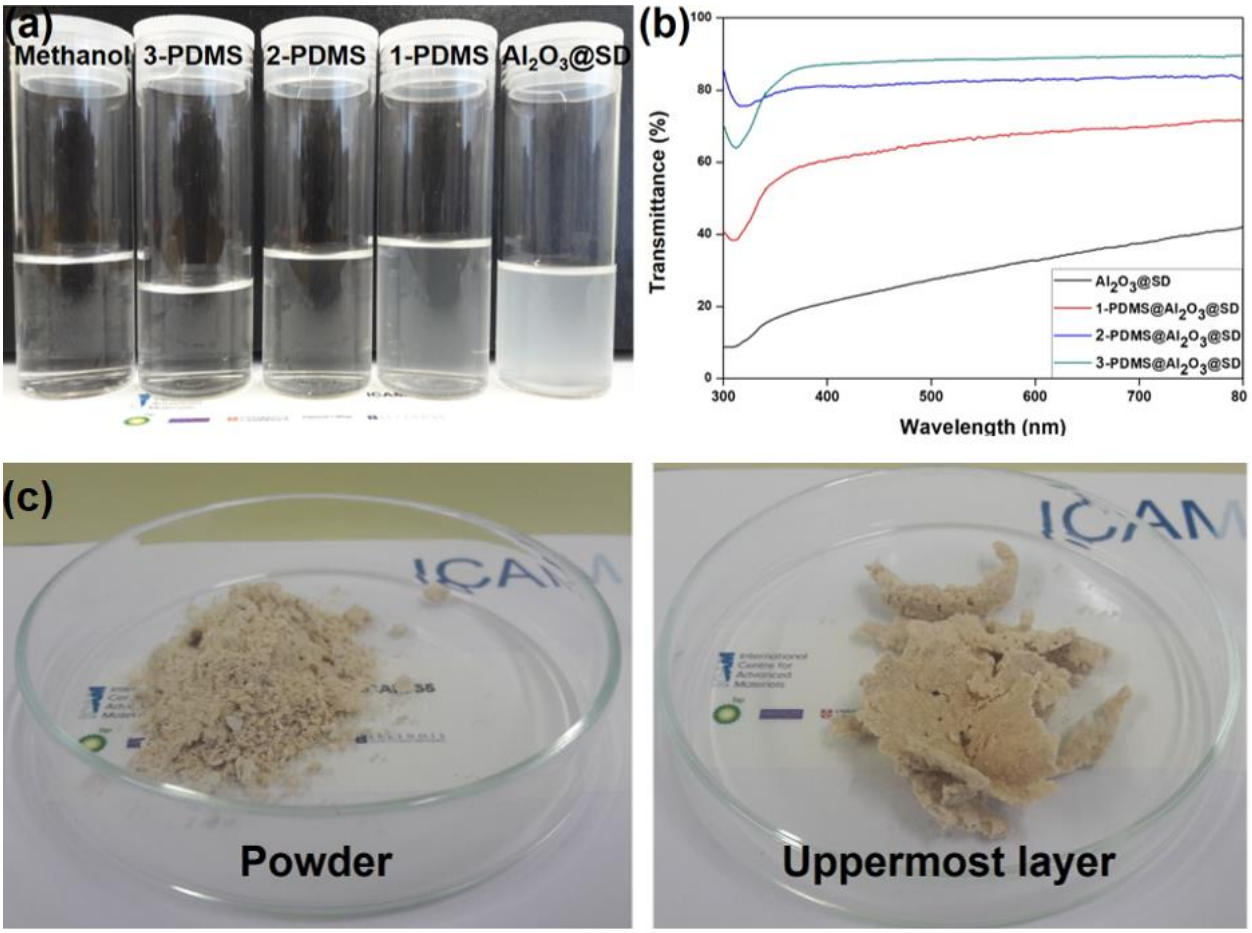

Figure S7: Digital images showing the filtrate (a) Transmittance spectra of samples before and

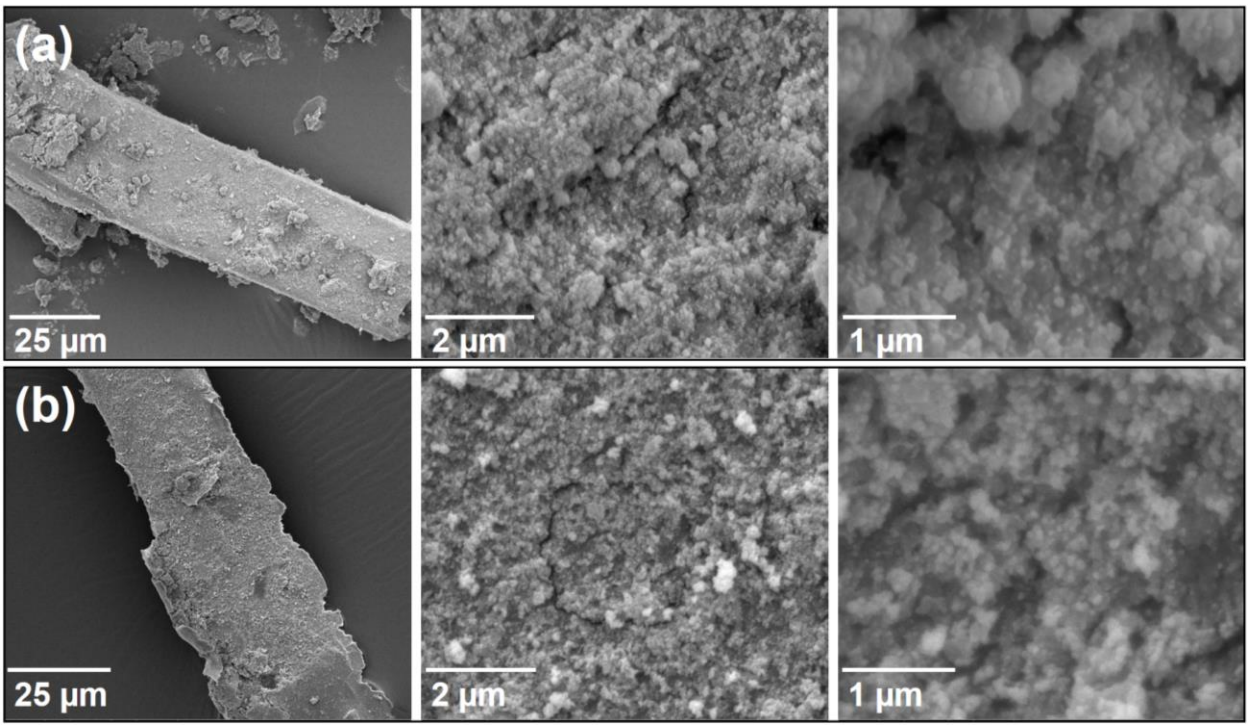

Figure S8: SEM images showing the morphology of the 1-PDMS@Al_2O_3@SD (a) and 2-PDMS@Al_2O_3@SD (b)

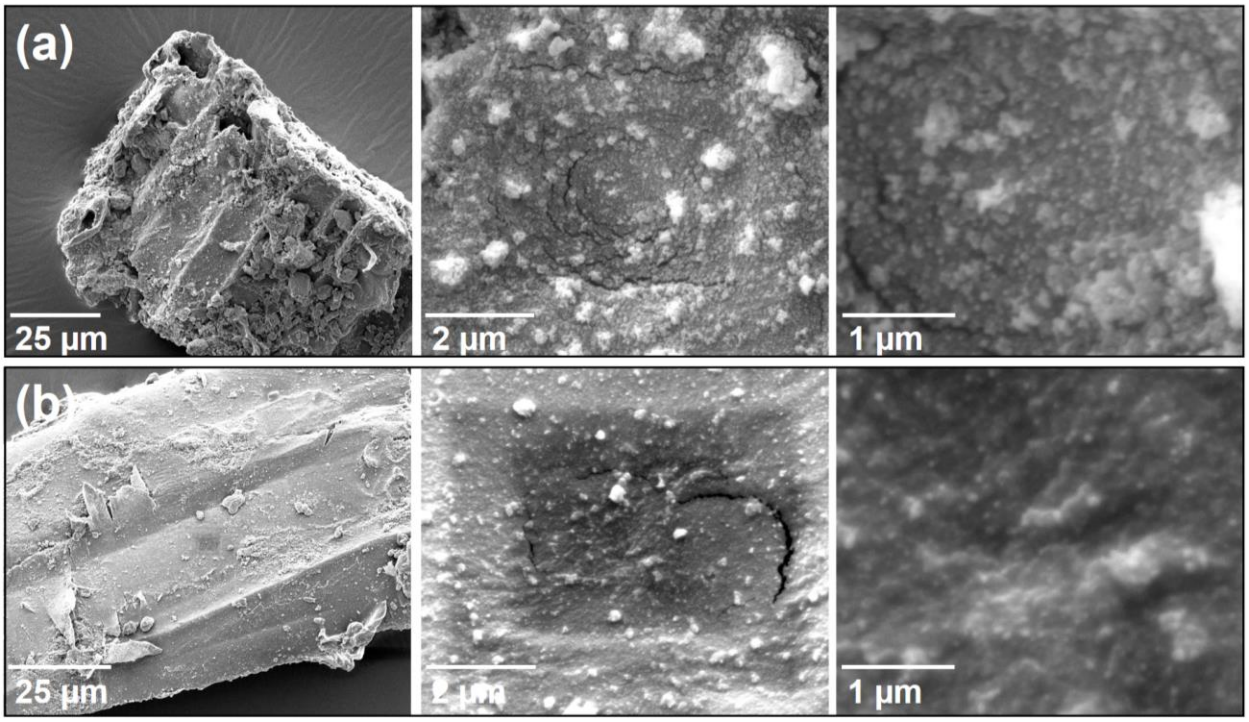

Figure S9: SEM images showing the morphology of two different particles of 3-PDMS@Al_2O_3@SD

To estimate the quantity of PDMS which is binding nanoparticles to the SD particles surface, TGA experiments were performed before and after PDMS deposition. Two different particles from the 3-PDM@ Al_2O_3 @SD samples were selected. One of them consisted of loose powder, the other of agglomerated flakes. It was suspected that the flakes contained a higher loading of PDMS compared to the loose particles. Fig. S10 and S11 show the TGA results for particles before and after PDMS deposition, while Fig. S12 shows the TGA for the flakes. These experiments were carried out in alumina crucibles and the samples were collected from the same batch to minimize the experimental errors. There are three stages of weight loss in all these results indicating the loss of moisture, cellulose, lignin and functional groups of Al_2O_3 NPs. An interesting behaviour can be found when the weight loss in all these results is compared. The weight loss from 240 to 345°C (corresponding to degradation of cellulose) is decreased in samples with PDMS coating. However, the weight loss from 345 to 490°C is increased in samples with PDMS coating, and is highest in the sample with the highest loading of PDMS. A previous study where thermal degradation of PDMS and its composite with graphene oxide was studied in N_2 environment found that PDMS degradation starts at 400 °C and completes at 600 °C with ~20 % residue [248]. This explains the increase in weight loss between 345 and 490°C. Also, a significant difference in the shape of curve can be observed as the curve becomes steeper with increased loading of PDMS. By subtracting the weight loss of lignin before coating of PDMS, it can be concluded that ~9.27% weight loss in particles and ~15.47% weight loss in flakes is from degradation of PDMS.

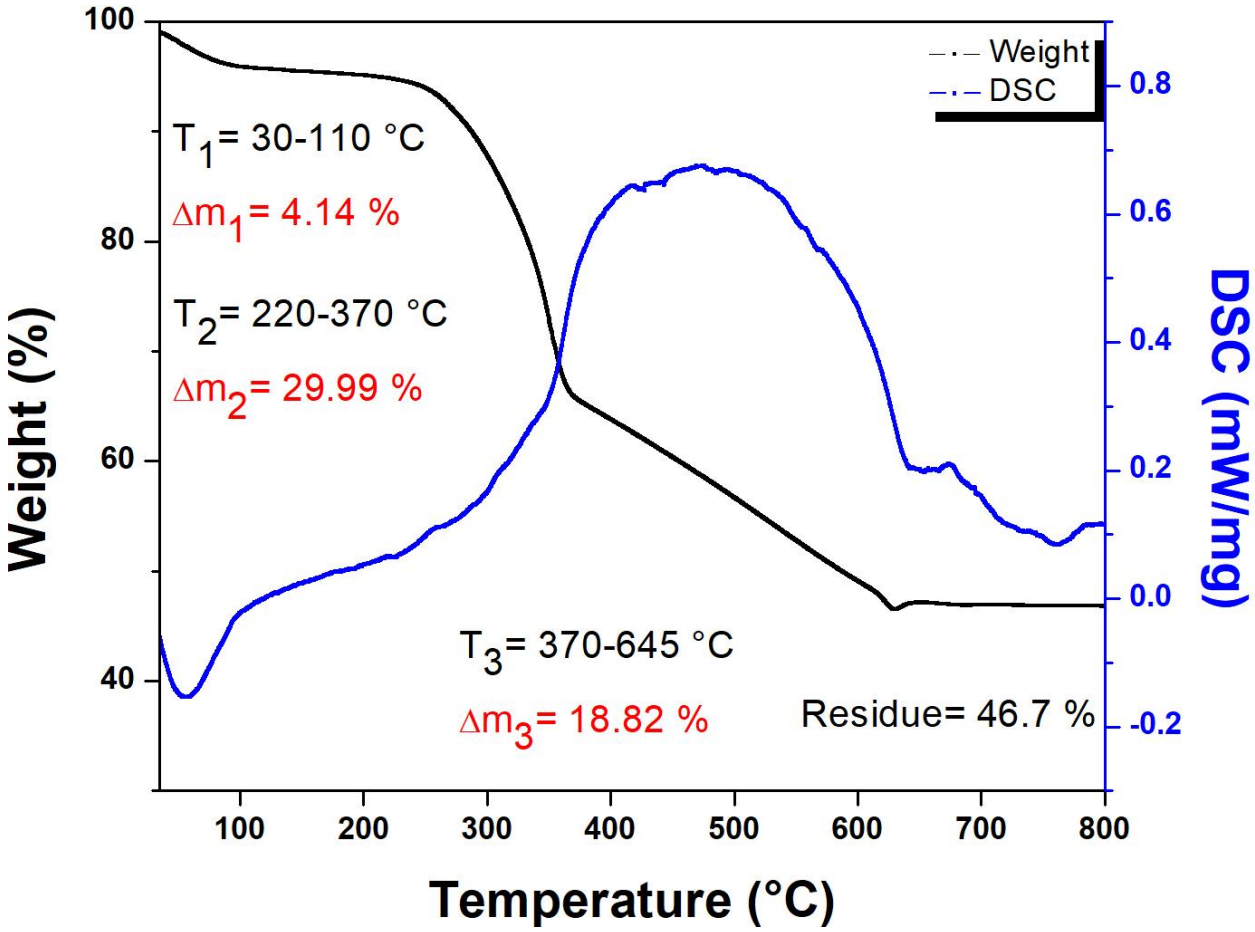

Figure S10: Thermal analysis of particles without PDMS

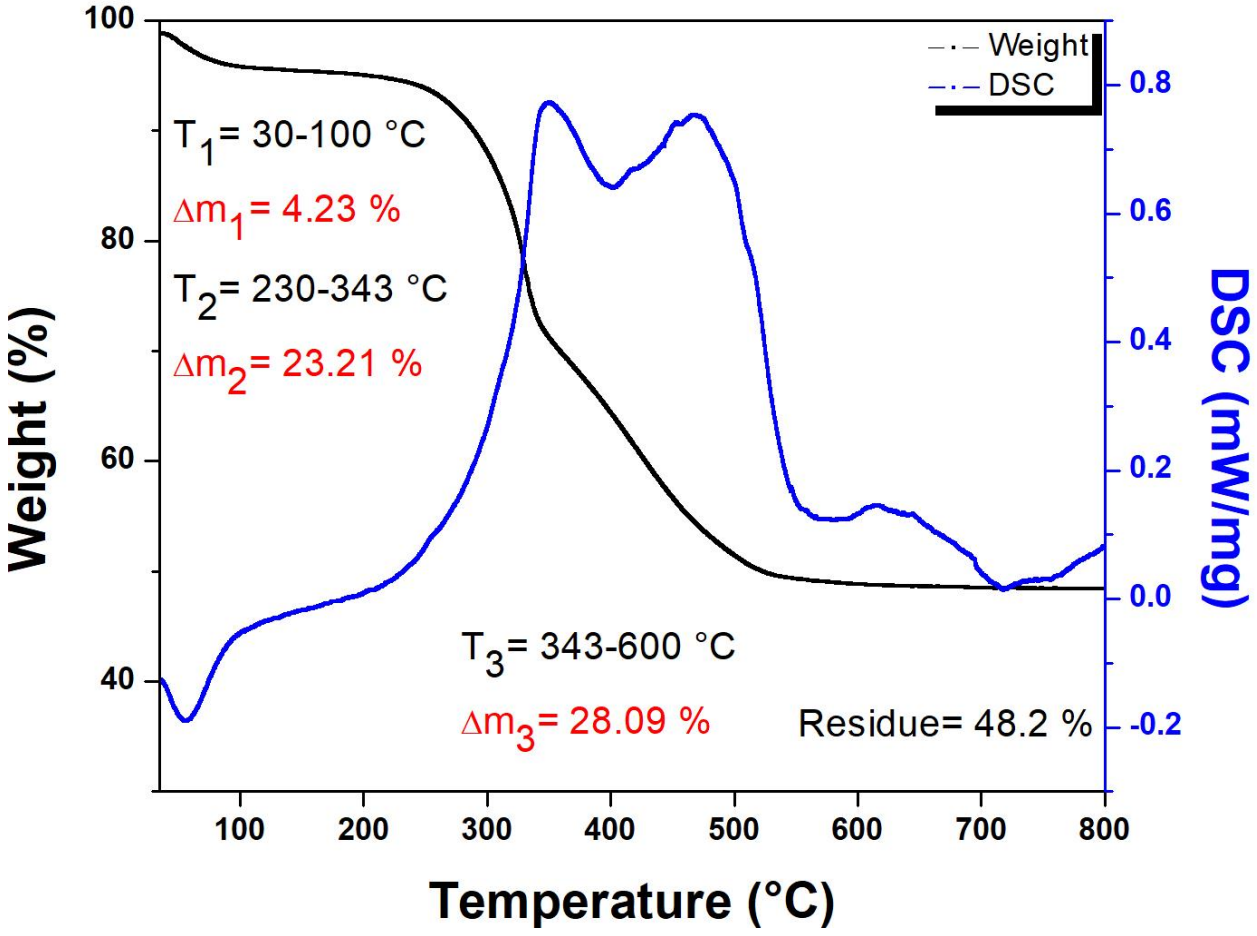

Figure S11: Thermal analysis of 3-PDMS@Al_2O_3@SD particles

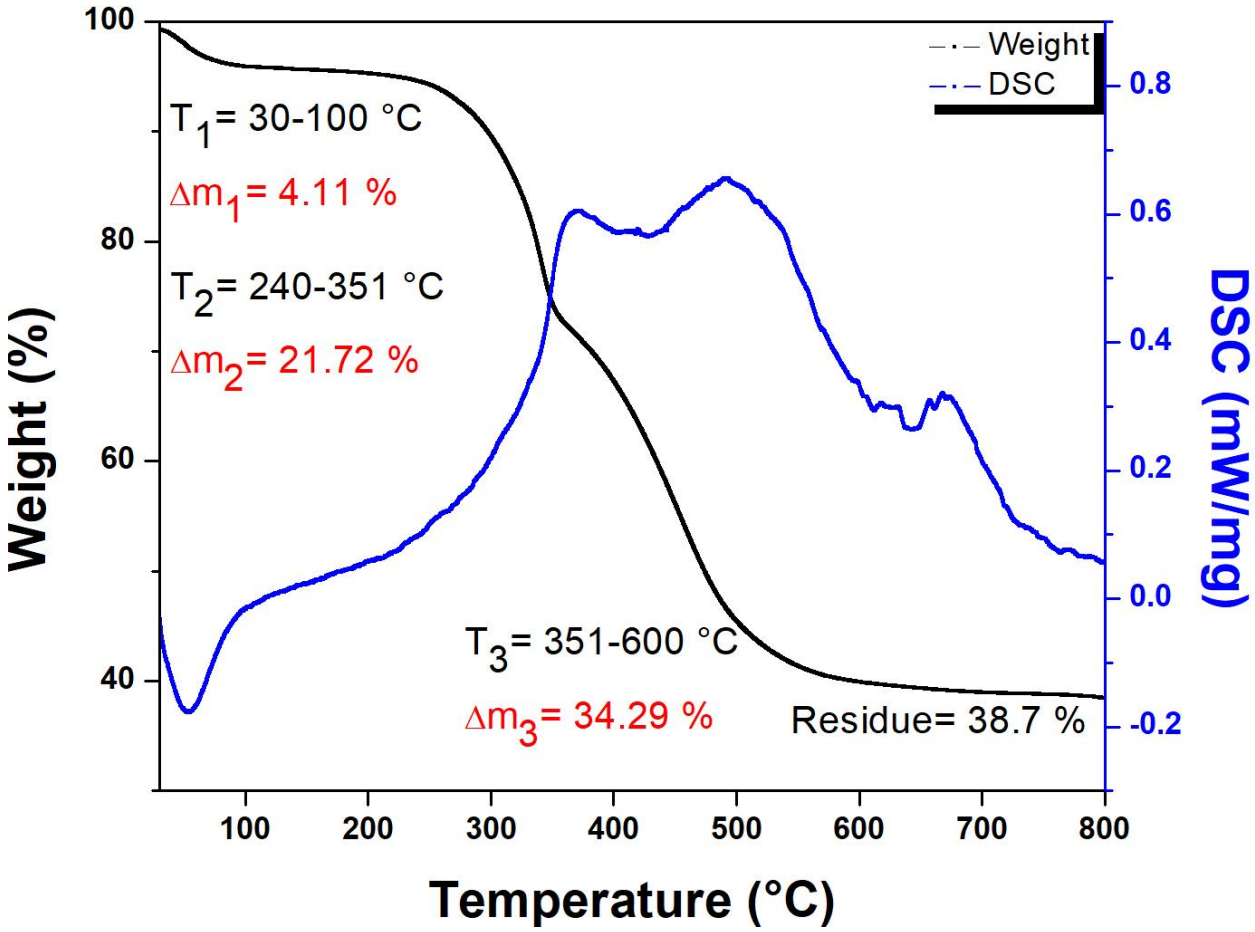

Figure S12: Thermal analysis of 3-PDMS@Al_2O_3@SD flakes

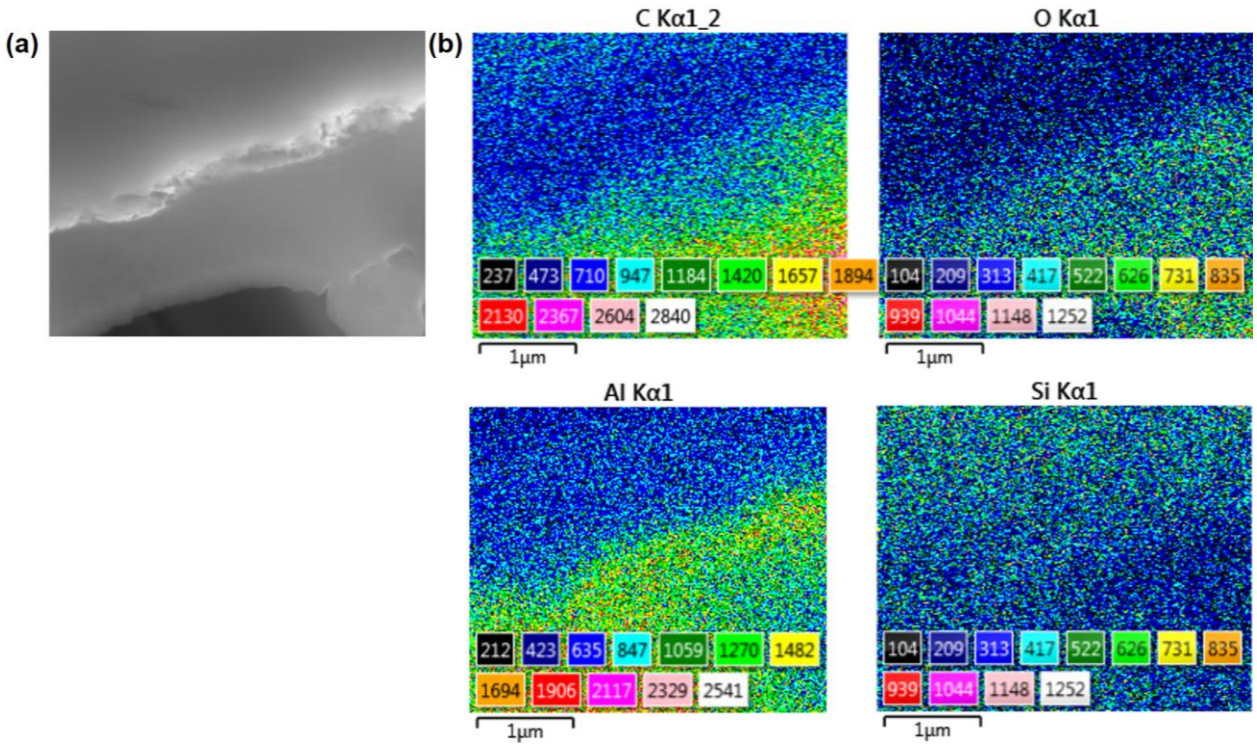

Figure S13: EDS spectra of the FIB cross section of 3-PDMS@Al_2O_3@SD

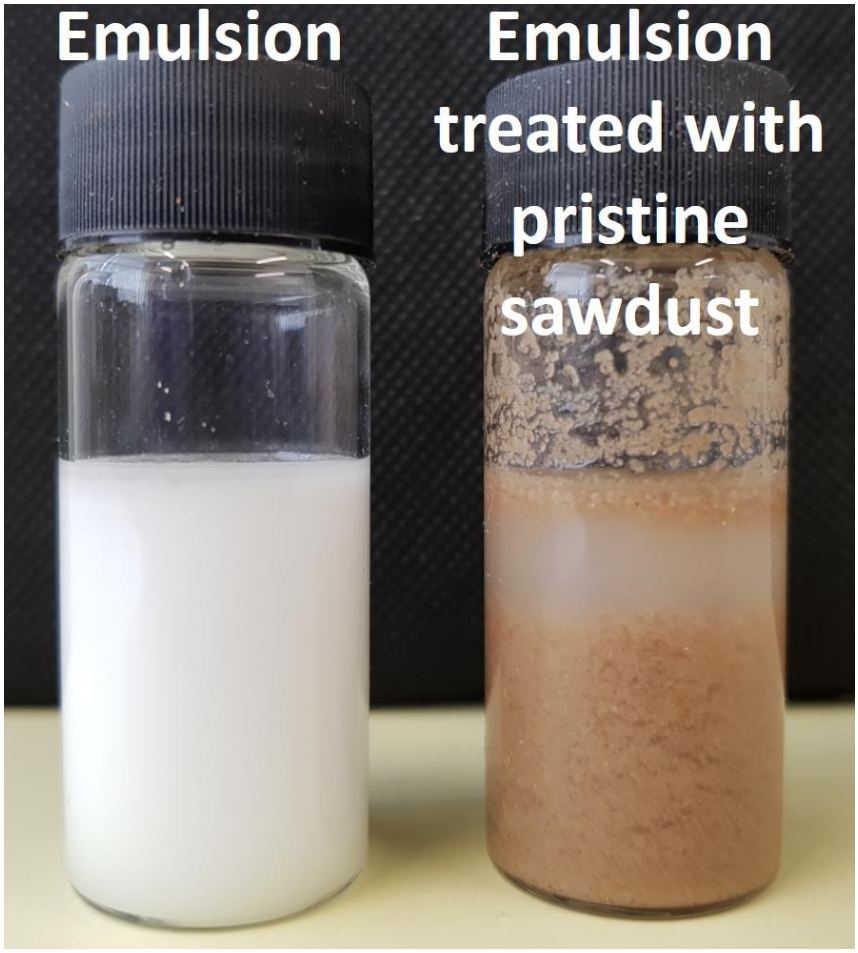

Figure S14: Digital images showing the performance of pristine sawdust on emulsion separation. The sawdust gets absorbed in the emulsion without having any effect on separation

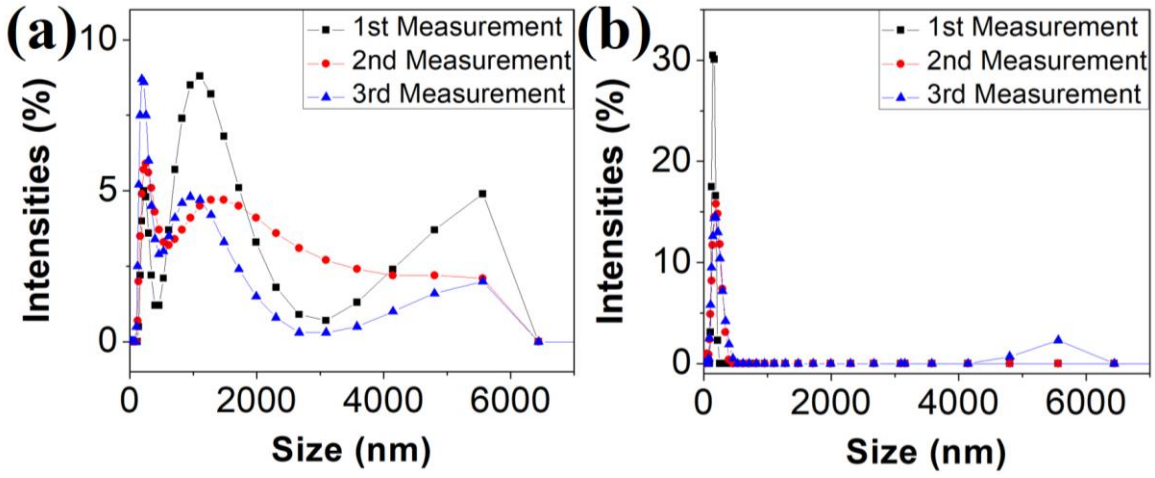

Figure S15: DLS of T4 emulsion (a) before and (b) after separation. Sample (T4) was diluted 5 times with water and tested again with DLS and the results are presented in the following images. Each sample is tested three times. Figure S15 shows the DLS of T4 emulsion before (a) and after

(b) separation. All three measurements show that emulsion contain different sizes of oil droplets ranging from nanometer to a few microns. After treatment with sawdust composite, most of the oil droplets have been removed and only small droplets are left as evidenced previously in the optical microscopy images.

Olive oil emulsion in water was prepared to see the performance of these composite particles in separation of triglycerides. The emulsion was prepared as mentioned in "Experimental section (T4)" and separation was performed under same conditions. It is important to mention here that emulsification was not same for olive oil in these conditions as very big droplets were formed in addition to small droplets as shown in optical microscopy images (Figure S16 and S17). The performance of sawdust composite was also different to the emulsions as the powder removed most of the big droplets but the water was not clean after 1st cycle of separation. When the emulsion was treated with sawdust composite powder 2nd time, the transparency was significantly improved and most of the oil droplets were removed. The digital images and optical microscopy images are shown below.

It can be inferred from these results that superhydrophobic absorbents have potential in separating glycerides, however, a detailed study is needed to understand the required design conditions and separation behavior.

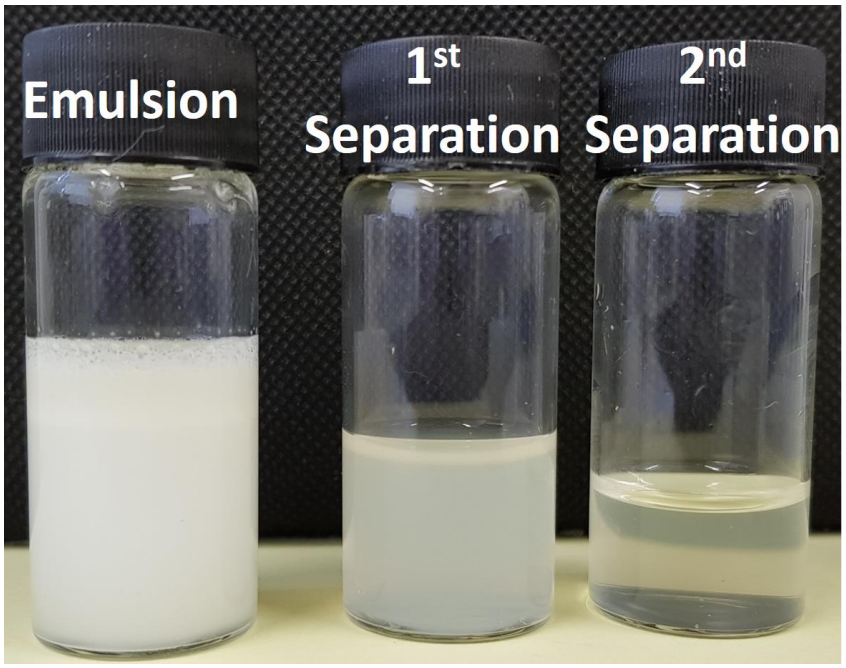

Figure S16: Digital images showing the separation of olive oil emulsions by two cycles of separations

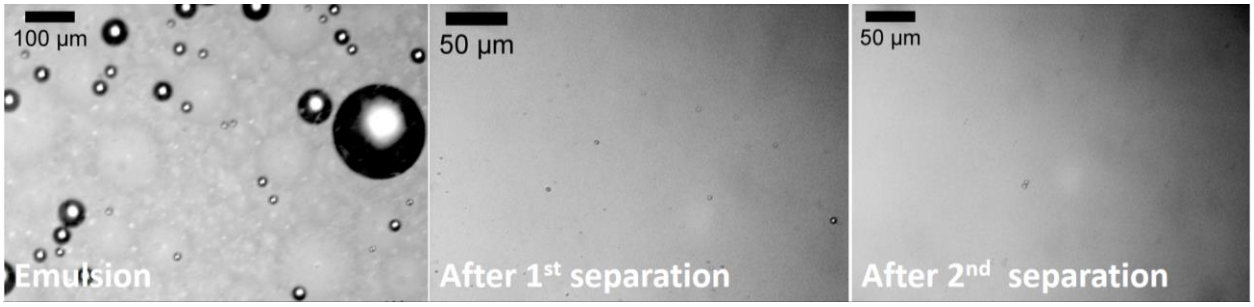

Figure S17: Optical microscopy images showing the olive oil emulsion before and after separation

Chapter 3: Hybrid magnetic nanocomposites for the separation of stable oil/water emulsions

Citation:

U. Zulfiqar, A. G. Thomas, K. Yearsley, L. W. Bolton, A. Matthews, and D. J. Lewis, "Hybrid magnetic nanocomposites for the separation of stable oil/water emulsions (To be submitted)

Author contributions:

All authors listed have made a substantial, direct and intellectual contribution to the work and approved it for publication. U. Zulfiqar carried out the experimental work and wrote the manuscript whilst A. Matthews, D. J. Lewis and A. G. Thomas were involved in supervision, critical analysis of results, editing and revision of the manuscript. A. G. Thomas helped with the XPS analysis of samples. K. Yearsley, L. W. Bolton provided supervision as industrial mentors and helped in editing the manuscript.

3.1 Abstract

Separation of a surfactant stabilised emulsion remains an industrial and environmental challenge despite significant progress in superhydrophobic materials for oil/water separation. Herein, two types of magnetic nanocomposite are presented, and their superhydrophobic and separation performance is evaluated in relation to surface area and nanoscale texture. Hybrid magnetic nanocomposite powders were synthesised by encapsulating magnetite nanoparticles in porous and non-porous silica shell through sol-gel process. The surface of both powders was grafted with silyl methyl groups to achieve the selective affinity towards oil. After surface modification, the powders show a water contact angle of >155º and have a combination of superhydrophobic and superoleophilic properties. The surface areas of the materials were found to be 213 m^2/g, and 860 m^2/g from both of the preparation routes reported. The combination of these properties allowed for the selective capture of oil from oil/water mixtures and emulsions. The powders were able to remove more than ca. 90% of organic content from the surfactant-stabilised emulsions. The magnetic properties assisted the facile removal of powder with oil entrained by a simple application of a magnetic field to the mixture. The separation process was studied in detail to demonstrate the applicability of superhydrophobic materials in the separation of stable emulsions.

3.2 Introduction

Biphasic mixtures form through both natural and industrial processes. It is essential to separate these mixtures of two immiscible liquids to purify or recover a product in some instances. One example is the separation of oil/water emulsions to refine crude oil or clean processed water before releasing into the environment [43,45,52,53,249]. Emulsions are produced due to several industrial operations in the oil industry, which start from the initial stages of oil production [52]. For example, uniform mixing of oil and water occurs due to high pressure and shear at wellbore and pipelines during crude oil drilling. The water content in oil increases as the life of an oil well nears its end.

Crude oil naturally contains fatty acids, waxes, clays and surface-active substances such as surfactants and asphaltenes, which tend to migrate to the oil/water interface and form an interfacial barrier [52,53]. These substances reduce coalescence and agglomeration and create very stable oil/water emulsions. The treatment of these types of stable emulsions is essential to increase the efficiency of oil production and prevent environmental contamination from the accidental release of effluent. Currently, there are various methods in practice to treat oil/water mixtures. Some examples include the in-situ combustion of oil, electrostatic separation, chemical demulsification, bioremediation, dispersants, solidifiers, skimmers and adsorbents [250,251]. Physical separation via absorption or filtration is considered one of the most efficient routes to treat oil/water mixtures due to the simplicity required for operation. [233,247,252,253]. Superhydrophobic and superoleophilic materials have recently been studied for the physical separation of oil/water mixtures and emulsions. A variety of architectures such as meshes [83,254–256], foams [132,257,258], membranes [90,259], aerogels [260–262] and fabrics [263,264] have been explored using a range of silica, titania, carbon, and zinc oxide-based nanostructured surface coatings. Most of these materials are successful in separating free mixtures where oil droplets are not stable. However, emulsions containing thoroughly distributed dispersants with droplet diameters of less than 150 μm are complicated to separate. They are often colloidally stable [265], and many oil/water emulsions contain dispersants with particle sizes < 20 μm and are stabilised by the surfactant, which exacerbates the problem.

Recently, superhydrophobic materials have been used to separate oil/water mixtures and emulsions. A polyimide nanofibrous membrane was modified with 1*H*, 2*H*, 2*H*-perfluorodecanethiol to achieve a combination of superhydrophobic and superoleophilic properties [88] and was subsequently used for separation of oil/water emulsions. In another example, a porous melamine based sponge was rendered superhydrophobic by creating a highly non-polar and low

energy surface coated with a monolayer of long-chain alkanes via the 1,4-conjugation reaction between amine and acrylate groups [266]. The resulting sponge is superhydrophobic and was used for the separation of oil/water mixtures. Emulsions were separated by tuning the pore size of the foam via compression. Superhydrophobic porous monoliths have also been fabricated by copolymerisation of styrene and glycidyl methacrylate by high internal phase emulsion template and used for the removal of oil from oil/water mixtures and surfactant-free emulsions [267]. The superhydrophobic membranes have been utilised to separate water-in-oil emulsions successfully; however, they have limited application in the separation of oil-in-water emulsions [107]. Alternative approaches to separation have included hierarchically structured particles made from sawdust, graphene oxide, silica, zinc oxide and manganese dioxide; these have been employed to selectively adsorb the oil phase from water [31,75,108,145,268]. The general strategy employed with these materials is to mix the superhydrophobic particles with emulsions under external force; the particles adsorb the oil phase from the emulsion and leave the clean water behind.

Step changes in separation processes can be effected with magnetic materials, as magnetic fields' application potentially allows spatial manipulation of the adsorbent. Magnetic separation has been widely explored in catalysis [269] and water treatment [270] to prevent losses, improve recyclability and reduce the overall cost of operation. Similarly, materials have been prepared with magnetic properties to adsorb oil from oil/water mixtures [271,272]. Magnetic melamine sponges were prepared by coating magnetite nanoparticles onto the sponge via dip coating and used to remove water from oil/water mixtures[273]. Similarly, silica sponges have been decorated with cobalt nanoparticles to produce nanostructured monoliths that exhibit magnetic properties [274]. The composite was coated with polydimethylsiloxane to attain superhydrophobic features and was used for the absorption of oil from oil/water mixtures.

In this work, we prepare superhydrophobic hybrid magnetic nanocomposite powders and test their use in the separation of surfactant-stabilised emulsions. In theory, these materials can then be physically extracted with a magnetic field post-separation. Two different types of silica and magnetite core-shell particles with different surface areas were synthesised for this purpose. Magnetite nanoparticles, prepared by a typical co-precipitation method [275], were encapsulated in non-porous and porous silica, herein referred to as HMN-1 and HMN-2, respectively. The magnetic particles were functionalised with hydrophobic organosilane groups to create a superhydrophobic nanoparticle surface. The powders were characterised using a range of bulk and surface-specific microscopies and spectroscopies to elucidate their physical and chemical properties. Finally, we tested the separation of surfactant-stabilised toluene in water emulsions followed by facile removal of the oil-imbued particles by applying a magnetic field to these hybrid particles.

3.3 Experimental

3.3.1 Materials

Tetraethyl orthosilicate ($Si(OCH_2CH_3)_4$ CAS Number 78-10-4), Dichlorodimethylsilane (CH_3SiHCl_2- CAS Number 75-78-5) ($\geq$ 98.5% (GC), Iron(II) chloride ($FeCl_2$ CAS 7758-94-3) and Iron(III) chloride ($FeCl_3$ CAS 7705-08-0) were procured from Sigma Aldrich. Span 80 ($C_{24}H_{44}O_6$-CAS Number 1338-43-8, viscosity 1000-2000 mPa.s) and Tween 80 ($C_{64}H_{124}O_{26}$-CAS Number 9005-65-6) were acquired from Sigma Aldrich and used as a surfactant to make stable oil-in-water emulsions. Ammonium hydroxide solution (25%) and other solvents such as methanol and acetone were acquired from Fisher Scientific.

3.3.2 Synthesis of Magnetite Nanoparticles

Magnetite nanoparticles were synthesised by a typical co-precipitation method. $FeCl_3$ (5 g) in water (100 ml) and $FeCl_2$ (2.5 g) in water (100 ml) were mixed and stirred for 10 min, and ammonium hydroxide (200 ml) was added. The solution was left stirring for 1 h. The magnetite (Fe_3O_4) nanoparticles formed were separated using a bar magnet, washed several times with water and acetone, and dried in an oven at 80°C for 2 h.

3.3.3 Synthesis of HMN-1 and HMN-2 magnetic nanocomposites

A portion of the magnetite nanoparticles (0.1 g) was dispersed in methanol (80 ml) for 6 h, then 20 ml water was added, and the mixture was sonicated for 10 min. Tetraethyl orthosilicate (TEOS, 1 ml) was added to the mixture which was sonicated before adding ammonia (10 ml). The solution was aged for 1 h at room temperature and the nanoparticles formed were collected by centrifugation and washed with acetone, and dried in an oven at 80 ºC. For the synthesis of mesoporous particles, 0.32 g CTAB was introduced in the reaction system before the addition of TEOS. 0.2 g of silica powders (HMN-1 standard SiO_2; HMN-2 mesoporous SiO_2) were suspended in 100 ml hexane via ultrasonication. Dichlorodimethylsilane (7 ml) was added to the mixtures under continuous stirring, and the solvents were then removed by distillation at 100 ºC. Dry powders were collected and washed with acetone several times. A bar magnet was used to collect the final particles which were dried in an oven at 80 ºC for 2 h.

3.3.4 Characterisation

Nanocomposites and surfaces were examined by field emission scanning electron microscope (Fe-SEM, FEI Magellan HR FEGSEM). The shell structure of silica was examined using a transmission electron microscope (TEM, Tecnai 20). The samples were made by making a dispersion of nanoparticles in methanol. A few drops of suspension were placed on a standard carbon-coated copper grid, and the solvent was evaporated in an oven at 80 ºC. Thermogravimetric

analysis (TGA, Mettler Toledo, TGA/DSC 1) of nanoparticles before and after functionalisation was performed in the air (heating rate of 10 °C/min). Fourier-transform infrared (FTIR) spectroscopy and X-ray photoelectron spectroscopy (XPS) was employed to study the chemical structure of nanoparticles. A Kratos Axis Ultra with a monochromatic Al K alpha X-ray source (sampling depth ca. 6nm) was used for the XPS analysis of samples. A small amount of powders was mounted on the carbon tape for XPS analysis, and the spectra were adjusted on the binding energy scale w.r.t C 1s peak. Quantification of elements and chemical state profiling was obtained by using CasaXPS. For measurement of contact angle, a smooth film was fabricated on a glass substrate by spray coating the suspension of nanoparticles (5 wt.%) on a glass slide. A KRUSS drop shape analyser was used to observe the water contact angles of surfaces. A MultiMode8 atomic force microscope (AFM) was used to compare the nanoscale features of surfaces formed by both types of nanoparticles. AFM samples were prepared by forming a thin film on a silicon substrate using the above-mentioned method. AFM images were processed by Gwyddion software to refine the result and obtain roughness values. UV/Vis spectrophotometer (Shimazu UV-1800) was used to record transmittance spectra in the visible range. The emulsions were prepared by mixing toluene, water and surfactant (1g/l) for 20 min at 1000 rpm with a magnetic stirrer. The emulsions were stabilised by two different surfactants to study the efficacy of nanoparticles in separating the tiny droplets of oil. Emulsions made by this method were stable for several days. The oil separation efficiency was examined by optical microscopy using an Olympus BH2 upright optical microscope (Zeiss camera) in tandem with a total organic carbon (TOC-Shimadzu, TOC-V CPN) analyser. Emulsion droplets were put on a glass slide and observed under the optical microscope before and after separation. Similarly, total organic carbon value was determined for the samples before and after separation to quantify the toluene and surfactant content in water.

3.4 Results and Discussion

Co-precipitation was used for the synthesis of magnetite nanoparticles which were then coated with a shell of organosilica by sol-gel processing. The following chemical equation describes the reaction to produce magnetite by this method:

$$Fe^{2+} + 2Fe^{3+} + 8OH^{-} \rightarrow Fe(OH)_2 + 2Fe(OH)_3 \rightarrow Fe_3O_4 + 4H_2O \quad (1)$$

The resulting magnetite nanoparticles were dispersed in methanol for 6 h to form a colloidally stable dispersion. Non-porous silica shells for HMN-1 were formed by the hydrolysis and condensation of tetraethyl orthosilicate (TEOS). The size of the produced particles depends upon several parameters such as concentration of reactants, catalyst, solvent, and temperature [128,276,277]. Mesoporous shells for HMN-2 were produced by the addition of cetyl ammonium bromide (CTAB) with TEOS. The powders produced are hydrophilic due to the presence of surface silanol (R-Si-OH) groups. In both cases, these were converted to hydrophobic surfaces by treatment with dichlorodimethyl silane, which installs dimethylsilane (R-Si-$(CH_3)_2$) groups at the surface in place of the silanol groups. **Figure 3-*1***a shows the FTIR spectra of HMN-1 before and after treatment with dichlorodimethyl silane. The peaks observed at 1040 cm^{-1}, 800 $cm^{-1,}$ and 432 cm^{-1} indicate the presence of silica (Si-O-Si, Si-OH and Si-O bonds). Compared to pristine HMN-1, a new band can be observed at 2965 cm^{-1} post-functionalisation. This peak arises due to the stretching from the dimethyl silane groups. **Figure 3-*1***b shows the FTIR spectra of HMN-2 before and after functionalisation. Similar behaviour can be observed in these particles as a peak for dimethyl silane groups appear after functionalisation in addition to the characteristic peaks of silica.

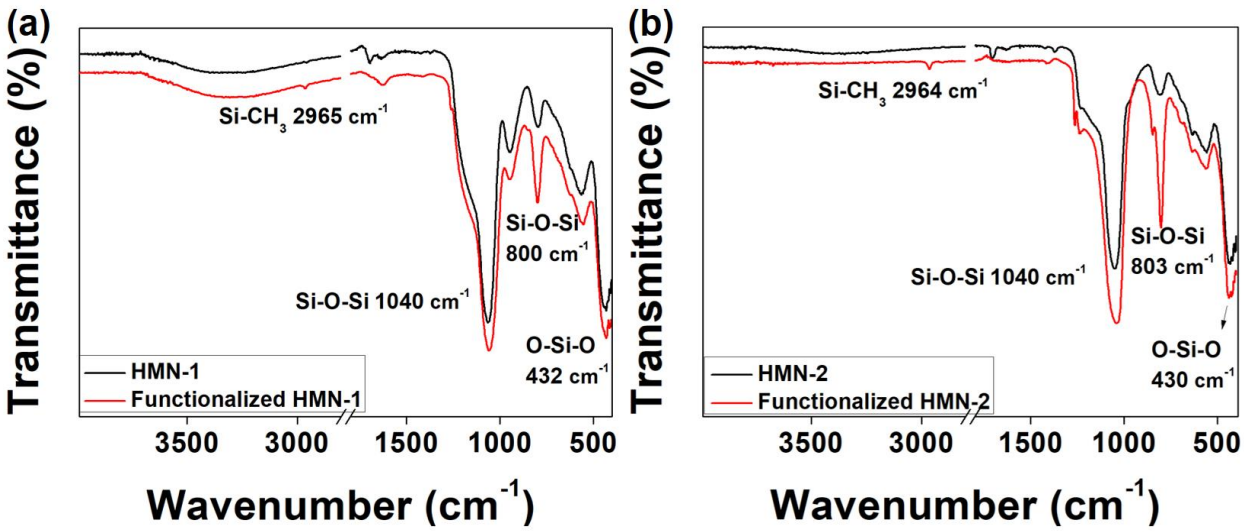

Figure 3-1: FTIR spectra of (a) HMN-1 and (b) HMN-2 showing the differences in functional groups before and after treatment of the surfaces with dichlorodimethyl silane.

Figure *0-2* shows the SEM images of HMN-1 and HMN-2. The HMN-1 particles show rough surface geometry, with most particles in the ca. 100nm size range. The rough morphology of particles is due to the magnetite nanoparticles as they tend to aggregate due to short-range magnetic ordering, i.e. as physically separate Weiss domains. **Figure *0-2***b shows the morphology of HMN-2. The particles are agglomerated, and broad size distribution is observed with some particles in the micron size range. The broad size distribution and large size of HMN-2 can be explained by the fact that surfactants such as CTAB cause aggregation during synthesis and affect the final particle size. The core/shell structure of both powders was observed by TEM (**Figure *0-2***). A characteristic contrast of a core-shell structure is observed; the dark regions indicate the magnetite nanoparticle while the light grey area is showing the uniform and thin coating of silica. The magnetite nanoparticles are encapsulated in a non-porous silica shell in the HMN-1 particles, while a mesoporous shell is present in HMN-2 particles. The grey area around magnetite nanoparticles contains very small and uniform pores in HMN-2 particles forming a mesoporous structure.

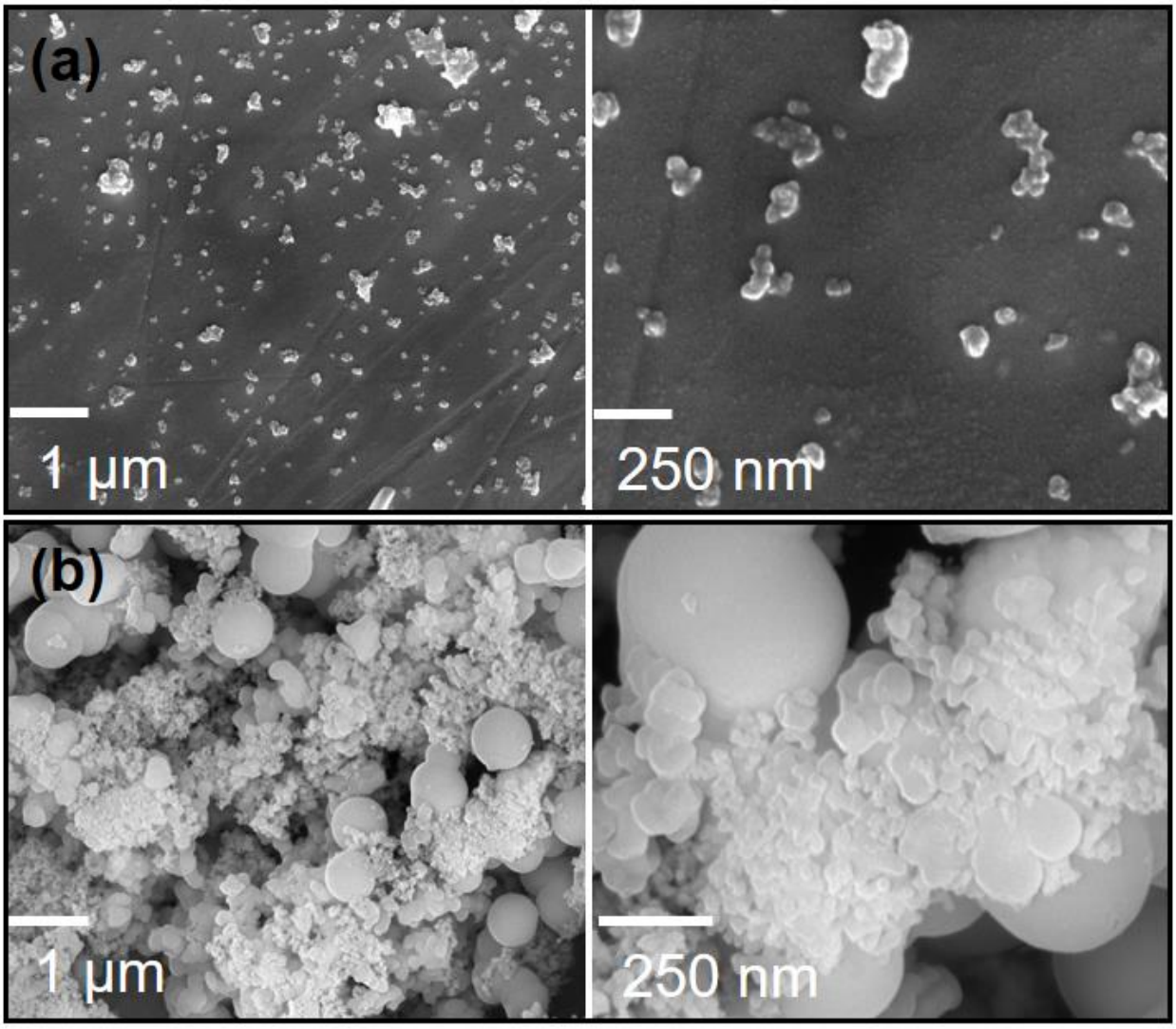

Figure 0-2: SEM images of (a) HMN-1 and(b) HMN-2 at different magnifications.

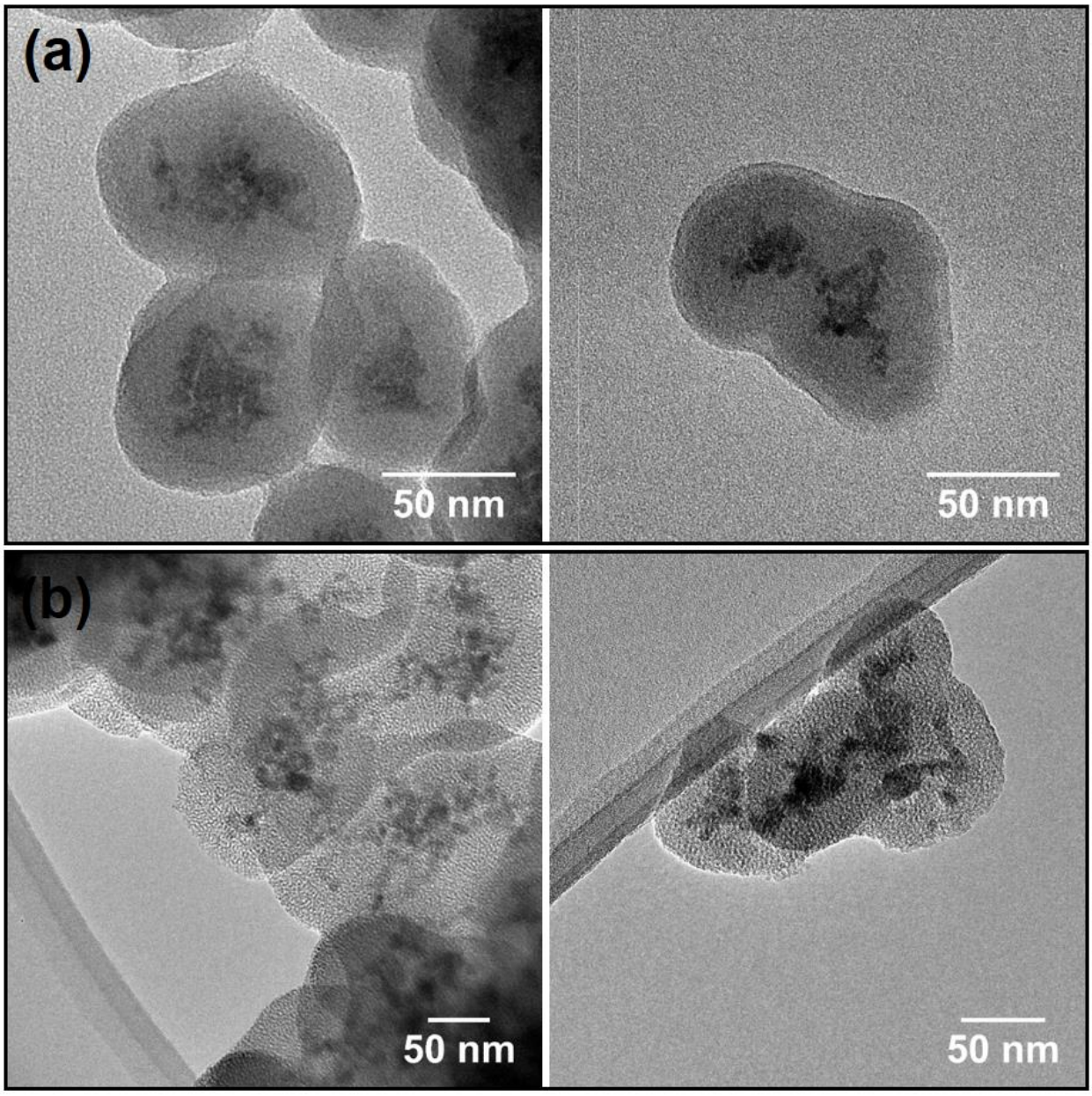

Figure 3-3: Bright field TEM (200 kV) images of nanoparticles of (a) HMN-1 and (b) HMN-2

The surface structure of HMN-1 and HMN-2 was studied with N_2 adsorption isotherms (**Figure 3-*4***a and b). HMN-1 shows a trivial isotherm typical for a non-porous material, whilst a Type IV isotherm is observed for HMN-2, typically manifested by mesoporous materials. The increases in adsorption after ca. P/P_0 = 0.15 in HMN-2 isotherm is associated with the adsorption of N_2 by the

porous structure. **Figure 3-*4***c shows the difference in pore size and pore volume of both particles. HMN-2 contains pores with diameters less than 2 nm with a pore volume of 0.497 cc/g, while HMN-1 did not indicate pores' presence in this size range. BET surface area measurements show that HMN-1 and HMN-2 have surface areas of 213 m^2/g and 860 m^2/g, respectively. The high surface area in HMN-2 particles is due to the silica shell's mesoporous structure around magnetite nanoparticles. **Figure 3-*4***d shows the powder XRD patterns of magnetite before and after coating with non-porous (HMN-1) and porous (HMN-2) silica shells. The XRD patterns for HMN-1 and HMN-2 have Bragg reflections indexed to cubic magnetite (ICDD No: 01-075-0449). The characteristic broad background of amorphous silica is also observed between $2\theta \sim 20°$- 27°. From these data, we conclude that the nanoparticles were successfully coated with non-porous (HMN-1) and mesoporous (HMN-2) silica shells without affecting their crystal structure. In particular, the mesoporous materials offer relatively high surface areas compared to non-porous analogues, as one may expect.

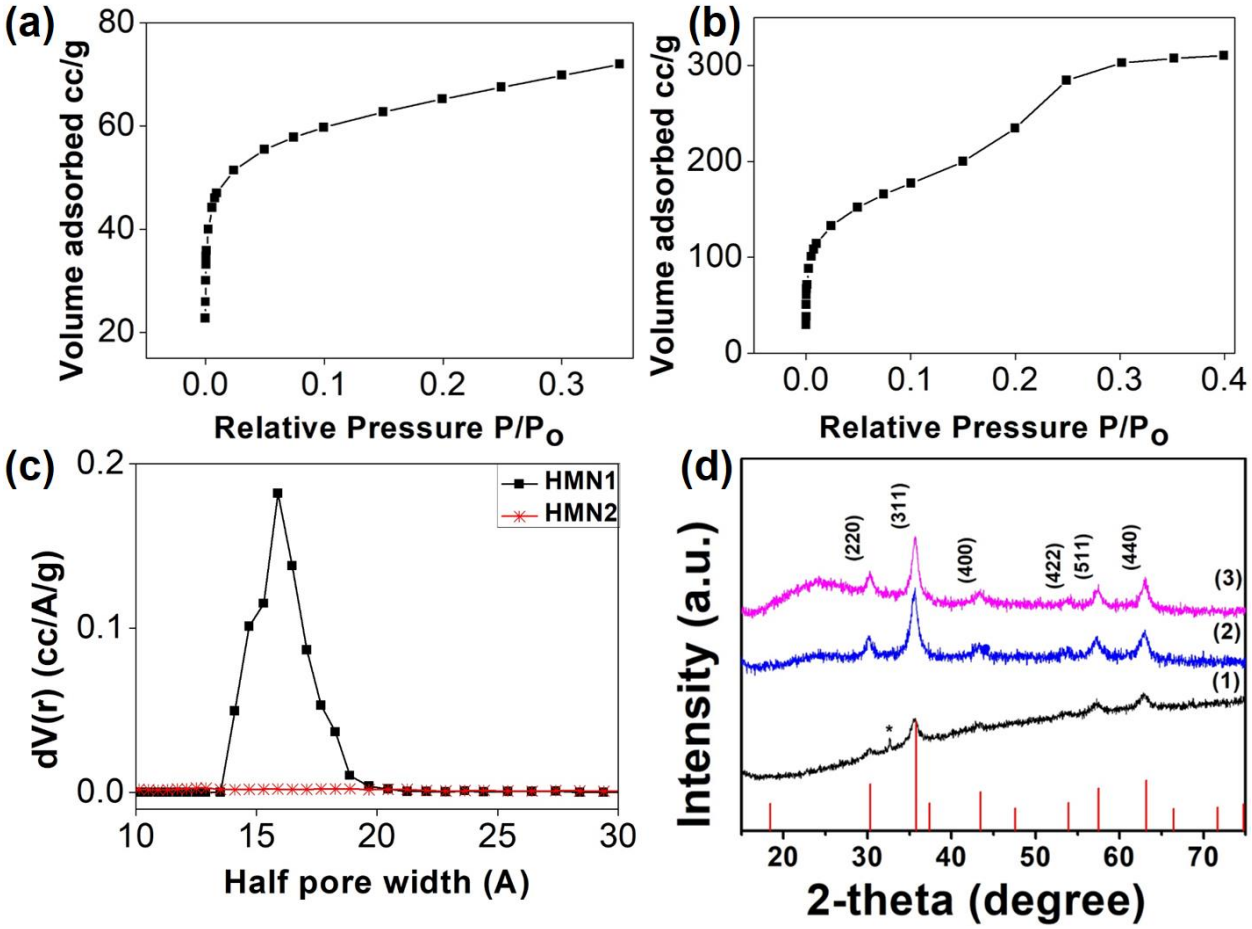

Figure 3-4: N_2 adsorption isotherms of (a) HMN-1 (b) HMN-2. (c) Pore size distribution of both powders measured from N_2 isotherms and (d) Powder XRD pattern of (1) pristine magnetite (2) HMN-1 and (3) HMN-2. The red line pattern is the library entry for cubic magnetite (ICDD No: 01-075-0449).

X-ray photoelectron spectroscopy was used to probe the surface chemistry of HMN-1 and HMN-2. Survey spectra show emission from silicon, oxygen, iron and carbon in both samples. The fitting of high-resolution spectra for each element shows that the surface of pristine HMN-1 contains 66.3 at% oxygen, 16.7 at% carbon, 15.8 at% silica and 1.5 at% iron. The surface composition changes to 56.1 at% oxygen, 20.3 at% carbon, 231.2 at% silica and 0.29 at% iron post-functionalisation. An increase in silica and carbon content post functionalisation is due to the presence of methyl silyl groups on particles' surface. A similar trend is observed in the HMN-2 sample, where the

composition changes from 65.6 at% oxygen, 12.7 at% carbon, 20.8 at% silica and 0.8 at% iron to 54.6 at% oxygen, 23 at% carbon, 21.9 at% silica and 0.37 at% iron. Both samples indicate an increase in the quantity of silica and carbon after functionalisation. The deconvolution of high-resolution spectra indicated the change in the chemical state of elements. **Figure 3-*5***a and b show the high-resolution XPS spectra of Si 2p and peak of pristine and functionalised HMN-1. The Si 2p peak appears at 103.49 eV, which confirms silicon's chemical state as silicon dioxide. The C 1s peak indicates three different chemical states of carbon (C-C, C-O and C=O). After modification with dimethyl silane, deconvolution of Si 2p reveals a new component at 102.29 eV, which implies the presence of another chemical state in addition to the silicon dioxide. We have ascribed this new component within the peak manifold to organosilica species ($Si(CH_3)_2O$-) arising from the surface modification step, i.e., installing methyl groups at the surface. The % area of the silica component is 91.3%, while that of the silane component is 8.7%. The area of the components corresponding to the three chemical states of carbon C-C, C-O and C=C observed changed from 78.4%, 7.6%, and 14.1% respectively to 91.6%, 2.4% and 6.0% post functionalisation. A considerable increase in C-C and decrease in C-O and C=O is therefore observed post-functionalisation. We ascribe these changes to the presence of methyl groups on the surface. The peak associated with Si-C appears very close to the C-C state. The presence of Si-C state in this region may add up to the area of C-C.

Similarly, a chemical state of silicon (oxide) is observed in the high-resolution spectra of Si 2p of pristine HMN-2 (Figure 5c and d) before and after functionalisation. The peak showing silyl methyl groups appeared at 102.15 eV; the ratio of inorganic silica to organosilica is 93.8% to 6.2%. Like the HMN-1 particles, a considerable change in the composition of chemical states of

carbon post-functionalisation is again observed in HMN-2 particles. The %age area of C-C, C-O and C=C changed from 80.76, 6.36, 12.88 to 90.51,7.84,1.65, respectively.

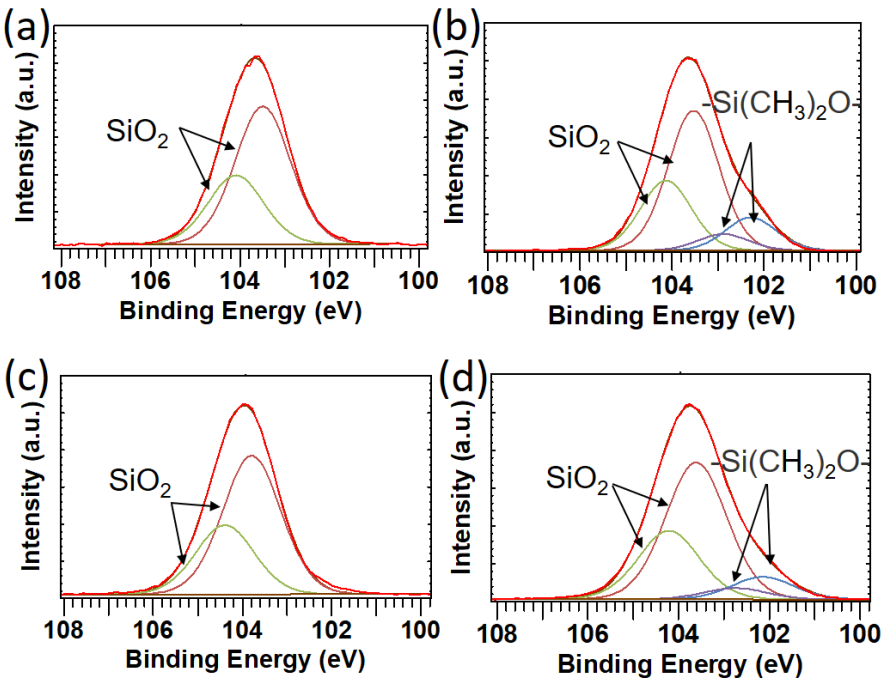

Figure 3-5: High resolution Si 2p XPS emission spectra of HMN-1 (a) before (b) and after functionalisation. High-resolution Si 2p XPS emission spectra of HMN-2 (c) before (d) and after functionalisation.

Figure 3-*6* shows the TGA results of HMN-1 and HMN-2 before and after functionalisation. HMN-1 shows various stages of mass loss, starting with removing water and moisture (5%), which completes at 150 °C. A uniform weight loss (5.5%) follows and finishes at ca. 800 °C due to silanol groups' dihydroxylation on the silica shell surface. After functionalisation, the weight loss due to moisture is reduced to 3.5% as the surface modification of particles reduces water adsorption. The 2nd weight loss (4.3%) is observed from 430 °C to 600 °C, which indicates the degradation of silyl methyl groups on the surface of particles. This weight loss may include some portion of unreacted silanol groups. HMN-2 shows significantly less weight loss due to

dihydroxylation as compared to the HMN-1 particles. It is found to be ca. 1.5% for moisture and water removal and ca. 3.5% for degradation of silanol groups. The difference in weight loss for moisture and silanol groups can be associated with the thermal treatment of HMN-2, as the high temperatures employed degrade pendant hydroxyl groups present on the surface of particles. After the functionalisation of HMN-2, the weight loss from 350 °C to 700 °C, which amounts to ca. 7% of the original weight, accounts for the removal of silyl methyl functional groups. The TGA analysis confirms that the polysiloxane network in both powders starts to degrade and is mostly volatilised at temperatures > 350 °C. It can also be inferred that particles do not lose their hydrophobic properties due to processing under about 300 °C. This is an attractive feature for emulsion separation applications as the powder may be subjected to cycles of heating at elevated temperatures to remove adsorbed oil for recycling.

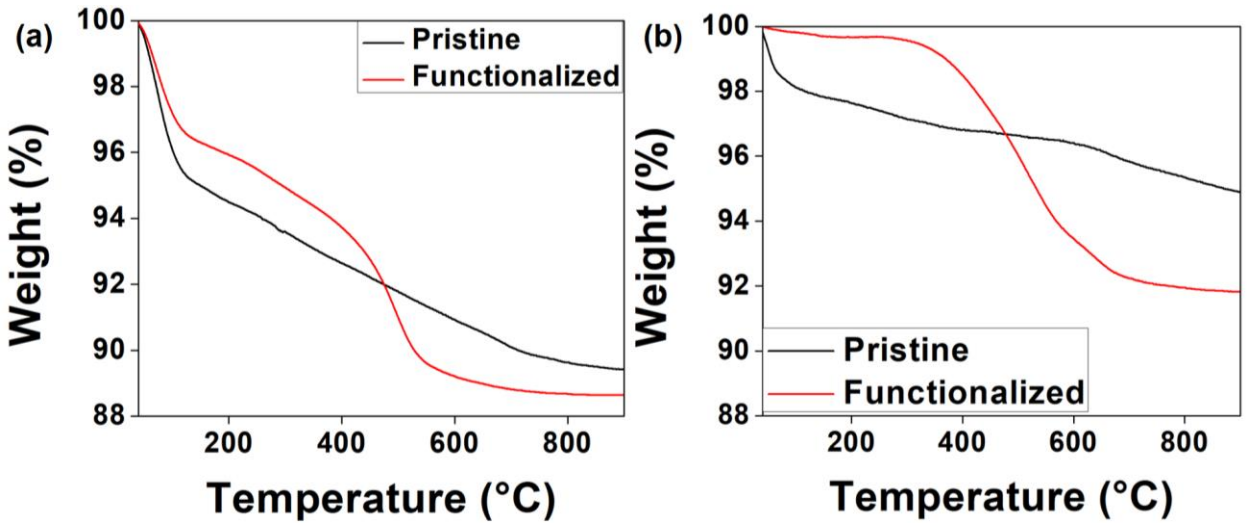

Figure 3-6: TGA profiles of (a) HMN-1 (b) HMN-2, showing in each case profiles before and after treatment with dimethyl dichlorosilane.

To determine the water contact angle and wettability of HMN-1 and HMN-2, the powders were suspended in methanol (5 wt.%) by ultrasonication and then spray coated on a glass slide and silicon substrate. Figure 3-7 shows the SEM and AFM images of both surfaces made from these

particles. The surfaces demonstrate water contact angles of ca. 154.8 ± 1.4º and 157.4 ± 1.6º for HMN-1 and HMN-2, respectively, and both surfaces are therefore superhydrophobic. HMN-2 particles demonstrate a slightly higher contact angle as compared to the surface formed by HMN-1 particles. **Figure 3-*7*** shows the rough structure of the surface observed by AFM and SEM, and the mean roughness value S_a of 334.8 nm and 549.9 nm is observed for HMN-1 and HMN-2, respectively. The difference in roughness can explain the difference in the water contact angle of these powders. It is well known that the water repellency of a surface is dependent upon the surface geometry and chemistry [122,123,278,279]. The surface contains irregular nanoscale and microscale features which contribute to an overall hierarchical roughness that bridges both length scales. The synergistic effect of roughness and silyl methyl groups present on the surface of nanoparticles delivers very high water repellency. The rough structure of a surface hosts the air pockets, which help in improving the water repellency. This type of surface contains a heterogeneous structure and makes two different interfaces, i.e., liquid–air and liquid-solid, during interaction with water.

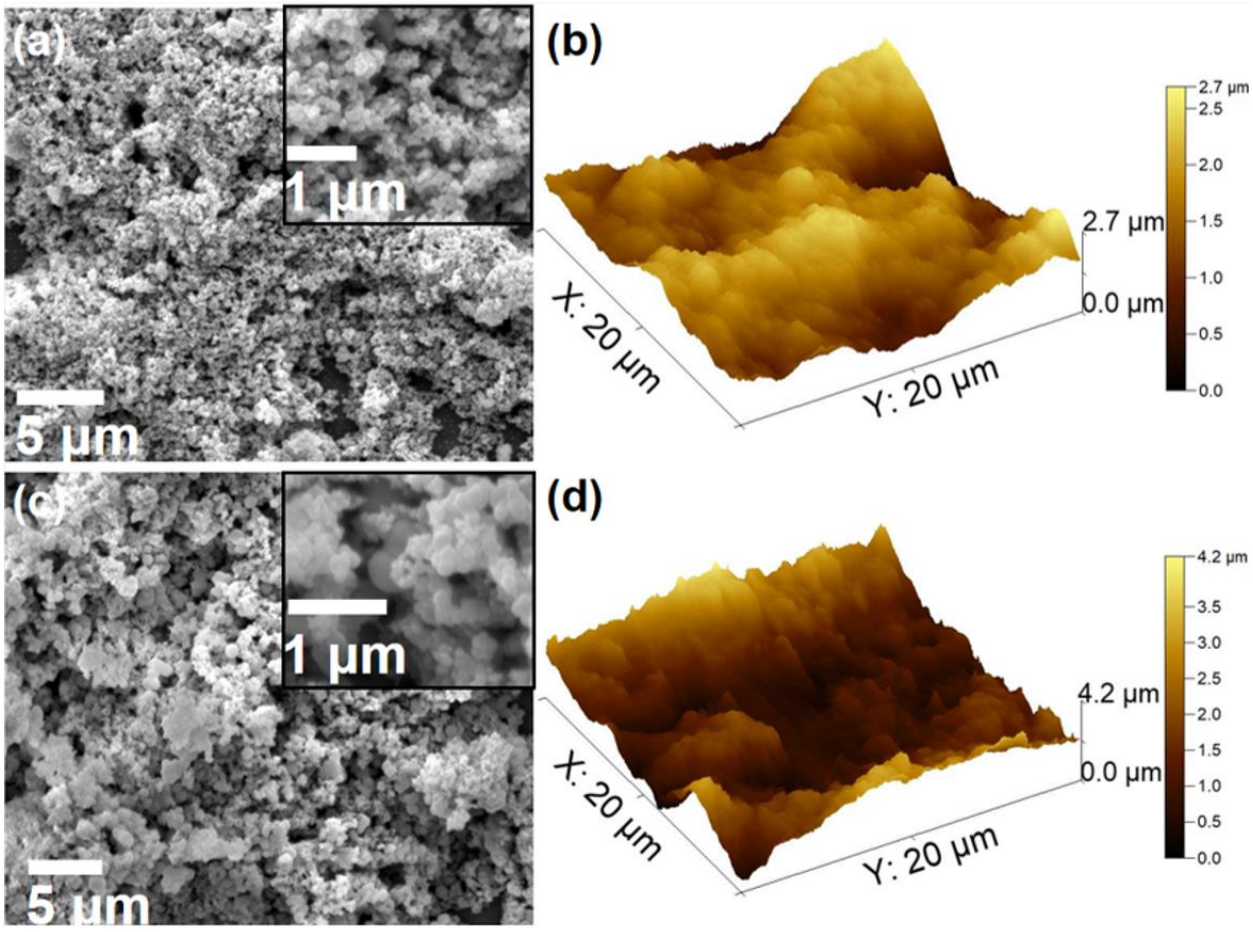

Figure 3-7: Physical analysis of the morphological features of surfaces decorated in HMN-1 and HMN-2. (a) low magnification SEM image of surface coated in HMN-1 and (b) AFM image of aforementioned surface, (c) low magnification SEM image of surface coated in HMN-2 and (d) AFM image of aforementioned surface.

The water repellency of the superhydrophobic surface is shown in **Figure 3-*8***a. Water droplets are observed to roll off upon contact with the surface. **Figure 3-*8***b shows that a continuous jet of water completely bounces off without affecting the surface.

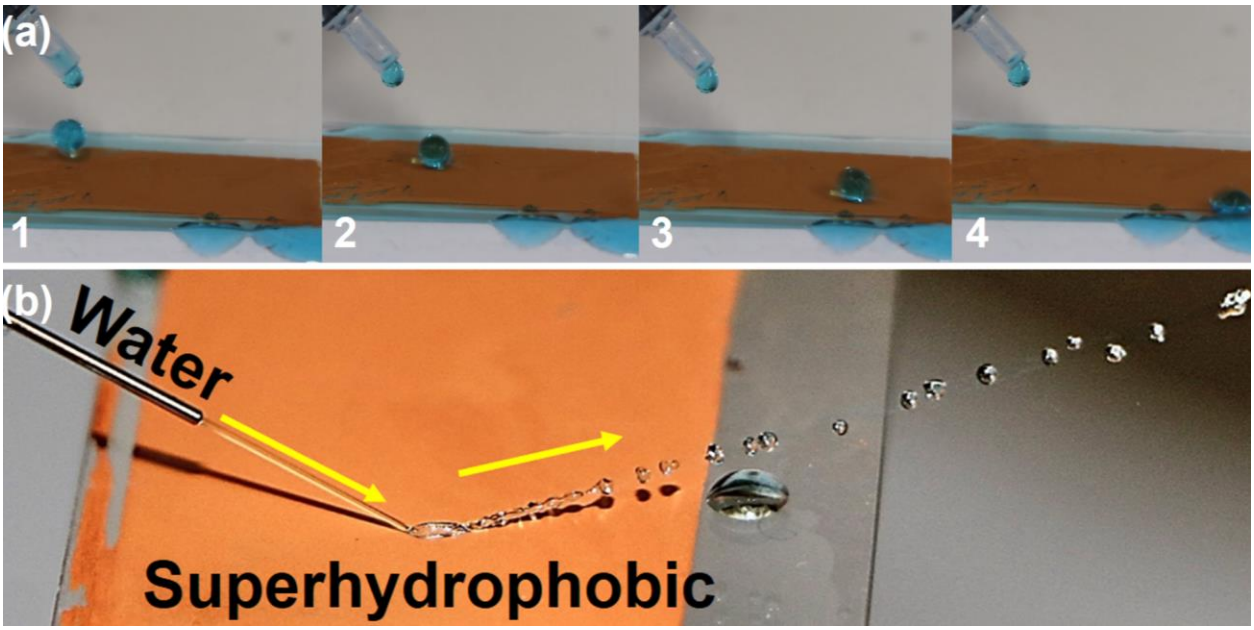

Figure 3-8: Digital images showing the (a) a water droplet rolling on the superhydrophobic surface(b) water jet bouncing off the surface

Another simple experiment demonstrates the selective affinity of HMN-1 towards organic liquids. The powder was immersed in a mixture of water and chloroform under magnetic force. **Figure 3-9**a shows the digital images: HMN-1 freely floats on the surface until it was forced to immerse in water under the influence of a magnet. Once immersed in water, a bubble forms around the powder, which appears as a silver mirror, while the particles remain dry. The bubble is formed due to the air entrapped inside the porous structure of particles. Upon contact with chloroform, the powder quickly adsorbs it due to high affinity towards organic fluids and releases the air bubbles.

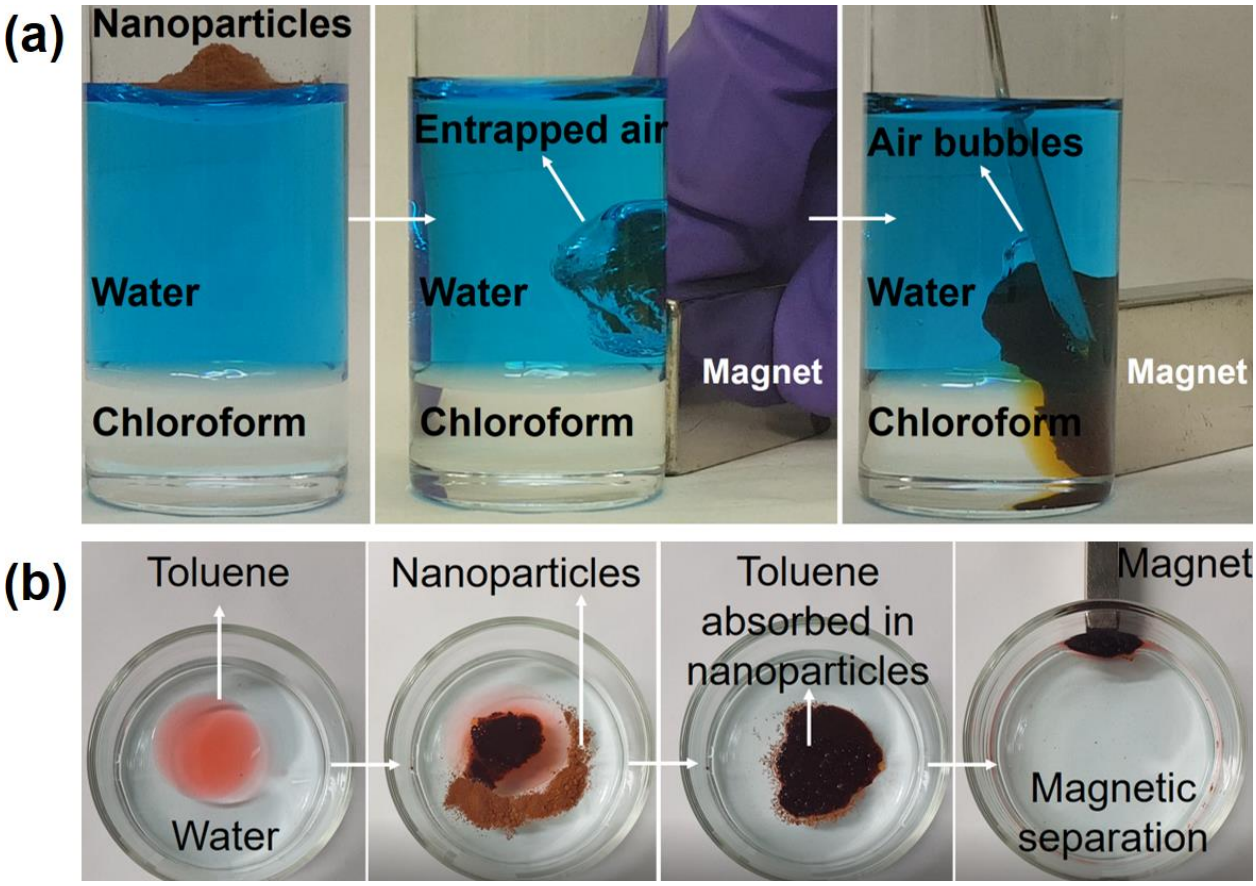

Figure 3-9: (a) Series of images showing the immersion of nanocomposite particles in a biphasic mixture of water and chloroform in a magnetic field; (b) series of images showing adsorption and collection of toluene (dyed with Sudan red) from the surface of water and separation of the particles from the mixture by the application of a magnetic field.

Figure 3-9b shows the oil absorption ability of HMN-1. Toluene was chosen as a model organic solvent and stained with Sudan red dye for identification. A few drops of toluene were added to the water which formed a thin film floating on the surface. When the powder was added, the oil film shrivelled immediately and was collected by the particles within a few minutes. After absorption, the oil/powder mixture floated on the surface of the water. This mixture can be separated from the water by applying a magnetic field.

The oil/water mixture where oil is homogeneously suspended in the water and stabilised with surfactant is challenging to separate due to the limited exposure of particles to the oil droplet inside the water phase. The ability of these powders to separate emulsions was tested. For this purpose, toluene was mixed in water and stabilised with two different surfactants (Span 80 and Tween 80). Surfactants help to stabilise oil droplets in water which otherwise separate immediately due to interfacial tension.

Different quantities of both types of powders were added in the emulsion, and the effect of the quantity of powders on the removal of toluene was observed. The emulsion and powder mixture was stirred by vortex mixture maximum contact between powder and oil droplets. Later, the particles were removed from water by using a magnet. **Figure 3-*10*** shows the emulsion before and after separation with the powder and separation of powder using a magnet.

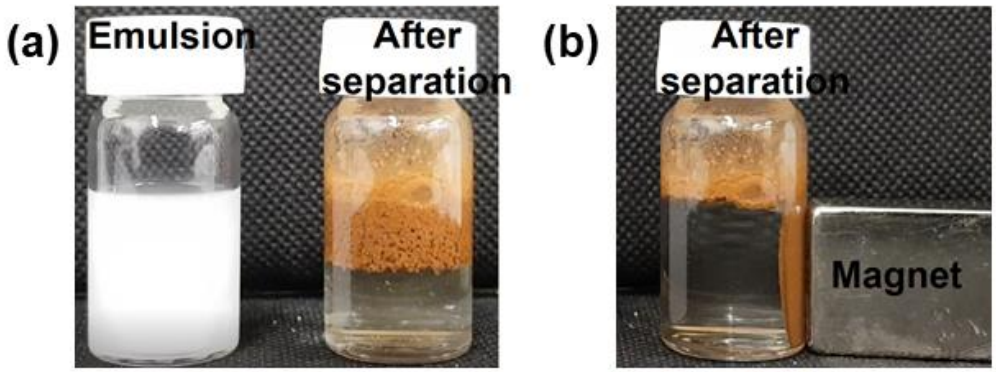

Figure 3-10: Digital images showing the (a) toluene-water emulsion and separation with HMN-1. (b) Extraction of HMN-1 from the solution by the imposition of an external magnetic field.

Figure 3-*11* shows the liquid obtained after treatment with three different quantities of HMN-1 particles. The emulsion is a milky colour mixture containing toluene droplets and surfactant. After treatment with 0.1 g HMN-1 particles (**Figure 3-*11***a), the colour has started to disappear, and

complete transparent water is obtained after treatment with 0.2 g and 0.3 g HMN-1. Similarly, the emulsions treated with HMN-2 particle (**Figure 3-*11***b) indicate transparent colour, which seems to get clearer with an increasing amount of HMN-2 particles. The samples were characterised to measure the change in light transmittance before and after treatment with powders (Figure 11c and d). The pristine emulsion shows ~0% transmittance, which significantly improved after treatment with HMN-1 particles. The transmittance increased to be more than 90% for all concentrations of HMN-1 particles. Similarly, the transmittance improved by increasing the amount of HMN-2 to 0.2 g and 0.3 g particles. The emulsions stabilised with Tween 80 were treated with 0.3 g of both particles using the same procedure as stated above. The transmittance of emulsion increased from 0% to more than 90% in both cases, which confirmed the effectiveness of these powders for both types of surfactants. The optical microscopy images of each kind of emulsion before and after separation are presented in **Figure 3-*12***. The optical microscopy images of the emulsions show the oil droplets distributed in the water phase, while the quantity of droplets decreases when the emulsions are treated with HMN-1 or HMN-2s. A few oil droplets can be observed in the emulsion treated with 0.1 g and 0.2 g powders, but the sample treated with 0.3 g powder shows very low oil trace.

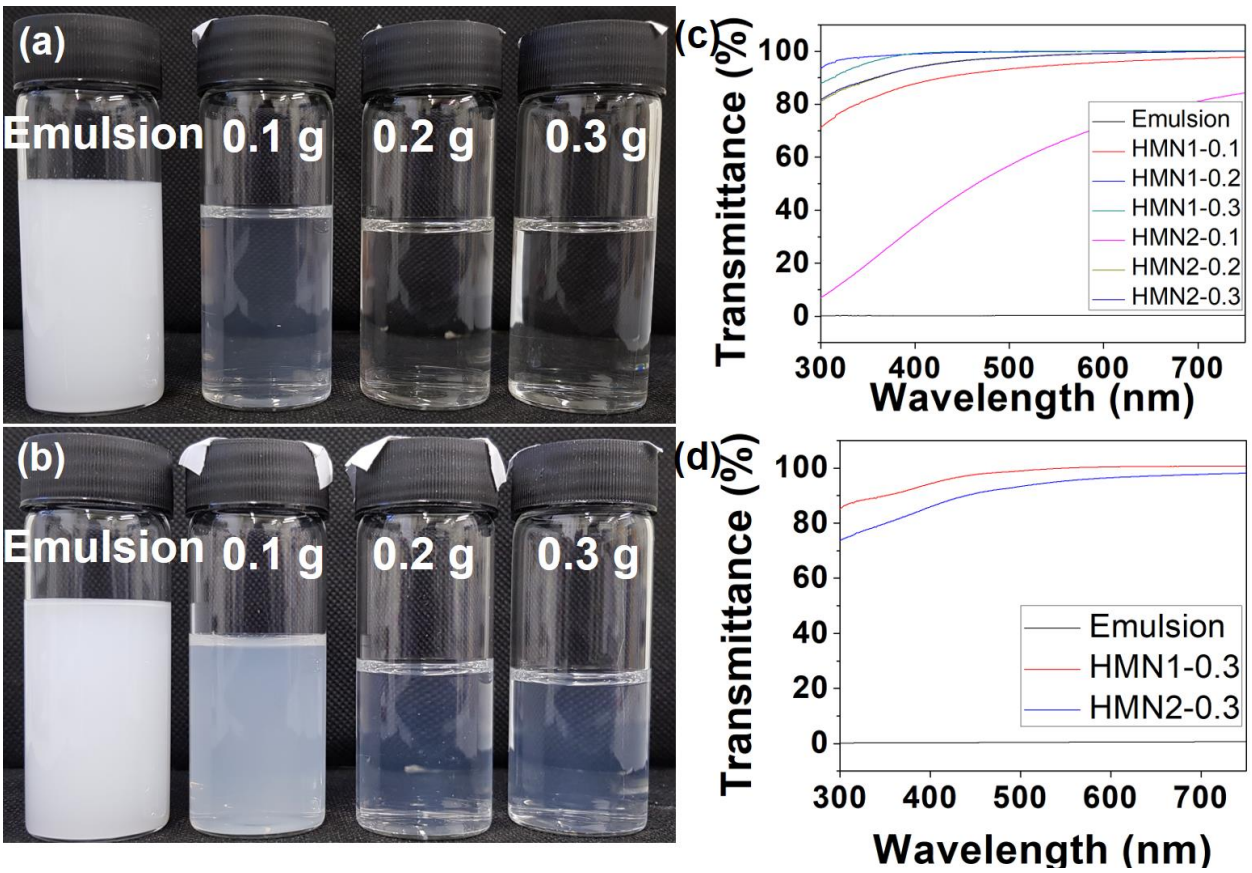

Figure 3-11: Separation of the emulsion by using different amount of (a) HMN-1(b) HMN-2 transmittance spectra of (c) emulsion stabilised by Span 80 (d) Tween 80

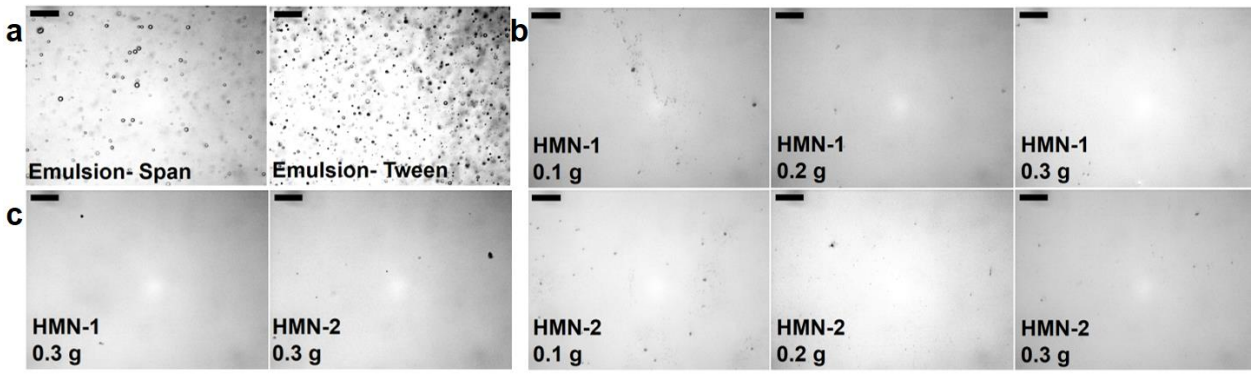

Figure 3-12: Optical microscopy images of emulsion and water obtained after treatment with powders. (a) emulsions (b) emulsion (Span) after treatment with powders (c) emulsion (Tween) after treatment with powders. The scale bar in all images is 50 µm.

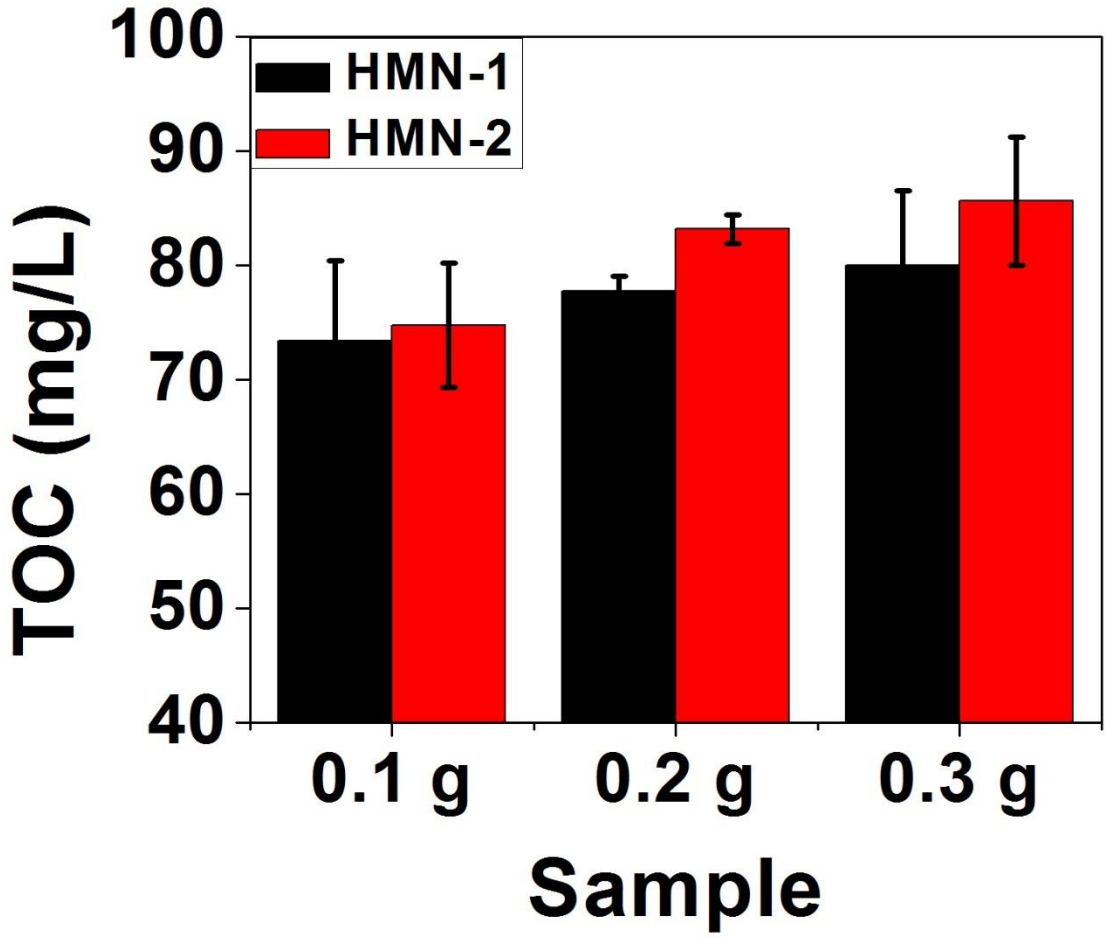

Figure 3-13: Separation efficiency of both HMN-1 and HMN-2 powders measured by TOC analysis.

The samples were characterised by a total organic carbon analyser (TOC) to quantify the organic content in the water before and after separation. TOC values were used to measure both powders' separation efficiency in removing surfactant stabilised emulsions (**Figure 3-*13***). Three measurements were performed for each sample, and an average value is used here, as shown in **Figure 3-*13***. A trend of decreasing organic content is observed with increasing powder in both cases (HMN-1, HMN-2). When the emulsion was treated with 0.1 g HMN-1, a separation

efficiency of 73.38 ± 7.06% was observed, which gradually increased to 79.99 ± 6.56% with the highest amount of powder. Similarly, the treatment with HMN-2 particles resulted in 85.61+5.62% removal of stable organic content from the emulsion.

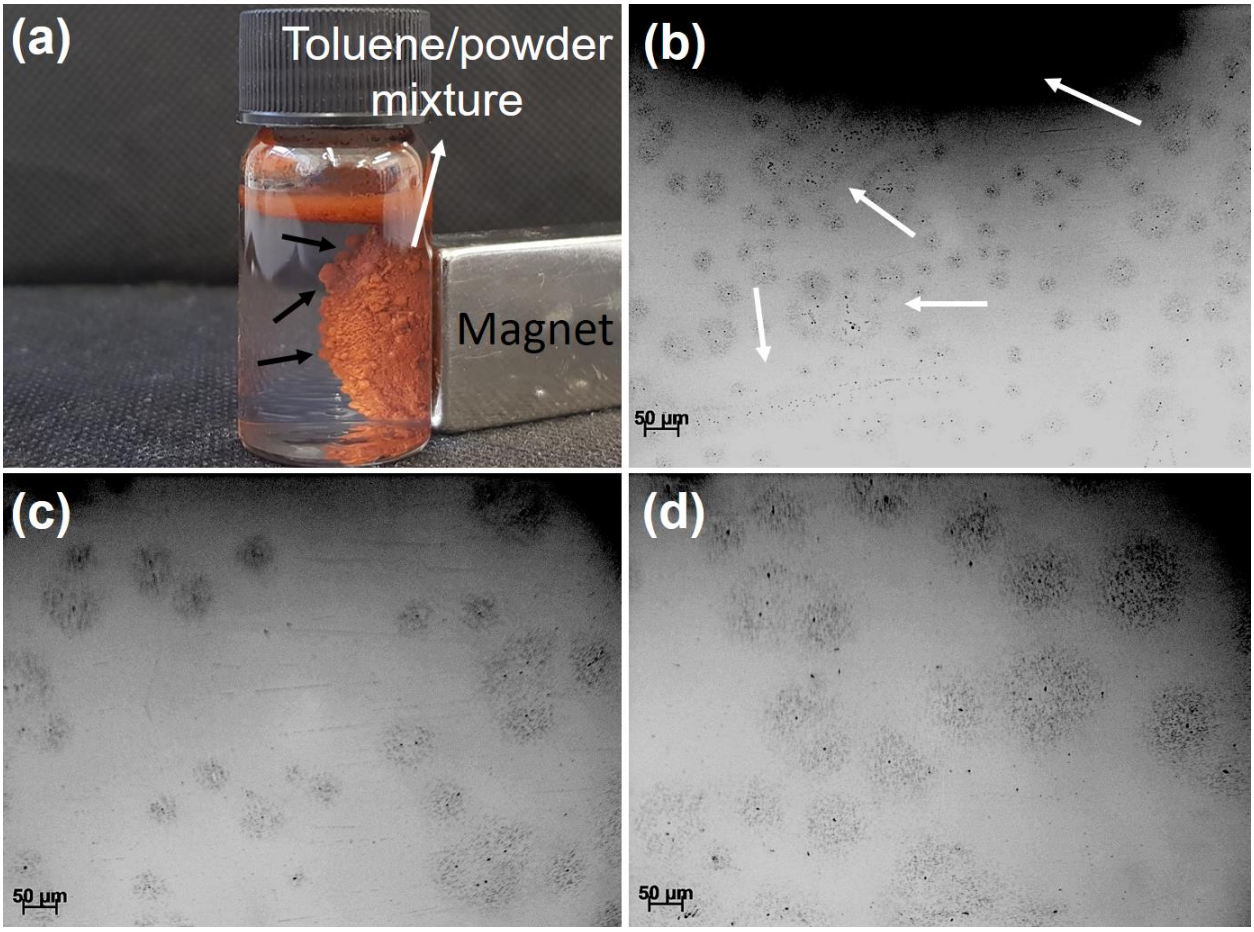

Figure 3-14: (a) Digital image shows the toluene/powder mixture after separation; (b, c and d) Optical microscopy images of toluene/powder mixture, the arrows point to the spherical pattern formed by nanoparticles in oil droplets. Scale bar in optical images is 50 µm.

After separation, the oil/powder mixture floats on water. When held underwater by the magnet, spherical-like structures can be seen on the surface of the mass of particles (**Figure 3-*14***a). The sample was observed under an optical microscope to understand the separation mechanism (**Figure 3-*14***b,c and d). It was difficult to focus on the lumps of powder due to their irregular

shape; however, the surrounding areas show spheres that could be from the toluene droplets containing nanoparticles. It seems that the particles go into the oil droplets under continuous stirring and then coalesce to form a bulk oil/powder mixture which comes to the top due to the difference in surface energy. During this process, the surface area of nanoparticles seems not to be an essential factor in separating surfactant-stabilised emulsions. An important feature could be the dispersion of the nanoparticles within the emulsion which could further enhance the ability of the nanoparticles to capture very small oil droplets.

3.5 Conclusions

Hybrid magnetic nanocomposites with different surface areas were synthesised and used to separate surfactant-stabilised emulsions. The synthesis was carried out by encapsulating magnetite nanoparticles in porous and non-porous silica shells, which were then functionalised with silane to lower the surface energy. The surfaces formed by these powders demonstrated superhydrophobic behaviour with water contact angles of more than 155º. The powders have a selective affinity towards organic solvents and can quickly adsorb oil floating on the surface of the water. The powders were used to separate surfactant-stabilised emulsions and were able to remove more than 95% of the oil. These powders' magnetic properties allow their fast and easy removal after separation of both oil/water mixtures and emulsions.

Chapter 4: Emulsion separation using a free-standing nanofibrous membrane produced by a spray method

Citation: U. Zulfiqar, A. G. Thomas, K. Yearsley, L. W. Bolton, A. Matthews, and D. J. Lewis, "Emulsion separation using nanofibrous hybrid membranes produced by a spray method.," (To be submitted)

Author contributions:

All authors listed have made a substantial, direct and intellectual contribution to the work and approved it for publication. U. Zulfiqar carried out the experimental work and wrote the manuscript whilst A. Matthews, D. J. Lewis and A. G. Thomas were involved in supervision, critical analysis of results, editing and revision of the manuscript. A. G. Thomas helped with the XPS analysis of samples. K. Yearsley, L. W. Bolton provided supervision as industrial mentors and helped in editing the manuscript.

4.1 Abstract

Complicated manufacturing routes and inefficiency in separating stable emulsions delimit commercial applications of superhydrophobic membranes. Herein, we propose a new scalable spray based method for fabricating nanofibrous superhydrophobic membrane for a range of separation applications. Alumina nanoparticles (13 nm) were coated with a nanoscale siloxane framework and later mixed with thermoplastic polyurethane and sprayed on water interface to form a superhydrophobic membrane via phase inversion. The spraying solution and conditions were adjusted to establish an optimum protocol for fabricating a superhydrophobic membrane. A hierarchically structured fibrous superhydrophobic (contact angle > 152°) and superoleophilic membrane was obtained with Young's modulus 1.4± 1.1 N/m^2 and tensile strength of 0.5± 0.1 MPa. Owing to the siloxane surface chemistry, fibrous morphology and micron-sized pores, the membrane shows high flux values (> 4000 $L/m^2.h$) for most organic solvents and maintained high separation efficiency for oil/water mixtures (<95%) for over ten cycles. In addition, the membrane can sieve micron-sized water droplets form surfactant stabilised toluene and hexane based emulsions. Membranes produced in the study are scalable and can be used for a range of filtration applications.

4.2 Introduction

Chemical separation is an essential part of production and waste management industries [280–282]. Among conventional separation techniques, membrane-based processes are favoured as they are scale-able, energy-efficient, and have a smaller carbon footprint due to low energy input [283,284]. A conventional multistage flash evaporation process requires 45 kWh/m^3, while a membrane-based reverse osmosis plant utilises a 4.5 kWh/m^3. Membranes have been used in various applications such as removal of colloids, bacteria and viruses [285–287], recovery of precious metals [288], petroleum refining, disinfection, heavy metals and media filtration [289–294], particulate [295],

carbon capture and gas separation [296–303]. Membranes with a suitable combination of molecular size, pore size, and physicochemical properties can act as a barrier layer to let the desired liquid pass through while blocking the undesired moieties [304–306]. With industries evolving to clean and energy-efficient practices, membrane technology is considered as a responsible route for industrial-scale separation and purification applications. Liquid/liquid separation is required at various industries to treat industrial effluents and sort organics from oil/water mixtures. Typical methods to separate oil/water mixtures such as skimmers, absorbents, flocculation, and cyclones suffer higher operational costs and low efficiency. A separator's efficiency is significantly compromised if the dispersant is uniformly distributed, as in the case of stable emulsions, which often result from surfactants [31,35]. Methods such as applying electric field or chemicals to separate emulsions have limited application due to the creation of secondary pollutant streams [35]. Membranes with selectivity towards organic and small pore size can have many advantages over traditional separation techniques.

A material with micro/nanoscale features and low surface energy can prevent water interaction due to non-polar surface chemistry and air pockets in its top surface layer. Water repellence known as superhydrophobicity has been endowed to several materials for applications in corrosion protection, drag reduction, self-cleaning and oil/water separation. Recently, membranes with superhydrophobic properties were studied to selectively remove a liquid from a biphasic mixture [221,254,307–314]. Hydrophobic membranes were engineered for applications such as desalination, oil/water separation, biogas upgrading, ammonia removal, recovery of methane and CO_2 absorption[289,315–320]. In a recent work, polyvinylidene fluoride (PVDF) membrane was coated with fluorinated silica nanoparticles to create a composite membrane for the separation of oil/water mixtures [104]. Functionalised silica nanoparticles were spray-coated on PVDF membrane to create

a Janus membrane for oil/water separation[321]. Asymmetric wettability of membranes allowed the separation of both oil/water and water/oil emulsions. Another work reported a polydopamine/reduced graphene oxide-based superhydrophobic membrane functionalised with fluoropolymer for separation of chloroform and water mixtures [93]. Despite some progress in this area, scalable separation systems entail better membrane materials with higher stability and selectivity.

Spray coating is a straightforward process and has been used for various coatings applications; however, there are a few reports on utilising this process to fabricate free-standing membranes. A recent study explored composite block copolymers membranes fabrication by spraying the solution on a macroporous substrate [322]. Another work used spray method to coat waterborne polymers such as polyethyleneimine and poly(glycidyl methacrylate-co-poly(ethylene glycol) methyl ether methacrylate) P(GMA-co-mPEGMA) on the surface of PVDF membranes [323]. In this work, polyurethane (PU) based nanocomposite membranes have been fabricated to separate stable emulsions. PU is a block copolymer with a unique set of properties, including flexibility, hardness, abrasion resistance and chemical resistance. It offers a window of processing with other materials to tailor its properties for advanced composites. It has been used in many application such as paints[324], adhesive[325], gas separation[192,326–328], fibers[329] and sealants[330]. Fibrous PU membranes with hydrophobic properties have been recently synthesised by electrospinning and modified with fluoroalkylsilane for protective clothing applications[331]. Herein, we report a spray based method for the fabrication of PU based free-standing superhydrophobic nanocomposite membranes. Surface modified Al_2O_3 nanoparticles (Al_2O_3 NPs) were grafted in situ on polyurethane framework, and a nanofibrous nanocomposite membraned was obtained via phase inversion method. Membranes were characterised by several advanced characterisation techniques

to optimise the synthesis protocol and later used for the separation of stable emulsions and oil/water mixtures for several cycles. The process used in this study can be used to fabricate membranes for a range of applications such as filtration energy and wearable devices.

4.3 Materials and Methods

4.3.1 Materials

Alumina nanoparticles (Al_2O_3- CAS Number 1344-28-1) and Span 80 ($C_{24}H_{44}O_6$-CAS Number 1338-43-8) were supplied by Sigma Aldrich. Dichlorodimethylsilane (CH_3SiHCl_2- CAS Number 75-78-5) and Tetrahydrofuran $(CH_2)_4O$ -CAS Number 109-99-9) were supplied by Fisher Chemical. Thermoplastic polyurethane (PU) beads (Elastollan® L 1185 A 12) were acquired from Goodfellow. Spray coating apparatus from Sparmax® was used for the fabrication of membranes. All the solvent (Hexane, Toluene, Tetrahydrofuran, Acetone and Methanol) were procured by Fisher and used without as received form.

4.3.2 Methods

2 g Al_2O_3 NPs (13 nm) were mixed with 100 ml hexane in a beaker under continuous stirring (500 rpm) using a hot plate and magnetic stirrer. Later, 25 ml dichloro dimethyl silane (DCDMS) was added to the mixture, and the temperature of the hotplate was raised to 100 ℃. The powder dried in the beaker at 200 ℃ for 2 hr after removal of solvent. The dried powder was mixed in acetone and centrifuged several times to remove the byproducts of the reaction and obtain pure functionalised nanoparticles. Finally, the powder was dried in an oven overnight (80 ℃).

3wt% mixture of thermoplastic polyurethane (PU) was prepared by dissolving the PU beads in tetrahydrofuran (THF) at 1000 rpm and 40 ℃. A known quantity (Table 1) of functionalised nanoparticles was introduced in the PU/THF mixture and left for stirring to prepare homogenous solutions. The solutions were sonicated in an ultrasonication bath to ensure the homogenous distribution of nanoparticle in PU mixture. Separately, a crystallisation dish was

filled with hot water (80 ℃) and placed on a hotplate (100 ℃) to maintain the temperature. The composite solution was sprayed on the surface of hot water using a spray gun at an angle of 45° from 10 cm distance and left to cure overnight. Membranes were collected from the surface of the water and washed with acetone several times and dried in an oven at 80 ℃. Synthesis of the membrane was carried out on the surface of hot water to remove the solvent quickly achieve a fibrous structure.

Table 0-1: Sample names for Al_2O_3 NP-coated SD particles

PU: Al_2O_3	**Sample Name**
1:0	PM
1:1	CM-1
1:1.66	CM-2
1:2.33	CM-3

4.3.3 Characterisation

Field emission scanning electron microscope (SEM) and Energy-dispersive X-ray spectroscopy (EDX) was used to observe the structure of samples and elemental mapping of the membrane. Samples were coated with a thin layer of platinum before SEM analysis to make them conductive. The chemical structure of samples was evaluated by Fourier-transform infrared spectroscopy (FTIR) whilst the information about surface chemistry was obtained by X-ray photoelectron spectroscopy (XPS). Thermal gravimetric analysis (TGA) of nanoparticles and membrane samples was performed in air with a heating rate of 10 °C/min. Tensile testing of membrane samples was done by using an Instron 3344L3928 instrument with a 100N load cell and a strain rate of 10mm/min. Membrane samples were used for the contact angle measurements using

a Kruss drop shape analyser. The surface topography of the membrane was profiled by using a MultiMode8 atomic force microscope.

Separation experiments were performed by using a 1:1 mixture of toluene and water dyed with Sudan III and methylene blue, respectively. For emulsions separation experiments, different volumes of water (5, 10 and 15%) were mixed with toluene and hexane in the presence of Span 80 as a surfactant. Span 80 is a nonionic surfactant with HLB 3-5 and helps to stabilise the water droplets in oil for more extended periods. The following formula calculated the oil/water separation efficiency of the membrane:

$e = (C°/ C) \times 100$

Where,

e= Separation efficiency of the membrane

C = Initial volume of oil in an oil/water mixture

C°= volume of the oil obtained after separation.

4.4 Results and Discussion

Figure 1 shows the TEM image of uniformly distributed spherical shaped Al_2O_3 NPs with a diameter of 13 nm. Figure 1b shows the FTIR spectra of Al_2O_3 NPs before and after functionalisation. Compared with the pristine Al_2O_3 NPs, four new peaks are observed at ca. 2960, 1260, 1013-1090, and 791 cm^{-1} post functionalisation. The peaks at ca. 2960, 1260, and 791 cm^{-1} assigned to the CH_3 and Si-CH_3 functional groups, whilst the broad band at ca. 1013-1090 $cm^{-1}$is characteristic to siloxane linkage (-Si-O-Si-). Whilst FTIR confirmed the grafting of dimethylsily groups on the surface of Al_2O_3 NPs, XPS was used to quantify the nanoscale surface chemical

composition. Four prominent peaks in XPS spectra of functionalised nanoparticles indicate Aluminum, Silicon, Carbon, and Oxygen. Quantification of spectra shows 25.38 at.% Aluminum, 3.01at.% silicon, 19.51 at.% carbon and 52.10 at.% oxygen. The peak appearing at ca. 102 eV is assigned to the silicon present in the polysiloxane network, which has supposedly covered the surface post functionalisation. As the surface film contains a polysiloxane structure, functional groups' depth appears to be less than 13 nm.

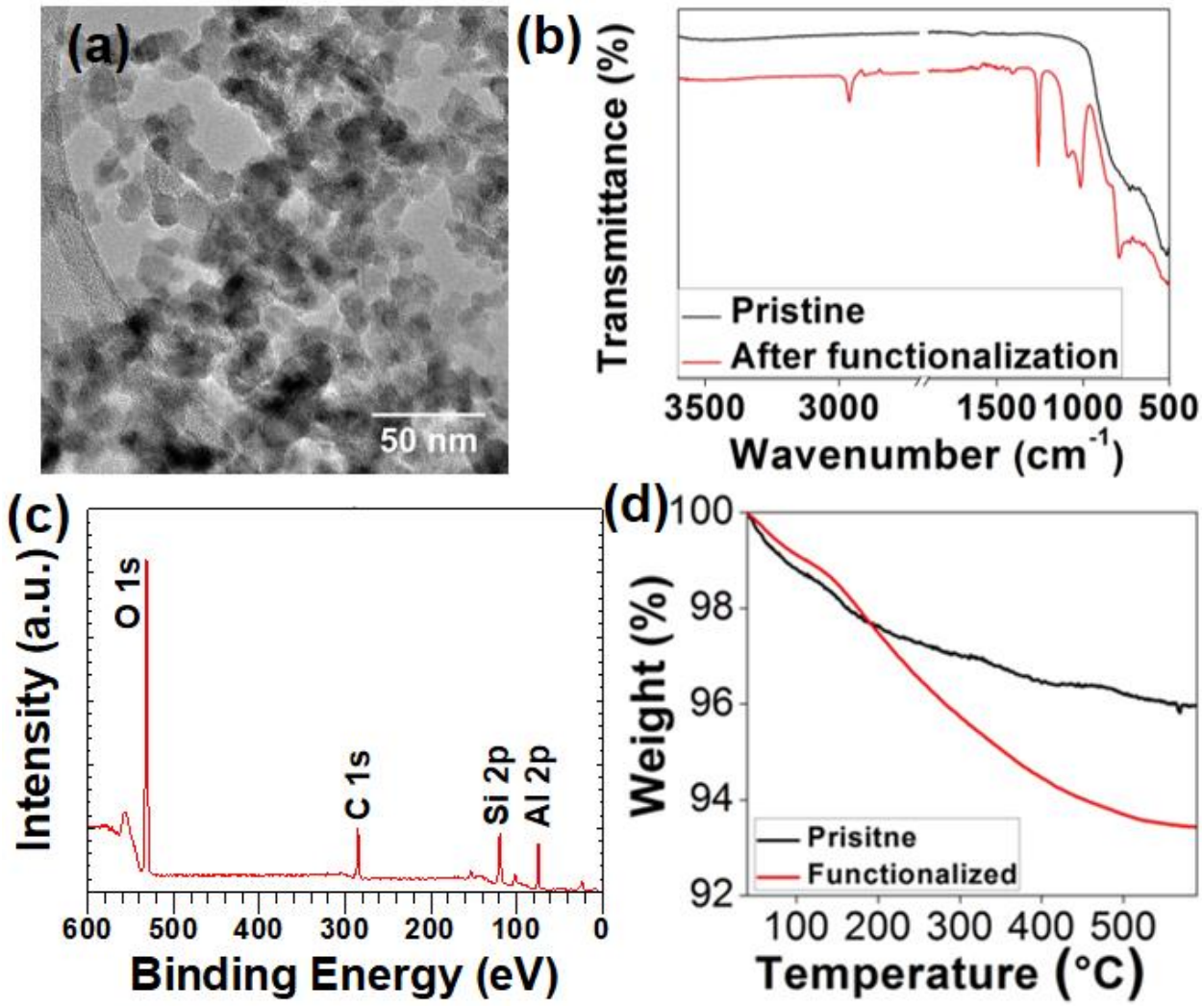

Figure 4-1 (a) Bright field TEM (200 kV) images of functionalised alumina nanoparticles (b) FTIR of pristine and functionalised nanoparticles (c) XPS spectra of functionalised nanoparticles (d) TGA of pristine and functionalised nanoparticles

TGA of functionalised nanoparticles was performed to observe the stability and measure the grafting density of functional groups. Figure 4-*1*d shows the TGA graph of pristine and functionalised nanoparticles. Nanoparticles contain a large number of hydroxyl surface functional groups due to their small size. Therefore, continuous weight loss with one step around 100℃ in pristine nanoparticle is ascribed to the moisture and dehydroxylation of surface groups.

Functionalised nanoparticles show two stages of weight loss; 1st stage corresponds to the removal of moisture whilst the 2nd region shows the degradation of dimethylsilyl functional groups. Surface coverage of functional groups can be calculated from the value of weight loss, size of nanoparticles and surface area using equation [332].

$$Grafting\ density = \left(\frac{wt\%}{100 - wt\%}\right)\left(\frac{6.022 \times 10^{23}}{Mw \times Surface\ area}\right)$$

Calculations from the equation mentioned above give the grafting density of 1.50 nm^{-2} in functionalised nanoparticles. FTIR, XPS and TGA analysis of nanoparticles concluded that surface hydroxyl groups of nanoparticles were replaced with a thin layer of polysiloxane groups due to functionalisation. Despite having a polarised backbone (Si-O), polysiloxane groups have the lowest surface tension due to the shielding effect of methyl groups oriented outside the silicone chain and responsible for hydrophobic characteristic. The surface tension of polysiloxane falls around 20-25 mN/m. A smooth film by dimethyldichlorosilane would give a contact angle in the range of 95-105°. However, a nanoscale polysiloxane film would bestow low surface energy to nano features making an ideal combination for the superhydrophobic effect. Al_2O_3 NPs containing a nanoscale polysiloxane film endow nanoscale roughness and low surface energy to the membrane. The superhydrophobic properties of the membrane are expected to improve with increasing wt.% of nanoparticles. Figure 2 shows the morphology of the control sample (pristine PU) and the membranes with different quantities of nanoparticles. The control sample shows a film-like structure with some interconnected fibres, which show planar surface morphology in high magnification images. With increasing concentrations of nanoparticles in the spray solution, the thinning of fibres and a more porous structure was observed in SEM images of CM1 and CM2.

NPs are present as clusters on the surface of fibres at low concentration but seem to form a more regular film with increasing wt/% in the solution.

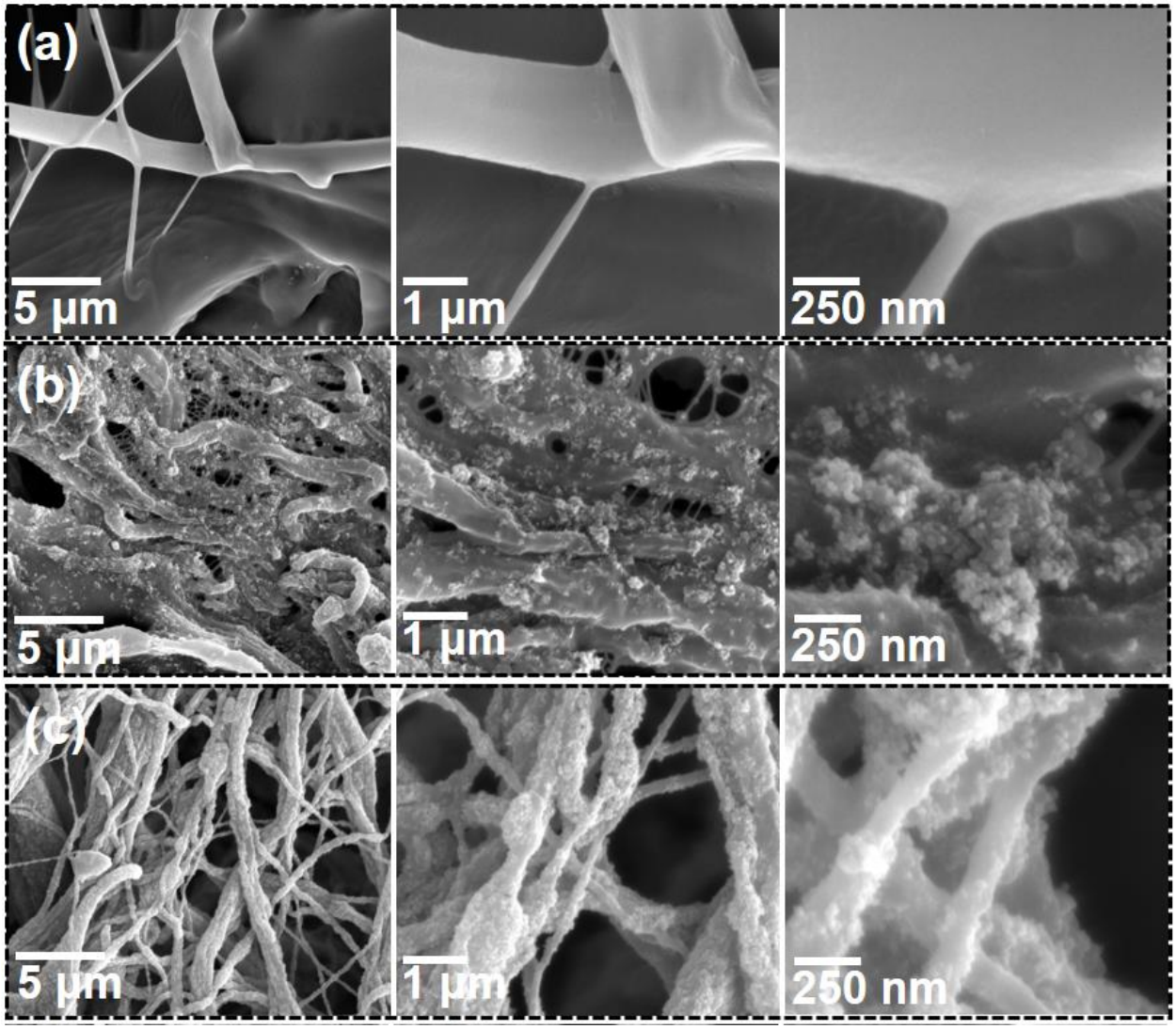

4-2: SEM images of (a) PM, (b) CM-1, and (c) CM-2 at different magnifications.

Figure 4-3a shows the membrane sample with the highest quantity of nanoparticles (CM-3). The membrane's fibrous structure is completely covered with nanoparticles, and individual fibres have formed a three-dimensional entwined porous network. Figure 4-3b shows the cross-section of CM-

3 membrane, which confirms that the membrane consists of entangled fibres and is porous throughout its structure without any PU film that could block the passage of liquids during filtration.

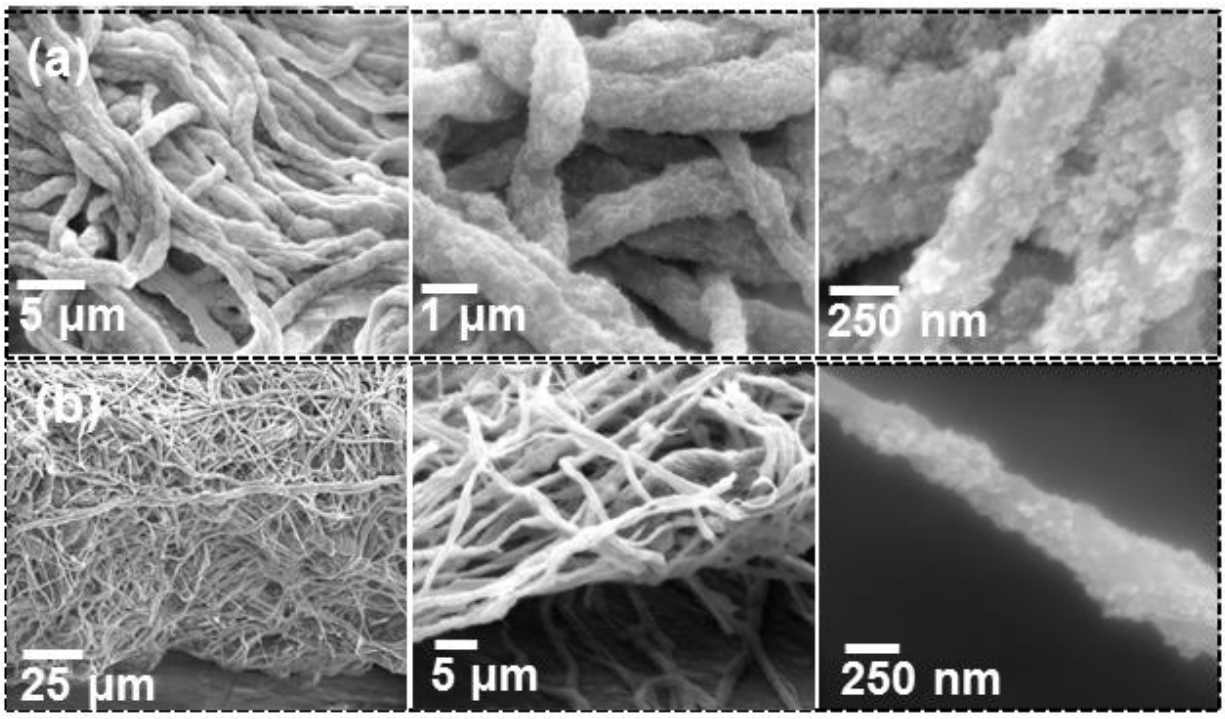

Figure 4-3: SEM images of (a) CM-3, (b) cross-section of CM-3.

Fig 4-4a shows the EDX mapping of the key elements on the surface of CM- 3 membranes. Elemental maps are presented with distinct colours and a black background to show the distribution of the membrane's single filament. Elemental spectra for Al indicates Al_2O_3 NPs is uniform and confirms the homogeneous distribution of nanoparticle coating on the filaments' top layer. EDX mapping also provided information about the uniform distribution of other elements such as Si, which is the characteristics of silane functional groups.

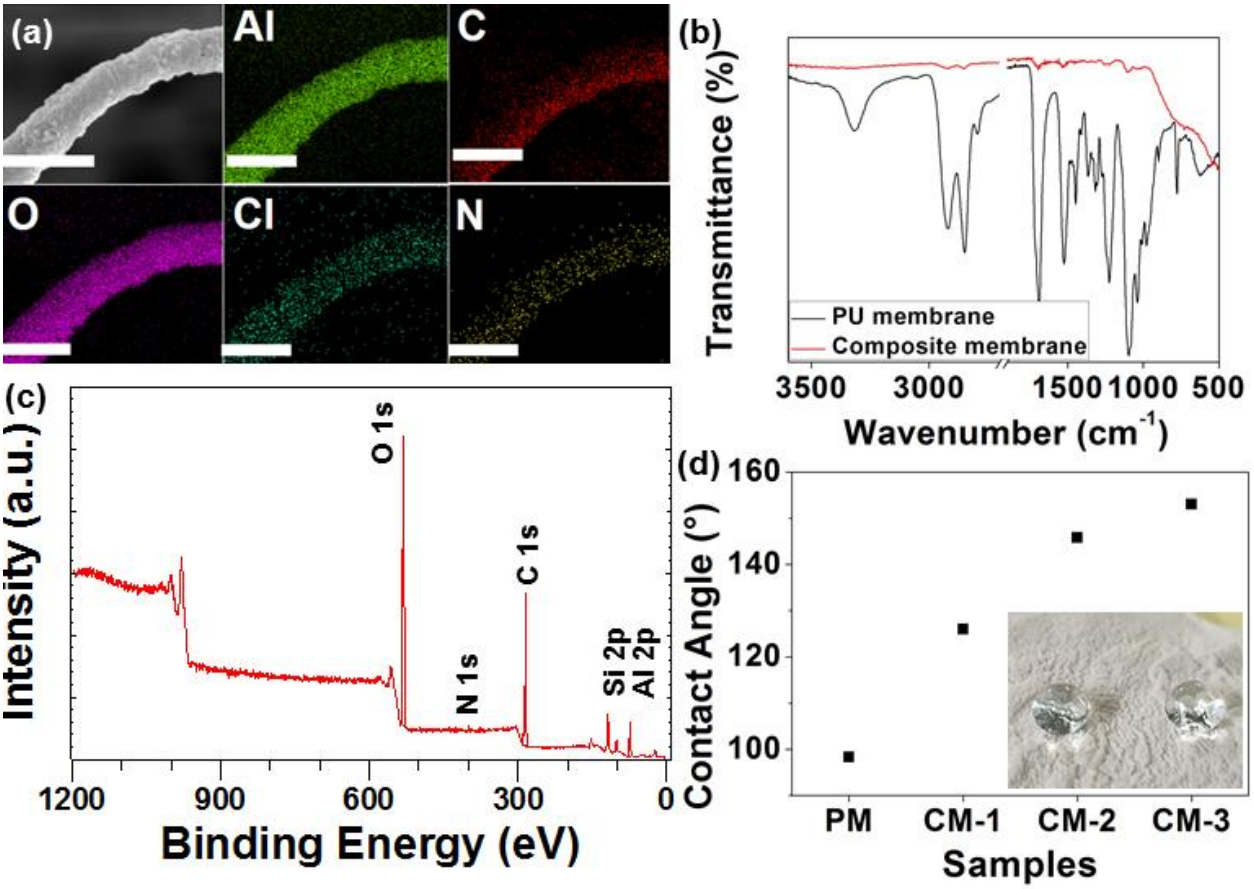

Figure 4-4: (a) EDX mapping of a single filament of membrane showing the uniform distribution of nanoparticles (b) FTIR spectra of CM-0 and CM- 3 (c) XPS spectra of CM-3, (d) contact angle measurement of all samples.

FTIR and XPS measurements were performed to study the chemical structure of composite membranes. Figure 4-4b shows the FTIR spectra of PU membranes and CM-3; the spectra show strong peaks for N-H and C-N bonding in the range of 1530 cm^{-1} and 1314 cm^{-1} typical for PU, peak appearing at 1700 cm^{-1} is assigned to the vibration from C=O bond. The FTIR spectrum of composite membrane shows weak signals for characteristic bonds of PU; however, a peak appearing around 1080 cm^{-1}can be assigned to the silyl methyl groups attached to the surface of alumina nanoparticles. XPS analysis of the membrane provides information about the nanoscale surface chemistry of the composite membrane. Fig 4-4c shows the main elements present on the surface, including carbon, nitrogen, oxygen, aluminium and silicon. Aluminium and silicon signals

are from functionalised nanoparticles present on the surface of the membrane. The quantification of XPS spectra shows the presence of 14.78 at.% Aluminum, 2.85 at.% silicon, 44.21 at.% carbon, 37.48 at.% oxygen and 0.68 at.% nitrogen. Silicon peak is an indicator of silyl methyl groups present on the surface of the membrane. The elemental composition of silicon in the composite membrane is comparable to the one detected in the XPS spectrum of functionalised Al_2O_3 NPs. It confirms that non-polar groups dominate the nanoscale surface composition of the membrane, which are essential to avoid water contact.

Figure 4-*4*d shows the contact angle measurement of all membrane samples. Pristine PU membrane sample shows a water contact angle of 98° which gradually increased to 153° with an increasing amount of nanoparticles. As discussed earlier, the gradual increase in contact angle directly relates to the loading of nanoparticles in the membrane. Uniformity in the distribution of nanoparticles on the membrane surface and roughness improves at higher loadings, ultimately leading to the highest contact angle in CM3. The addition of nanoparticles gradually enhanced porosity and surface roughness in the membrane, ultimately resulting in higher contact angles of the composite membrane. AFM further explained the surface texture of the CM3 membrane and quantified the roughness needed for superhydrophobic properties. It is important to note that the AFM analysis of this material was complicated due to the irregular, rough and fibrous structure of the membrane; however, two AFM images are presented, and the roughness values were calculated by processing the high-resolution image using Gwyddion software. Topography analysis by AFM suggests a rough and fibrous structure of the membrane. The root mean square roughness (S_q) was calculated to be 210 nm. Uniformly distributed tiny protrusions in AFM mages indicate the presence of nanoparticles on the fibre surface. Micron sized fibres with nanoscale particles on their surface lead to a heterogeneous structure creating air pockets that help achieve Cassie Baxter state

during interaction with water. An air layer entrapped between solid and liquid interface due to nanoscale roughness bestows water-repellant properties to the membrane. SEM images and AFM results confirm that CM-3 contains nanoscale features in tandem with microscale fibres providing an ideal 3D porous platform to sort organics from oil/water mixtures selectively.

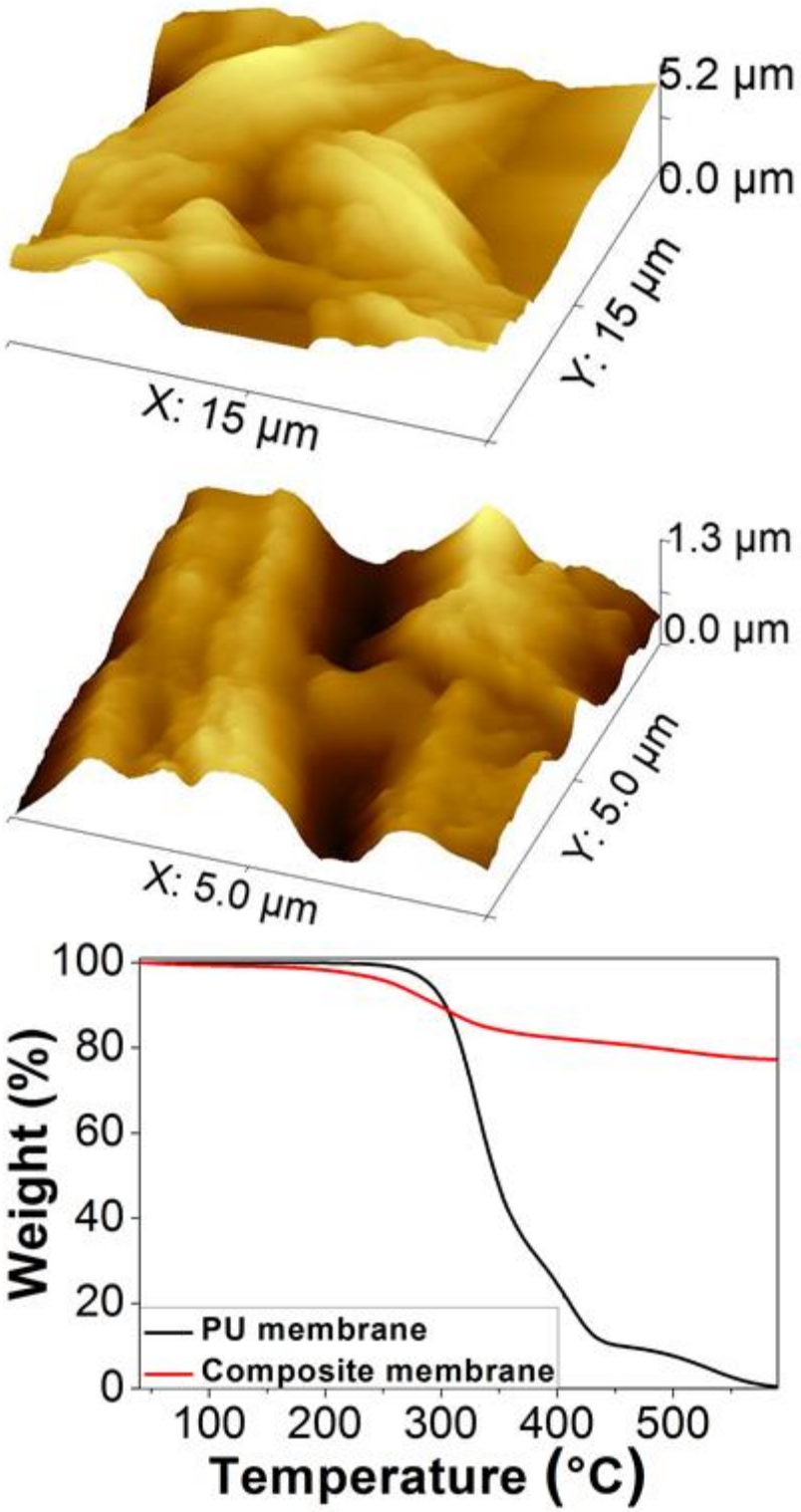
5.2 µm
0.0 µm
Y: 15 µm
X: 15 µm
1.3 µm
0.0 µm
Y: 5.0 µm
X: 5.0 µm
Weight (%)
100
80
60
40
20
0
PU membrane
Composite membrane
100
200
300
400
500
Temperature (°C)

Figure 4-5: (a) AFM images showing the morphology of the membrane at two different magnifications. (b) TGA of PM and CM-3.

Fig. 4-5c shows the TGA of PU-M and CM-3. The weight loss curve for PU-M shows two stages of degradation with shoulders around 300 ºC and 400 ºC. The curve ends before 600 ºC with ca. 0% residue left. This two-stage weight loss is attributed to hard and soft segments in thermoplastic polyurethane. The degradation starts with urethane's dissociation, followed by the degradation of polyols in the soft segment in the second stage. Different degradation behaviour is observed in the TGA curve of CM-3 membrane as the curve has shifted to a lower temperature and indicates a significantly higher residue after 600 ºC. Nanoparticles may contain unreacted hydroxyl groups on the surface, which triggered the early weight loss and lead to a steep degradation curve showing the combined weight loss due to hydroxyl, silyl methyl group and PU. The residue left after 600 ºC indicates the inorganic content present in the membranes. It implies that the dissociation of the PU framework will cause the membrane's thermal degradation whilst alumina nanoparticles remain intact due to their inorganic nature.

Figure 4-6a shows the tensile stress-strain curve of PU membrane and CM-3 membrane. It is important to note that an average of three measurements is used for each sample. The fibrous structure of the membrane suggests the non-uniform distribution of load; therefore, multiple measurements were made, and an average value is used in this manuscript. PU membrane has Young's modulus of 0.79± 0.2 N/m^2, %age elongation at breaking point 152.3± 36.8 and tensile strength 1± 0.4 MPa. CM-3 membrane shows relatively higher Young's modulus (1.4± 1.1 N/m^2) but the reduction in %elongation at breaking point 69.78± 9.81 and lower tensile strength 0.5± 0.1 MPa as compared to the PU membrane. Mechanical properties of membranes are controlled by various parameters such as fibrous morphology. In addition, surface throughout the matrix,

manufacturing route and loading of nanoparticles. Surface texture and fibre size contribute to mechanical behaviour; any crack or fracture on the surface would accelerate mechanical failure [333].

Similarly, fibres with small radius are prone to cracks due to the small surface area per unit length. PU membrane has a sheet-like structure, whilst CM-3 contains hierarchically structured entangled nanoscale fibres. The difference in morphology could have triggered disparate response during uniaxial load. Besides, nanomaterials have a significant impact on the mechanical properties of polyurethane depending upon the processing and impregnation methods.

In a previous report, three different types of nanoparticles (Al_2O_3, SiO_2, $CaCO_3$) were incorporated in a thermosetting polyurethane matrix via a shearing device and their effect on mechanical properties was studied. Nanoparticles initially increased the tensile strength and Young's modulus but had the opposite effect after a particular threshold concentration (ca. 10%) [334]. Similar behaviour was observed in other studies with nanosized clay and $CaCO_3$. Another study reported significantly lower tensile strength and Young's modulus for carbon nanofiber reinforced porous thermoplastic polyurethane film prepared by solution casting [335]. A decrease of %elongation in amorphous poly(tetramethylene oxide)-based polyurethane–urea copolymer was observed due to ca. 10% colloidal SiO_2 [336]. We conclude that nanoparticles' addition to the polyurethane matrix enhanced the porosity significantly and resulted in a fibrous morphology that ultimately reduced the tensile strength and %elongation but enhanced the brittleness (higher Young's modulus). Nevertheless, the membrane still shows some flexibility despite having inorganic content in the matrix.

Fig. 4-6b shows the digital images of membranes produced in various sizes. Fig. 4-6c shows a filtration setup with CM-3 membrane. Water is unable to penetrate through the membrane due to

strong repellence. The filtration setup was connected with a pump to demonstrate the breathability and porous structure of the membrane. The turbulence in water (Figure 4-6c) due to pressurised air and air bubbles demonstrates the breathability of CM-3 membrane. The membrane is composed of a fibrous porous structure and lets the air pass through and restrict water entry.

Superhydrophobic properties and fibrous structure helped selectively capture oil from oil/water mixtures, as shown in Fig. 4-6d. Toluene (dyed with Sudan red) floats on the surface of the water and form a thin layer. When a small piece of the membrane was immersed in the oil/water mixtures, it immediately absorbed the oil from the water surface as indicated by the red colour due to Sudan red dye in oil.

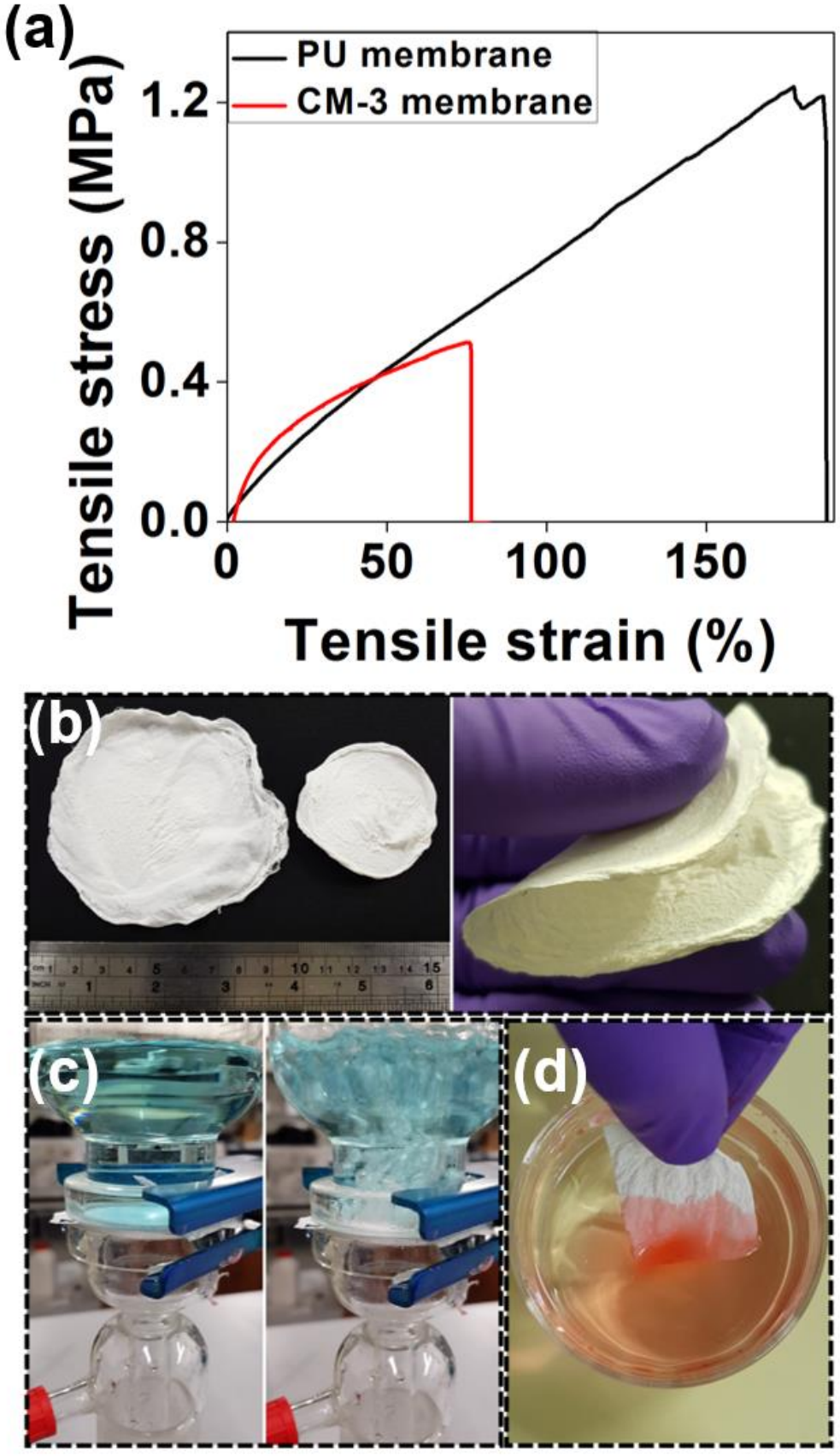
(a)
PU membrane
CM-3 membrane
Tensile stress (MPa)
1.2
0.8
0.4
0.0
0
50
100
150
Tensile strain (%)
(b)
(c)
(d)

Figure 4-6: (a) A typical stress-strain curve of PU-membrane and CM-3 membrane, (b) digital images showing the different sizes of membranes which can be formed by this method, (c) images shows that membrane does not let the water pass through, and the porous and breathable structure of membranes; the pump was connected to the inlet, and air bubbles can be observed coming through the membrane, (d) images showing the absorption of toluene (red) from the surface of the water using CM-3 membrane.

The flux of a membrane is an essential parameter for separation applications. The flux of CM-3 membrane was calculated by observing the flow volume of various organic solvents through the membrane. Figure 4-7a shows flux for different solvents. The flux values of 4049, 3630, 4387 and 5012 $L/m^2.h$ are observed for Toluene, Hexane, Diethyl ether, and Acetonitrile, respectively. Flux value is relatively high for most solvents, implying that the membrane can separate various oils with different viscosities. Table 2 shows a comparison of different membranes reported recently in the literature.

Figure 4-7b shows the oil/water separation set up for a typical oil/water mixture prepared by mixing dyed toluene and water (inset Fig. 4-7b). The membrane was fixed in the filtration setup, and separation of oil/water mixtures was performed under gravity without any external pressure. Oil/water mixture was poured from the top, and oil quickly transferred through the membrane to the flask. The water could not pass through the membrane, as shown in Fig 4-7b. The separation was repeated ten times to observe the recyclability and efficiency for various separation cycles. It was observed that the membrane maintains efficiency of more than 95% for ten cycles, as shown in Fig 4-7c.

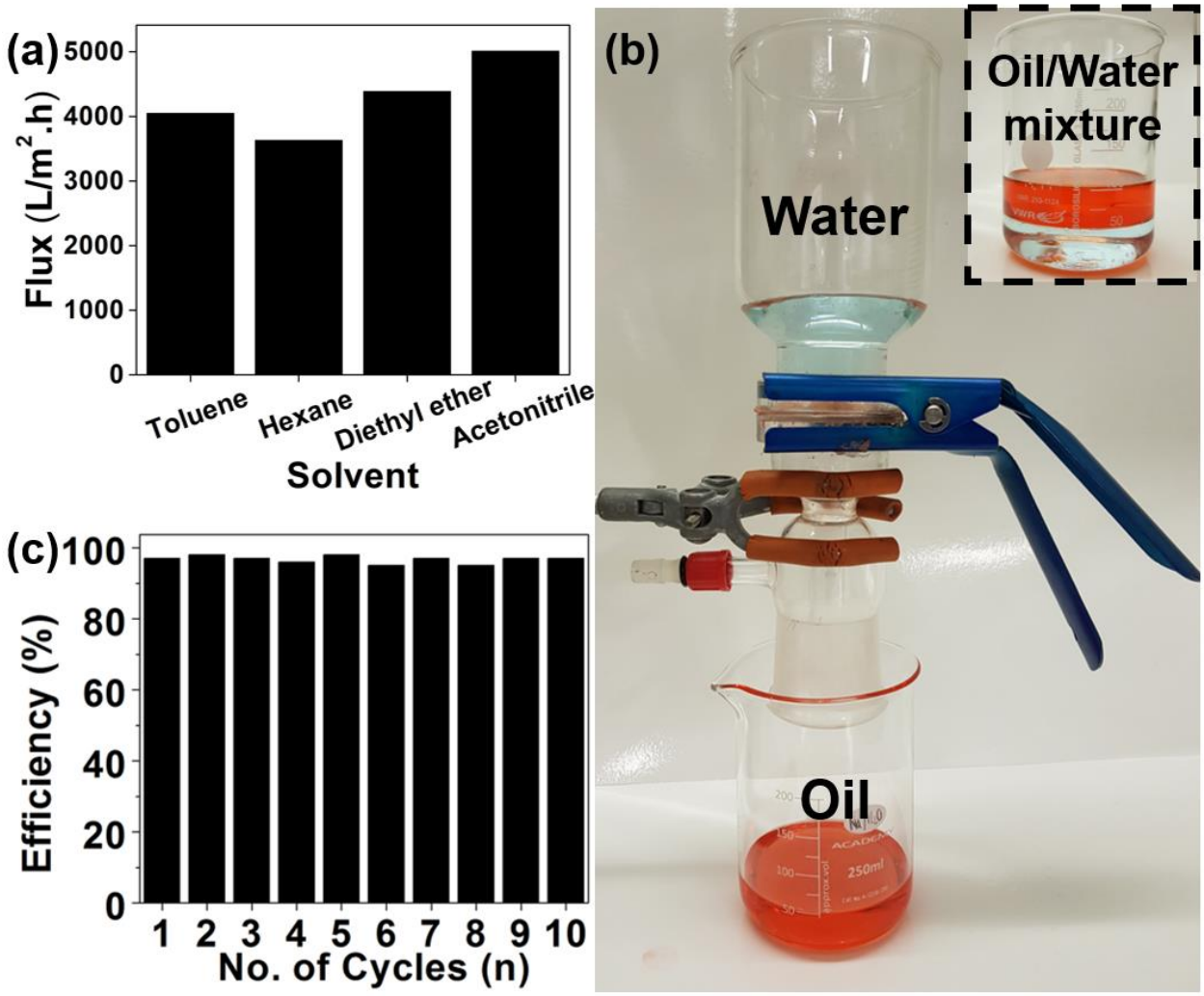

Figure 4-7: (a) Graph showing the flux of different solvent through membranes (b) images showing the setup for separation of oil/water mixtures; inset shows a typical oil/water mixture, (c) graph showing the separation efficiency of membrane for ten cycles of separation.

Table 4-2: Comparison of different types of membranes used for gravity-based oil/water separation

Membrane	Method	Contact angle	Permeate	Flux	Ref.
Polytetrafluoroethylene	Laser ablation	154.6 ± 2°	1,2-dichloroethane	65.9 ± 2.3	[337]
Polytetrafluoroethylene	Electrospinning/sintering	155.0°	Oil	1215	[338]
Polysulfone /fluorinated ethylene propylene	Phase separation	153.3	Diesel	668.8	[339]
PVDF-HFP/Cu($CH_3COO)_2$	Electrospinning	152.4°	Hexane	>2050	[340]
Polyvinylidene fluoride-co-hexafluoropropylene/ Carbon nanoparticles	Electrospinning	160.8°	Hexane	2163 ± 29	[341]
Polyvinylidene fluoride/ Ovalbumin/Tannic acid	Adsorption	Superhydrophilic	Water	2008 ± 88	[342]

Separation of oil/water mixture is relatively easy when they exist as two separate phases due to the different polarities of both liquids. In most practical scenarios, oil/water mixtures are emulsified due to surfactants, and it becomes tricky to separate the finely dispersed droplets from an emulsion. Emulsion separation is vital from an industrial point of view as most practical scenario mixtures are stabilised by naturally occurring surfactants. Different types of hexane and toluene-based emulsion were prepared using a surfactant (Span 80 (HLB=3-5) to simulate such a situation in this work. Two different emulsion systems based on toluene and hexane were prepared by mixing the surfactant and a known amount of water in oil via stirring at 1000 rpm. This method produces homogenised oil/water mixtures that are stable for several days. Toluene based emulsions

containing 5, 10 and 15% water were designated as T1, T2 and T3, respectively, while the hexane based emulsion with the same volume %ages of water was denoted as H1, H2 and H3. Figure 4-8a shows a typical separation cycle for an emulsion using CM3 membrane. The emulsion was poured into the separation setup containing the CM-3 membrane. The membrane retained the dispersed water droplets, and clean oil was collected as a permeate in a glass vial. Figure 4-8a shows a milky coloured liquid (emulsion) on top while the transparent liquid(oil) is collected at the bottom. Figure 4-8b shows the digital images of emulsion before and after filtration.

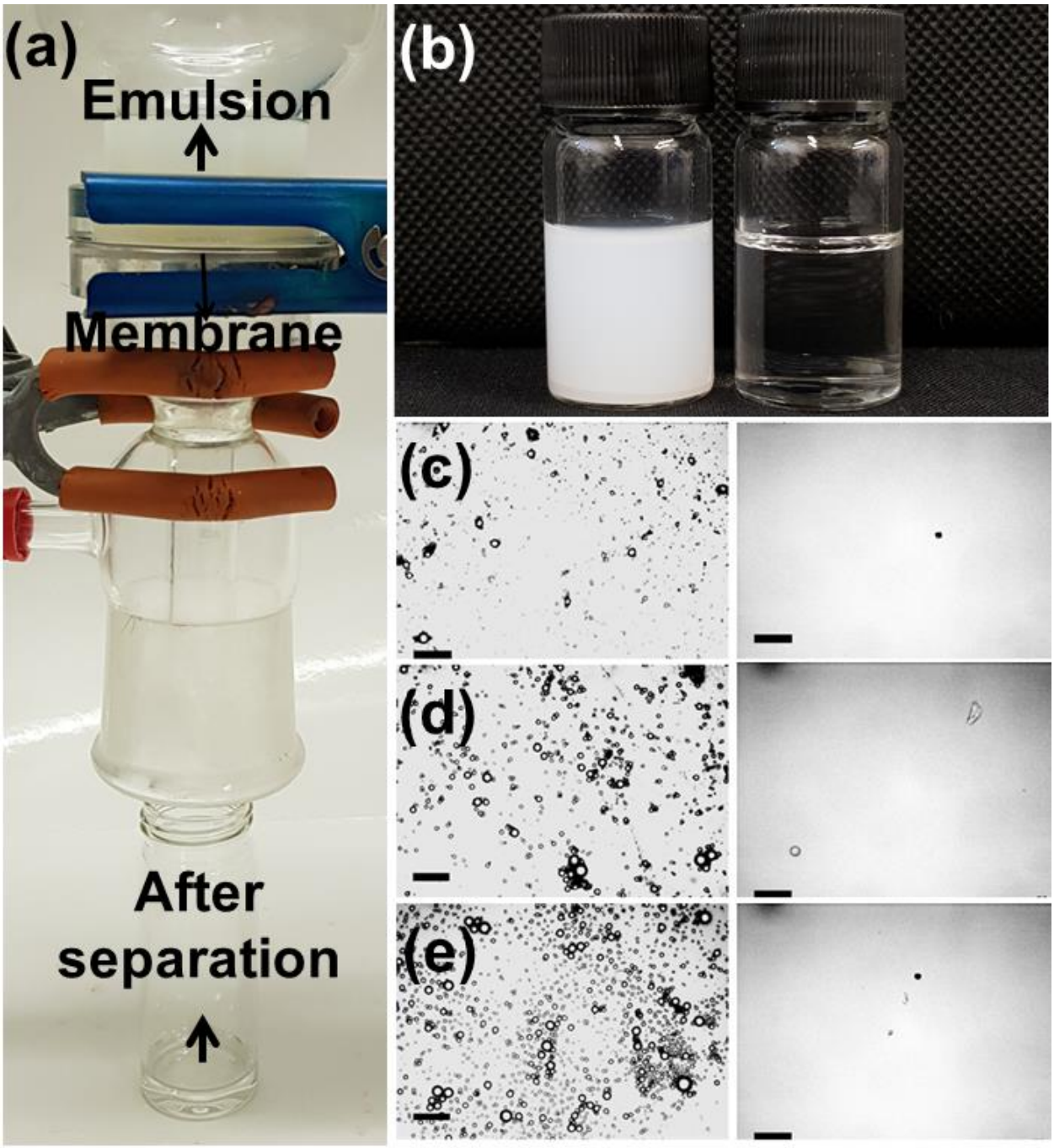

Figure 4-8: (a) Separation setup for the separation of emulsions using CM-3 membrane (b) digital images showing the emulsion before (white liquid) and after (permeate) separation, optical microscopy images of emulsions (c) T1, (d) T2, (e) T3. Scale bar on optical images is 50 µm.

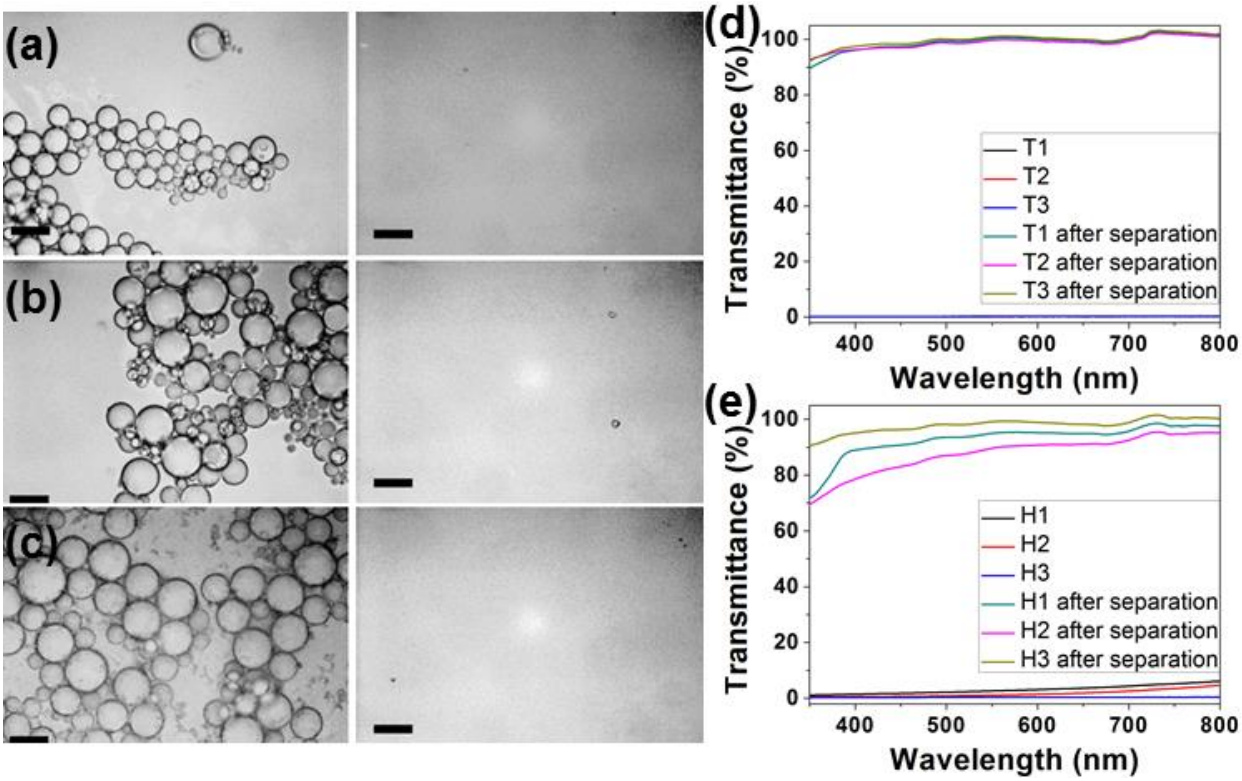

Figure 4-9: (a) Separation setup for the separation of emulsions using CM-3 membrane (b) digital images showing the emulsion before and after separation, optical microscopy images of emulsions (c) T1, (d) T2, (e) T3. Scale bar on optical images is 50 µm

Fig. 4-8c shows the optical microscopy images of emulsion and filtrate. A difference in the phase composition of emulsions and filtrate is observed. Emulsions contain densely packed spherical shaped water droplets in a range of sizes. Micron sized water droplets are uniformly distributed throughout the oil phase due to Tween 80, which acts as an emulsifier for water in oil emulsions by directing its hydrophilic head towards the water and hydrophobic tail towards oil. Optical microscopy images show that the CM-3 membrane has removed most water droplets from the emulsion. Similar behaviour was observed for the hexane based emulsion system, as shown in Fig. 4-9(a-c). The emulsion contains water droplets which are absent in images of filtrate after treatment with CM-3 membrane. UV-vis was used to characterise the emulsions and filtrate to

observe the transmittance of samples. Figure 9d shows the transmittance spectra for toluene-based emulsions while Fig.4-9e presents spectra of hexane based emulsions. Toluene based emulsion show ca. 0% transmittance in visible range due to the presence of microscale water droplets. The transmittance of all three toluene-based emulsion goes up to ~95% after treatment with CM-3 membrane.

Similarly, the hexane based emulsion shows zero transmittance, but it significantly improved after filtration. It can be concluded from these results that the nanostructured fibrous membranes produced in this study are a viable approach towards the separation of oil/water mixtures and stabilised emulsion. The highly porous nature and small pore channels of membrane allow for sieving the droplets in micron range whilst the selective affinity of the membrane towards organic liquids allow the purification of biphasic mixtures. The three-dimensional structure of the membrane effectively captures emulsion droplets and promotes coalescence during the separation process.

4.5 Conclusion

In summary, a versatile spray based process is proposed in this study for the fabrication of superhydrophobic hybrid membranes from alumina nanoparticles and polyurethane. Various synthesis parameters such as surface chemistry, volume ratios and temperature were optimised to achieve membranes with a uniformly interconnected fibrous structure. The optimum sample contains hierarchal multiscale roughness and silyl methyl surface groups on its surface, which endows a combination of superhydrophobic and superoleophilic properties. The resultant membrane has a fairly high flux value for most organic solvents and shows excellent performance in separating oil/water mixtures and surfactant stabilised emulsions.

Chapter 5 Conclusion and Future work

The project started with a comprehensive literature review of superhydrophobic materials for oil/water separation (**Chapter 1**). Later, a range of superhydrophobic materials was engineered with a focus on the separation of stable emulsions. These materials could be divided into 1) particulate systems for batch scale separation of emulsions and 2) continuous porous superhydrophobic structures for continuous separation. Extensive work on particulate systems for batch scale separation (sawdust based adsorbents (**Chapter 2**), magnetic nanocomposites (**Chapter 3**) and some other powder-based materials such as self-assembled silica nanostructures and magnetic sawdust composites) guided the efforts towards materials for continuous separation. Results from the powder-based superhydrophobic adsorbent and advice from the industrial partners lead to the efforts for continuous separation materials. Therefore, superhydrophobic membranes (**Chapter 4**), meshes, GNPs composite sponges, and activated carbon-based structures were fabricated and used for continuous separation of mixtures.

Stable and recyclable superhydrophobic nanocomposites were prepared by coating surface modified alumina NPs and coating with PDMS. The inherent hierarchical structure of sawdust provides a suitable platform to host superhydrophobic coating. The composite particles separate surfactant-stabilised oil in water emulsions for various cycles. From the application point of view, the particles could be mixed with the emulsion and then separated via pressure or inline filtration once they have completely absorbed the oil. In comparison, the magnetic nanocomposite particles reported in **Chapter 2** provides a fast separation and facile removal after separation. However, they require more synthesis steps and reagents, which will add up to the final cost of the process. The superhydrophobic magnetic nanocomposites were synthesised by the sol-gel process. and used to separate surfactant-stabilised emulsions. For this purpose, the magnetite nanoparticles were

encapsulated in porous and non-porous silica shells and later modified with silane to lower the surface energy. The powders were able to separate surfactant-stabilised emulsions and removed more than 95% of the oil. Magnetic nanocomposites allow their fast and easy removal after the separation compared to the sawdust based composites studied in **Chapter 1**. In addition, these powders can be integrated into a separation system with an electromagnet to separate batches of stable emulsions.

Compared to the powder-based materials reported in **Chapters 2** and **3**, a spray-based process was proposed in Ch.4 to fabricate superhydrophobic hybrid membranes for continuous separation of emulsions. A uniformly interconnected fibrous structure of composite polyurethane containing alumina NPs was achieved. The resulting membrane contains hierarchal roughness and silyl methyl surface groups on its surface, which endows a combination of superhydrophobic and superoleophilic properties. The resultant membrane has a fairly high flux value for most organic solvents and excellently separates oil/water mixtures, and surfactant stabilised emulsions. The membrane-based process offers a viable solution to the continuous separation as compared to the particulate systems.

In the next stage of the project, the work on advanced Janus membranes should be resumed. The fabrication process can be optimised to obtain nanoscale fibres and further smaller the pore size. The membrane should be characterised for permeation pressure, flow rate, bio-fouling, and emulsion separation under harsh conditions. These materials should be characterised using industrial complex mixtures at the project's next stage, simulating the field conditions and containing various surfactants and solid residues. The solid particles in the mixtures could block the membrane's pores, so the separation process should be combined with a subsequent cleaning mechanism or a relation between the volume of the separation mixture. The pore size and thickness

of the membrane should be studied concerning the flow rate, types of emulsions, fouling and type of oil. The membrane fabrication process can be advanced to several functional membranes by using different types of nanoparticles and 2D materials for separation and energy applications. In addition, biofouling experiments should be performed as membrane fouling can reduce efficiency and produce secondary pollution.

Similarly, pressure-driven separation and energy applications should be explored. An extension of this project is carbon conversion via electrochemical processing by using superhydrophobic electrodes. Hierarchically structured superhydrophobic materials produced in this project could be modified as electrodes where inorganic nanoparticles are grafted onto the surface of conducting supports. Nanostructured electrodes create a triphase boundary (gas/electrolyte/electrode) at the water-CO_2- electrode interface, which will significantly enhance the CO_2 reduction and capture capability by providing nanoscale storage space for gas, thus solving the mass transfer problem while preventing the electrolyte flow into pores which at the same time solves the hydrogen evolution problem encountered by traditional electrodes.

References

(1) Barthlott, W.; Neinhuis, C. Purity of the Sacred Lotus, or Escape from Contamination in Biological Surfaces. *Planta* **1997**, *202* (1), 1–8. https://doi.org/10.1007/s004250050096.

(2) Koch, K.; Bhushan, B.; Barthlott, W. Multifunctional Surface Structures of Plants: An Inspiration for Biomimetics. *Prog. Mater. Sci.* **2009**, *54* (2), 137–178. https://doi.org/10.1016/J.PMATSCI.2008.07.003.

(3) Perez Goodwyn, P.; Maezono, Y.; Hosoda, N.; Fujisaki, K. Waterproof and Translucent Wings at the Same Time: Problems and Solutions in Butterflies. *Naturwissenschaften* **2009**, *96* (7), 781–787. https://doi.org/10.1007/s00114-009-0531-z.

(4) Crawford, R. J.; Ivanova, E. P.; Crawford, R. J.; Ivanova, E. P. Chapter Two – Natural Superhydrophobic Surfaces. In *Superhydrophobic Surfaces*; 2015; pp 7–25. https://doi.org/10.1016/B978-0-12-801109-6.00002-1.

(5) Ivanova, E. P.; Nguyen, S. H.; Webb, H. K.; Hasan, J.; Truong, V. K.; Lamb, R. N.; Duan, X.; Tobin, M. J.; Mahon, P. J.; Crawford, R. J. Molecular Organization of the Nanoscale Surface Structures of the Dragonfly Hemianax Papuensis Wing Epicuticle. *PLoS One* **2013**, *8* (7), e67893. https://doi.org/10.1371/journal.pone.0067893.

(6) Liao, Y.; Zheng, G.; Huang, J. J.; Tian, M.; Wang, R. Development of Robust and Superhydrophobic Membranes to Mitigate Membrane Scaling and Fouling in Membrane Distillation. *J. Memb. Sci.* **2020**, *601*, 117962. https://doi.org/10.1016/j.memsci.2020.117962.

(7) Ge, M.; Cao, C.; Liang, F.; Liu, R.; Zhang, Y.; Zhang, W.; Zhu, T.; Yi, B.; Tang, Y.; Lai, Y. A “PDMS-in-Water” Emulsion Enables Mechanochemically Robust Superhydrophobic

Surfaces with Self-Healing Nature. *Nanoscale Horizons* **2020**, *5* (1), 65–73. https://doi.org/10.1039/c9nh00519f.

(8) Shao, Y.; Zhao, J.; Fan, Y.; Wan, Z.; Lu, L.; Zhang, Z.; Ming, W.; Ren, L. Shape Memory Superhydrophobic Surface with Switchable Transition between "Lotus Effect" to "Rose Petal Effect." *Chem. Eng. J.* **2020**, *382*, 122989. https://doi.org/10.1016/j.cej.2019.122989.

(9) Cheng, Y.; Lu, S.; Xu, W.; Boukherroub, R.; Szunerits, S.; Liang, W. Controlled Fabrication of NiO/ZnO Superhydrophobic Surface on Zinc Substrate with Corrosion and Abrasion Resistance. *J. Alloys Compd.* **2017**, *723*, 225–236. https://doi.org/10.1016/J.JALLCOM.2017.06.241.

(10) Tang, M.-K.; Huang, X.-J.; Yu, J.-G.; Li, X.-W.; Zhang, Q.-X. Simple Fabrication of Large-Area Corrosion Resistant Superhydrophobic Surface with High Mechanical Strength Property on TiAl-Based Composite. *J. Mater. Process. Technol.* **2017**, *239*, 178–186. https://doi.org/10.1016/j.jmatprotec.2016.08.024.

(11) Gao, L.; Yang, S.; Yang, H.; Ma, T. One-Stage Method for Fabricating Superhydrophobic Stainless Steel Surface and Its Anti-Corrosion Performance. *Adv. Eng. Mater.* **2017**, *19* (2), 1600511. https://doi.org/10.1002/adem.201600511.

(12) Zhang, H.; Tuo, Y.; Wang, Q.; Jin, B.; Yin, L.; Liu, X. Fabrication and Drag Reduction of Superhydrophobic Surface on Steel Substrates. *Surf. Eng.* **2017**, 1–7. https://doi.org/10.1080/02670844.2017.1317423.

(13) Cho, E. C.; Chang-Jian, C. W.; Chen, H. C.; Chuang, K. S.; Zheng, J. H.; Hsiao, Y. S.; Lee, K. C.; Huang, J. H. Robust Multifunctional Superhydrophobic Coatings with

Enhanced Water/Oil Separation, Self-Cleaning, Anti-Corrosion, and Anti-Biological Adhesion. *Chem. Eng. J.* **2017**, *314*, 347–357. https://doi.org/10.1016/j.cej.2016.11.145.

(14) Siddiqui, A. R.; Maurya, R.; Balani, K. Superhydrophobic Self-Floating Carbon Nanofiber Coating for Efficient Gravity-Directed Oil/Water Separation. *J. Mater. Chem. A* **2017**, *5* (6), 2936–2946. https://doi.org/10.1039/C6TA10411H.

(15) Kang, H.; Zhang, X.; Li, L.; Zhao, B.; Ma, F.; Zhang, J. Polydopamine and Poly(Dimethylsiloxane) Modified Superhydrophobic Fiberglass Membranes for Efficient Water-in-Oil Emulsions Separation. *J. Colloid Interface Sci.* **2020**, *559*, 178–185. https://doi.org/10.1016/j.jcis.2019.10.016.

(16) Nine, M. J.; Kabiri, S.; Sumona, A. K.; Tung, T. T.; Moussa, M. M.; Losic, D. Superhydrophobic/Superoleophilic Natural Fibres for Continuous Oil-Water Separation and Interfacial Dye-Adsorption. *Sep. Purif. Technol.* **2020**, *233*, 116062. https://doi.org/10.1016/j.seppur.2019.116062.

(17) Zhu, H.; Wu, L.; Meng, X.; Wang, Y.; Huang, Y.; xia, fan. Anti-UV Superhydrophobic Material with Photocatalysis, Self-Cleaning, Self-Healing and Oil/Water Separation. *Nanoscale* **2020**. https://doi.org/10.1039/d0nr01038c.

(18) Zhang, Q.; Liu, N.; Cao, Y.; Zhang, W.; Wei, Y.; Feng, L.; Jiang, L. A Facile Method to Prepare Dual-Functional Membrane for Efficient Oil Removal and in Situ Reversible Mercury Ions Adsorption from Wastewater. *Appl. Surf. Sci.* **2018**, *434*, 57–62. https://doi.org/10.1016/j.apsusc.2017.09.230.

(19) Lu, J.; Zhu, X.; Wang, B.; Liu, L.; Song, Y.; Miao, X.; Ren, G.; Li, X. A Slippery Oil-Repellent Hydrogel Coating. *Cellulose* **2020**, *27* (5), 2817–2827.

https://doi.org/10.1007/s10570-019-02953-5.

(20) Ren, G.; Song, Y.; Li, X.; Wang, B.; Zhou, Y.; Wang, Y.; Ge, B.; Zhu, X. A Simple Way to an Ultra-Robust Superhydrophobic Fabric with Mechanical Stability, UV Durability, and UV Shielding Property. *J. Colloid Interface Sci.* **2018**, *522*, 57–62. https://doi.org/10.1016/j.jcis.2018.03.038.

(21) Lu, J.; Zhu, X.; Miao, X.; Song, Y.; Liu, L.; Ren, G.; Li, X. Photocatalytically Active Superhydrophilic/Superoleophobic Coating. *ACS Omega* **2020**, acsomega.0c00474. https://doi.org/10.1021/acsomega.0c00474.

(22) Khatib, Z.; Verbeek, P. Water to Value - Produced Water Management for Sustainable Field Development of Mature and Green Fields. In *International Conference on Health, Safety and Environment in Oil and Gas Exploration and Production*; Society of Petroleum Engineers (SPE), 2002; pp 91–94. https://doi.org/10.2118/73853-ms.

(23) Veil, J. A.; Puder, M. G.; Elcock, D.; Redweik, R. J., Jr. *A White Paper Describing Produced Water from Production of Crude Oil, Natural Gas, and Coal Bed Methane.*; Argonne, IL (United States), 2004. https://doi.org/10.2172/821666.

(24) Kang, L.; Wang, B.; Zeng, J.; Cheng, Z.; Li, J.; Xu, J.; Gao, W.; Chen, K. Degradable Dual Superlyophobic Lignocellulosic Fibers for High-Efficiency Oil/Water Separation. *Green Chem.* **2020**, *22* (2), 504–512. https://doi.org/10.1039/c9gc03861b.

(25) Guo, Z.; Long, B.; Gao, S.; Luo, J.; Wang, L.; Huang, X.; Wang, D.; Xue, H.; Gao, J. Carbon Nanofiber Based Superhydrophobic Foam Composite for High Performance Oil/Water Separation. *J. Hazard. Mater.* **2021**, *402*, 123838. https://doi.org/10.1016/j.jhazmat.2020.123838.

(26) Yan, S.; Li, Y.; Xie, F.; Wu, J.; Jia, X.; Yang, J.; Song, H.; Zhang, Z. Environmentally Safe and Porous MS@TiO2@PPy Monoliths with Superior Visible-Light Photocatalytic Properties for Rapid Oil-Water Separation and Water Purification. *ACS Sustain. Chem. Eng.* **2020**, *8* (13), 5347–5359. https://doi.org/10.1021/acssuschemeng.0c00360.

(27) Wang, M.; Wang, M.; Zhang, Z.; Zhang, Z.; Wang, Y.; Zhao, X.; Men, X.; Yang, M. Ultrafast Fabrication of Metal-Organic Framework-Functionalized Superwetting Membrane for Multichannel Oil/Water Separation and Floating Oil Collection. *ACS Appl. Mater. Interfaces* **2020**, *12* (22), 25512–25520. https://doi.org/10.1021/acsami.0c08731.

(28) Liu, H.; Chen, X.; Zheng, Y.; Zhang, D.; Zhao, Y.; Wang, C.; Pan, C.; Liu, C.; Shen, C. Lightweight, Superelastic, and Hydrophobic Polyimide Nanofiber /MXene Composite Aerogel for Wearable Piezoresistive Sensor and Oil/Water Separation Applications. *Adv. Funct. Mater.* **2021**, 2008006. https://doi.org/10.1002/adfm.202008006.

(29) Zulfiqar, U.; Thomas, A. G.; Matthews, A.; Lewis, D. J. Surface Engineering of Ceramic Nanomaterials for Separation of Oil/Water Mixtures. *Frontiers in Chemistry*. Frontiers Media S.A. November 19, 2020, p 578. https://doi.org/10.3389/fchem.2020.00578.

(30) Latthe, S. S.; Kodag, V. S.; Sutar, R. S.; Bhosale, A. K.; Nagappan, S.; Ha, C. S.; Sadasivuni, K. K.; Kulal, S. R.; Liu, S.; Xing, R. Sawdust-Based Superhydrophobic Pellets for Efficient Oil-Water Separation. *Mater. Chem. Phys.* **2020**, *243*, 122634. https://doi.org/10.1016/j.matchemphys.2020.122634.

(31) Zulfiqar, U.; Thomas, A. G.; Yearsley, K.; Bolton, L. W.; Matthews, A.; Lewis, D. J. Renewable Adsorbent for the Separation of Surfactant-Stabilized Oil in Water Emulsions Based on Nanostructured Sawdust. *ACS Sustain. Chem. Eng.* **2019**,

acssuschemeng.9b04294. https://doi.org/10.1021/acssuschemeng.9b04294.

(32) Zhu, L.; Li, H.; Yin, Y.; Cui, Z.; Ma, C.; Li, X.; Xue, Q. One-Step Synthesis of a Robust and Anti-Oil-Fouling Biomimetic Cactus-like Hierarchical Architecture for Highly Efficient Oil/Water Separation. *Environ. Sci. Nano* **2020**, *7* (3), 903–911. https://doi.org/10.1039/c9en01140d.

(33) Zhang, M.; Wu, Z.; Meng, F.; Lin, H. Facile Preparation of Grass-like Hierarchical Structured γ-AlOOH Coated Stainless Steel Mesh with Superhydrophobic and Superoleophilic for Highly Efficient Oil-Water Separation. *Sep. Purif. Technol.* **2019**, *212*, 347–354. https://doi.org/10.1016/J.SEPPUR.2018.08.069.

(34) Ma, W.; Li, Y.; Zhang, M.; Gao, S.; Cui, J.; Huang, C.; Fu, G. Biomimetic Durable Multifunctional Self-Cleaning Nanofibrous Membrane with Outstanding Oil/Water Separation, Photodegradation of Organic Contaminants, and Antibacterial Performances. *ACS Appl. Mater. Interfaces* **2020**, *12* (31), 34999–35010. https://doi.org/10.1021/acsami.0c09059.

(35) Zulfiqar, U.; Thomas, A. G.; Matthews, A.; Lewis, D. J. Surface Engineering of Ceramic Nanomaterials for Separation of Oil/Water Mixtures. *Frontiers in Chemistry*. Frontiers Media S.A. November 19, 2020, p 578. https://doi.org/10.3389/fchem.2020.00578.

(36) Li, Y.; Gong, H.; Dong, M.; Liu, Y. Separation of Water-in-Heavy Oil Emulsions Using Porous Particles in a Coalescence Column. *Sep. Purif. Technol.* **2016**, *166*, 148–156. https://doi.org/10.1016/j.seppur.2016.04.004.

(37) Wang, C.-F.; Yang, S.-Y.; Kuo, S.-W. Eco-Friendly Superwetting Material for Highly Effective Separations of Oil/Water Mixtures and Oil-in-Water Emulsions. *Sci. Rep.* **2017**,

7, 43053. https://doi.org/10.1038/srep43053.

(38) Liu, N.; Zhang, Q.; Qu, R.; Zhang, W.; Li, H.; Wei, Y.; Feng, L. Nanocomposite Deposited Membrane for Oil-in-Water Emulsion Separation with in Situ Removal of Anionic Dyes and Surfactants. *Langmuir* **2017**, acs.langmuir.7b01281. https://doi.org/10.1021/acs.langmuir.7b01281.

(39) Chen, X.; Liang, Y. N.; Tang, X. Z.; Shen, W.; Hu, X. Additive-Free Poly (Vinylidene Fluoride) Aerogel for Oil/Water Separation and Rapid Oil Absorption. *Chem. Eng. J.* **2017**, *308*, 18–26. https://doi.org/10.1016/j.cej.2016.09.038.

(40) Liu, M.; Li, J.; Guo, Z. Electrochemical Route to Prepare Polyaniline-Coated Meshes with Controllable Pore Size for Switchable Emulsion Separation. *Chem. Eng. J.* **2016**, *304*, 115–120. https://doi.org/10.1016/j.cej.2016.06.073.

(41) Yu, Y.; Chen, H.; Liu, Y.; Craig, V. S. J.; Lai, Z. Selective Separation of Oil and Water with Mesh Membranes by Capillarity. *Adv. Colloid Interface Sci.* **2016**, *235*, 46–55. https://doi.org/10.1016/J.CIS.2016.05.008.

(42) Poulopoulos, S. G.; Voutsas, E. C.; Grigoropoulou, H. P.; Philippopoulos, C. J. Stripping as a Pretreatment Process of Industrial Oily Wastewater. *J. Hazard. Mater.* **2005**, *117* (2–3), 135–139. https://doi.org/10.1016/J.JHAZMAT.2004.08.033.

(43) Yu, L.; Han, M.; He, F. A Review of Treating Oily Wastewater. *Arab. J. Chem.* **2017**, *10*, S1913–S1922. https://doi.org/10.1016/J.ARABJC.2013.07.020.

(44) Huang, X.; Wang, W.; Liu, Y.; Wang, H.; Zhang, Z.; Fan, W.; Li, L. Treatment of Oily Waste Water by PVP Grafted PVDF Ultrafiltration Membranes. *Chem. Eng. J.* **2015**, *273*,

421–429. https://doi.org/10.1016/J.CEJ.2015.03.086.

(45) Gebreslase, G. A. Review on Membranes for the Filtration of Aqueous Based Solution: Oil in Water Emulsion. *J. Membr. Sci. Technol.* **2018**, *08* (02), 1–16. https://doi.org/10.4172/2155-9589.1000188.

(46) Shin, J. H.; Heo, J.-H.; Jeon, S.; Park, J. H.; Kim, S.; Kang, H.-W. Bio-Inspired Hollow PDMS Sponge for Enhanced Oil–Water Separation. *J. Hazard. Mater.* **2018**. https://doi.org/10.1016/J.JHAZMAT.2018.10.078.

(47) Wan, Z.; Li, D.; Jiao, Y.; Ouyang, X.; Chang, L.; Wang, X. Bifunctional MoS2 Coated Melamine-Formaldehyde Sponges for Efficient Oil–Water Separation and Water-Soluble Dye Removal. *Appl. Mater. Today* **2017**, *9*, 551–559. https://doi.org/10.1016/J.APMT.2017.09.013.

(48) Brody, T. M.; Bianca, P. Di; Krysa, J. Analysis of Inland Crude Oil Spill Threats, Vulnerabilities, and Emergency Response in the Midwest United States. *Risk Anal.* **2012**, *32* (10), 1741–1749. https://doi.org/10.1111/j.1539-6924.2012.01813.x.

(49) Han, Y.; Nambi, I. M.; Prabhakar Clement, T. Environmental Impacts of the Chennai Oil Spill Accident – A Case Study. *Sci. Total Environ.* **2018**, *626*, 795–806. https://doi.org/10.1016/J.SCITOTENV.2018.01.128.

(50) Chang, S. E.; Stone, J.; Demes, K.; Piscitelli, M. Consequences of Oil Spills: A Review and Framework for Informing Planning. *Ecol. Soc.* **2014**, *19* (2), art26. https://doi.org/10.5751/ES-06406-190226.

(51) Major, D. N.; Wang, H. How Public Health Impact Is Addressed: A Retrospective View

on Three Different Oil Spills. *Toxicol. Environ. Chem.* **2012**, *94* (3), 442–467. https://doi.org/10.1080/02772248.2012.654633.

(52) Wong, S. F.; Lim, J. S.; Dol, S. S. Crude Oil Emulsion: A Review on Formation, Classification and Stability of Water-in-Oil Emulsions. *J. Pet. Sci. Eng.* **2015**, *135*, 498–504. https://doi.org/10.1016/J.PETROL.2015.10.006.

(53) Umar, A. A.; Saaid, I. B. M.; Sulaimon, A. A.; Pilus, R. B. M. A Review of Petroleum Emulsions and Recent Progress on Water-in-Crude Oil Emulsions Stabilized by Natural Surfactants and Solids. *J. Pet. Sci. Eng.* **2018**, *165*, 673–690. https://doi.org/10.1016/J.PETROL.2018.03.014.

(54) Aziz, H. M. A.; Darwish, S. F.; Abdeen, F. M. Downhole Emulsion Problem, The Causes and Remedy, Ras Budran Field. In *SPE Asia Pacific Oil and Gas Conference and Exhibition*; Society of Petroleum Engineers, 2002. https://doi.org/10.2118/77847-MS.

(55) Becker, J. R. *Crude Oil Waxes, Emulsions, and Asphaltenes*; Pennwell Books, 1997.

(56) Ghosh, S.; Rousseau, D. Emulsion Breakdown in Foods and Beverages. *Chem. Deterior. Phys. Instab. Food Beverages* **2010**, 260–295. https://doi.org/10.1533/9781845699260.2.260.

(57) What Is an Emulsion? In *Pharmaceutical Emulsions*; John Wiley & Sons, Ltd: Chichester, UK, 2013; pp 15–48. https://doi.org/10.1002/9781118648384.ch2.

(58) Lim, J. S.; Wong, S. F.; Law, M. C.; Samyudia, Y.; Dol, S. S. A Review on the Effects of Emulsions on Flow Behaviours and Common Factors Affecting the Stability of Emulsions. *J. Appl. Sci.* **2015**, *15* (2), 167–172. https://doi.org/10.3923/jas.2015.167.172.

(59) Sjöblom, J.; Aske, N.; Harald Auflem, I.; Brandal, Ø.; Erik Havre, T.; Sæther, Ø.; Westvik, A.; Eng Johnsen, E.; Kallevik, H. Our Current Understanding of Water-in-Crude Oil Emulsions.: Recent Characterization Techniques and High Pressure Performance. *Adv. Colloid Interface Sci.* **2003**, *100–102*, 399–473. https://doi.org/10.1016/S0001-8686(02)00066-0.

(60) Fingas, M.; Fieldhouse, B. Studies of the Formation Process of Water-in-Oil Emulsions. *Mar. Pollut. Bull.* **2003**, *47* (9–12), 369–396. https://doi.org/10.1016/S0025-326X(03)00212-1.

(61) Fingas, M.; Fieldhouse, B. Formation of Water-in-Oil Emulsions and Application to Oil Spill Modelling. *J. Hazard. Mater.* **2004**, *107* (1–2), 37–50. https://doi.org/10.1016/J.JHAZMAT.2003.11.008.

(62) US EPA, O. EPA's Response Techniques.

(63) Ornitz, B. E.; Champ, M. A. *Oil Spills First Principles : Prevention and Best Response*; Elsevier, 2002.

(64) Ivshina, I. B.; Kuyukina, M. S.; Krivoruchko, A. V.; Elkin, A. A.; Makarov, S. O.; Cunningham, C. J.; Peshkur, T. A.; Atlas, R. M.; Philp, J. C. Oil Spill Problems and Sustainable Response Strategies through New Technologies. *Environ. Sci. Process. Impacts* **2015**, *17* (7), 1201–1219. https://doi.org/10.1039/C5EM00070J.

(65) Saththasivam, J.; Loganathan, K.; Sarp, S. An Overview of Oil–Water Separation Using Gas Flotation Systems. *Chemosphere* **2016**, *144*, 671–680. https://doi.org/10.1016/J.CHEMOSPHERE.2015.08.087.

(66) Aulenbach, D. B.; Shammas, N. K.; Wang, L. K.; Marvin, R. C. Algae Removal by Flotation. In *Flotation Technology*; Humana Press: Totowa, NJ, 2010; pp 363–399. https://doi.org/10.1007/978-1-60327-133-2_11.

(67) Jiang, J.-Q. The Role of Coagulation in Water Treatment. *Curr. Opin. Chem. Eng.* **2015**, *8*, 36–44. https://doi.org/10.1016/J.COCHE.2015.01.008.

(68) Sillanpää, M.; Ncibi, M. C.; Matilainen, A.; Vepsäläinen, M. Removal of Natural Organic Matter in Drinking Water Treatment by Coagulation: A Comprehensive Review. *Chemosphere* **2018**, *190*, 54–71. https://doi.org/10.1016/J.CHEMOSPHERE.2017.09.113.

(69) Wei, H.; Gao, B.; Ren, J.; Li, A.; Yang, H. Coagulation/Flocculation in Dewatering of Sludge: A Review. *Water Res.* **2018**, *143*, 608–631. https://doi.org/10.1016/J.WATRES.2018.07.029.

(70) Padaki, M.; Surya Murali, R.; Abdullah, M. S.; Misdan, N.; Moslehyani, A.; Kassim, M. A.; Hilal, N.; Ismail, A. F. Membrane Technology Enhancement in Oil–Water Separation. A Review. *Desalination* **2015**, *357*, 197–207. https://doi.org/10.1016/J.DESAL.2014.11.023.

(71) Han, S. W.; Kim, K.-D.; Seo, H. O.; Kim, I. H.; Jeon, C. S.; An, J. E.; Kim, J. H.; Uhm, S.; Kim, Y. D. Oil-Water Separation Using Superhydrophobic PET Membranes Fabricated Via Simple Dip-Coating Of PDMS-SiO_2 Nanoparticles. *Macromol. Mater. Eng.* **2017**, 1700218. https://doi.org/10.1002/mame.201700218.

(72) Sun, S.; Zhu, L.; Liu, X.; Wu, L.; Dai, K.; Liu, C.; Shen, C.; Guo, X.; Zheng, G.; Guo, Z. Superhydrophobic Shish-Kebab Membrane with Self-Cleaning and Oil/Water Separation Properties. *ACS Sustain. Chem. Eng.* **2018**, *6* (8), 9866–9875.

https://doi.org/10.1021/acssuschemeng.8b01047.

(73) Li, F.; Wang, Z.; Huang, S.; Pan, Y.; Zhao, X. Flexible, Durable, and Unconditioned Superoleophobic/Superhydrophilic Surfaces for Controllable Transport and Oil-Water Separation. *Adv. Funct. Mater.* **2018**, *28* (20), 1706867. https://doi.org/10.1002/adfm.201706867.

(74) Qu, M.; Ma, L.; Zhou, Y.; Zhao, Y.; Wang, J.; Zhang, Y.; Zhu, X.; Liu, X.; He, J. Durable and Recyclable Superhydrophilic–Superoleophobic Materials for Efficient Oil/Water Separation and Water-Soluble Dyes Removal. *ACS Appl. Nano Mater.* **2018**, *1* (9), 5197–5209. https://doi.org/10.1021/acsanm.8b01249.

(75) Guo, F.; Wen, Q.; Guo, Z. Low Cost and Non-Fluoride Flowerlike Superhydrophobic Particles Fabricated for Both Emulsions Separation and Dyes Adsorption. *J. Colloid Interface Sci.* **2017**, *507*, 421–428. https://doi.org/10.1016/J.JCIS.2017.08.021.

(76) Jia, S.; Deng, S.; Luo, S.; Qing, Y.; Yan, N.; Wu, Y. Texturing Commercial Epoxy with Hierarchical and Porous Structure for Robust Superhydrophobic Coatings. *Appl. Surf. Sci.* **2019**, *466*, 84–91. https://doi.org/10.1016/J.APSUSC.2018.10.017.

(77) Lv, X.; Tian, D.; Peng, Y.; Li, J.; Jiang, G. Superhydrophobic Magnetic Reduced Graphene Oxide-Decorated Foam for Efficient and Repeatable Oil-Water Separation. *Appl. Surf. Sci.* **2019**, *466*, 937–945. https://doi.org/10.1016/J.APSUSC.2018.10.110.

(78) Zhu, X.; Zhang, Z.; Song, Y.; Yan, J.; Wang, Y.; Ren, G. A Waterproofing Textile with Robust Superhydrophobicity in Either Air or Oil Surroundings. *J. Taiwan Inst. Chem. Eng.* **2017**, *71*, 421–425. https://doi.org/10.1016/j.jtice.2016.11.029.

(79) Ge, B.; Ren, G.; Miao, X.; Li, X.; Zhang, T.; Pu, X.; Jin, C.; Zhao, L.; Li, W. Visible Light Activation of Superhydrophobic BiOBr/Ag Loaded Copper Mesh for Degradation and Their Use in Oil/Water Separation. *J. Taiwan Inst. Chem. Eng.* **2019**, *102*, 233–241. https://doi.org/10.1016/j.jtice.2019.06.007.

(80) Ge, B.; Yang, X.; Li, H.; Zhao, L.; Ren, G.; Miao, X.; Pu, X.; Li, W. A Durable Superhydrophobic BiOBr/PFW Cotton Fabric for Visible Light Response Degradation and Oil/Water Separation Performance. *Colloids Surfaces A Physicochem. Eng. Asp.* **2020**, *585*, 124027. https://doi.org/10.1016/j.colsurfa.2019.124027.

(81) Wang, J.; Han, F.; Chen, Y.; Wang, H. A Pair of MnO2 Nanocrystal Coatings with Inverse Wettability on Metal Meshes for Efficient Oil/Water Separation. *Sep. Purif. Technol.* **2019**, *209*, 119–127. https://doi.org/10.1016/J.SEPPUR.2018.07.024.

(82) Nanda, D.; Sahoo, A.; Kumar, A.; Bhushan, B. Facile Approach to Develop Durable and Reusable Superhydrophobic/Superoleophilic Coatings for Steel Mesh Surfaces. *J. Colloid Interface Sci.* **2019**, *535*, 50–57. https://doi.org/10.1016/J.JCIS.2018.09.088.

(83) Zhang, M.; Wu, Z.; Meng, F.; Lin, H. Facile Preparation of Grass-like Hierarchical Structured γ-AlOOH Coated Stainless Steel Mesh with Superhydrophobic and Superoleophilic for Highly Efficient Oil-Water Separation. *Sep. Purif. Technol.* **2019**, *212*, 347–354. https://doi.org/10.1016/J.SEPPUR.2018.08.069.

(84) Jiang, B.; Zhang, H.; Zhang, L.; Sun, Y.; Xu, L.; Sun, Z.; Gu, W.; Chen, Z.; Yang, H. Novel One-Step, in Situ Thermal Polymerization Fabrication of Robust Superhydrophobic Mesh for Efficient Oil/Water Separation. *Ind. Eng. Chem. Res.* **2017**, *56* (41), 11817–11826. https://doi.org/10.1021/acs.iecr.7b03063.

(85) Zhang, F.; Shi, Z.; Xu, C.; Huo, D.; Zhang, W.; Peng, C. Self-Fibering Growth in the Soot-Templated CVD Coating of Silica on Mesh for Efficient Oil/Water Separation. *Mater. Des.* **2018**, *154*, 370–377. https://doi.org/10.1016/J.MATDES.2018.05.038.

(86) Gong, Z.; Yang, N.; Chen, Z.; Jiang, B.; Sun, Y.; Yang, X.; Zhang, L. Fabrication of Meshes with Inverse Wettability Based on the TiO2 Nanowires for Continuous Oil/Water Separation. *Chem. Eng. J.* **2020**, *380*, 122524. https://doi.org/10.1016/j.cej.2019.122524.

(87) Huang, X.; Li, B.; Song, X.; Wang, L.; Shi, Y.; Hu, M.; Gao, J.; Xue, H. Stretchable, Electrically Conductive and Superhydrophobic/Superoleophilic Nanofibrous Membrane with a Hierarchical Structure for Efficient Oil/Water Separation. *J. Ind. Eng. Chem.* **2018**. https://doi.org/10.1016/J.JIEC.2018.10.021.

(88) Ma, W.; Zhao, J.; Oderinde, O.; Han, J.; Liu, Z.; Gao, B.; Xiong, R.; Zhang, Q.; Jiang, S.; Huang, C. Durable Superhydrophobic and Superoleophilic Electrospun Nanofibrous Membrane for Oil-Water Emulsion Separation. *J. Colloid Interface Sci.* **2018**, *532*, 12–23. https://doi.org/10.1016/J.JCIS.2018.06.067.

(89) Zhao, F.; Ma, Z.; Xiao, K.; Xiang, C.; Wang, H.; Huang, X.; Liang, S. Hierarchically Textured Superhydrophobic Polyvinylidene Fluoride Membrane Fabricated via Nanocasting for Enhanced Membrane Distillation Performance. *Desalination* **2018**, *443*, 228–236. https://doi.org/10.1016/J.DESAL.2018.06.003.

(90) Subramanian, N.; Qamar, A.; Alsaadi, A.; Gallo, A.; Ridwan, M. G.; Lee, J.-G.; Pillai, S.; Arunachalam, S.; Anjum, D.; Sharipov, F.; Ghaffour, N.; Mishra, H. Evaluating the Potential of Superhydrophobic Nanoporous Alumina Membranes for Direct Contact Membrane Distillation. *J. Colloid Interface Sci.* **2019**, *533*, 723–732.

https://doi.org/10.1016/J.JCIS.2018.08.054.

(91) Qing, W.; Shi, X.; Zhang, W.; Wang, J.; Wu, Y.; Wang, P.; Tang, C. Y. Solvent-Thermal Induced Roughening: A Novel and Versatile Method to Prepare Superhydrophobic Membranes. *J. Memb. Sci.* **2018**, *564*, 465–472. https://doi.org/10.1016/J.MEMSCI.2018.07.035.

(92) Attia, H.; Johnson, D. J.; Wright, C. J.; Hilal, N. Robust Superhydrophobic Electrospun Membrane Fabricated by Combination of Electrospinning and Electrospraying Techniques for Air Gap Membrane Distillation. *Desalination* **2018**, *446*, 70–82. https://doi.org/10.1016/J.DESAL.2018.09.001.

(93) Cheng, Y.; Barras, A.; Lu, S.; Xu, W.; Szunerits, S.; Boukherroub, R. Fabrication of Superhydrophobic/Superoleophilic Functionalized Reduced Graphene Oxide/Polydopamine/PFDT Membrane for Efficient Oil/Water Separation. *Sep. Purif. Technol.* **2020**, *236*, 116240. https://doi.org/10.1016/j.seppur.2019.116240.

(94) Li, Z.-T.; Wu, H.-T.; Chen, W.-Y.; He, F.-A.; Li, D.-H. Preparation of Magnetic Superhydrophobic Melamine Sponges for Effective Oil-Water Separation. *Sep. Purif. Technol.* **2019**, *212*, 40–50. https://doi.org/10.1016/J.SEPPUR.2018.11.002.

(95) Li, X.; Cao, M.; Shan, H.; Handan Tezel, F.; Li, B. Facile and Scalable Fabrication of Superhydrophobic and Superoleophilic PDMS-Co-PMHS Coating on Porous Substrates for Highly Effective Oil/Water Separation. *Chem. Eng. J.* **2019**, *358*, 1101–1113. https://doi.org/10.1016/J.CEJ.2018.10.097.

(96) Huang, Z.-S.; Quan, Y.-Y.; Mao, J.-J.; Wang, Y.-L.; Lai, Y.; Zheng, J.; Chen, Z.; Wei, K.; Li, H. Multifunctional Superhydrophobic Composite Materials with Remarkable

Mechanochemical Robustness, Stain Repellency, Oil-Water Separation and Sound-Absorption Properties. *Chem. Eng. J.* **2019**, *358*, 1610–1619. https://doi.org/10.1016/J.CEJ.2018.10.123.

(97) Zhou, Q.; Yan, B.; Xing, T.; Chen, G. Fabrication of Superhydrophobic Caffeic Acid/Fe@cotton Fabric and Its Oil-Water Separation Performance. *Carbohydr. Polym.* **2019**, *203*, 1–9. https://doi.org/10.1016/J.CARBPOL.2018.09.025.

(98) Cheng, Q.-Y.; Guan, C.-S.; Wang, M.; Li, Y.-D.; Zeng, J.-B. Cellulose Nanocrystal Coated Cotton Fabric with Superhydrophobicity for Efficient Oil/Water Separation. *Carbohydr. Polym.* **2018**, *199*, 390–396. https://doi.org/10.1016/J.CARBPOL.2018.07.046.

(99) Chauhan, P.; Kumar, A.; Bhushan, B. Self-Cleaning, Stain-Resistant and Anti-Bacterial Superhydrophobic Cotton Fabric Prepared by Simple Immersion Technique. *J. Colloid Interface Sci.* **2019**, *535*, 66–74. https://doi.org/10.1016/J.JCIS.2018.09.087.

(100) Lin, D.; Zeng, X.; Li, H.; Lai, X.; Wu, T. One-Pot Fabrication of Superhydrophobic and Flame-Retardant Coatings on Cotton Fabrics via Sol-Gel Reaction. *J. Colloid Interface Sci.* **2019**, *533*, 198–206. https://doi.org/10.1016/J.JCIS.2018.08.060.

(101) Dan, Y.; Popowski, Y.; Buzhor, M.; Menashe, E.; Rachmani, O.; Amir, E. Covalent Surface Modification of Cellulose-Based Textiles for Oil–Water Separation Applications. *Ind. Eng. Chem. Res.* **2020**, *59* (13), 5456–5465. https://doi.org/10.1021/acs.iecr.9b05785.

(102) Ferrero, G.; Sandgren Bock, M.; Stenby, E. H.; Hou, C.; Zhang, J. Reduced Graphene Oxide-Coated Microfibers for Oil-Water Separation. *Environ. Sci. Nano* **2019**, *6* (11), 3215–3224. https://doi.org/10.1039/c9en00549h.

(103) Topuz, F.; Abdulhamid, M. A.; Nunes, S. P.; Szekely, G. Hierarchically Porous Electrospun Nanofibrous Mats Produced from Intrinsically Microporous Fluorinated Polyimide for the Removal of Oils and Non-Polar Solvents. *Environ. Sci. Nano* **2020**. https://doi.org/10.1039/d0en00084a.

(104) Lin, J.; Lin, F.; Liu, R.; Li, P.; Fang, S.; Ye, W.; Zhao, S. Scalable Fabrication of Robust Superhydrophobic Membranes by One-Step Spray-Coating for Gravitational Water-in-Oil Emulsion Separation. *Sep. Purif. Technol.* **2020**, *231*. https://doi.org/10.1016/j.seppur.2019.115898.

(105) Zhang, J.; Chen, F.; Lu, Y.; Zhang, Z.; Liu, J.; Chen, Y.; Liu, X.; Yang, X.; Carmalt, C. J.; Parkin, I. P. Superhydrophilic–Superhydrophobic Patterned Surfaces on Glass Substrate for Water Harvesting. *J. Mater. Sci.* **2020**, *55* (2), 498–508. https://doi.org/10.1007/s10853-019-04046-x.

(106) Guo, F.; Wen, Q.; Guo, Z. Low Cost and Non-Fluoride Flowerlike Superhydrophobic Particles Fabricated for Both Emulsions Separation and Dyes Adsorption. *J. Colloid Interface Sci.* **2017**, *507*, 421–428. https://doi.org/10.1016/J.JCIS.2017.08.021.

(107) Duan, C.; Zhu, T.; Guo, J.; Wang, Z.; Liu, X.; Wang, H.; Xu, X.; Jin, Y.; Zhao, N.; Xu, J. Smart Enrichment and Facile Separation of Oil from Emulsions and Mixtures by Superhydrophobic/Superoleophilic Particles. *ACS Appl. Mater. Interfaces* **2015**, *7* (19), 10475–10481. https://doi.org/10.1021/acsami.5b01901.

(108) Chen, H.-J.; Hang, T.; Yang, C.; Liu, G.; Lin, D.; Wu, J.; Pan, S.; Yang, B.; Tao, J.; Xie, X. Anomalous Dispersion of Magnetic Spiky Particles for Enhanced Oil Emulsions/Water Separation. *Nanoscale* **2018**, *10* (4), 1978–1986. https://doi.org/10.1039/C7NR07995H.

(109) Guo, F.; Wen, Q.; Peng, Y.; Guo, Z. Multifunctional Hollow Superhydrophobic SiO2 Microspheres with Robust and Self-Cleaning and Separation of Oil/Water Emulsions Properties. *J. Colloid Interface Sci.* **2017**, *494*, 54–63. https://doi.org/10.1016/j.jcis.2017.01.070.

(110) Dong, J.; Zhang, J. Biomimetic Super Anti-Wetting Coatings from Natural Materials: Superamphiphobic Coatings Based on Nanoclays. *Sci. Rep.* **2018**, *8* (1), 12062. https://doi.org/10.1038/s41598-018-30586-4.

(111) Kwak, W.; Hwang, W. Facile Method for Preparing Superoleophobic Surfaces with Hierarchical Microcubic/Nanowire Structures. *Nanotechnology* **2016**, *27* (5), 055301. https://doi.org/10.1088/0957-4484/27/5/055301.

(112) Nosonovsky, M.; Bhushan, B. Why Re-Entrant Surface Topography Is Needed for Robust Oleophobicity. *Philos. Trans. A. Math. Phys. Eng. Sci.* **2016**, *374* (2073), 20160185. https://doi.org/10.1098/rsta.2016.0185.

(113) Hong, S. K.; Bae, S.; Jeon, H.; Kim, M.; Cho, S. J.; Lim, G. An Underwater Superoleophobic Nanofibrous Cellulosic Membrane for Oil/Water Separation with High Separation Flux and High Chemical Stability. *Nanoscale* **2018**, *10* (6), 3037–3045. https://doi.org/10.1039/C7NR08199E.

(114) Obaid, M.; Yang, E.; Kang, D.-H.; Yoon, M.-H.; Kim, I. S. Underwater Superoleophobic Modified Polysulfone Electrospun Membrane with Efficient Antifouling for Ultrafast Gravitational Oil-Water Separation. *Sep. Purif. Technol.* **2018**, *200*, 284–293. https://doi.org/10.1016/J.SEPPUR.2018.02.043.

(115) Xiong, L.; Guo, W.; Alameda, B. M.; Sloan, R. K.; Walker, W. D.; Patton, D. L. Rational

Design of Superhydrophilic/Superoleophobic Surfaces for Oil–Water Separation via Thiol–Acrylate Photopolymerization. *ACS Omega* **2018**, *3* (8), 10278–10285. https://doi.org/10.1021/acsomega.8b01461.

(116) Zhao, Y.; Zhang, M.; Wang, Z. Underwater Superoleophobic Membrane with Enhanced Oil-Water Separation, Antimicrobial, and Antifouling Activities. *Adv. Mater. Interfaces* **2016**, *3* (13), 1500664. https://doi.org/10.1002/admi.201500664.

(117) Qian, D.; Chen, D.; Li, N.; Xu, Q.; Li, H.; He, J.; Lu, J. Multilayer Network Membranes Based on Evenly Dispersed Nanofibers/Co_3O_4 Nanoneedles for High-Efficiency Separation of Micrometer-Scale Oil/Water Emulsions. *Adv. Mater. Interfaces* **2018**, *5* (21), 1801004. https://doi.org/10.1002/admi.201801004.

(118) Wu, Z.; Zhang, C.; Peng, K.; Wang, Q.; Wang, Z. Hydrophilic/Underwater Superoleophobic Graphene Oxide Membrane Intercalated by TiO2 Nanotubes for Oil/Water Separation. *Front. Environ. Sci. Eng.* **2018**, *12* (3), 15. https://doi.org/10.1007/s11783-018-1042-y.

(119) Wang, B.; Chen, C.; Liu, H.; Xia, B.; Fan, Y.; Chen, T. WO3/TiO2 Superhydrophilic and Underwater Superoleophobic Membrane for Effective Separation of Oil-in-Water Emulsions. *Thin Solid Films* **2018**, *665*, 9–16. https://doi.org/10.1016/J.TSF.2018.08.039.

(120) Yong, J.; Chen, F.; Yang, Q.; Huo, J.; Hou, X. Superoleophobic Surfaces. *Chem. Soc. Rev.* **2017**, *46* (14), 4168–4217. https://doi.org/10.1039/C6CS00751A.

(121) Wang, J.; Wang, H. Integrated Device Based on Cauliflower-like Nickel Hydroxide Particles–Coated Fabrics with Inverse Wettability for Highly Efficient Oil/Hot Alkaline Water Separation. *J. Colloid Interface Sci.* **2019**, *534*, 228–238.

https://doi.org/10.1016/J.JCIS.2018.09.028.

(122) Simpson, J. T.; Hunter, S. R.; Aytug, T. Superhydrophobic Materials and Coatings: A Review. *Reports Prog. Phys.* **2015**, *78* (8), 086501. https://doi.org/10.1088/0034-4885/78/8/086501.

(123) Jeevahan, J.; Chandrasekaran, M.; Britto Joseph, G.; Durairaj, R. B.; Mageshwaran, G. Superhydrophobic Surfaces: A Review on Fundamentals, Applications, and Challenges. *J. Coatings Technol. Res.* **2018**, *15* (2), 231–250. https://doi.org/10.1007/s11998-017-0011-x.

(124) Shirtcliffe, N. J.; McHale, G.; Atherton, S.; Newton, M. I. An Introduction to Superhydrophobicity. *Adv. Colloid Interface Sci.* **2010**, *161* (1–2), 124–138. https://doi.org/10.1016/J.CIS.2009.11.001.

(125) Li, J.-J.; Zhou, Y.-N.; Luo, Z.-H. Polymeric Materials with Switchable Superwettability for Controllable Oil/Water Separation: A Comprehensive Review. *Prog. Polym. Sci.* **2018**, *87*, 1–33. https://doi.org/10.1016/J.PROGPOLYMSCI.2018.06.009.

(126) Darmanin, T.; Guittard, F. Superhydrophobic and Superoleophobic Properties in Nature. *Mater. Today* **2015**, *18* (5), 273–285. https://doi.org/10.1016/J.MATTOD.2015.01.001.

(127) Khan, S. A.; Zulfiqar, U.; Hussain, S. Z.; Zaheer, U.; Hussain, I.; Husain, S. W.; Subhani, T. Fabrication of Superhydrophobic Filter Paper and Foam for Oil–Water Separation Based on Silica Nanoparticles from Sodium Silicate. *J. Sol-Gel Sci. Technol.* **2016**, 1–9. https://doi.org/10.1007/s10971-016-4250-6.

(128) Zulfiqar, U.; Subhani, T.; Wilayat Husain, S. Towards Tunable Size of Silica Particles

from Rice Husk. *J. Non. Cryst. Solids* **2015**, *429*. https://doi.org/10.1016/j.jnoncrysol.2015.08.037.

(129) Rahman, Z. U.; Wei, N.; Li, Z.; Sun, W.; Wang, D. Preparation of Hollow Mesoporous Silica Nanospheres: Controllable Template Synthesis and Their Application in Drug Delivery. *New J. Chem.* **2017**, *41* (23), 14122–14129. https://doi.org/10.1039/C7NJ02804K.

(130) Lalchhingpuii; Tiwari, D.; Lalhmunsiama; Lee, S. M. Chitosan Templated Synthesis of Mesoporous Silica and Its Application in the Treatment of Aqueous Solutions Contaminated with Cadmium(II) and Lead(II). *Chem. Eng. J.* **2017**, *328*, 434–444. https://doi.org/10.1016/J.CEJ.2017.07.053.

(131) Pirzada, T.; Ashrafi, Z.; Xie, W.; Khan, S. A. Cellulose Silica Hybrid Nanofiber Aerogels: From Sol–Gel Electrospun Nanofibers to Multifunctional Aerogels. *Adv. Funct. Mater.* **2020**, *30* (5), 1907359. https://doi.org/10.1002/adfm.201907359.

(132) Wang, H.; Zhang, C.; Zhou, B.; Zhang, Z.; Shen, J.; Du, A. Hydrophobic Silica Nanorod Arrays Vertically Grown on Melamine Foams for Oil/Water Separation. *ACS Appl. Nano Mater.* **2020**, *3* (2), 1479–1488. https://doi.org/10.1021/acsanm.9b02303.

(133) Anjum, A. S.; Ali, M.; Sun, K. C.; Riaz, R.; Jeong, S. H. Self-Assembled Nanomanipulation of Silica Nanoparticles Enable Mechanochemically Robust Super Hydrophobic and Oleophilic Textile. *J. Colloid Interface Sci.* **2020**, *563*, 62–73. https://doi.org/10.1016/j.jcis.2019.12.056.

(134) Ebrahimi, F.; Farazi, R.; Karimi, E. Z.; Beygi, H. Dichlorodimethylsilane Mediated One-Step Synthesis of Hydrophilic and Hydrophobic Silica Nanoparticles. *Adv. Powder*

Technol. **2017**, *28* (3), 932–937. https://doi.org/10.1016/J.APT.2016.12.022.

(135) Ma, W.; Guo, Z.; Zhao, J.; Yu, Q.; Wang, F.; Han, J.; Pan, H.; Yao, J.; Zhang, Q.; Samal, S. K.; De Smedt, S. C.; Huang, C. Polyimide/Cellulose Acetate Core/Shell Electrospun Fibrous Membranes for Oil-Water Separation. *Sep. Purif. Technol.* **2017**, *177*, 71–85. https://doi.org/10.1016/j.seppur.2016.12.032.

(136) Zhang, F.; Shi, Z.; Chen, L.; Jiang, Y.; Xu, C.; Wu, Z.; Wang, Y.; Peng, C. Porous Superhydrophobic and Superoleophilic Surfaces Prepared by Template Assisted Chemical Vapor Deposition. *Surf. Coatings Technol.* **2017**. https://doi.org/10.1016/j.surfcoat.2017.02.058.

(137) Yang, S.; Chen, L.; Wang, C.; Rana, M.; Ma, P. C. Surface Roughness Induced Superhydrophobicity of Graphene Foam for Oil-Water Separation. *J. Colloid Interface Sci.* **2017**, *508*, 254–262. https://doi.org/10.1016/j.jcis.2017.08.061.

(138) Li, H.; Liang, T.; Lai, X.; Su, X.; Zhang, L.; Zeng, X. Vapor-Liquid Interfacial Reaction to Fabricate Superhydrophilic and Underwater Superoleophobic Thiol-Ene/Silica Hybrid Decorated Fabric for Oil/Water Separation. *Appl. Surf. Sci.* **2018**, *427*, 92–101. https://doi.org/10.1016/j.apsusc.2017.08.022.

(139) Su, X.; Li, H.; Lai, X.; Zhang, L.; Wang, J.; Liao, X.; Zeng, X. Vapor–Liquid Sol–Gel Approach to Fabricating Highly Durable and Robust Superhydrophobic Polydimethylsiloxane@Silica Surface on Polyester Textile for Oil–Water Separation. *ACS Appl. Mater. Interfaces* **2017**, *9* (33), 28089–28099. https://doi.org/10.1021/acsami.7b08920.

(140) Kusworo, T. D.; Utomo, D. P.; Aryanti, N.; Qudratun. Synergistic Effect of UV

Irradiation and Thermal Annealing to Develop High Performance Polyethersulfone-Nano Silica Membrane for Produced Water Treatment. *J. Environ. Chem. Eng.* **2017**, *5* (4), 3290–3301. https://doi.org/10.1016/j.jece.2017.06.035.

(141) Tang, X.; Shen, C.; Zhu, W.; Zhang, S.; Xu, Y.; Yang, Y.; Gao, M.; Dong, F. A Facile Procedure to Modify Filter Paper for Oil–Water Separation. *RSC Adv.* **2017**, *7* (48), 30495–30499. https://doi.org/10.1039/C7RA03754F.

(142) Zhu, X.; Zhang, Z.; Song, Y.; Yan, J.; Wang, Y.; Ren, G. A Waterproofing Textile with Robust Superhydrophobicity in Either Air or Oil Surroundings. *J. Taiwan Inst. Chem. Eng.* **2017**, *71*, 421–425. https://doi.org/10.1016/j.jtice.2016.11.029.

(143) Salehabadi, S.; Seyfi, J.; Hejazi, I.; Davachi, S. M.; Naeini, A. H.; Khakbaz, M. Nanosilica-Decorated Sponges for Efficient Oil/Water Separation: Role of Nanoparticle's Type and Concentration. *J. Mater. Sci.* **2017**, *52* (12), 7017–7027. https://doi.org/10.1007/s10853-017-0935-7.

(144) Zhi, D.; Lu, Y.; Sathasivam, S.; Parkin, I. P.; Zhang, X. Large-Scale Fabrication of Translucent and Repairable Superhydrophobic Spray Coatings with Remarkable Mechanical, Chemical Durability and UV Resistance. *J. Mater. Chem. A* **2017**, *5* (21), 10622–10631. https://doi.org/10.1039/C7TA02488F.

(145) Guo, F.; Wen, Q.; Peng, Y.; Guo, Z. Multifunctional Hollow Superhydrophobic SiO2 Microspheres with Robust and Self-Cleaning and Separation of Oil/Water Emulsions Properties. *J. Colloid Interface Sci.* **2017**, *494*, 54–63. https://doi.org/10.1016/j.jcis.2017.01.070.

(146) Yu, M.; Wang, Q.; Zhang, M.; Deng, Q.; Chen, D. Facile Fabrication of Raspberry-like

Composite Microspheres for the Construction of Superhydrophobic Films and Applications in Highly Efficient Oil–Water Separation. *RSC Adv.* **2017**, *7* (63), 39471–39479. https://doi.org/10.1039/C7RA07250C.

(147) Gao, J.; Huang, X.; Xue, H.; Tang, L.; Li, R. K. Y. Facile Preparation of Hybrid Microspheres for Super-Hydrophobic Coating and Oil-Water Separation. *Chem. Eng. J.* **2017**, *326*, 443–453. https://doi.org/10.1016/j.cej.2017.05.175.

(148) Li, Y.; Zhang, Z.; Ge, B.; Men, X.; Xue, Q. A Versatile and Efficient Approach to Separate Both Surfactant-Stabilized Water-in-Oil and Oil-in-Water Emulsions. *Sep. Purif. Technol.* **2017**, *176*, 1–7. https://doi.org/10.1016/j.seppur.2016.11.072.

(149) Zhai, W.; Srikanth, N.; Kong, L. B.; Zhou, K. Carbon Nanomaterials in Tribology. *Carbon N. Y.* **2017**, *119*, 150–171. https://doi.org/10.1016/J.CARBON.2017.04.027.

(150) Liu, Y.; Zhang, F.; Zhu, W.; Su, D.; Sang, Z.; Yan, X.; Li, S.; Liang, J.; Dou, S. X. A Multifunctional Hierarchical Porous SiO2/GO Membrane for High Efficiency Oil/Water Separation and Dye Removal. *Carbon N. Y.* **2020**, *160*, 88–97. https://doi.org/10.1016/j.carbon.2020.01.002.

(151) Zhang, B.; Huang, K.; Wang, Q.; Li, G.; Wu, T.; Li, Y. Highly Efficient Treatment of Oily Wastewater Using Magnetic Carbon Nanotubes/Layered Double Hydroxides Composites. *Colloids Surfaces A Physicochem. Eng. Asp.* **2020**, *586*, 124187. https://doi.org/10.1016/j.colsurfa.2019.124187.

(152) Chen, X. Q.; Zhang, B.; Xie, L.; Wang, F. MWCNTs Polyurethane Sponges with Enhanced Super-Hydrophobicity for Selective Oil–Water Separation. *Surf. Eng.* **2020**. https://doi.org/10.1080/02670844.2019.1711303.

(153) Qu, J. Y.; Han, Q.; Gao, F.; Qiu, J. S. Carbon Foams Produced from Lignin-Phenol-Formaldehyde Resin for Oil/Water Separation. *Xinxing Tan Cailiao/New Carbon Mater.* **2017**, *32* (1), 86–91. https://doi.org/10.1016/S1872-5805(17)60109-4.

(154) Singh, V.; Joung, D.; Zhai, L.; Das, S.; Khondaker, S. I.; Seal, S. Graphene Based Materials: Past, Present and Future. *Prog. Mater. Sci.* **2011**, *56* (8), 1178–1271. https://doi.org/10.1016/j.pmatsci.2011.03.003.

(155) Randviir, E. P.; Brownson, D. A. C.; Banks, C. E. A Decade of Graphene Research: Production, Applications and Outlook. *Materials Today*. Elsevier November 1, 2014, pp 426–432. https://doi.org/10.1016/j.mattod.2014.06.001.

(156) Dai, J.; Wang, L.; Wang, Y.; Tian, S.; Tian, X.; Xie, A.; Zhang, R.; Yan, Y.; Pan, J. Robust Nacrelike Graphene Oxide-Calcium Carbonate Hybrid Mesh with Underwater Superoleophobic Property for Highly Efficient Oil/Water Separation. *ACS Appl. Mater. Interfaces* **2020**, *12* (4), 4482–4493. https://doi.org/10.1021/acsami.9b18664.

(157) Tang, W.; Sun, D.; Liu, S.; Li, B.; Sun, W.; Fu, J.; Li, B.; Hu, D.; Yu, J. One Step Electrochemical Fabricating of the Biomimetic Graphene Skins with Superhydrophobicity and Superoleophilicity for Highly Efficient Oil-Water Separation. *Sep. Purif. Technol.* **2020**, *236*, 116293. https://doi.org/10.1016/j.seppur.2019.116293.

(158) Alammar, A.; Park, S. H.; Williams, C. J.; Derby, B.; Szekely, G. Oil-in-Water Separation with Graphene-Based Nanocomposite Membranes for Produced Water Treatment. *J. Memb. Sci.* **2020**, *603*, 118007. https://doi.org/10.1016/j.memsci.2020.118007.

(159) Zhang, X.; Liu, D.; Ma, Y.; Nie, J.; Sui, G. Super-Hydrophobic Graphene Coated Polyurethane (GN@PU) Sponge with Great Oil-Water Separation Performance. *Appl.*

Surf. Sci. **2017**, *422*, 116–124. https://doi.org/10.1016/j.apsusc.2017.06.009.

(160) Kong, Z.; Wang, J.; Lu, X.; Zhu, Y.; Jiang, L. In Situ Fastening Graphene Sheets into a Polyurethane Sponge for the Highly Efficient Continuous Cleanup of Oil Spills. *Nano Res.* **2017**, *10* (5), 1756–1766. https://doi.org/10.1007/s12274-017-1484-8.

(161) Liu, J.; Wang, H.; Li, X.; Jia, W.; Zhao, Y.; Ren, S. Recyclable Magnetic Graphene Oxide for Rapid and Efficient Demulsification of Crude Oil-in-Water Emulsion. *Fuel* **2017**, *189*, 79–87. https://doi.org/10.1016/j.fuel.2016.10.066.

(162) Gu, J.; Fan, H.; Li, C.; Caro, J.; Meng, H. Robust Superhydrophobic/Superoleophilic Wrinkled Microspherical MOF@rGO Composites for Efficient Oil-Water Separation. *Angew. Chemie Int. Ed.* **2019**, *58* (16), 5297–5301. https://doi.org/10.1002/anie.201814487.

(163) Yang, H. J.; Cho, J. Y.; Kim, J. H.; Kim, H. Y.; Lee, J. W.; Wang, J. W.; Kwak, J. H.; Jung, S.; Park, J. H.; Jeong, H. J.; Jeong, S. Y.; Seo, S. H.; Lee, G. W.; Han, J. T. Efficient Oxidation and Rational Reduction of Long Carbon Nanotubes for Multifunctional Superhydrophobic Surfaces. *Carbon N. Y.* **2020**, *157*, 649–655. https://doi.org/10.1016/j.carbon.2019.11.006.

(164) Zarghami, S.; Mohammadi, T.; Sadrzadeh, M.; Van der Bruggen, B. Bio-Inspired Anchoring of Amino-Functionalized Multi-Wall Carbon Nanotubes (N-MWCNTs) onto PES Membrane Using Polydopamine for Oily Wastewater Treatment. *Sci. Total Environ.* **2020**, *711*, 134951. https://doi.org/10.1016/j.scitotenv.2019.134951.

(165) Saadati, J.; Pakizeh, M. Separation of Oil/Water Emulsion Using a New PSf/Pebax/F-MWCNT Nanocomposite Membrane. *J. Taiwan Inst. Chem. Eng.* **2017**, *71*, 265–276.

https://doi.org/10.1016/j.jtice.2016.12.024.

(166) Lu, Y.; Yuan, W. Superhydrophobic/Superoleophilic and Reinforced Ethyl Cellulose Sponges for Oil/Water Separation: Synergistic Strategies of Cross-Linking, Carbon Nanotube Composite, and Nanosilica Modification. *ACS Appl. Mater. Interfaces* **2017**, *9* (34), 29167–29176. https://doi.org/10.1021/acsami.7b09160.

(167) Lin, X.; Choi, M.; Heo, J.; Jeong, H.; Park, S.; Hong, J. Cobweb-Inspired Superhydrophobic Multiscaled Gating Membrane with Embedded Network Structure for Robust Water-in-Oil Emulsion Separation. *ACS Sustain. Chem. Eng.* **2017**, *5* (4), 3448–3455. https://doi.org/10.1021/acssuschemeng.7b00124.

(168) Iqbal, R.; Majhy, B.; Sen, A. K. Facile Fabrication and Characterization of a PDMS-Derived Candle Soot Coated Stable Biocompatible Superhydrophobic and Superhemophobic Surface. *ACS Appl. Mater. Interfaces* **2017**, *9* (36), 31170–31180. https://doi.org/10.1021/acsami.7b09708.

(169) Sahoo, B. N.; Nanda, S.; Kozinski, J. A.; Mitra, S. K. PDMS/Camphor Soot Composite Coating: Towards a Self-Healing and a Self-Cleaning Superhydrophobic Surface. *RSC Adv.* **2017**, *7* (25), 15027–15040. https://doi.org/10.1039/C6RA28581C.

(170) Qahtan, T. F.; Gondal, M. A.; Alade, I. O.; Dastageer, M. A. Fabrication of Water Jet Resistant and Thermally Stable Superhydrophobic Surfaces by Spray Coating of Candle Soot Dispersion. *Sci. Rep.* **2017**, *7* (1), 7531. https://doi.org/10.1038/s41598-017-06753-4.

(171) Ju, G.; Liu, J.; Li, D.; Cheng, M.; Shi, F. Chemical and Equipment-Free Strategy To Fabricate Water/Oil Separating Materials for Emergent Oil Spill Accidents. *Langmuir* **2017**, *33* (10), 2664–2670. https://doi.org/10.1021/acs.langmuir.6b04548.

(172) Chandrasekaran, S.; Campbell, P. G.; Baumann, T. F.; Worsley, M. A. Carbon Aerogel Evolution: Allotrope, Graphene-Inspired, and 3D-Printed Aerogels. *J. Mater. Res.* **2017**, *32* (22), 4166–4185. https://doi.org/10.1557/jmr.2017.411.

(173) Gorgolis, G.; Galiotis, C. Graphene Aerogels: A Review. *2D Materials*. IOP Publishing June 22, 2017, p 032001. https://doi.org/10.1088/2053-1583/aa7883.

(174) Lin, Z.; Zeng, Z.; Gui, X.; Tang, Z.; Zou, M.; Cao, A. Carbon Nanotube Sponges, Aerogels, and Hierarchical Composites: Synthesis, Properties, and Energy Applications. *Adv. Energy Mater.* **2016**, *6* (17), 1600554. https://doi.org/10.1002/aenm.201600554.

(175) Pauzauskie, P. J.; Crowhurst, J. C.; Worsley, M. A.; Laurence, T. A.; Kilcoyne, A. L. D.; Wang, Y.; Willey, T. M.; Visbeck, K. S.; Fakra, S. C.; Evans, W. J.; Zaug, J. M.; Satcher, J. H. Synthesis and Characterization of a Nanocrystalline Diamond Aerogel. *Proc. Natl. Acad. Sci. U. S. A.* **2011**, *108* (21), 8550–8553. https://doi.org/10.1073/pnas.1010600108.

(176) Maleki, H. Recent Advances in Aerogels for Environmental Remediation Applications: A Review. *Chemical Engineering Journal*. Elsevier September 15, 2016, pp 98–118. https://doi.org/10.1016/j.cej.2016.04.098.

(177) Luo, Y.; Jiang, S.; Xiao, Q.; Chen, C.; Li, B. Highly Reusable and Superhydrophobic Spongy Graphene Aerogels for Efficient Oil/Water Separation. *Sci. Rep.* **2017**, *7* (1), 7162. https://doi.org/10.1038/s41598-017-07583-0.

(178) Li, L.; Li, B.; Sun, H.; Zhang, J. Compressible and Conductive Carbon Aerogels from Waste Paper with Exceptional Performance for Oil/Water Separation. *J. Mater. Chem. A* **2017**, *5* (28), 14858–14864. https://doi.org/10.1039/C7TA03511J.

(179) Dai, J.; Zhang, R.; Ge, W.; Xie, A.; Chang, Z.; Tian, S.; Zhou, Z.; Yan, Y. 3D Macroscopic Superhydrophobic Magnetic Porous Carbon Aerogel Converted from Biorenewable Popcorn for Selective Oil-Water Separation. *Mater. Des.* **2018**, *139*, 122–131. https://doi.org/10.1016/j.matdes.2017.11.001.

(180) Li, L.; Hu, T.; Sun, H.; Zhang, J.; Wang, A. Pressure-Sensitive and Conductive Carbon Aerogels from Poplars Catkins for Selective Oil Absorption and Oil/Water Separation. *ACS Appl. Mater. Interfaces* **2017**, *9* (21), 18001–18007. https://doi.org/10.1021/acsami.7b04687.

(181) Lee, N.; Yoo, D.; Ling, D.; Cho, M. H.; Hyeon, T.; Cheon, J. Iron Oxide Based Nanoparticles for Multimodal Imaging and Magnetoresponsive Therapy. *Chem. Rev.* **2015**, *115* (19), 10637–10689. https://doi.org/10.1021/acs.chemrev.5b00112.

(182) Kandasamy, G.; Maity, D. Recent Advances in Superparamagnetic Iron Oxide Nanoparticles (SPIONs) for in Vitro and in Vivo Cancer Nanotheranostics. *Int. J. Pharm.* **2015**, *496* (2), 191–218. https://doi.org/10.1016/J.IJPHARM.2015.10.058.

(183) Ali, A.; Zafar, H.; Zia, M.; ul Haq, I.; Phull, A. R.; Ali, J. S.; Hussain, A. Synthesis, Characterization, Applications, and Challenges of Iron Oxide Nanoparticles. *Nanotechnol. Sci. Appl.* **2016**, *Volume 9*, 49–67. https://doi.org/10.2147/NSA.S99986.

(184) Mirabello, G.; Lenders, J. J. M.; Sommerdijk, N. A. J. M. Bioinspired Synthesis of Magnetite Nanoparticles. *Chem. Soc. Rev.* **2016**, *45* (18), 5085–5106. https://doi.org/10.1039/C6CS00432F.

(185) Wu, W.; Jiang, C. Z.; Roy, V. A. L. Designed Synthesis and Surface Engineering Strategies of Magnetic Iron Oxide Nanoparticles for Biomedical Applications. *Nanoscale*

2016, *8* (47), 19421–19474. https://doi.org/10.1039/C6NR07542H.

(186) Zhang, S.; Lü, T.; Qi, D.; Cao, Z.; Zhang, D.; Zhao, H. Synthesis of Quaternized Chitosan-Coated Magnetic Nanoparticles for Oil-Water Separation. *Mater. Lett.* **2017**, *191*, 128–131. https://doi.org/10.1016/j.matlet.2016.12.092.

(187) Lü, T.; Zhang, S.; Qi, D.; Zhang, D.; Vance, G. F.; Zhao, H. Synthesis of PH-Sensitive and Recyclable Magnetic Nanoparticles for Efficient Separation of Emulsified Oil from Aqueous Environments. *Appl. Surf. Sci.* **2017**, *396*, 1604–1612. https://doi.org/10.1016/J.APSUSC.2016.11.223.

(188) Su, C.; Yang, H.; Song, S.; Lu, B.; Chen, R. A Magnetic Superhydrophilic/Oleophobic Sponge for Continuous Oil-Water Separation. *Chem. Eng. J.* **2016**. https://doi.org/10.1016/j.cej.2016.10.082.

(189) Guselnikova, O.; Barras, A.; Addad, A.; Sviridova, E.; Szunerits, S.; Postnikov, P.; Boukherroub, R. Magnetic Polyurethane Sponge for Efficient Oil Adsorption and Separation of Oil from Oil-in-Water Emulsions. *Sep. Purif. Technol.* **2020**, *240*, 116627. https://doi.org/10.1016/j.seppur.2020.116627.

(190) Yang, L.; Wang, Z.; Yang, L.; Li, X.; Zhang, Y.; Lu, C. Coco Peat Powder as a Source of Magnetic Sorbent for Selective Oil–Water Separation. *Ind. Crops Prod.* **2017**, *101*, 1–10. https://doi.org/10.1016/J.INDCROP.2017.02.040.

(191) Beshkar, F.; Khojasteh, H.; Salavati-Niasari, M. Recyclable Magnetic Superhydrophobic Straw Soot Sponge for Highly Efficient Oil/Water Separation. *J. Colloid Interface Sci.* **2017**, *497*, 57–65. https://doi.org/10.1016/J.JCIS.2017.02.016.

(192) Tran, V.-H. T.; Lee, B.-K. Novel Fabrication of a Robust Superhydrophobic PU@ZnO@Fe3O4@SA Sponge and Its Application in Oil-Water Separations. *Sci. Rep.* **2017**, *7* (1), 17520. https://doi.org/10.1038/s41598-017-17761-9.

(193) Li, Z.-T.; Lin, B.; Jiang, L.-W.; Lin, E.-C.; Chen, J.; Zhang, S.-J.; Tang, Y.-W.; He, F.-A.; Li, D.-H. Effective Preparation of Magnetic Superhydrophobic Fe3O4/PU Sponge for Oil-Water Separation. *Appl. Surf. Sci.* **2018**, *427*, 56–64. https://doi.org/10.1016/J.APSUSC.2017.08.183.

(194) Liu, S.; Xu, Q.; Latthe, S. S.; Gurav, A. B.; Xing, R. Superhydrophobic/Superoleophilic Magnetic Polyurethane Sponge for Oil/Water Separation. *RSC Adv.* **2015**, *5* (84), 68293–68298. https://doi.org/10.1039/C5RA12301A.

(195) Wu, L.; Li, L.; Li, B.; Zhang, J.; Wang, A. Magnetic, Durable, and Superhydrophobic Polyurethane@Fe $_3$ O $_4$ @SiO $_2$ @Fluoropolymer Sponges for Selective Oil Absorption and Oil/Water Separation. *ACS Appl. Mater. Interfaces* **2015**, *7* (8), 4936–4946. https://doi.org/10.1021/am5091353.

(196) Zhang, S.; Lü, T.; Qi, D.; Cao, Z.; Zhang, D.; Zhao, H. *Synthesis of Quaternized Chitosan-Coated Magnetic Nanoparticles for Oil-Water Separation*; 2017; Vol. 191. https://doi.org/10.1016/j.matlet.2016.12.092.

(197) Theivasanthi, T. Review on Titania Nanopowder- Processing and Applications. **2017**.

(198) Tudu, B. K.; Gupta, V.; Kumar, A.; Sinhamahapatra, A. Freshwater Production via Efficient Oil-Water Separation and Solar-Assisted Water Evaporation Using Black Titanium Oxide Nanoparticles. *J. Colloid Interface Sci.* **2020**, *566*, 183–193. https://doi.org/10.1016/j.jcis.2020.01.079.

(199) Yang, M.; Liu, W.; Liang, L.; Jiang, C.; Liu, C.; Xie, Y.; Shi, H.; Zhang, F.; Pi, K. A Mild Strategy to Construct Superhydrophobic Cotton with Dual Self-Cleaning and Oil–Water Separation Abilities Based on TiO2 and POSS via Thiol-Ene Click Reaction. *Cellulose* **2020**, *27* (5), 2847–2857. https://doi.org/10.1007/s10570-019-02963-3.

(200) Wang, F.; He, M.; Su, Y.; Wang, W.; Liu, Y.; Xue, J.; Cao, J.; Shen, J.; Zhang, R.; Jiang, Z. In Situ Construction of Chemically Heterogeneous Hydrogel Surfaces toward Near-Zero-Flux-Decline Membranes for Oil-Water Separation. *J. Memb. Sci.* **2020**, *594*, 117455. https://doi.org/10.1016/j.memsci.2019.117455.

(201) Nakata, K.; Fujishima, A. TiO2 Photocatalysis: Design and Applications. *J. Photochem. Photobiol. C Photochem. Rev.* **2012**, *13* (3), 169–189. https://doi.org/10.1016/J.JPHOTOCHEMREV.2012.06.001.

(202) Gunatilake, U. B.; Bandara, J. Efficient Removal of Oil from Oil Contaminated Water by Superhydrophilic and Underwater Superoleophobic Nano/Micro Structured TiO2nanofibers Coated Mesh. *Chemosphere* **2017**, *171*, 134–141. https://doi.org/10.1016/j.chemosphere.2016.12.031.

(203) Patowary, M.; Ananthakrishnan, R.; Pathak, K. Effective Oil Removal from Water by Magnetically Driven Superhydrophobic and Oleophilic Magnetic Titania Nanotubes. *Environ. Sci. Pollut. Res.* **2017**, *24* (22), 18063–18072. https://doi.org/10.1007/s11356-017-9458-7.

(204) Gao, S.; Huang, J.; Li, S.; Liu, H.; Li, F.; Li, Y.; Chen, G.; Lai, Y. Facile Construction of Robust Fluorine-Free Superhydrophobic TiO2@fabrics with Excellent Anti-Fouling, Water-Oil Separation and UV-Protective Properties. *Mater. Des.* **2017**, *128*, 1–8.

https://doi.org/10.1016/J.MATDES.2017.04.091.

(205) Xiong, Z.; Lin, H.; Zhong, Y.; Qin, Y.; Li, T.; Liu, F. Robust Superhydrophilic Polylactide (PLA) Membranes with a TiO_2 Nano-Particle Inlaid Surface for Oil/Water Separation. *J. Mater. Chem. A* **2017**, *5* (14), 6538–6545. https://doi.org/10.1039/C6TA11156D.

(206) Ong, C. B.; Ng, L. Y.; Mohammad, A. W. A Review of ZnO Nanoparticles as Solar Photocatalysts: Synthesis, Mechanisms and Applications. *Renew. Sustain. Energy Rev.* **2018**, *81*, 536–551. https://doi.org/10.1016/J.RSER.2017.08.020.

(207) Agarwal, H.; Venkat Kumar, S.; Rajeshkumar, S. A Review on Green Synthesis of Zinc Oxide Nanoparticles – An Eco-Friendly Approach. *Resour. Technol.* **2017**, *3* (4), 406–413. https://doi.org/10.1016/J.REFFIT.2017.03.002.

(208) Sirelkhatim, A.; Mahmud, S.; Seeni, A.; Kaus, N. H. M.; Ann, L. C.; Bakhori, S. K. M.; Hasan, H.; Mohamad, D. Review on Zinc Oxide Nanoparticles: Antibacterial Activity and Toxicity Mechanism. *Nano-Micro Lett.* **2015**, *7* (3), 219–242. https://doi.org/10.1007/s40820-015-0040-x.

(209) Huang, A.; Kan, C. C.; Lo, S. C.; Chen, L. H.; Su, D. Y.; Soesanto, J. F.; Hsu, C. C.; Tsai, F. Y.; Tung, K. L. Nanoarchitectured Design of Porous ZnO@copper Membranes Enabled by Atomic-Layer-Deposition for Oil/Water Separation. *J. Memb. Sci.* **2019**, *582*, 120–131. https://doi.org/10.1016/j.memsci.2019.03.093.

(210) Lorwanishpaisarn, N.; Kasemsiri, P.; Srikhao, N.; Jetsrisuparb, K.; Knijnenburg, J. T. N.; Hiziroglu, S.; Pongsa, U.; Chindaprasirt, P. Fabrication of Durable Superhydrophobic Epoxy/Cashew Nut Shell Liquid Based Coating Containing Flower-like Zinc Oxide for

Continuous Oil/Water Separation. *Surf. Coatings Technol.* **2019**, *366*, 106–113. https://doi.org/10.1016/j.surfcoat.2019.03.021.

(211) Li, M.; Chen, F.; Liu, C.; Qian, J.; Wu, Z.; Chen, Z. Electrospun Fibrous PTFE Supported ZnO for Oil–Water Separation. *J. Inorg. Organomet. Polym. Mater.* **2019**, *29* (5), 1738–1745. https://doi.org/10.1007/s10904-019-01135-x.

(212) Agrawal, N.; Munjal, S.; Ansari, M. Z.; Khare, N. Superhydrophobic Palmitic Acid Modified ZnO Nanoparticles. *Ceram. Int.* **2017**, *43* (16), 14271–14276. https://doi.org/10.1016/J.CERAMINT.2017.07.176.

(213) Wang, X.; He, Y.; Liu, X.; Zhu, J. Synthesis of Hierarchical Flower-like Particles and Its Application as Super-Hydrophobic Coating. *Powder Technol.* **2017**, *319*, 408–414. https://doi.org/10.1016/J.POWTEC.2017.07.005.

(214) Zhang, X.; Si, Y.; Mo, J.; Guo, Z. Robust Micro-Nanoscale Flowerlike ZnO/Epoxy Resin Superhydrophobic Coating with Rapid Healing Ability. *Chem. Eng. J.* **2017**, *313*, 1152–1159. https://doi.org/10.1016/J.CEJ.2016.11.014.

(215) Raturi, P.; Yadav, K.; Singh, J. P. ZnO-Nanowires-Coated Smart Surface Mesh with Reversible Wettability for Efficient On-Demand Oil/Water Separation. *ACS Appl. Mater. Interfaces* **2017**, *9* (7), 6007–6013. https://doi.org/10.1021/acsami.6b14448.

(216) Scarratt, L. R. J.; Steiner, U.; Neto, C. A Review on the Mechanical and Thermodynamic Robustness of Superhydrophobic Surfaces. *Adv. Colloid Interface Sci.* **2017**, *246*, 133–152. https://doi.org/10.1016/J.CIS.2017.05.018.

(217) Mortazavi, V.; Khonsari, M. M. On the Degradation of Superhydrophobic Surfaces: A

Review. *Wear* **2017**, *372–373*, 145–157. https://doi.org/10.1016/J.WEAR.2016.11.009.

(218) Gupta, R. K.; Dunderdale, G. J.; England, M. W.; Hozumi, A.; Long, X.; Gao, S.; Li, R.; Yao, Y.; Hou, X.; Xu, J.; Xu, J.; Fan, C. Oil/Water Separation Techniques: A Review of Recent Progresses and Future Directions. *J. Mater. Chem. A* **2017**, *2*, 1980–1984. https://doi.org/10.1039/C7TA02070H.

(219) Razavi, S. M. R.; Oh, J.; Sett, S.; Feng, L.; Yan, X.; Hoque, M. J.; Liu, A.; Haasch, R. T.; Masoomi, M.; Bagheri, R.; Miljkovic, N. Superhydrophobic Surfaces Made from Naturally Derived Hydrophobic Materials. *ACS Sustain. Chem. Eng.* **2017**, *5* (12), 11362–11370. https://doi.org/10.1021/acssuschemeng.7b02424.

(220) Khew, S. Y.; Tan, C. F.; Yan, H.; Lin, S.; Thian, E. S.; Zhou, R.; Hong, M. Nanosecond Laser Ablation for Enhanced Adhesion of CuO Nanowires on Copper Substrate and Its Application for Oil-Water Separation. *Appl. Surf. Sci.* **2019**, *465*, 995–1002. https://doi.org/10.1016/J.APSUSC.2018.09.256.

(221) Chen, C.; Wang, B.; Liu, H.; Chen, T.; Zhang, H.; Qiao, J. Synthesis of 3D Dahlia-like Co3O4 and Its Application in Superhydrophobic and Oil-Water Separation. *Appl. Surf. Sci.* **2019**, *471*, 289–299. https://doi.org/10.1016/J.APSUSC.2018.12.023.

(222) Zhang, B.; Li, J.; Zhao, X.; Hu, X.; Yang, L.; Wang, N.; Li, Y.; Hou, B. Biomimetic One Step Fabrication of Manganese Stearate Superhydrophobic Surface as an Efficient Barrier against Marine Corrosion and Chlorella Vulgaris-Induced Biofouling. *Chem. Eng. J.* **2016**, *306*, 441–451. https://doi.org/10.1016/j.cej.2016.07.062.

(223) Martin, S.; Bhushan, B. Transparent, Wear-Resistant, Superhydrophobic and Superoleophobic Poly(Dimethylsiloxane) (PDMS) Surfaces. *J. Colloid Interface Sci.*

2017, *488*, 118–126. https://doi.org/10.1016/j.jcis.2016.10.094.

(224) Shah, S. M.; Zulfiqar, U.; Hussain, S. Z.; Ahmad, I.; Habib-ur-Rehman; Hussain, I.; Subhani, T. *A Durable Superhydrophobic Coating for the Protection of Wood Materials*; 2017; Vol. 203. https://doi.org/10.1016/j.matlet.2017.05.126.

(225) Cheng, Q.-Y.; An, X.-P.; Li, Y.-D.; Huang, C.-L.; Zeng, J.-B. Sustainable and Biodegradable Superhydrophobic Coating from Epoxidized Soybean Oil and ZnO Nanoparticles on Cellulosic Substrates for Efficient Oil/Water Separation. *ACS Sustain. Chem. Eng.* **2017**, *5* (12), 11440–11450. https://doi.org/10.1021/acssuschemeng.7b02549.

(226) Yang, R.-L.; Zhu, Y.-J.; Chen, F.-F.; Qin, D.-D.; Xiong, Z.-C. Recyclable, Fire-Resistant, Superhydrophobic, and Magnetic Paper Based on Ultralong Hydroxyapatite Nanowires for Continuous Oil/Water Separation and Oil Collection. *ACS Sustain. Chem. Eng.* **2018**, *6* (8), 10140–10150. https://doi.org/10.1021/acssuschemeng.8b01463.

(227) Lv, X.; Tian, D.; Peng, Y.; Li, J.; Jiang, G. Superhydrophobic Magnetic Reduced Graphene Oxide-Decorated Foam for Efficient and Repeatable Oil-Water Separation. *Appl. Surf. Sci.* **2019**, *466*, 937–945. https://doi.org/10.1016/J.APSUSC.2018.10.110.

(228) Jiang, C.; Liu, W.; Yang, M.; Liu, C.; He, S.; Xie, Y.; Wang, Z. Robust Multifunctional Superhydrophobic Fabric with UV Induced Reversible Wettability, Photocatalytic Self-Cleaning Property, and Oil-Water Separation via Thiol-Ene Click Chemistry. *Appl. Surf. Sci.* **2019**, *463*, 34–44. https://doi.org/10.1016/J.APSUSC.2018.08.197.

(229) Li, Z.-T.; Wu, H.-T.; Chen, W.-Y.; He, F.-A.; Li, D.-H. Preparation of Magnetic Superhydrophobic Melamine Sponges for Effective Oil-Water Separation. *Sep. Purif. Technol.* **2019**, *212*, 40–50. https://doi.org/10.1016/J.SEPPUR.2018.11.002.

(230) Cao, H.; Gu, W.; Fu, J.; Liu, Y.; Chen, S. Preparation of Superhydrophobic/Oleophilic Copper Mesh for Oil-Water Separation. *Appl. Surf. Sci.* **2017**, *412*, 599–605. https://doi.org/10.1016/j.apsusc.2017.04.012.

(231) Cao, C.; Ge, M.; Huang, J.; Li, S.; Deng, S.; Zhang, S.; Chen, Z.; Zhang, K.; Al-Deyab, S. S.; Lai, Y.; Al-Deyab, S. S.; Lai, Y. K. Robust Fluorine-Free Superhydrophobic PDMS–Ormosil@fabrics for Highly Effective Self-Cleaning and Efficient Oil–Water Separation. *J. Mater. Chem. A* **2016**, *4* (31), 12179–12187. https://doi.org/10.1039/C6TA04420D.

(232) Chen, K.; Gou, W.; Wang, X.; Zeng, C.; Ge, F.; Dong, Z.; Wang, C. UV-Cured Fluoride-Free Polyurethane Functionalized Textile with PH-Induced Switchable Superhydrophobicity and Underwater Superoleophobicity for Controllable Oil/Water Separation. *ACS Sustain. Chem. Eng.* **2018**, *6* (12), 16616–16628. https://doi.org/10.1021/acssuschemeng.8b03851.

(233) Gao, R.; Xiao, S.; Gan, W.; Liu, Q.; Amer, H.; Rosenau, T.; Li, J.; Lu, Y. Mussel Adhesive-Inspired Design of Superhydrophobic Nanofibrillated Cellulose Aerogels for Oil/Water Separation. *ACS Sustain. Chem. Eng.* **2018**, *6* (7), 9047–9055. https://doi.org/10.1021/acssuschemeng.8b01397.

(234) Li, Z.; Wang, B.; Qin, X.; Wang, Y.; Liu, C.; Shao, Q.; Wang, N.; Zhang, J.; Wang, Z.; Shen, C.; Guo, Z. Superhydrophobic/Superoleophilic Polycarbonate/Carbon Nanotubes Porous Monolith for Selective Oil Adsorption from Water. *ACS Sustain. Chem. Eng.* **2018**, *6* (11), 13747–13755. https://doi.org/10.1021/acssuschemeng.8b01637.

(235) Han, X.; Hu, J.; Chen, K.; Wang, P.; Zhang, G.; Gu, J.; Ding, C.; Zheng, X.; Cao, F. Self-Assembly and Epitaxial Growth of Multifunctional Micro-Nano-Spheres for Effective

Separation of Water-in-Oil Emulsions with Ultra-High Flux. *Chem. Eng. J.* **2018**, *352*, 530–538. https://doi.org/10.1016/J.CEJ.2018.07.006.

(236) Jain, A.; Jayaraman, S.; Ulaganathan, M.; Balasubramanian, R.; Aravindan, V.; Srinivasan, M. P.; Madhavi, S. Highly Mesoporous Carbon from Teak Wood Sawdust as Prospective Electrode for the Construction of High Energy Li-Ion Capacitors. *Electrochim. Acta* **2017**, *228*, 131–138. https://doi.org/10.1016/J.ELECTACTA.2017.01.060.

(237) Kazmierczak-Razna, J.; Gralak-Podemska, B.; Nowicki, P.; Pietrzak, R. The Use of Microwave Radiation for Obtaining Activated Carbons from Sawdust and Their Potential Application in Removal of NO2 and H2S. *Chem. Eng. J.* **2015**, *269*, 352–358. https://doi.org/10.1016/J.CEJ.2015.01.057.

(238) Kataria, N.; Garg, V. K. Green Synthesis of Fe 3 O 4 Nanoparticles Loaded Sawdust Carbon for Cadmium (II) Removal from Water: Regeneration and Mechanism. *Chemosphere* **2018**. https://doi.org/10.1016/j.chemosphere.2018.06.022.

(239) Reguyal, F.; Sarmah, A. K.; Gao, W. Synthesis of Magnetic Biochar from Pine Sawdust via Oxidative Hydrolysis of FeCl2 for the Removal Sulfamethoxazole from Aqueous Solution. *J. Hazard. Mater.* **2017**, *321*, 868–878. https://doi.org/10.1016/J.JHAZMAT.2016.10.006.

(240) Islam, M. N.; Islam, M. S. Mechanical Properties of Chemically Treated Sawdust-Reinforced Recycled Polyethylene Composites. *Ind. Eng. Chem. Res.* **2011**, *50* (19), 11124–11129. https://doi.org/10.1021/ie201077k.

(241) Setyono, D.; Valiyaveettil, S. Chemically Modified Sawdust as Renewable Adsorbent for

Arsenic Removal from Water. *ACS Sustain. Chem. Eng.* **2014**, *2* (12), 2722–2729. https://doi.org/10.1021/sc500458x.

(242) Prado, L. A. S. A.; Sriyai, M.; Ghislandi, M.; Barros-Timmons, A.; Schulte, K. Surface Modification of Alumina Nanoparticles with Silane Coupling Agents. *J. Braz. Chem. Soc.* **2010**, *21* (12), 2238–2245. https://doi.org/10.1590/S0103-50532010001200010.

(243) Al-Shatty, W.; Lord, A. M.; Alexander, S.; Barron, A. R. Tunable Surface Properties of Aluminum Oxide Nanoparticles from Highly Hydrophobic to Highly Hydrophilic. *ACS Omega* **2017**, *2* (6), 2507–2514. https://doi.org/10.1021/acsomega.7b00279.

(244) Dai, C.; Wang, S.; Li, Y.; Gao, M.; Liu, Y.; Sun, Y.; Zhao, M. The First Study of Surface Modified Silica Nanoparticles in Pressure-Decreasing Application. *RSC Adv.* **2015**, *5* (76), 61838–61845. https://doi.org/10.1039/C5RA09883A.

(245) Saetun, V.; Chiachun, C.; Riyajan, S.-A.; Kaewtatip, K. Green Composites Based on Thermoplastic Starch and Rubber Wood Sawdust. *Polym. Compos.* **2017**, *38* (6), 1063–1069. https://doi.org/10.1002/pc.23669.

(246) Wang, H.; Yao, Q.; Wang, C.; Ma, Z.; Sun, Q.; Fan, B.; Jin, C.; Chen, Y. Hydrothermal Synthesis of Nanooctahedra $MnFe_2O_4$ onto the Wood Surface with Soft Magnetism, Fire Resistance and Electromagnetic Wave Absorption. *Nanomater. (Basel, Switzerland)* **2017**, *7* (6). https://doi.org/10.3390/nano7060118.

(247) Ma, W.; Zhao, J.; Oderinde, O.; Han, J.; Liu, Z.; Gao, B.; Xiong, R.; Zhang, Q.; Jiang, S.; Huang, C. Durable Superhydrophobic and Superoleophilic Electrospun Nanofibrous Membrane for Oil-Water Emulsion Separation. *J. Colloid Interface Sci.* **2018**, *532*, 12–23. https://doi.org/10.1016/J.JCIS.2018.06.067.

(248) Ghosh, R.; Reddy, S. K.; Sridhar, S.; Misra, A. Temperature Dependent Compressive Behavior of Graphene Mediated Three-Dimensional Cellular Assembly. *Carbon N. Y.* **2016**, *96*, 439–447. https://doi.org/10.1016/J.CARBON.2015.09.089.

(249) Doshi, B.; Sillanpää, M.; Kalliola, S. A Review of Bio-Based Materials for Oil Spill Treatment. *Water Res.* **2018**, *135*, 262–277. https://doi.org/10.1016/J.WATRES.2018.02.034.

(250) Wang, N.; Wang, Y.; Shang, B.; Wen, P.; Peng, B.; Deng, Z. Bioinspired One-Step Construction of Hierarchical Superhydrophobic Surfaces for Oil/Water Separation. *J. Colloid Interface Sci.* **2018**, *531*, 300–310. https://doi.org/10.1016/J.JCIS.2018.07.056.

(251) Wang, J.; Wang, H. Ultra-Hydrophobic and Mesoporous Silica Aerogel Membranes for Efficient Separation of Surfactant-Stabilized Water-in-Oil Emulsion Separation. *Sep. Purif. Technol.* **2019**, *212*, 597–604. https://doi.org/10.1016/J.SEPPUR.2018.11.078.

(252) Chen, C.; Weng, D.; Mahmood, A.; Chen, S.; Wang, J. Separation Mechanism and Construction of Surfaces with Special Wettability for Oil/Water Separation. *ACS Appl. Mater. Interfaces* **2019**, *11* (11), 11006–11027. https://doi.org/10.1021/acsami.9b01293.

(253) Yogapriya, R.; Kasibhatta, K. R. D. Hydrophobic-Superoleophilic Fluorinated Graphene Nanosheet Composites with Metal–Organic Framework HKUST-1 for Oil–Water Separation. *ACS Appl. Nano Mater.* **2020**, *3* (6), 5816–5825. https://doi.org/10.1021/acsanm.0c00980.

(254) Yu, T.; Lu, S.; Xu, W.; Boukherroub, R. Preparation of Superhydrophobic/Superoleophilic Copper Coated Titanium Mesh with Excellent Ice-Phobic and Water-Oil Separation Performance. *Appl. Surf. Sci.* **2019**, *476*, 353–362.

https://doi.org/10.1016/J.APSUSC.2019.01.117.

(255) Liu, Y.; Zhang, K.; Yao, W.; Zhang, C.; Han, Z.; Ren, L. A Facile Electrodeposition Process for the Fabrication of Superhydrophobic and Superoleophilic Copper Mesh for Efficient Oil–Water Separation. *Ind. Eng. Chem. Res.* **2016**, *55* (10), 2704–2712. https://doi.org/10.1021/acs.iecr.5b03503.

(256) Li, J.; Kang, R.; Tang, X.; She, H.; Yang, Y.; Zha, F. Superhydrophobic Meshes That Can Repel Hot Water and Strong Corrosive Liquids Used for Efficient Gravity-Driven Oil/Water Separation. *Nanoscale* **2016**, 7638–7645. https://doi.org/10.1039/C6NR01298A.

(257) Wang, J.; Wang, H.; Geng, G. Flame-Retardant Superhydrophobic Coating Derived from Fly Ash on Polymeric Foam for Efficient Oil/Corrosive Water and Emulsion Separation. *J. Colloid Interface Sci.* **2018**, *525*, 11–20. https://doi.org/10.1016/J.JCIS.2018.04.069.

(258) Li, Z.; Xu, J.; Sun, D.; Lin, T.; Huang, F. Nanoporous Carbon Foam for Water and Air Purification. *ACS Appl. Nano Mater.* **2020**, *3* (2), 1564–1570. https://doi.org/10.1021/acsanm.9b02347.

(259) Wang, Y.; He, G.; Shao, Y.; Zhang, D.; Ruan, X.; Xiao, W.; Li, X.; Wu, X.; Jiang, X. Enhanced Performance of Superhydrophobic Polypropylene Membrane with Modified Antifouling Surface for High Salinity Water Treatment. *Sep. Purif. Technol.* **2019**, *214*, 11–20. https://doi.org/10.1016/J.SEPPUR.2018.02.011.

(260) Jing, Z.; Ding, J.; Zhang, T.; Yang, D.; Qiu, F.; Chen, Q.; Xu, J. Flexible, Versatility and Superhydrophobic Biomass Carbon Aerogels Derived from Corn Bracts for Efficient Oil/Water Separation. *Food Bioprod. Process.* **2019**, *115*, 134–142.

https://doi.org/10.1016/J.FBP.2019.03.010.

(261) Lu, Y.; Niu, Z.; Yuan, W. Multifunctional Magnetic Superhydrophobic Carbonaceous Aerogel with Micro/Nano-Scale Hierarchical Structures for Environmental Remediation and Energy Storage. *Appl. Surf. Sci.* **2019**, *480*, 851–860. https://doi.org/10.1016/J.APSUSC.2019.03.060.

(262) Wang, J.; Wang, H. Facile Synthesis of Flexible Mesoporous Aerogel with Superhydrophobicity for Efficient Removal of Layered and Emulsified Oil from Water. *J. Colloid Interface Sci.* **2018**, *530*, 372–382. https://doi.org/10.1016/J.JCIS.2018.07.002.

(263) Liao, X.; Li, H.; Zhang, L.; Su, X.; Lai, X.; Zeng, X. Superhydrophobic MGO/PDMS Hybrid Coating on Polyester Fabric for Oil/Water Separation. *Prog. Org. Coatings* **2018**, *115*, 172–180. https://doi.org/10.1016/J.PORGCOAT.2017.12.001.

(264) Hu, L.; Liu, Y.; Wang, Z.; Zhou, Y.; Zhang, Y.; Liu, Y.; Li, B. A General in Situ Deposition Strategy for Synthesis of Janus Composite Fabrics with Co(CO3)0.5OH·0.11H2O Nanoneedles for Oil-Water Separation. *ACS Appl. Nano Mater.* **2020**, *3* (4), 3779–3786. https://doi.org/10.1021/acsanm.0c00464.

(265) Liang, Y.; Kim, S.; Kallem, P.; Choi, H. Capillary Effect in Janus Electrospun Nanofiber Membrane for Oil/Water Emulsion Separation. *Chemosphere* **2019**, *221*, 479–485. https://doi.org/10.1016/J.CHEMOSPHERE.2019.01.048.

(266) Yang, J.; Wang, H.; Tao, Z.; Liu, X.; Wang, Z.; Yue, R.; Cui, Z. 3D Superhydrophobic Sponge with a Novel Compression Strategy for Effective Water-in-Oil Emulsion Separation and Its Separation Mechanism. *Chem. Eng. J.* **2019**, *359*, 149–158. https://doi.org/10.1016/J.CEJ.2018.11.125.

(267) Guo, Z.; Gu, H.; Chen, Q.; He, Z.; Xu, W.; Zhang, J.; Liu, Y.; Xiong, L.; Zheng, L.; Feng, Y. Macroporous Monoliths with PH-Induced Switchable Wettability for Recyclable Oil Separation and Recovery. *J. Colloid Interface Sci.* **2019**, *534*, 183–194. https://doi.org/10.1016/J.JCIS.2018.09.021.

(268) Velayi, E.; Norouzbeigi, R. Synthesis of Hierarchical Superhydrophobic Zinc Oxide Nano-Structures for Oil/Water Separation. *Ceram. Int.* **2018**, *44* (12), 14202–14208. https://doi.org/10.1016/J.CERAMINT.2018.05.023.

(269) Abu-Dief, A. M.; Abdel-Fatah, S. M. Development and Functionalization of Magnetic Nanoparticles as Powerful and Green Catalysts for Organic Synthesis. *Beni-Suef Univ. J. Basic Appl. Sci.* **2018**, *7* (1), 55–67. https://doi.org/10.1016/J.BJBAS.2017.05.008.

(270) Mu, B.; Tang, J.; Zhang, L.; Wang, A. Facile Fabrication of Superparamagnetic Graphene/Polyaniline/Fe3O4 Nanocomposites for Fast Magnetic Separation and Efficient Removal of Dye. *Sci. Rep.* **2017**, *7* (1), 5347. https://doi.org/10.1038/s41598-017-05755-6.

(271) Singh, A. K.; Bhuyan, T.; Maity, S.; Mandal, T. K.; Bandyopadhyay, D. Magnetically Actuated Carbon Soot Nanoparticle-Based Catalytic CARBOts Coated with Ni/Pt Nanofilms for Water Detoxification and Oil-Spill Recovery. *ACS Appl. Nano Mater.* **2020**, *3* (4), 3459–3470. https://doi.org/10.1021/acsanm.0c00199.

(272) Ieamviteevanich, P.; Palaporn, D.; Chanlek, N.; Poo-Arporn, Y.; Mongkolthanaruk, W.; Eichhorn, S. J.; Pinitsoontorn, S. Carbon Nanofiber Aerogel/Magnetic Core-Shell Nanoparticle Composites as Recyclable Oil Sorbents. *ACS Appl. Nano Mater.* **2020**, *3* (4), 3939–3950. https://doi.org/10.1021/acsanm.0c00818.

(273) Su, C.; Yang, H.; Song, S.; Lu, B.; Chen, R. A Magnetic Superhydrophilic/Oleophobic Sponge for Continuous Oil-Water Separation. *Chem. Eng. J.* **2017**, *309*, 366–373. https://doi.org/10.1016/J.CEJ.2016.10.082.

(274) Mi, H.-Y.; Jing, X.; Xie, H.; Huang, H.-X.; Turng, L.-S. Magnetically Driven Superhydrophobic Silica Sponge Decorated with Hierarchical Cobalt Nanoparticles for Selective Oil Absorption and Oil/Water Separation. *Chem. Eng. J.* **2018**, *337*, 541–551. https://doi.org/10.1016/J.CEJ.2017.12.135.

(275) Yazdani, F.; Seddigh, M. Magnetite Nanoparticles Synthesized by Co-Precipitation Method: The Effects of Various Iron Anions on Specifications. *Mater. Chem. Phys.* **2016**, *184*, 318–323. https://doi.org/10.1016/j.matchemphys.2016.09.058.

(276) Zulfiqar, U.; Hussain, S. Z.; Awais, M.; Khan, M. M. J.; Hussain, I.; Husain, S. W.; Subhani, T. In-Situ Synthesis of Bi-Modal Hydrophobic Silica Nanoparticles for Oil-Water Separation. *Colloids Surfaces A Physicochem. Eng. Asp.* **2016**, *508*. https://doi.org/10.1016/j.colsurfa.2016.08.074.

(277) Zulfiqar, U.; Subhani, T.; Wilayat Husain, S. Synthesis of Silica Nanoparticles from Sodium Silicate under Alkaline Conditions. *J. Sol-Gel Sci. Technol.* **2016**, *77* (3). https://doi.org/10.1007/s10971-015-3950-7.

(278) Das, S.; Kumar, S.; Samal, S. K.; Mohanty, S.; Nayak, S. K. A Review on Superhydrophobic Polymer Nanocoatings: Recent Development and Applications. *Ind. Eng. Chem. Res.* **2018**, *57* (8), 2727–2745. https://doi.org/10.1021/acs.iecr.7b04887.

(279) Yu, S.; Guo, Z.; Liu, W.; Watanabe, T.; Kim, Y. S.; Zhang, G.; Pei, M.; Fu, Q.; Fujishima, A.; Zhu, D. Biomimetic Transparent and Superhydrophobic Coatings: From Nature and

beyond Nature. *Chem. Commun.* **2015**, *51* (10), 1775–1794. https://doi.org/10.1039/C4CC06868H.

(280) Hou, J.; Zhang, H.; Simon, G. P.; Wang, H. Polycrystalline Advanced Microporous Framework Membranes for Efficient Separation of Small Molecules and Ions. *Adv. Mater.* **2020**, *32* (18), 1902009. https://doi.org/10.1002/adma.201902009.

(281) Wang, Q.; Yu, L.; Nagasawa, H.; Kanezashi, M.; Tsuru, T. High-performance Molecular-separation Ceramic Membranes Derived from Oxidative Cross-linked Polytitanocarbosilane. *J. Am. Ceram. Soc.* **2020**, *103* (8), 4473–4488. https://doi.org/10.1111/jace.17108.

(282) Wu, Y.; Xing, W.; Yan, J.; Cui, J.; Ma, F.; Gao, J.; Lu, J.; Yu, C.; Yan, M. Multilevel Mineral-Coated Imprinted Nanocomposite Membranes for Template-Dependent Recognition and Separation: A Well-Designed Strategy with PDA/CaCO3-Based Loading Structure. *J. Colloid Interface Sci.* **2020**, *575*, 356–366. https://doi.org/10.1016/j.jcis.2020.04.095.

(283) Yusuf, A.; Sodiq, A.; Giwa, A.; Eke, J.; Pikuda, O.; De Luca, G.; Di Salvo, J. L.; Chakraborty, S. A Review of Emerging Trends in Membrane Science and Technology for Sustainable Water Treatment. *Journal of Cleaner Production*. Elsevier Ltd September 1, 2020, p 121867. https://doi.org/10.1016/j.jclepro.2020.121867.

(284) Ramkumar, J. Nafion Perfluorosulphonate Membrane: Unique Properties and Various Applications. In *Functional Materials*; Elsevier Inc., 2012; pp 549–577. https://doi.org/10.1016/B978-0-12-385142-0.00013-1.

(285) Palika, A.; Rahimi, A.; Bolisetty, S.; Handschin, S.; Fischer, P.; Mezzenga, R. Amyloid

Hybrid Membranes for Bacterial & Genetic Material Removal from Water and Their Anti-Biofouling Properties. *Nanoscale Adv.* **2020**, *2* (10), 4665–4670. https://doi.org/10.1039/d0na00189a.

(286) Németh, Z.; Szekeres, G. P.; Schabikowski, M.; Schrantz, K.; Traber, J.; Pronk, W.; Hernádi, K.; Graule, T. Enhanced Virus Filtration in Hybrid Membranes with MWCNT Nanocomposite. *R. Soc. Open Sci.* **2019**, *6* (1). https://doi.org/10.1098/rsos.181294.

(287) Sun, T.; Hao, S.; Fan, R.; Qin, M.; Chen, W.; Wang, P.; Yang, Y. Hydrophobicity-Adjustable MOF Constructs Superhydrophobic MOF-RGO Aerogel for Efficient Oil-Water Separation. *ACS Appl. Mater. Interfaces* **2020**, *12* (50), 56435–56444. https://doi.org/10.1021/acsami.0c16294.

(288) Yang, F.; Yan, Z.; Zhao, J.; Miao, S.; Wang, D.; Yang, P. Rapid Capture of Trace Precious Metals by Amyloid-like Protein Membrane with High Adsorption Capacity and Selectivity. *J. Mater. Chem. A* **2020**, *8* (6), 3438–3449. https://doi.org/10.1039/c9ta12124b.

(289) Goh, P. S.; Naim, R.; Rahbari-Sisakht, M.; Ismail, A. F. Modification of Membrane Hydrophobicity in Membrane Contactors for Environmental Remediation. *Separation and Purification Technology*. Elsevier B.V. November 15, 2019. https://doi.org/10.1016/j.seppur.2019.115721.

(290) Chen, X.; Chen, D.; Li, N.; Xu, Q.; Li, H.; He, J.; Lu, J. Modified-MOF-808-Loaded Polyacrylonitrile Membrane for Highly Efficient, Simultaneous Emulsion Separation and Heavy Metal Ion Removal. *ACS Appl. Mater. Interfaces* **2020**, *12* (35), 39227–39235. https://doi.org/10.1021/acsami.0c10290.

(291) Wang, Y.; Gao, Z.; Shang, Y.; Qi, Z.; Zhao, W.; Peng, Y. Proportional Modulation of Zinc-Based MOF/Carbon Nanotube Hybrids for Simultaneous Removal of Phosphate and Emerging Organic Contaminants with High Efficiency. *Chem. Eng. J.* **2020**, 128063. https://doi.org/10.1016/j.cej.2020.128063.

(292) Kong, X.; Ma, J.; Le-Clech, P.; Wang, Z.; Tang, C. Y.; Waite, T. D. Management of Concentrate and Waste Streams for Membrane-Based Algal Separation in Water Treatment: A Review. *Water Research*. Elsevier Ltd September 15, 2020, p 115969. https://doi.org/10.1016/j.watres.2020.115969.

(293) Ismail, N. H.; Salleh, W. N. W.; Ismail, A. F.; Hasbullah, H.; Yusof, N.; Aziz, F.; Jaafar, J. Hydrophilic Polymer-Based Membrane for Oily Wastewater Treatment: A Review. *Separation and Purification Technology*. Elsevier B.V. February 15, 2020, p 116007. https://doi.org/10.1016/j.seppur.2019.116007.

(294) Al-Attabi, R.; Dumée, L. F.; Kong, L.; Schütz, J. A.; Morsi, Y. High Efficiency Poly(Acrylonitrile) Electrospun Nanofiber Membranes for Airborne Nanomaterials Filtration. *Adv. Eng. Mater.* **2018**, *20* (1), 1700572. https://doi.org/10.1002/adem.201700572.

(295) Zhang, S.; Liu, H.; Tang, N.; Ali, N.; Yu, J.; Ding, B. Highly Efficient, Transparent, and Multifunctional Air Filters Using Self-Assembled 2D Nanoarchitectured Fibrous Networks. *ACS Nano* **2019**, acsnano.9b07293. https://doi.org/10.1021/acsnano.9b07293.

(296) Luo, S.; Zhang, Q.; Zhu, L.; Lin, H.; Kazanowska, B. A.; Doherty, C. M.; Hill, A. J.; Gao, P.; Guo, R. Highly Selective and Permeable Microporous Polymer Membranes for Hydrogen Purification and CO_2 Removal from Natural Gas. *Chem. Mater.* **2018**, *30* (15),

5322–5332. https://doi.org/10.1021/acs.chemmater.8b02102.

(297) Baena-Moreno, F. M.; le Saché, E.; Pastor-Pérez, L.; Reina, T. R. Membrane-Based Technologies for Biogas Upgrading: A Review. *Environmental Chemistry Letters*. Springer September 1, 2020, pp 1649–1658. https://doi.org/10.1007/s10311-020-01036-3.

(298) Kárászová, M.; Zach, B.; Petrusová, Z.; Červenka, V.; Bobák, M.; Šyc, M.; Izák, P. Post-Combustion Carbon Capture by Membrane Separation, Review. *Separation and Purification Technology*. Elsevier B.V. May 1, 2020, p 116448. https://doi.org/10.1016/j.seppur.2019.116448.

(299) Kanehashi, S.; Scholes, C. A. Perspective of Mixed Matrix Membranes for Carbon Capture. *Front. Chem. Sci. Eng.* **2020**, *14* (3), 460–469. https://doi.org/10.1007/s11705-019-1881-5.

(300) Siagian, U. W. R.; Raksajati, A.; Himma, N. F.; Khoiruddin, K.; Wenten, I. G. Membrane-Based Carbon Capture Technologies: Membrane Gas Separation vs. Membrane Contactor. *Journal of Natural Gas Science and Engineering*. Elsevier B.V. July 1, 2019, pp 172–195. https://doi.org/10.1016/j.jngse.2019.04.008.

(301) Shah, S.; Shah, M.; Shah, A.; Shah, M. Evolution in the Membrane-Based Materials and Comprehensive Review on Carbon Capture and Storage in Industries. *Emergent Mater.* **2020**, *3* (1), 33–44. https://doi.org/10.1007/s42247-020-00069-2.

(302) Chakrabortty, S.; Nayak, J.; Ruj, B.; Pal, P.; Kumar, R.; Banerjee, S.; Sardar, M.; Chakraborty, P. Photocatalytic Conversion of CO2 to Methanol Using Membrane-Integrated Green Approach: A Review on Capture, Conversion and Purification. *Journal of Environmental Chemical Engineering*. Elsevier Ltd August 1, 2020, p 103935.

https://doi.org/10.1016/j.jece.2020.103935.

(303) Ang, E. Y. M.; Toh, W.; Yeo, J.; Lin, R.; Liu, Z.; Geethalakshmi, K. R.; Ng, T. Y. A Review on Low Dimensional Carbon Desalination and Gas Separation Membrane Designs. *Journal of Membrane Science*. Elsevier B.V. March 15, 2020, p 117785. https://doi.org/10.1016/j.memsci.2019.117785.

(304) Zhao, X.; Zhang, R.; Liu, Y.; He, M.; Su, Y.; Gao, C.; Jiang, Z. Antifouling Membrane Surface Construction: Chemistry Plays a Critical Role. *Journal of Membrane Science*. Elsevier B.V. April 1, 2018, pp 145–171. https://doi.org/10.1016/j.memsci.2018.01.039.

(305) Zhao, F.; Chu, H.; Yu, Z.; Jiang, S.; Zhao, X.; Zhou, X.; Zhang, Y. The Filtration and Fouling Performance of Membranes with Different Pore Sizes in Algae Harvesting. *Sci. Total Environ.* **2017**, *587–588*, 87–93. https://doi.org/10.1016/j.scitotenv.2017.02.035.

(306) Yin, X.; Zhang, Z.; Ma, H.; Venkateswaran, S.; Hsiao, B. S. Ultra-Fine Electrospun Nanofibrous Membranes for Multicomponent Wastewater Treatment: Filtration and Adsorption. *Sep. Purif. Technol.* **2020**, *242*, 116794. https://doi.org/10.1016/j.seppur.2020.116794.

(307) He, S.; Zhan, Y.; Bai, Y.; Hu, J.; Li, Y.; Zhang, G.; Zhao, S. Gravity-Driven and High Flux Super-Hydrophobic/Super-Oleophilic Poly(Arylene Ether Nitrile) Nanofibrous Composite Membranes for Efficient Water-in-Oil Emulsions Separation in Harsh Environments. *Compos. Part B Eng.* **2019**, *177*, 107439. https://doi.org/10.1016/j.compositesb.2019.107439.

(308) Wang, J.; Wang, H. Ultra-Hydrophobic and Mesoporous Silica Aerogel Membranes for Efficient Separation of Surfactant-Stabilized Water-in-Oil Emulsion Separation. *Sep.*

Purif. Technol. **2019**, *212*, 597–604. https://doi.org/10.1016/J.SEPPUR.2018.11.078.

(309) Deng, Y.; Zhang, G.; Bai, R.; Shen, S.; Zhou, X.; Wyman, I. Fabrication of Superhydrophilic and Underwater Superoleophobic Membranes via an in Situ Crosslinking Blend Strategy for Highly Efficient Oil/Water Emulsion Separation. *J. Memb. Sci.* **2019**, *569*, 60–70. https://doi.org/10.1016/J.MEMSCI.2018.09.069.

(310) Ding, L.; Gao, J.; Chung, T.-S. Schiff Base Reaction Assisted One-Step Self-Assembly Method for Efficient Gravity-Driven Oil-Water Emulsion Separation. *Sep. Purif. Technol.* **2019**, *213*, 437–446. https://doi.org/10.1016/J.SEPPUR.2018.12.055.

(311) Long, Y.; Shen, Y.; Tian, H.; Yang, Y.; Feng, H.; Li, J. Superwettable Coprinus Comatus Coated Membranes Used toward the Controllable Separation of Emulsified Oil/Water Mixtures. *J. Memb. Sci.* **2018**, *565*, 85–94. https://doi.org/10.1016/j.memsci.2018.08.013.

(312) Pan, Z.; Cao, S.; Li, J.; Du, Z.; Cheng, F. Anti-Fouling TiO2 Nanowires Membrane for Oil/Water Separation: Synergetic Effects of Wettability and Pore Size. *J. Memb. Sci.* **2019**, *572*, 596–606. https://doi.org/10.1016/j.memsci.2018.11.056.

(313) Xing, R.; Yang, B.; Huang, R.; Qi, W.; Su, R.; Binks, B. P.; He, Z. Three-Dimensionally Printed Bioinspired Superhydrophobic Packings for Oil-in-Water Emulsion Separation. *Langmuir* **2019**, *35* (39), 12799–12806. https://doi.org/10.1021/acs.langmuir.9b02131.

(314) Wu, J.; Li, H.; Lai, X.; Chen, Z.; Zeng, X. Superhydrophobic Polydimethylsiloxane@Multiwalled Carbon Nanotubes Membrane for Effective Water-in-Oil Emulsions Separation and Quick Deicing. *Ind. Eng. Chem. Res.* **2019**. https://doi.org/10.1021/acs.iecr.9b00994.

(315) Huang, A.; Chen, L. H.; Chen, C. H.; Tsai, H. Y.; Tung, K. L. Carbon Dioxide Capture Using an Omniphobic Membrane for a Gas-Liquid Contacting Process. *J. Memb. Sci.* **2018**, *556*, 227–237. https://doi.org/10.1016/j.memsci.2018.03.089.

(316) Lin, Y. F.; Wang, W. W.; Chang, C. Y. Environmentally Sustainable, Fluorine-Free and Waterproof Breathable PDMS/PS Nanofibrous Membranes for Carbon Dioxide Capture. *J. Mater. Chem. A* **2018**, *6* (20), 9489–9497. https://doi.org/10.1039/c8ta00275d.

(317) Lee, H. J.; Park, Y. G.; Kim, M. K.; Lee, S. H.; Park, J. H. Study on CO2 Absorption Performance of Lab-Scale Ceramic Hollow Fiber Membrane Contactor by Gas/Liquid Flow Direction and Module Design. *Sep. Purif. Technol.* **2019**, *220*, 189–196. https://doi.org/10.1016/j.seppur.2019.03.011.

(318) Guo, J.; Deka, B. J.; Kim, K. J.; An, A. K. Regeneration of Superhydrophobic TiO2 Electrospun Membranes in Seawater Desalination by Water Flushing in Membrane Distillation. *Desalination* **2019**, *468*. https://doi.org/10.1016/j.desal.2019.06.020.

(319) Xu, Y.; Lin, Y.; Lee, M.; Malde, C.; Wang, R. Development of Low Mass-Transfer-Resistance Fluorinated TiO2-SiO2/PVDF Composite Hollow Fiber Membrane Used for Biogas Upgrading in Gas-Liquid Membrane Contactor. *J. Memb. Sci.* **2018**, *552*, 253–264. https://doi.org/10.1016/j.memsci.2018.02.016.

(320) Yu, X.; An, L.; Yang, J.; Tu, S. T.; Yan, J. CO 2 Capture Using a Superhydrophobic Ceramic Membrane Contactor. *J. Memb. Sci.* **2015**, *496*, 1–12. https://doi.org/10.1016/j.memsci.2015.08.062.

(321) Zuo, J. H.; Gu, Y. H.; Wei, C.; Yan, X.; Chen, Y.; Lang, W. Z. Janus Polyvinylidene Fluoride Membranes Fabricated with Thermally Induced Phase Separation and Spray-

Coating Technique for the Separations of Both W/O and O/W Emulsions. *J. Memb. Sci.* **2020**, *595*, 117475. https://doi.org/10.1016/j.memsci.2019.117475.

(322) Ma, D.; Zhou, J.; Wang, Z.; Wang, Y. Block Copolymer Ultrafiltration Membranes by Spray Coating Coupled with Selective Swelling. *J. Memb. Sci.* **2020**, *598*, 117656. https://doi.org/10.1016/j.memsci.2019.117656.

(323) Xing, J.; Zhang, G.; Jia, X.; Liu, D.; Wyman, I. Preparation of Multipurpose Polyvinylidene Fluoride Membranes via a Spray-Coating Strategy Using Waterborne Polymers. *ACS Appl. Mater. Interfaces* **2021**, *13*, 4485–4498. https://doi.org/10.1021/acsami.0c18788.

(324) Song, J.; Batra, A.; Rego, J. M.; MacOsko, C. W. Polyethylene/Polyurethane Blends for Improved Paint Adhesion. *Prog. Org. Coatings* **2011**, *72* (3), 492–497. https://doi.org/10.1016/j.porgcoat.2011.06.008.

(325) Joshi, M.; Adak, B.; Butola, B. S. Polyurethane Nanocomposite Based Gas Barrier Films, Membranes and Coatings: A Review on Synthesis, Characterization and Potential Applications. *Progress in Materials Science*. Elsevier Ltd August 1, 2018, pp 230–282. https://doi.org/10.1016/j.pmatsci.2018.05.001.

(326) Gharibi, R.; Ghadimi, A.; Yeganeh, H.; Sadatnia, B.; Gharedaghi, M. Preparation and Evaluation of Hybrid Organic-Inorganic Poly(Urethane-Siloxane) Membranes with Build-in Poly(Ethylene Glycol) Segments for Efficient Separation of CO2/CH4 and CO2/H2. *J. Memb. Sci.* **2018**, *548*, 572–582. https://doi.org/10.1016/j.memsci.2017.11.058.

(327) Molki, B.; Aframehr, W. M.; Bagheri, R.; Salimi, J. Mixed Matrix Membranes of Polyurethane with Nickel Oxide Nanoparticles for CO2 Gas Separation. *J. Memb. Sci.*

2018, *549*, 588–601. https://doi.org/10.1016/j.memsci.2017.12.056.

(328) Mozaffari, V.; Sadeghi, M.; Fakhar, A.; Khanbabaei, G.; Ismail, A. F. Gas Separation Properties of Polyurethane/Poly(Ether-Block-Amide) (PU/PEBA) Blend Membranes. *Sep. Purif. Technol.* **2017**, *185*, 202–214. https://doi.org/10.1016/j.seppur.2017.05.028.

(329) He, Z.; Byun, J. H.; Zhou, G.; Park, B. J.; Kim, T. H.; Lee, S. B.; Yi, J. W.; Um, M. K.; Chou, T. W. Effect of MWCNT Content on the Mechanical and Strain-Sensing Performance of Thermoplastic Polyurethane Composite Fibers. *Carbon N. Y.* **2019**, *146*, 701–708. https://doi.org/10.1016/j.carbon.2019.02.060.

(330) Report Analyses Polyurethane Sealant Market. *Seal. Technol.* **2017**, *2017* (4), 6. https://doi.org/10.1016/s1350-4789(17)30121-6.

(331) Gu, J.; Gu, H.; Cao, J.; Chen, S.; Li, N.; Xiong, J. Robust Hydrophobic Polyurethane Fibrous Membranes with Tunable Porous Structure for Waterproof and Breathable Application. *Appl. Surf. Sci.* **2018**, *439*, 589–597. https://doi.org/10.1016/j.apsusc.2017.12.267.

(332) Alexander, S.; Eastoe, J.; Lord, A. M.; Guittard, F.; Barron, A. R. Branched Hydrocarbon Low Surface Energy Materials for Superhydrophobic Nanoparticle Derived Surfaces. *ACS Appl. Mater. Interfaces* **2016**, *8* (1), 660–666. https://doi.org/10.1021/acsami.5b09784.

(333) Roodbar Shojaei, T.; Hajalilou, A.; Tabatabaei, M.; Mobli, H.; Aghbashlo, M. Characterization and Evaluation of Nanofiber Materials. In *Handbook of Nanofibers*; Springer International Publishing, 2019; pp 491–522. https://doi.org/10.1007/978-3-319-53655-2_15.

(334) Rodríguez, R.; Pérez, B.; Flórez, S. Effect of Different Nanoparticles on Mechanical Properties and Curing Behavior of Thermoset Polyurethane Adhesives. In *Journal of Adhesion*; Taylor and Francis Inc., 2014; Vol. 90, pp 848–859. https://doi.org/10.1080/00218464.2014.893509.

(335) Wu, T.; Chen, B. Facile Fabrication of Porous Conductive Thermoplastic Polyurethane Nanocomposite Films via Solution Casting. *Sci. Rep.* **2017**, *7* (1), 1–11. https://doi.org/10.1038/s41598-017-17647-w.

(336) Oguz, O.; Candau, N.; Bernhard, S. H. F.; Kosak Soz, C.; Heinz, O.; Stochlet, G.; Plummer, C. J. G.; Yilgor, E.; Yilgor, I.; Menceloglu, Y. Z. Effect of Surface Modification of Colloidal Silica Nanoparticles on the Rigid Amorphous Fraction and Mechanical Properties of Amorphous Polyurethane–Urea–Silica Nanocomposites. *J. Polym. Sci. Part A Polym. Chem.* **2019**, *57* (24), 2543–2556. https://doi.org/10.1002/pola.29529.

(337) Qin, Z.; Xiang, H.; Liu, J.; Zeng, X. High-Performance Oil-Water Separation Polytetrafluoroethylene Membranes Prepared by Picosecond Laser Direct Ablation and Drilling. *Mater. Des.* **2019**, *184*, 108200. https://doi.org/10.1016/j.matdes.2019.108200.

(338) Qing, W.; Shi, X.; Deng, Y.; Zhang, W.; Wang, J.; Tang, C. Y. Robust Superhydrophobic-Superoleophilic Polytetrafluoroethylene Nanofibrous Membrane for Oil/Water Separation. *J. Memb. Sci.* **2017**, *540*, 354–361. https://doi.org/10.1016/j.memsci.2017.06.060.

(339) Ji, D.; Xiao, C.; An, S.; Liu, H.; Chen, K.; Hao, J.; Zhang, T. Preparation of PSF/FEP Mixed Matrix Membrane with Super Hydrophobic Surface for Efficient Water-in-Oil Emulsion Separation. *RSC Adv.* **2018**, *8* (18), 10097–10106.

https://doi.org/10.1039/c8ra00055g.

(340) Liu, Z.; Qin, D.; Zhao, J.; Feng, Q.; Li, Z.; Bai, H.; Sun, D. D. Efficient Oil/Water Separation Membrane Derived from Super-Flexible and Superhydrophilic Core-Shell Organic/Inorganic Nanofibrous Architectures. *Polymers (Basel).* **2019**, *11* (6). https://doi.org/10.3390/polym11060974.

(341) Seyed Shahabadi, S. M.; Brant, J. A. Bio-Inspired Superhydrophobic and Superoleophilic Nanofibrous Membranes for Non-Aqueous Solvent and Oil Separation from Water. *Sep. Purif. Technol.* **2019**, *210*, 587–599. https://doi.org/10.1016/j.seppur.2018.08.038.

(342) Wang, Z.; Ji, S.; Zhang, J.; Liu, Q.; He, F.; Peng, S.; Li, Y. Tannic Acid Encountering Ovalbumin: A Green and Mild Strategy for Superhydrophilic and Underwater Superoleophobic Modification of Various Hydrophobic Membranes for Oil/Water Separation. *J. Mater. Chem. A* **2018**, *6* (28), 13959–13967. https://doi.org/10.1039/c8ta03794a.